Volume 6, Issue 1 (VI)
January - March 2019

ISSN 2394 - 7780

ज्ञान-विज्ञान विमुक्तये
UGC
University Grants Commission
Journal No.: 63571

International Journal of
Advance and Innovative Research

(University Special)

Indian Academicians and Researchers Association
www.iaraedu.com

EXCELLENCE IN EDUCATION
VELS 25 YEARS
1992 - 2017

VELS
INSTITUTE OF SCIENCE, TECHNOLOGY
& ADVANCED STUDIES (VISTAS)
(DEEMED TO BE UNIVERSITY Estd. u/s 3 OF THE UGC ACT, 1956)
NAAC ACCREDITED
PALLAVARAM - CHENNAI - INDIA

SPECIAL ISSUE

OF

VELS INSTITUTE OF SCIENCE, TECHNOLOGY & ADVANCED STUDIES (VISTAS)

CHENNAI

Department of Chemistry

School of Basic Sciences

Publication Partner

Indian Academicians and Researcher’s Association

Guest Editors of Special Issue

Dr. T. Somanathan
Associate Professor,
Department of Chemistry, School of Basic Sciences,
Vels Institute of Science Technology and Advanced Studies (VISTAS)
Chennai

Dr. R. Sasikala
Assistant Professor,
Department of Chemistry, School of Basic Sciences,
Vels Institute of Science Technology and Advanced Studies (VISTAS)
Chennai

Dr. S. Sowmya
Assistant Professor
Department of Chemistry, School of Basic Sciences,
Vels Institute of Science Technology and Advanced Studies (VISTAS)
Chennai

International Journal of Advance and Innovative Research

Volume 6, Issue 1 (VI): January - March 2019

Editor- In-Chief **Dr. Tazyn Rahman**

Members of Editorial Advisory Board

Mr. Nakibur Rahman
Ex. General Manager (Project)
Bongaigoan Refinery, IOC Ltd, Assam

Dr. Alka Agarwal
Director,
Mewar Institute of Management, Ghaziabad

Prof. (Dr.) Sudhansu Ranjan Mohapatra
Dean, Faculty of Law,
Sambalpur University, Sambalpur

Dr. P. Malyadri
Principal,
Government Degree College, Hyderabad

Prof.(Dr.) Shareef Hoque
Professor,
North South University, Bangladesh

Prof.(Dr.) Michael J. Riordan
Professor,
Sanda University, Jiashan, China

Prof.(Dr.) James Steve
Professor,
Fresno Pacific University, California, USA

Prof.(Dr.) Chris Wilson
Professor,
Curtin University, Singapore

Prof. (Dr.) Amer A. Taqa
Professor, DBS Department,
University of Mosul, Iraq

Dr. Nurul Fadly Habidin
Faculty of Management and Economics,
Universiti Pendidikan Sultan Idris, Malaysia

Dr. Neetu Singh
HOD, Department of Biotechnology,
Mewar Institute, Vasundhara, Ghaziabad

Dr. Mukesh Saxena
Pro Vice Chancellor,
University of Technology and Management, Shillong

Dr. Archana A. Ghatule
Director,
SKN Sinhgad Business School, Pandharpur

Prof. (Dr.) Monoj Kumar Chowdhury
Professor, Department of Business Administration,
Guahati University, Guwahati

Prof. (Dr.) Baljeet Singh Hothi
Professor,
Gitarattan International Business School, Delhi

Prof. (Dr.) Badiuddin Ahmed
Professor & Head, Department of Commerce,
Maulana Azad Nationl Urdu University, Hyderabad

Dr. Anindita Sharma
Dean & Associate Professor,
Jaipuria School of Business, Indirapuram, Ghaziabad

Prof. (Dr.) Jose Vargas Hernandez
Research Professor,
University of Guadalajara,Jalisco, México

Prof. (Dr.) P. Madhu Sudana Rao
Professor,
Mekelle University, Mekelle, Ethiopia

Prof. (Dr.) Himanshu Pandey
Professor, Department of Mathematics and Statistics
Gorakhpur University, Gorakhpur

Prof. (Dr.) Agbo Johnson Madaki
Faculty, Faculty of Law,
Catholic University of Eastern Africa, Nairobi, Kenya

Prof. (Dr.) D. Durga Bhavani
Professor,
CVR College of Engineering, Hyderabad, Telangana

Prof. (Dr.) Shashi Singhal
Professor,
Amity University, Jaipur

Prof. (Dr.) Alireza Heidari
Professor, Faculty of Chemistry,
California South University, California, USA

Prof. (Dr.) A. Mahadevan
Professor
S. G. School of Business Management, Salem

Prof. (Dr.) Hemant Sharma
Professor,
Amity University, Haryana

Dr. C. Shalini Kumar
Principal,
Vidhya Sagar Women's College, Chengalpet

Prof. (Dr.) Badar Alam Iqbal
Adjunct Professor,
Monarch University, Switzerland

Prof.(Dr.) D. Madan Mohan
Professor,
Indur PG College of MBA, Bodhan, Nizamabad

Dr. Sandeep Kumar Sahratia
Professor
Sreyas Institute of Engineering & Technology

Dr. S. Balamurugan
Director - Research & Development,
Mindnotix Technologies, Coimbatore

Dr. Dhananjay Prabhakar Awasarikar
Associate Professor,
Suryadutta Institute, Pune

Dr. Mohammad Younis
Associate Professor,
King Abdullah University, Saudi Arabia

Dr. Kavita Gidwani
Associate Professor,
Chanakya Technical Campus, Jaipur

Dr. Vijit Chaturvedi
Associate Professor,
Amity University, Noida

Dr. Marwan Mustafa Shammot
Associate Professor,
King Saud University, Saudi Arabia

Prof. (Dr.) Aradhna Yadav
Professor,
Krupanidhi School of Management, Bengaluru

Prof.(Dr.) Robert Allen
Professor
Carnegie Mellon University, Australia

Prof. (Dr.) S. Nallusamy
Professor & Dean,
Dr. M.G.R. Educational & Research Institute,Chennai

Prof. (Dr.) Ravi Kumar Bommisetti
Professor,
Amrita Sai Institute of Science & Technology, Paritala

Dr. Syed Mehartaj Begum
Professor,
Hamdard University, New Delhi

Dr. Darshana Narayanan
Head of Research,
Pymetrics, New York, USA

Dr. Rosemary Ekechukwu
Associate Dean,
University of Port Harcourt, Nigeria

Dr. P.V. Praveen Sundar
Director,
Shanmuga Industries Arts and Science College

Dr. Manoj P. K.
Associate Professor,
Cochin University of Science and Technology

Dr. Indu Santosh
Associate Professor,
Dr. C. V.Raman University, Chhattisgath

Dr. Pranjal Sharma
Associate Professor, Department of Management
Mile Stone Institute of Higher Management, Ghaziabad

Dr. Lalata K Pani
Reader,
Bhadrak Autonomous College, Bhadrak, Odisha

Dr. Pradeepta Kishore Sahoo
Associate Professor,
B.S.A, Institute of Law, Faridabad

Dr. R. Navaneeth Krishnan
Associate Professor,
Bharathiyan College of Engg & Tech, Puducherry

Dr. Mahendra Daiya
Associate Professor,
JIET Group of Institutions, Jodhpur

Dr. Parbin Sultana
Associate Professor,
University of Science & Technology Meghalaya

Dr. Kalpesh T. Patel
Principal (In-charge)
Shree G. N. Patel Commerce College, Nanikadi

Dr. Juhab Hussain
Assistant Professor,
King Abdulaziz University, Saudi Arabia

Dr. V. Tulasi Das
Assistant Professor,
Acharya Nagarjuna University, Guntur, A.P.

Dr. Urmila Yadav
Assistant Professor,
Sharda University, Greater Noida

Dr. M. Kanagarathinam
Head, Department of Commerce
Nehru Arts and Science College, Coimbatore

Dr. V. Ananthaswamy
Assistant Professor
The Madura College (Autonomous), Madurai

Dr. S. R. Boselin Prabhu
Assistant Professor,
SVS College of Engineering, Coimbatore

Dr. A. Anbu
Assistant Professor,
Achariya College of Education, Puducherry

Dr. C. Sankar
Assistant Professor,
VLB Janakiammal College of Arts and Science

Dr. G. Valarmathi
Associate Professor,
Vidhya Sagar Women's College, Chengalpet

Dr. M. I. Qadir
Assistant Professor,
Bahauddin Zakariya University, Pakistan

Dr. Brijesh H. Joshi
Principal (In-charge)
B. L. Parikh College of BBA, Palanpur

Dr. Namita Dixit
Assistant Professor,
ITS Institute of Management, Ghaziabad

Dr. Nidhi Agrawal
Associate Professor,
Institute of Technology & Science, Ghaziabad

Dr. Ashutosh Pandey
Assistant Professor,
Lovely Professional University, Punjab

Dr. Subha Ganguly
Scientist (Food Microbiology)
West Bengal University of A. & F Sciences, Kolkata

Dr. R. Suresh
Assistant Professor, Department of Management
Mahatma Gandhi University

Dr. V. Subba Reddy
Assistant Professor,
RGM Group of Institutions, Kadapa

Dr. R. Jayanthi
Assistant Professor,
Vidhya Sagar Women's College, Chengalpattu

Dr. Manisha Gupta
Assistant Professor,
Jagannath International Management School

Copyright @ 2019 Indian Academicians and Researchers Association, Guwahati
All rights reserved.

No part of this publication may be reproduced or transmitted in any form or by any means, or stored in any retrieval system of any nature without prior written permission. Application for permission for other use of copyright material including permission to reproduce extracts in other published works shall be made to the publishers. Full acknowledgment of author, publishers and source must be given.

The views expressed in the articles are those of the contributors and not necessarily of the Editorial Board or the IARA. Although every care has been taken to avoid errors or omissions, this publication is being published on the condition and understanding that information given in this journal is merely for reference and must not be taken as having authority of or binding in any way on the authors, editors and publishers, who do not owe any responsibility for any damage or loss to any person, for the result of any action taken on the basis of this work. All disputes are subject to Guwahati jurisdiction only.

International Journal of Advance and Innovative Research

IJAIR

IMPACT FACTOR

7.36

ISSN : 2394-7780

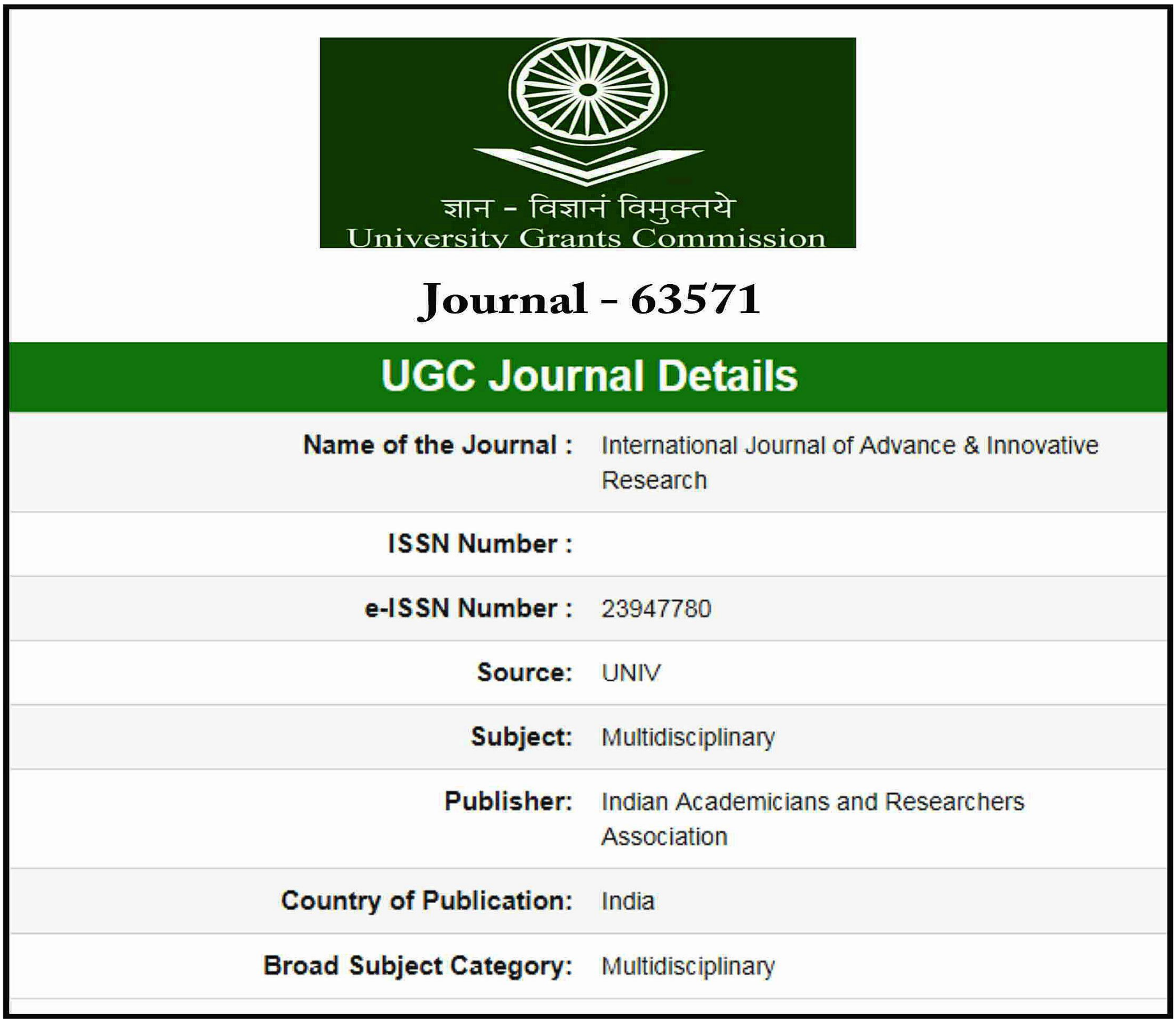

ज्ञान - विज्ञानं विमुक्तये
University Grants Commission

Journal - 63571

UGC Journal Details

Name of the Journal :	International Journal of Advance & Innovative Research
ISSN Number :	
e-ISSN Number :	23947780
Source:	UNIV
Subject:	Multidisciplinary
Publisher:	Indian Academicians and Researchers Association
Country of Publication:	India
Broad Subject Category:	Multidisciplinary

International Journal of Advance and Innovative Research

Volume 6, Issue 1 (VI) : January – March 2019

CONTENTS

Research Papers

International Journal of Advance and Innovative Research
Volume 6, Issue 1 (VI): January - March, 2019

ISSN 2394 - 7780

ENHANCED ELECTROCATALYTIC ACTIVITY OF PD–SN–CO CATALYSTS FOR THE ANODIC OXIDATION OF FORMIC ACID IN MEMBRANELESS FUEL CELLS

M. Elumalai[1], R. Siva[2], Meyyappan Revathi[3], M. Raja[4], and. A. Rajasekaran[5]
Department of Chemistry[1, 2, 3], School of Basic Science, VISTAS, Chennai
Assistant Professsor[4], Tagore Arts and Science College, Chennai
Assistant Professsor[5], Dhanalakshmi Srinivasan College of Engineering and Technology, Chennai
E-mail: elumalai.sbs@velsuniv.ac.in

ABSTRACT

In this study, a Graphene supported Pd–Sn–Co (40:40:20), Pd–Sn (60:40), Pd–Co (60:40), and Pd (100) were synthesized by a borohydride reduction method. These catalysts were characterized by using X-ray diffraction (XRD), transmission electron microscopy (TEM), energy dispersive X-ray spectroscopy (EDX). The electrocatalytic activities were characterized by cyclic voltammetry (CV) and chronoamperometry (CA). As compared with PdSn/G, the trimetallic catalysts show a significant activity enhancement for ethanol and formic acid electro-oxidation. Moreover, the Pd−Sn−Co/G catalyst exhibits the highest activity together with much better stability. The electrochemical results obtained at room temperature showed that the ternary Pd−Sn−Co/G (40:40:20) catalyst displayed better catalytic activity for formic acid oxidation compared with the binary catalysts. During the experiments performed on single membraneless fuel cells, Pd−Sn−Co/G (40:40:20) performed better among all the catalysts prepared with power density of 32.4 mW/cm^2.

Keywords: Palladium, Catalysts, Membraneless Formic acid Fuel Cells and power density.

1. INTRODUCTION

Microfluidic membraneless fuel cells have attracted extensive interest for applications as portable and transportation power sources mainly due to their high efficiency, high energy density and low environmental pollution [1-3]. It is known that methanol is a toxic and harmful chemical. In comparison, ethanol is less toxic, more environmentally friendly and can be easily produced in large quantities by fermentation of sugar-containing raw materials [4-6]. Apart from ethanol, formic acid is another promising candidate for fuel cells because it is nontoxic, nonflammable and easy to store/handle [7]. Therefore, much effort has been devoted to the development of membraneless formic acid fuel cell (MLFAFC). Over the past decade, lots of investigations have been focused upon Pt and Pt-based materials, which were believed to be the best catalysts for low temperature fuel cells [8]. Unfortunately, high cost and limited resource ultimately hinder its use at a commercial level. Thus, numerous studies have been aimed at searching for alternative non-platinum electrocatalysts [9].

Pd is considered to be a promising candidate for Pt since Pd is in the same group within the periodic table of elements and has similar electronic structure. Moreover, Pd is more cost-effective than Pt and its abundance is at least fifty times more than that of Pt on earth. Nowadays, various Pd nanostructures have increasing interest regarding to their excellent electrocatalytic activities toward formic acid oxidation. It is found that Pd catalysts not only exhibit high catalytic activity for formic acid oxidation, but also greatly overcome the CO poisoning effect [10]. Compared to pure Pd, Pd-based alloys show further enhanced electrocatalytic activity because incorporation of alloying elements or oxides can facilitate fresh molecules adsorption, dissociation as well as desorption of poisoning intermediates. Recent reports have shown an improved activity for various Pd–based catalysts, such as Pd–Co, Pd–Ni, Pd–Fe, Pd–Au, Pd–Sn, Pd–Ru, Pd–Cu and Pd–Mo compositions [11-15].

In general, the presence of a second transition metal not only has a significant impact on optimizing the activity and stability, but also can greatly reduce Pd loading, thereby lowering the cost of electrocatalyst. Among Pd-based bimetallic catalysts, Pd–Sn has been receiving special attention due to its excellent catalytic performance towards ethanol and formic acid electro-oxidation [16]. Generally, Sn promoter exists in several chemical states in Pt- and Pd-based catalysts, including fully alloyed, partially alloyed as well as SnO_x (x = 1 or/and 2) oxides, depending on the fabricating and pretreating procedure synthesized a series of Pd_xSn_y/C catalysts and found that a comparable atomic ratio between Pd and Sn can bring on a promising activity enhancement for formic acid electro-oxidation.

To the best of our knowledge, there exist few reports on the activity of ternary Pd–Sn–M catalysts for ethanol and formic acid oxidation, especially with a comparable Pd and Sn atomic ratio. Although the influence of monometallic Ni, Co, Ag or Sn on Pd has been widely reported [17], the possible synergistic effect between Sn and M in ternary electrocatalysts is not available in the literature. In this work, we successfully synthesized a series of Graphene supported ternary Pd–Sn–Co catalysts with the borohydride reduction method. Based upon the co-operative effect of Sn and Co, these ternary catalysts reveal superior electro-catalytic activities toward formic acid oxidation, and will find great potential as less expensive anodic electrocatalysts for MLFAFCs.

2. EXPERIMENTAL

2.1 Materials

The metal precursors used for the preparation of electrocatalysts were adequate amounts of the Pd salt ($Pd(NO_3)_2{\cdot}2H_2O$, Aldrich Chem. Co.), Sn salt ($SnCl_2{\cdot}2H_2O$, Aldrich Chem. Co.), and Co salt ($Co(NO_3)_2{\cdot}6H_2O$, Aldrich Chem. Co.) and $NaBH_4$ (from Merck) reducing agent. Graphene (from Cabot Corp.) was used as a support for the catalysts. Graphite plates (3 cm long and 0.1 cm wide, from E-TEK) were used as substrates for the catalyst to prepare the electrodes. Formic acid (from Merck), sodium perborate (from Riedel) and H_2SO_4 (from Merck) were used as the fuel, the oxidant and as the electrolyte for electrochemical analysis, respectively. All the chemicals were of analytical grade. Pd/G (40-wt%, from E-TEK) was used as the cathode catalyst.

2.2 Catalyst Preparation

Graphene supported ternary Pd–Sn–Co nanoparticles were synthesized by the conventional sodium borohydride reduction method [18]. First, the required amounts of Graphene (from Cabot Corp.,) were ultrasonically dispersed in a mixture of ultrapure water (Millipore MilliQ, 18 MΩ cm), and then, adequate amounts of the precursors were added to the solution. After mixing the solutions, the metal salts were reduced by $NaBH_4$. The prepared materials were washed with distilled water and dried in a vacuum oven at 70◦C. For comparison, the monometallic Pd/G, bimetallic Pd–Sn/G and Pd–Co/G catalysts were synthesized under the same conditions. The electrocatalytic mixtures and atomic ratios were Pd/G (100), Pd–Co/G (60:40), Pd–Sn/G (60:40), and Pd–Sn–Co/G (40:40:20). The nominal loading of metals in the electrocatalysts was 40 %wt and rest 60 % wt. was Graphene.

3 RESULTS AND DISCUSSIONS

3.1 Physical Characterization

3.1.1 X-ray Diffraction (XRD)

Fig. 1 shows the XRD profiles of Pd/G (100), Pd–Co/G (60:40), Pd–Sn/G (60:40), and Pd–Sn–Co/G (40:40:20) catalysts. For all the samples, the broad peak at about 25° is associated with the (002) crystalline plane of graphite with a hexagonal structure for Graphene.

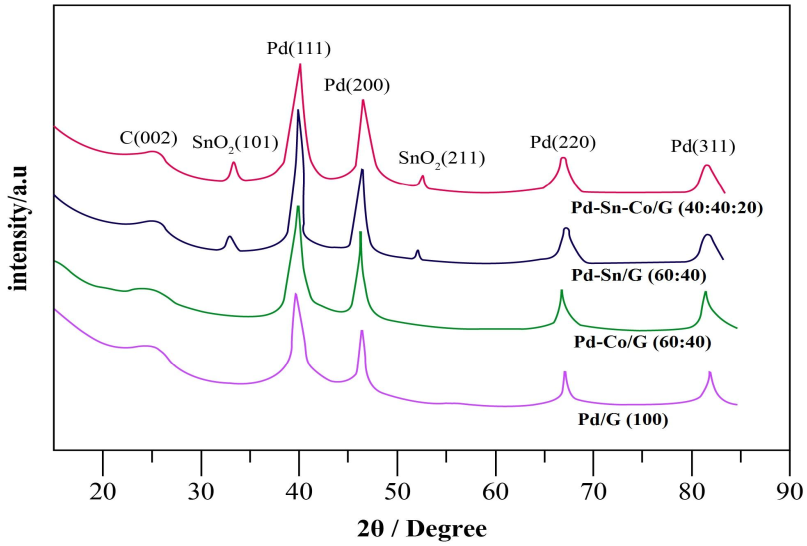

Fig-1: X-ray diffraction patterns of Pd–Sn–Co/G (40:40:20), Pd–Sn/G (60:40), Pd–Co/G (60:40), and Pd/G (100) catalysts.

The peaks at around 39.5°, 46.1° and 67.2° can be assigned to the diffraction planes (111), (200), (220) and (311), indicating that these catalysts have a face-centered cubic (fcc) structure. The present results are well consistent with the reported Pd-based catalysts. Apart from the five main diffraction peaks, there also exist tiny peaks of SnO_2 (101) and SnO_2 (211) at around 34° and 52°, which can also be detected in a series of Pd–Sn based catalysts. All the diffraction peaks were obviously shifted to lower 2θ values with respect to the corresponding peaks of the Pd/G catalyst, indicating a lattice expansion arising from the incorporation of the second and third atoms into the Pd lattice due to the formation of Pd–Sn–Co/G alloys. The XRD patterns of Pd–Sn–Co/G do not show any peaks of Co or Co oxides. However, their presence cannot be ruled out, because the Co particles may be of significantly small size and be present in a small amount or even in an amorphous form.

The average crystallite sizes, calculated from the (2 2 0) plane using a Scherrer equation, of the Pd/G (100), Pd−Co/G (60:40), Pd−Sn/G (60:40) and Pd−Sn−Co/G (40:40:20) alloy catalysts prepared with the Pd content. The mean crystallite sizes of Pd−Co/G, Pd−Sn/G and Pd−Sn−Co/G are smaller than that of the Pd/G prepared with similar procedure shown in Table 1.

Table-1: The EDX composition, XRD and TEM particle size obtained for different atomic ratios of electrocatalysts

Electrocatalyst	Nominal atomic ratio			EDX atomic ratio			Lattice parameter (nm)	Crystallite size (nm)	Particle size from TEM (nm)
	Pd	Sn	Co	Pd	Sn	Co			
Pd/G	100	-	-	100	-	-	0.3936	7.8	7.3
Pd−Co/G	60	-	40	58.9	41.1	-	0.3986	7.1	6.9
Pd−Sn/G	60	40	-	58.7	-	41.3	0.3951	6.7	6.6
Pd−Sn−Co/G	40	40	20	41.3	40.4	18.3	0.3928	6.5	6.1

3.1.2 Transmission Electron Microscopy (TEM)

Fig. 2 shows the typical TEM and histogram of the synthesized Pd–Sn–Co/G catalysts. The metal particle distribution on the Graphene support is heterogeneous with some agglomerates over Graphene particles. However, the distribution of particle size is uniform in a narrow range to some extent. The particle size distribution can be analyzed by randomly choosing more than 100 particles in the corresponding TEM image. It is clear that the particle sizes of the catalysts are in the range of 6.0–7.5 nm, with an average diameter of 6.5 nm for Pd–Sn–Co/G, catalysts. Obviously, the mean particle size of the catalysts is in good agreement with those calculated from XRD.

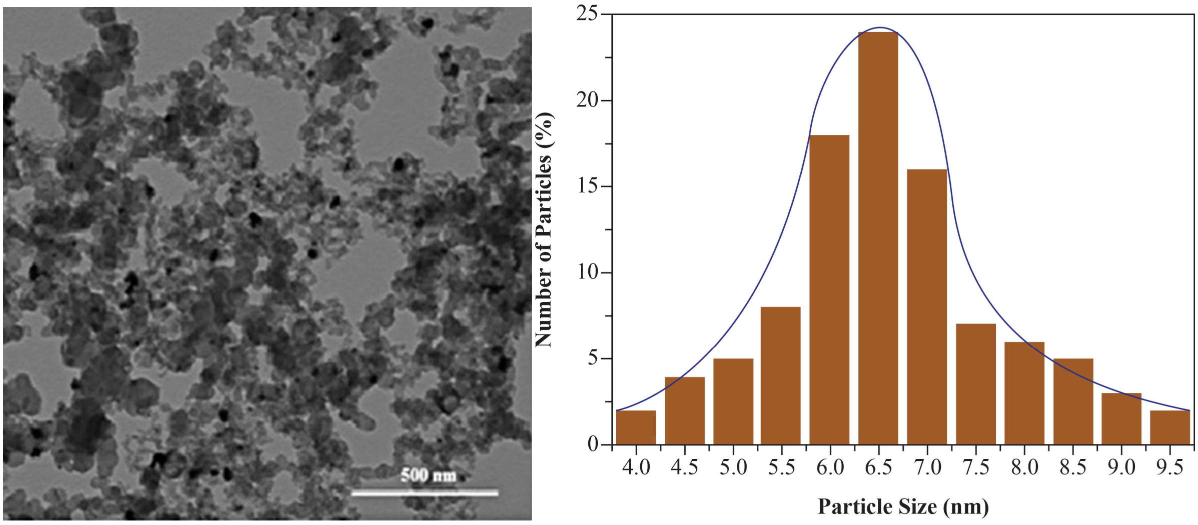

Fig-2: TEM and histogram of Pd–Sn–Co/G catalysts

3.1.3 Energy Dispersive X-ray (EDX) Analysis

The chemical composition of the synthesized Pd–Sn–Co/G (40:40:20) catalysts were evaluated using energy dispersive X-ray spectroscopy (EDX) and the corresponding results are shown in Fig. 3, which indicates the presence of Pd, Sn, Co and Graphene. The EDX results are shown in Table 1. The catalysts prepared had the desired elements with some variation in composition. Clearly, the actual metallic ratio of the synthesized catalyst agrees well with the nominal value.

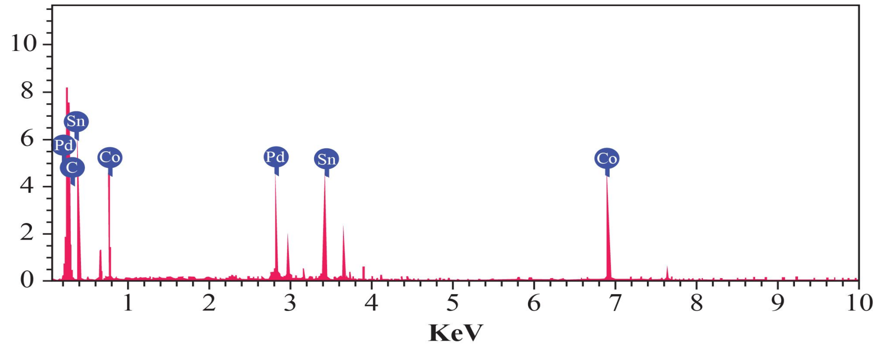

Fig-3: EDX spectra of Pd–Sn–Co/G catalysts

3.2 Electrochemical Characterization

3.2.1 Cyclic Voltammetry (CV)

The catalytic activity of cyclic voltammetry for formic acid electro-oxidation of Pd/G (100), Pd–Co/G (60:40), Pd–Sn/G (60:40) and Pd–Sn–Co/G (40:40:20) alloys are shown in Fig. 4. The Pd–Sn–Co/G (40:40:20) exhibited the highest catalytic activity. For comparison, the catalytic activity of Pd/G, Pd–Co/G, and Pd–Sn/G, was tested. Fig. 4 shows cyclic voltammetry scan of formic acid oxidation of Pd–Sn–Co/G (40:40:20), Pd–Sn/G (60:40), Pd–Co/G (60:40) and Pd/G (100) in 0.5 M H_2SO_4 with 2.0 M HCOOH solution in the potential range of 0.2 V to 0.7 V vs. Ag/AgCl. There were two oxidation peaks when formic acid CV was carried out on the Pd–Sn–Co/G catalyst one during the forward scan and the other during the reverse scan. The onset potential of formic acid oxidation for Pd–Sn–Co/G (40:40:20) catalyst is earlier at about 200 mV was more negative than those of Pd–Sn/G (60:40), Pd–Co/G (60:40) and Pd/G (100) catalysts, indicating good electrocatalytic activity as shown in Table 2.

Table-2: CV results of Pd−Sn−Co/G (40:40:20), Pd–Sn/G (60:40), and Pd–Co/G (60:40) electrocatalysts at room temperature

Catalyst	Scan rate 50 mV/s	
	Positive peak potential (V vs. Ag/AgCl)	Peak current density (mA/cm^2)
Pd–Co/G (60:40)	0.541	42.7
Pd–Sn/G (60:40)	0.542	51.4
Pd–Sn–Co/G (40:40:20)	0.574	182.2

The first electro-oxidation peak of formic acid on Pd–Sn–Co/G (40:40:20) is at 0.574V (vs. Ag/AgCl). The current density at the first peak of formic acid on Pd–Sn–Co/G (40:40:20) is 182.2 mA/cm^2 which is higher than that of Pd–Sn/G (60:40) 51.4 and Pd–Co/G (60:40) 42.7 mA/cm^2 respectively.

The experimental results showed that the Pd–Sn–Co/G (40:40:20) catalyst exhibits the highest activity in formic acid electro-oxidation. The Pd–Sn–Co/G (40:40:20) shows highest peak current density at 0.574 V peak potential, and hence possesses highest catalytic activity towards formic acid oxidation than Pd–Sn/G (60:40), Pd–Co/G (60:40), and Pd/G (100) catalysts, indicating that Pd–Sn–Co/G (40:40:20) is a promising catalyst for formic acid electrooxidation.

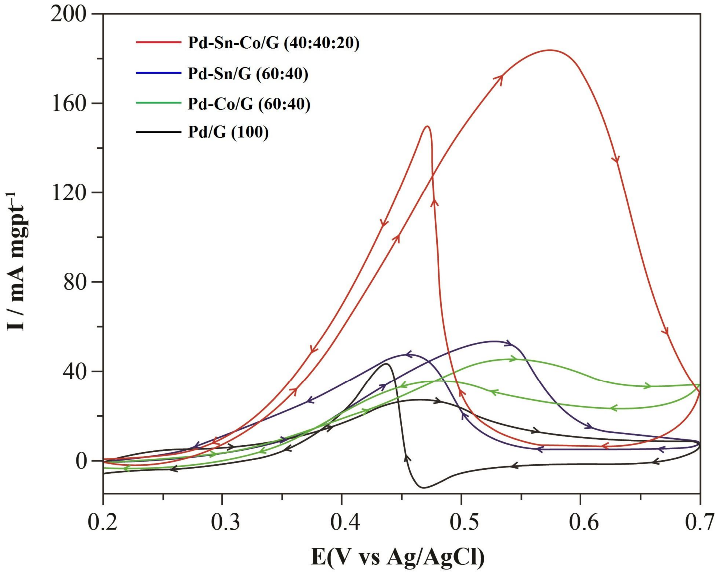

Fig-4: Cyclic Voltammetry of Pd/G, Pd–Co/G, Pd–Sn/G and Pd–Sn–Co/G Electrocatalysts in 0.5 M H_2SO_4 and 2.0 M formic acid.

3.2.2 Chronoamperometry (CA)

The long-term operation test chronoamperometry (CA) of Pd/G (100), Pd–Co/G (60:40), Pd–Sn/G (60:40), and Pd–Sn–Co/G (40:40:20) electrocatalyst performances for formic acid oxidation were studied by chronoamperometry at 0.35 V. Fig. 5 shows representative chronoamperograms obtained for the different electrocatalysts whose current densities were normalized by Pd mass. During the experiment, there was a sharp decrease in the current density and after five minutes, it becomes relatively stable. This behavior can be explained assuming that initially the active sites are free from adsorbed formic acid molecules, but a new adsorption of formic acid molecules is a function of the liberation of the active sites by formic acid oxidation. The ternary Pd–Sn–Co/G (40:40:20) electrocatalysts gave higher current than the binary

Pd–Sn/G (60:40) and Pd–Co/G (60:40) electrocatalysts. This is attributed to the change of electronic structure induced by ternary Pd–Sn–Co/G (40:40:20) electrocatalysts. The results showed that the ternary Pd–Sn–Co/G (40:40:20) electrocatalysts shows the highest activity for formic acid oxidation.

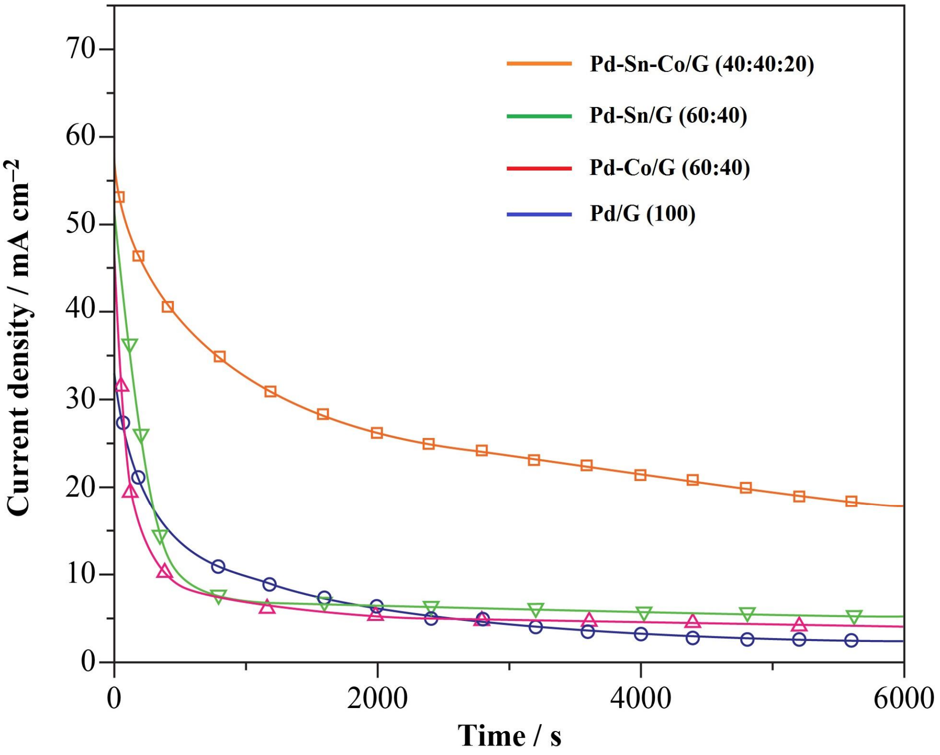

Fig-5: Chronoamperometry of Pd/G, Pd–Co/G, Pd–Sn/G, and Pd–Sn–Co/G Electrocatalysts

3.3 Single Cell Performance

The microfluidic architecture of laminar flow-based membraneless fuel cells overcomes the fuel crossover and water management issues that plague membrane-based fuel cells (i.e., PEMFC, DMFC) and enables independent control of stream characteristics (i.e., flow-rate and composition). Here we focused on maximizing cell performance, in terms of power density, by tailoring various structural characteristics and catalytic activity of Graphene supported ternary Pd–Sn–Co catalysts. The single membraneless formic acid fuel cell (MLFAFC) of Pd–Co/G (60:40), Pd–Sn/G (60:40), Pd–Sn–Co/G (40:40:20) and Pd/G (100) catalysts were evaluated as anode catalysts for formic acid electro-oxidation are showed in Fig. 6. When Pd/G (100), Pd–Co/G (60:40), Pd–Sn/G (60:40) was used as the anode catalytic activity towards formic acid electro-oxidation the performance of single cell was poor as compared to ternary Pd–Sn–Co/G (40:40:20). The maximum power density for Pd−Sn/G (60:40), Pd−Co/G (60:40) and Pd/G (100) is 22.5, 18.4 and 6.1 mW/cm^2. The results of MLFAFC adapting to different catalysts are summarized in Table 3. It was observed that the cell performance of Pd–Sn–Co/G (40:40:20) catalyst was better than other catalysts with peak power density value of 32.4 mW/cm^2.

Table-3: Summary of performance of single fuel cell tests using (2 mg cm^{-2} catalyst loading, 40 wt% catalyst on Graphene)

Anode Catalysts	Open circuit voltage (V)	Maximum power density (mW/cm^2)	Current density at maximum power density (mA/cm^2)
Pd/G (100)	0.51	6.1	52.4
Pd–Co/G (60:40)	0.63	18.4	115.8
Pd–Sn/G (60:40)	0.69	22.5	126.7
Pd–Sn–Co/G (40:40:20)	0.82	32.4	184.3

In the single membraneless formic acid fuel cell test of tri-metallic combinations of Pd, Sn, and Co, the addition of Co increases the cell performances. Pd/G (100), Pd–Co/G (60:40), Pd–Sn/G (60:40), Pd–Sn–Co/G (40:40:20) the current densities are 52.4, 115.8, 126.7 and 184.3 mA/cm^2, respectively. The enhanced catalytic performance of Pd–Sn–Co/G (40:40:20) may be attributed to its special composition and surface electronic state in electro-oxidation of formic acid.

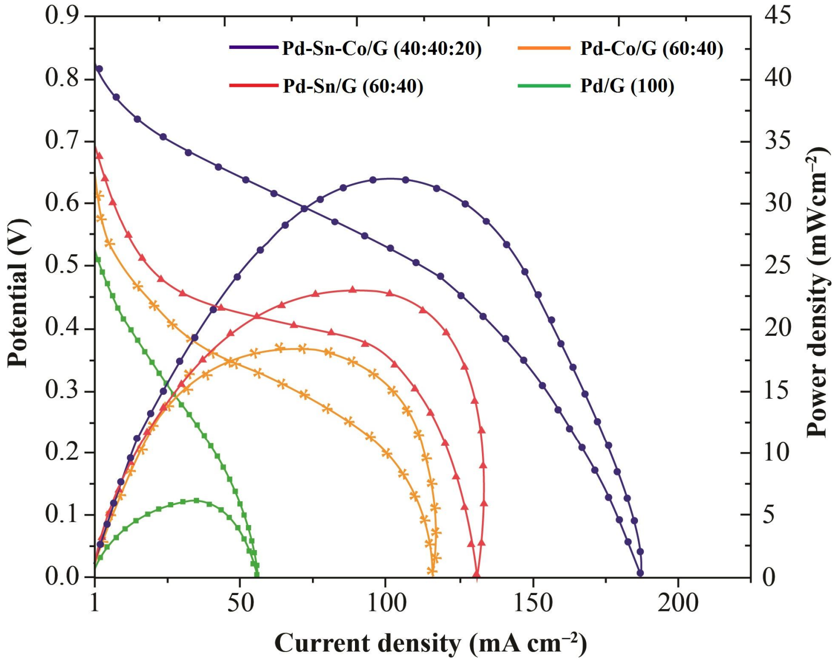

Fig-6: Polarization and power density curves of different catalyst at 2 mg cm^{-2} catalyst loading on anode and cathode at room temperature.

4. CONCLUSIONS

In summary, Pd–Co/G, Pd–Sn/G and Pd–Sn–Co/G electrocatalysts were prepared by the borohydride reduction method. The nano-sized particles catalysts were well dispersed on the Graphene supports. The prepared catalysts are characterized by XRD, TEM, EDX, CV, CA. The X-ray diffractograms of the Pd–Co/G, Pd–Sn/G and Pd–Sn–Co/G electrocatalyst showed a structure of the Pd alloys. The Pd metal was the predominant material in all the samples, with peaks attributed to the face-centered cubic (fcc) crystalline structure. The TEM analysis and histograms showed that the catalysts on Graphene support are uniformly dispersed having the average particle size of 6.5 nm. Additionally EDX analysis indicated that the experimental composition is in agreement with the nominal composition of the catalyst. Cyclic voltammetry results showed that Pd–Sn–Co/G (40:40:20) is more active in formic acid electro-oxidation than other catalysts. The long-term operation test chronoamperometry was performed successfully, revealing that the maximum power density behavior of Pd–Sn–Co/G (40:40:20) catalyst gave higher current than the binary Pd–Sn/G (60:40) and Pd–Co/G (60:40) catalysts at steady condition. In this work, Graphene-supported binary Pd–Sn/G, Pd–Co/G and ternary Pd–Sn–Co/G anode catalysts were successfully tested in a single membraneless fuel cell using 2.0 M formic acid as the fuel and 0.1 M sodium perborate as the oxidant in the presence of 0.5 M H_2SO_4 as the electrolyte. Based on peak power density drawn from a single cell, Pd–Sn–Co/G (40:40:20) is the best anode catalyst with peak power density value of 32.4 mW/cm^2 among the catalysts tested. The enhanced catalytic performance of Pd–Sn–Co/G (40:40:20) may be attributed to its special composition and surface electronic state. This implies that the Pd–Sn–Co/G (40:40:20) catalysts would become alternatives to membraneless formic acid fuel cells.

REFERENCES

1. M. Elumalai, M. Priya, S. Kiruthika and B. Muthukumaran, afinidad, 72, 572 (2015).
2. M. Priya, M. Elumalai, S. Kiruthika and B. Muthukumaran, Int. J. of Innovative Research in Science and eng., 2, 108 (2018).
3. M. Elumalai, S. Kiruthika and B. Muthukumaran, Int. J. of Indust. Eng., 3, 114 (2017).
4. E. Antolini, and E. R. Gonzalez, *J. of Pow. Sour.*, 195, 3431 (2010).
5. L. Y. Chen, N. Chen, Y. Hou, Z. C. Wang, S. H. Lv, T. Fujita, J. H. Jiang, A. Hirata and M. W. Chen, *ACS Cat.*, 3, 1220 (2013).
6. W. Du, K. E. Mackenzie, D. F. Milano, N. A. Deskins, D. Su and X. Teng, *ACS Cat.*, 2, 287 (2012).
7. G. L. Li, L. H. Jiang, Q. Jiang, S. L. Wang and G. Q. Sun, *Electrochim. Acta*, 56, 7703 (2011).
8. M. Priya, A. Arun, M. Elumalai, S. Kiruthika and B. Muthukumaran, Advan. in Phys. Chem., 8, 2014 (2014).

ISSN 2394 - 7780

9. Z. L. Liu and X. H. Zhang, *Electrochem. Commun.*, 11, 1667 (2009).
10. C. C. Qiu, R. Shang, Y. F. Xie, Y. R. Bu, C. Y. Li and H. Y. Ma, *Mater. Chem. and Phys.*, 120, 323 (2010).
11. M. Elumalai and B. Muthukumaran, int. j. of ChemTech Research, 7, 3033 (2015).
12. G. R. Sanchez, H. Y. Madeira and O. S. Feria, *Inter. J. of Hyd. Ener.*, 33, 3596 (2008).
13. A. Sarkar, A. V. Murugan and A. Manthiram, *J. of Phys. Chem.C*, 112, 12037 (2008).
14. L. P. Shen, H. Z. Li, L. Lu, Y. F. Luo, Y. W. Tang, Y. Chen and T. H. Lu, *Electrochim. Acta*, 89, 497 (2013).
15. D. D. Tu, B. Wu, B. X. Wang, C. Deng and Y. Gao, *Appl. Catal.B*, 103, 163 (2011).
16. Y. Wang, X. Wang and C. M. Li, *Appl. Catal.B*, 99, 229 (2010).
17. J. B. Xu, T. S. Zhao, S. Y. Shen and Y. S. Li, *Inter. J. of Hyd. Ener.*, 35, 6490 (2010).
18. F. C. Zhu, G. S. Ma, Z. C. Bai, R. Q. Hang, B. Tang, Z. H. Zhang and X. G. Wang, *J. of Pow. Sour.*, 242, 610 (2013).

International Journal of Advance and Innovative Research
Volume 6, Issue 1 (VI): January - March, 2019
ISSN 2394 - 7780

HIGHLY EFFICIENT, UV ACTIVE AND REUSABLE PHOTOCATALYST: LANTHANUM LOADED COPPER OXIDE FOR METHYL ORANGE AND TRYPAN BLUE DYES DEGRADATION WITH SYNERGISTIC EFFECT

R. Sasikala[1], B. Subash[2] and S. Kutti Rani[3]
Department of Chemistry[1], Vel's Institute of Science, Technology and Advanced Studies, Chennai
Department of Chemistry[2], St. Joseph's College of Engineering, Chennai
Department of Chemistry[3], B. S. Abdur Rahman University, Chennai
E-mail: sasiram.sbs@velsuniv.ac.in

ABSTRACT

A simple precipitation - thermal decomposition method was adopted for the synthesis of Lanthanum loaded CuO (La-CuO). The synthesized catalyst was characterized by (XRD), field emission scanning electron microscopy (FE-SEM), energy dispersive spectra (EDS), diffuse reflectance spectra (DRS), photoluminescence (PL), Fourier transform infrared (FT-IR) spectra, BET surface area and cyclic voltammetry (CV) measurements. The photo catalytic activity of bare, commercial and optimized La-CuO catalyst is used for the degradation of toxic azo dyes Methyl Orange (MO) and Trypan Blue (TB) under UV light irradiation. La-CuO have more effective in the degradation of two azo dyes than pure and commercial CuO. The mineralization of MO and TB has been confirmed by Chemical Oxygen Demand (COD) measurements. A possible mechanism is proposed for the higher efficiency of La-CuO under UV light. This catalyst was reusable and stable under UV light illuminations.

Keywords: La loaded CuO, Methyl Orange, Photocatalysis, Reusability, Trypan Blue, UV light.

INTRODUCTION

The importance of the wastewater treatment, management and its disposal progressively increases in the present times and it converts a foremost fretfulness for public health scientific attention. At present protocols focused on, the wastewater treatment is based on the properties of physical, chemical and biological process [1]. The chronological and contemporaneous use of those processes collectively have a tendency to produce a more efficient method in removing the all types of impurity aspects in liquid dregs. Limitations in terms of implementation, efficiency, and cost are a factor, nevertheless, biological methods, as an example, have been widely used and show potential towards dairy and agricultural wastewater treatment [2]. Especially chemical procedure focused with suitable semiconductors photocatalytic materials like TiO_2, ZnO, CdS, WO_3, ZnS, CuO, CdO., etc mediated environmental remediation of industrial wastewater [3-9]. Conversely, due to hasty recombination of photo generated e^- and h^+ pairs on semicondors unavoidably hinders the superficial diffusion of the charge carrier's activity, which drops the photocatalyzed degradation reaction occurring at the semiconductor/liquid interface [10-12].

To overwhelmed this drawback or restraining factor, several methods have been used to progress the charge separation and improve the light response of semiconductor based photocatalysts. Catalytic activity of semiconducting materials through modification with different metals [13-16]. Among the photocatalysts, CuO is a eminent p-type semiconductor with a small bandgap of 1.2 eV in bulk, it has been considered passionately is supposed to be the most capable material due to its higher photocatalytic activity, non-toxicity, low price and reusability or long-term stability. CuO is widely used in the heterogeneous catalyst due to its versatile properties and budding applications. It is mainly used as gas sensors, field-emission sources, lithium ion electrode materials, etc., [17-19]. Numerous methods such as metal/non-metal/anion doping or loading and surface variation with porous substances have been practiced for modification of CuO [20-23]. Enhanced photocatalytic activity is mainly due to the defeating the fast recombination of charge carriers by metals or non-metals are loaded with CuO, by the action of charge transferal takes place from the CuO to the metal surface. In our present studies mainly inspired on the synthesis, characterization and photo catalytic activity of La loaded CuO by simple precipitation - thermal decomposition method and also detoxification studies of both Tryphan Blue and Methyl Orange dyes. The mineralization of both dyes established by Chemical Oxygen Demand (COD) measurement.

EXPERIMENTAL

Materials and Methods

The commercial azo dyes Trypan Blue (TB), Methyl Orange (MB) from (s.d.Fine), copper nitrate pentahydrate (99%) and Oxalic acid dihydrate (99%) were found from Himedia chemicals. $La(NO_3)_3$. $6H_2O$ (CAS) were got from Spectrochem, commercial CuO (Himedia), Ag_2SO_4 (s.d.fine), $K_2Cr_2O_7$ (s.d.fine), $HgSO_4$ and $FeSO_4.7H_2O$

(Qualigens) were used as received. The pH of the solutions was adjusted by using diluted sulphuric acid or sodium hydroxide. Double distilled water was also used to prepared experimental solutions.

Analytical Methods

IR spectra was recorded using avatar-330 FT-IR spectrophotometer. Morphology of the catalyst was recorded by gold coated samples using the model of JEOL-JSM 5610 LV Scanning electron microscope, equipped with OXFORD energy dispersive spectra. Cyclic voltammetry CHI 60AC of Electrochemical analyzer was used to measure the presence of metal in the catalyst.

Photocatalytic experiments

Degradation was employed by using standard Heber multilamp photoreactor HML-MP 88 [4] by UV-A light at 365 nm. It consists of 8W medium pressure Hg vapor standard lamp set in parallel at 365 nm. It also consisting of has a chamber with specially premeditated reflector made of polished Al foil and constructed in cooling fan. 50 mL of reaction glass tubes fixed with magnetic stirrer. The light exposure length is about 330 mm. Only four parallel 8W medium pressure Hg light was used carried out the irradiation procedure. Absolute mixing of dye solution and catalyst was constantly aerated by a pump to supply of oxygen.

Both the TB and MO dyes (25 mL) with suitable quantity of catalyst was stirred for half hour in absence of light to reach the maximum adsorption of dye on the catalyst surface. During the reaction time, no evaporation of the solvent was noticed. The mixture of solution and catalyst were continuously stirred for complete mixing at specific time intervals. The centrifugation was used to remove the catalyst from 2-3 mL of sample was withdrawn from reaction mixture. 1 mL of the filterate was suitably diluted and the solution was used to measure the concentration of the dyes at particular wavelength. The percentage of dye remaining was also determined from the concentration of the dyes.

Chemical oxygen demand (COD) measurements

COD was determined by the following procedure for the mineralization process. A known volume of $K_2Cr_2O_7$, Ag_2SO_4 and H_2SO_4 were refluxed with appropriate amount of $HgSO_4$ and 1ML of dye sample for two hours. After 2 hours the mixture was titrated against standard Ferrous Ammonium Sulfate (FAS). The end point of the titration was identified by using Ferroin indicator. Instead of dye sample, distilled water was also used to carried out the blank titration. COD was determined using the following equation (1).

$$\text{COD}=\frac{(\text{Blank titre value} - \text{dye sample titre value}) \times \text{normality of FAS} \times 8 \times 1000}{\text{Volume of sample}} \qquad \ldots (1)$$

RESULTS AND DISCUSSION

Characterization of catalyst

Sasikala et al, were reported the synthesis and characterization of La-CuO and its catalytic activity for A^3 and click reaction [24]. XRD analysis shows that all the diffraction peaks exactly matched with CuO nanoparticles (monoclinic phase) (JCPDS File no. 048-1548). The 2θ values such as 35.45, 38.73, 42.50, 48.92, 61.99 and 66.49, matching to the hkl values of (002), (111), (200), (202), (220) and (113) planes of CuO nanoparticles were displayed. The agglomerated with spherical shaped CuO nanoparticles was identified by FE-SEM images. The presence of La, Cu and O were confirmed by energy dispersive spectrum (EDS) analysis. DRS spectra of La-CuO shows a higher adsorption in visible region than pure CuO, due to the higher adsorption in visible region, this may enhance the catalytic activity. The PL intensity decreases when compared to bare CuO, due to the loading of La with CuO. This is because of the reduces the recombination of electron-hole pairs by loading of La. BET surface shows that, La loaded CuO (4.26 m^2g^{-1}) is higher surface area than that of bare CuO (1.82 m^2g^{-1}) (Table 1). Higher surface area of the catalyst, improves the catalytic activity.

FT-IR Spectral study

FT-IR spectra of virgin CuO and La-CuO are shown in Fig. 1, respectively. The broad absorption band in the region of 3200 – 3400 cm^{-1} is the distinguishing of the -OH stretching vibration of surface hydroxyl groups. The broad band at 528.4 cm^{-1} is due to the stretching vibration of archetypal La with Cu-O bond in CuO nanoparticles. When compared to the spectrum of virgin copper oxide, La-CuO peaks broad absorption band in the region is appeared from 458.9 - 1809.8 cm^{-1} for La in CuO. This type of broad peak reveals that La metal may be presence in the catalyst.

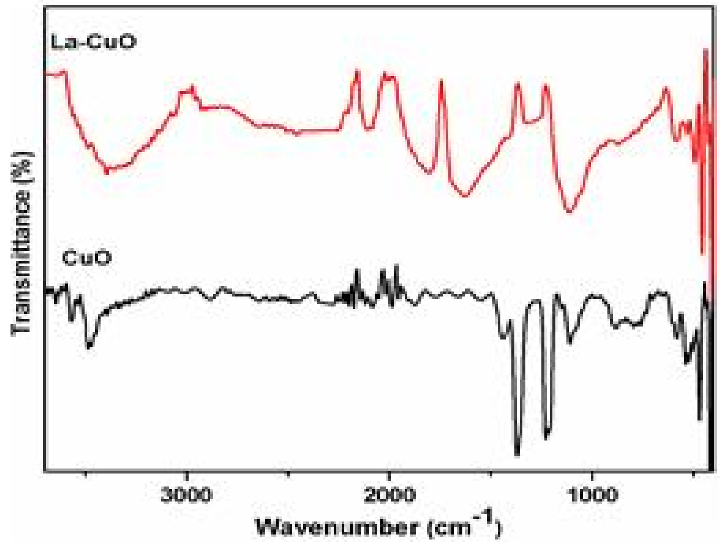

Fig-1: FT-IR spectra of (a) bare CuO and (b) La-CuO.

Cyclic voltammetry study

In Fig. 2 shows the cyclic voltammetry measurements of bare CuO and La-CuO were used in the reaction of potassium ferrocyanide. Cathodic potential (E_{pc}) is shifted from 0.046 to 0.318 V and the cathodic current (i_{pc}) also increases from - 3.08×10^{-5}A to - 8.35×10^{-5}A by La loading on CuO material (Fig. 4). While the current achieved by bare CuO is very less when compared to metal loaded CuO. This enlarge in potential and current entitled the presence of metal (La) in the catalyst [25, 26].

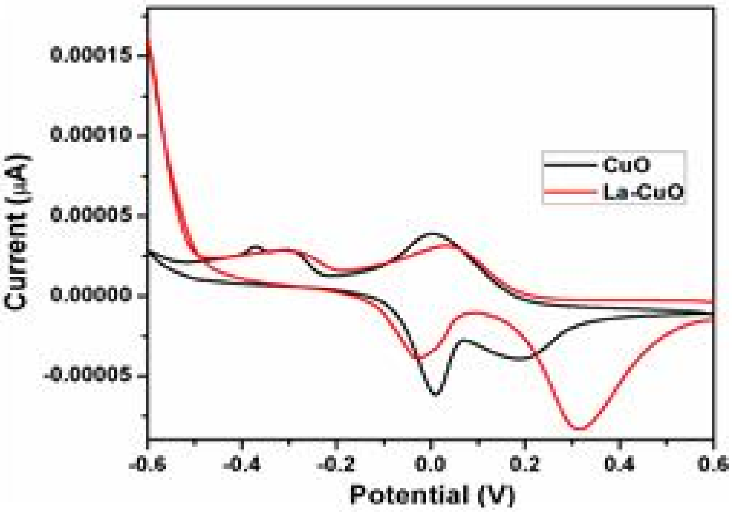

Fig-2: Cyclic voltammograme of: (a) bare CuO and (b) La-CuO

Major analysis of photocatalytic degradations of these two dyes (TB and MO) with different wt% La on CuO catalysts was carried out. The heterogeneous photocatalysis follows *pseudo*-first order kinetics were reported earlier [3,4, 16]. *Pseudo*-first order rate constants determined for 0.5, 1.0, 1.5 and 2.0 wt% La loading were 0.071, 0.091, 0.079 and 0.060 min^{-1} for TB, 0.052, 0.075, 0.0580 and 0.053 min^{-1} for MO dyes. From this results 1 wt% of La-CuO catalyst was found be highest efficient for both TB and MO dyes.

Photocatalytic degradability of TB and stability of the catalyst

TB dye degradation analysis was carried out under control condition, in the presence of La loaded CuO with and without light irradiation, as displayed in Fig. 3. In the absence of UV light, there is no degradation was observed (curve c). The experiment results also gave you an idea about that there was negligible degradation (0.2 %) when the reaction was endorsed to occur in the presence of UV light without any catalyst. Below 1% of dye degradation was obtained with the mixture of dye and La-CuO catalyst in the absence of UV light, it reveals that the adsorption of dye molecule on the surface catalyst (curve b). Almost 100 % degradation was attained in presence La-CuO with UV light at 300 min irradiation (curve a). When bare CuO, and commercial CuO were used as photocatalyst under alike conditions only 82.9 (curve d) and 77.9 (curve e) percentages of degradation was achieved. From the above results shows that La-CuO is highly efficient in TB dye degradation than other prepared and commercial CuO catalysts.

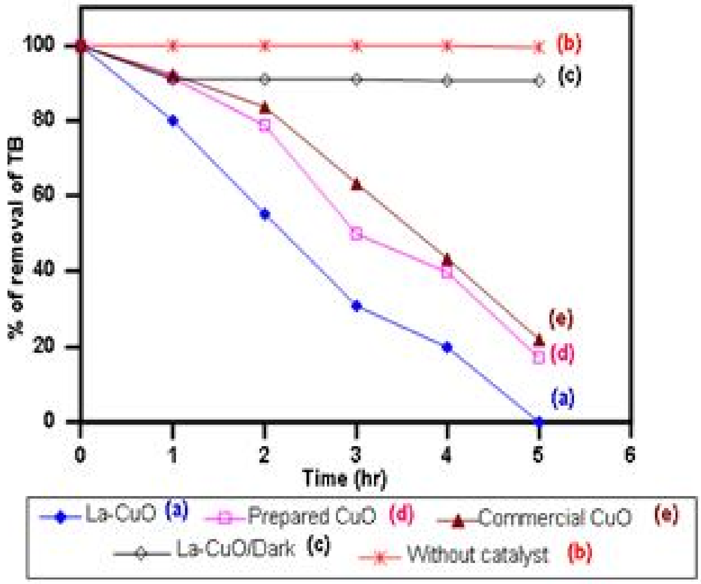

Fig-3: Photodegradability of TB; [TB] = 2×10^{-4} M, catalyst suspended = 1 g L^{-1}, pH = 7, airflow rate = 8.1 mL s^{-1}, $I_{UV} = 1.381 \times 10^{-6}$ einstein L^{-1} s^{-1}

Life time of semiconductor photocatalyst is a most important parameter of the catalytic process because of its use for a lengthy period of time which may leads to a sizeable expense reduction of the treatment. The life time was tested persistently by carrying out the degradation with the used catalyst. The results for three cycles of the catalyst are shown in Fig. 4. Degradation effectiveness at first, second, and third cycles are 100, 98.9 and 96.9% respectively. La-CuO NPs revealed prominent photostability without any noticeable loss of photocatalytic activity even at third cycles. These outcomes indicate that La-CuO catalyst remains more active and reusable.

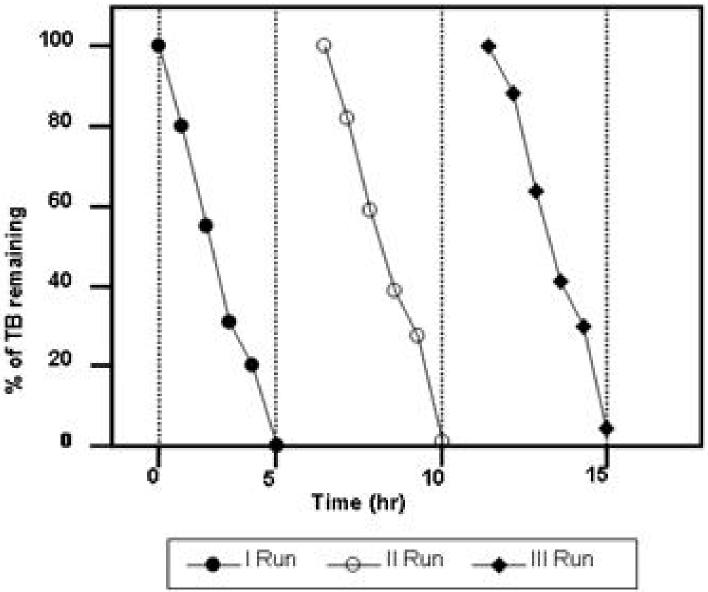

Fig-4: Catalyst reusability, [TB] = 2×10^{-4} M, 1 wt% La-CuO suspended = 1 g L^{-1}, pH = 7, airflow rate = 8.1 mL s^{-1}, $I_{UV} = 1.381 \times 10^{-6}$ einstein L^{-1} s^{-1}

Photocatalytic degradation of MO and stability of the catalyst

After receiving equilibrium in dark, according to the desorption test from the adsorbed sample, approximately 1 % of MO (curve b) was adsorbed. This may be owing to adsorption of the dye on the catalyst surface (Fig. 5). When the reaction was allowed to take place in the presence of UV light without any catalyst only insignificant degradation (0.2 %) was occurred. The colour of the catalysts are the same for both before and after use (not shown here). Curve a indicate that adsorbed dye has been completely degraded. From these clarifications, it shown that the UV light and photocatalyst were highly essential for effective degradation of MO dye. When the both catalyst (bare CuO and commercial CuO) were used under similar conditions only 80.9 (curve d) and 80.6 (curve e) percentages of degradations was resulted, respectively. From the above results, both UV light and catalyst were needed for effective degradation of MO dye than other prepared and commercial catalysts.

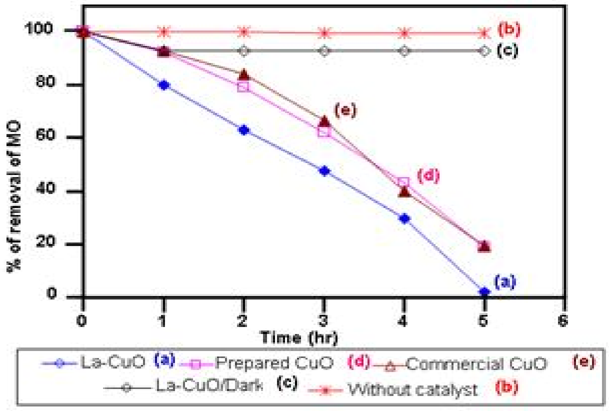

Fig-5: Photodegradability of MO; [MO] = 5 × 10^{-4} M, catalyst suspended = 1 g L^{-1}, pH = 7, airflow rate = 8.1 mL s^{-1}, I_{UV} = 1.381 × 10^{-6} einstein L^{-1} s^{-1}

With the aim of determine the solidity of photocatalyst during the photo catalytic degradation of MO, La-CuO catalyst was used repetitively for 3 runs. The results are displayed in Fig. 6. Almost 91.3% was achieved after 3rd run, it reveals that the prepared catalyst is found to be more stable and reusable.

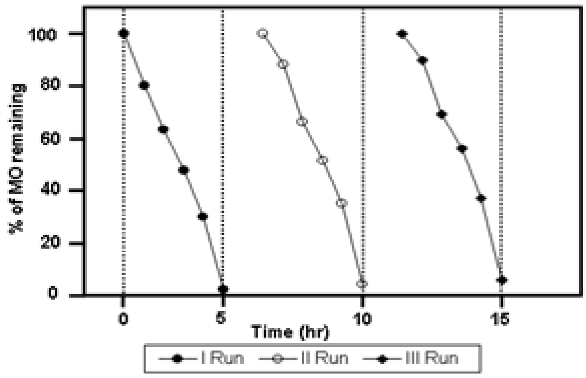

Fig-6: Catalyst reusability, [MO] = 5×10^{-4} M, 1 wt% La-CuO suspended = 1 g L^{-1}, pH = 7, airflow rate = 8.1 mL s^{-1}, I_{UV} = 1.381 × 10^{-6} einstein L^{-1} s^{-1}

UV-visible spectra of the dyes at different time of irradiation

The perceptible changes in the absorbance spectra (200 nm to 700 nm) of TB and MO dyes with La loaded CuO photocatalyst at different time intermissions under UV light irradiation are showed in Fig. 7a and b. The colour of azo dyes, due to the n→π* transition of the -N=N- and hydrazone forms above 400 nm. The peak at 200–400 nm (π→π*) transition owing to the presence of benzene ring, and its lessening the absorption maxima is mainly owing to the degradation of aromatic portion of the dye [3, 8]. The total peaks in dye molecules was decreased in constantly by the reaction time increased up to 300 min. There were no new peaks are showed throughout treatment in the analyzed wavelength range. It's clearly indicated that the aromatic fragment and main chromophores in the original dye solution were overcome in the presence of La-CuO under UV light irradiation. Additionally, the UV spectra also does not shows any intermediate in adsorption spectrum.

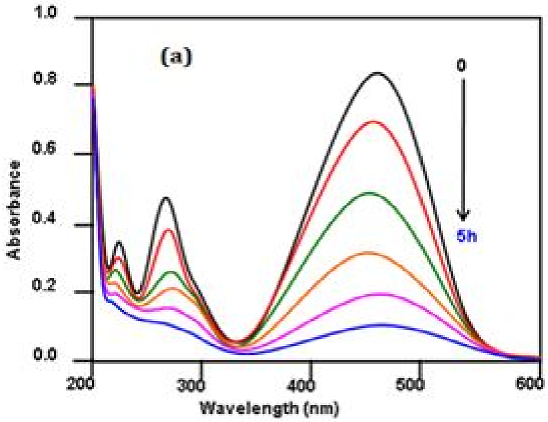

Fig-7a: The changes in UV-vis spectra of TB on irradiation with UV light in the presence La-CuO : [TB] = 2× 10^{-4} M; pH = 7; catalyst suspended = 1 g L^{-1}; airflow rate = 8.1 mL s^{-1}; I_{UV} = 1.381 × 10^{-6} einstein L^{-1} s^{-1}

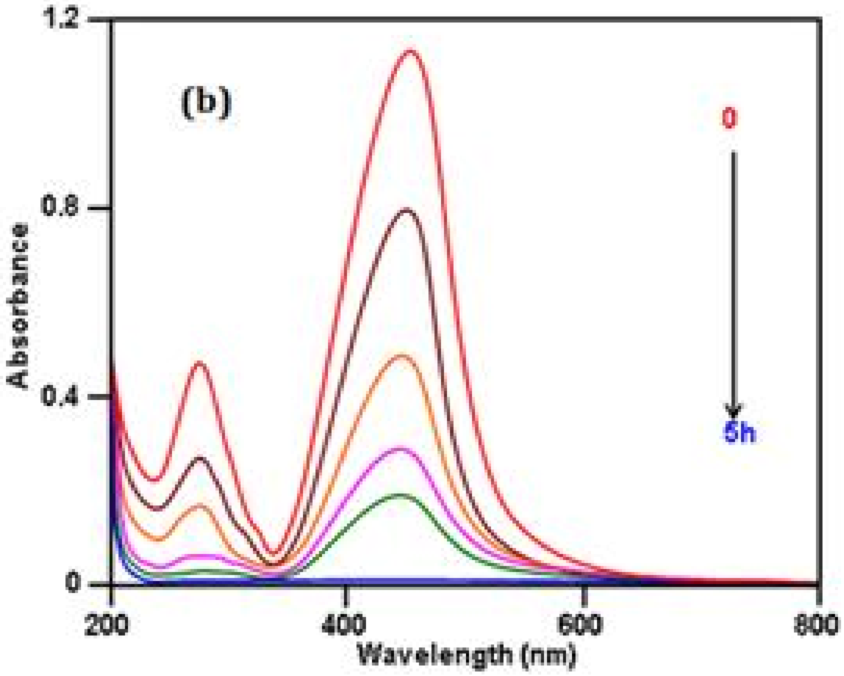

Fig-7b: The changes in UV-vis spectra of MO and TB on irradiation with UV light in the presence La-CuO : [MO] = 5× 10^{-4} M; [TB] = 2× 10^{-4} M; pH = 7; catalyst suspended = 1 g L^{-1}; airflow rate = 8.1 mL s^{-1}; I_{UV} = 1.381 × 10^{-6} einstein $L^{-1}s^{-1}$

COD analysis TB & MO dyes

COD is a significant factor for assessing the concentration of untreated contaminants in water resources. It is an indicative measure of the amount of oxygen that can be consumed by reactions in a measured solution. It is commonly expressed in mass of oxygen consumed over volume of solution which in SI units is milligrams per litre (mg/L) or ppm [8]. The mineralization of these dyes (TB and MO) was accounted by measuring the COD values at various time interval of irradiated solution under suitable UV light source. Table 1, represented the percentages of COD reduction at different times of irradiation. COD reduction were observed for TB dye 98.1% and MO dye 93.4% respectively. It clearly indicates the both dye molecules were complete mineralization takes place.

Table-1: COD measurements of La-CuO NPs

Time (hr)	COD removal (TB)[a]	COD removal (MO)[b]
0	0	0
1	17.9	13.5
3	60.0	56.0
4	98.1	93.4

[a] [TB] = 2 × 10^{-4} M; 1 wt% La-CuO suspended=1 g L^{-1}; pH = 7; airflow rate = 8.1 mL s^{-1}; I_{UV} = 1.381 × 10^{-6} einstein L^{-1} s^{-1}.

[b] [MO] = 5 × 10^{-4} M; 1 wt% La-CuO suspended=1 g L^{-1}; pH = 7; airflow rate = 8.1 mL s^{-1}; I_{UV} = 1.381 × 10^{-6} einstein L^{-1} s^{-1}.

Mechanism of dye degradation

A mechanistic method of the charge separation and catalytic reaction for La-CuO photocatalyst is shown in Scheme 1. The electron from valance band (VB) to conductance band (CB), leave a hole in valance band by the illumination of CuO semiconductor. Generally, the recombination of both electron-holes reduces the catalytic activity of CuO semiconductors. But the presence of ‘La’ it traps the electron from CB of CuO and also reduces, which inhibit the electron-hole recombination. It is well-known that rare earths metals are having extremely electron trapping nature from the conduction band of semiconductor oxide. This fact evidently tells that the enhanced the detoxification by using La-CuO catalyst of both TB and MO dyes under UV light illumination.

ISSN 2394 - 7780

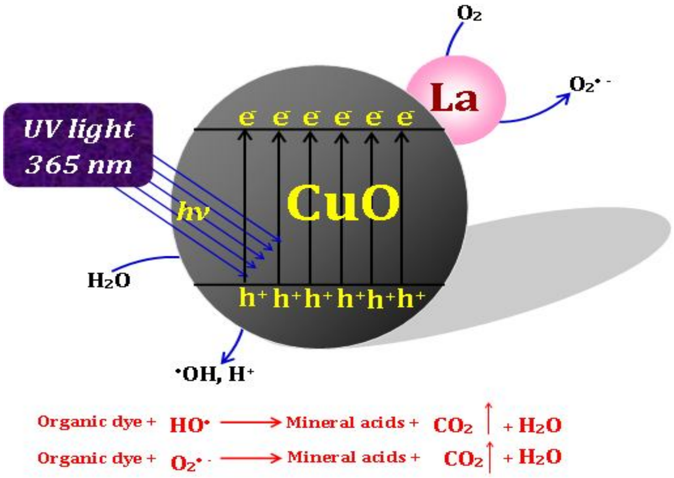

Scheme-1: Mechanism of degradation of dyes by La-CuO NPs

CONCLUSIONS

A fresh La-CuO was synthesized by simple precipitation-decomposition method and characterized by XRD, CV and BET surface area measurements. La-CuO was found to be more competent than bare and commercial CuO for degradation of dyes under UV light illumination. This catalyst was found to be reusable and more stable. COD measurements confirm the almost complete mineralization of the dye molecules. A mechanism is suggested for the higher photocatalytic activity of the La-CuO. This process using La-CuO photocatalytic material would be more useful for industrial effluent treatment due to the advantages of its “Cleanness”, “Low-priced”, “Long term-stability”, and “Tremendous performance”.

REFERENCES

1. Neppolian B, Choi HC, Sakthivel S, Arabindoo B, Murugesan V. (2002) Solar/UV-induced photocatalytic degradation of three commercial textile dyes. Journal of Hazardous Materials, 89(2-3), 303–17..

2. Sin J-C, Lam S-M, Mohamed AR, Lee K-T. (2012) Degrading endocrine isrupting chemicals from wastewater by TiO2 photocatalysis: A review. International Journal of Photoenergy , 185159.

3. B.Subash, B.Krishanakumar, R.Velmurugan, M.Swaminathan and M.Shanthi, Synthesis of Ce co-doped Ag-ZnO Photocatalyst with excellent performance for NBB dye degradation under natural sunlight illumination, catalysis science and technology, 2012, 2, 2319–2326.

4. B.Subash, B.Krishnakumar, V.Pandiyan, M.Swaminathan and M.Shanthi, Synthesis and characterization of novel WO_3 loaded Ag-ZnO and its photocatalytic activity, Materials Research Bulletin, 48 (2013) 63–69.

5. Kundu, P.; Deshpande, P. A.; Madras, G.; Ravishankar, N. Nanoscale ZnO/CdS Heterostructures with Engineered Interfaces for High Photocatalytic Activity under Solar Radiation.J. Mater. Chem. 2011, 21, 4209−4216.

6. B. Subash, B. Krishnakumar, M. Swaminathan and M. Shanthi, Ag_2S-ZnO-An efficient photocatalyst for the mineralization of Acid Black 1 with UV light, Spectrochimica Acta Part A: Molecular and Biomolecular Spectroscopy, 105 (2013) 314–319.

7. Li, Q.; Easter, N. J.; Shang, J. K. As(III) Removal by PalladiumModified Nitrogen-Doped Titanium Oxide Nanoparticle Photocatalyst. Environ. Sci. Technol. 2009, 43, 1534−1539.

8. B. Subash, B. Krishnakumar, M. Swaminathan and M. Shanthi, ZnS-Ag-ZnO as an Excellent UV light active Photocatalyst for the Degradation of AV 7, AB 1, RR 120 and RY 84 Dyes; Synthesis, Characterization and Catalytic Applications, Industrial & Engineering Chemistry Research, 2014, 53, 12953−12963.

9. R.Srivastava, M.U.A.Prathap and R.Kore, Morphologically Controlled Synthesis of Copper Oxides and their Catalytic Applications in the Synthesis of Propargylamine and Oxidative Degradation of Methylene Blue, Colloids and Surfaces A: Physicochemical and Engineering Aspects, 392, 2011, 271–282.

10. K. Hirano, H. Asayama, A. Hoshino, H. Wakatsuki, J. Photochem. Photobiol. A: Chem. 110 (1997) (1996) 307–311.
11. A. Sclafani, J.M. Herrmann, J. Photochem. Photobiol. A: Chem. 113 (1998) 181–188.
12. A. Blazkova, I. Csolleova, V. Brezova, J. Photochem. Photobiol. A: Chem. 113 (1998) 251–256.
13. Etacheri, V.; Roshan, R.; Kumar, V. Mg-Doped ZnO Nanoparticles for Efficient Sunlight-Driven Photocatalysis. ACS Appl. Mater. Interfaces2012, 4, 2717−2725.
14. A. Sclafani, L. Palmisano, G. MarcI and A. M. Venezia, Sol.Energy Mater. Sol. Cells, 1998, 51, 203–219.
15. S. Sakthivel, M. V. Shankar, M. Palanichamy, B. Arabindoo, D. W. Bahnemann and V. Murugesan,Water Res., 2004, 38, 3001–3008.
16. B. Subash, M. Shanthi, Photocatalytic Detoxification of NBB Dye Over Cerium Loaded Ag–ZnO Photocatalyst Under UV-A Light Irradiation, DJ Journal of Engineering Chemistry and Fuel, Vol. 2(1) 2017, 30-40.
17. R. Jayaseelan, M. Gopalakrishnan, Synthesis and Characterization of Virgin and Ag doped CuO: SnO_2 Mixed Composites, DJ Journal of Engineering Chemistry and Fuel, Vol. 2(1) 2017, 10-20
18. C. Karunakaran, J. Jayabharathi, K. Jayamoorthy, P. Vinayagamoorthy, Inhibition of fluorescence enhancement of benzimidazole derivative on doping ZnO with Cu and Ag, J. Photochem. Photobiol. A: 247 (2012) 16-23.
19. Poizot, P., Laruelle, S., Grugeon, S., Dupont, L., Taracon, J.M., 2000. Nano-sized transition-metal oxides as negative-electrode materials for lithium-ion batteries. Nature407, 496–499.
20. M. Enhessaria,M. Shaterian, M. Javad Esfahani, M. Nasser Motaharian, Synthesis, characterization and optical band gap of La_2CuO_4 nanoparticles, Materials Science in Semiconductor Processing 16 (2013) 1517–1520.
21. R.Sasikala, S. Kutti Rani, K. Karthikeyan, D. Easwaramoorthy, and I. Moham med Bilal, Detoxification of Methyl Orange and Trypan Blue Dyes by using Erbium loaded CuO nanoparticles, International Journal of ChemTech Research, 9, 2016, 440-452.
22. R. Sasikala, K. Karthikeyan, D. Easwaramoorthy, I. Mohammed Bilal and S. Kutti Rani, Photocatalytic degradation of trypan blue and methyl orange azo dyes by cerium loaded CuO nanoparticles, Environmental Nanotechnology, Monitoring & Management, (2016).
23. Jingbiao Cui, A Simple Two-Step Electrodeposition of Cu_2O/ZnO Nanopillar Solar Cells, J. Phys. Chem. C2010,114,6408–6412.
24. Sasikala, R., Kutti Rani, S., Easwaramoorthy, D., Karthikeyan, K., 2015. Lanthanum loaded CuO nanoparticles: synthesis and characterization of a recyclable catalyst for the synthesis of 1, 4-disubstituted 1,2,3-triazoles and propargylamines. RSC Adv. 5, 56507–56517.
25. B. Subash, B. Krishnakumar, R. Velmurugan and M. Swaminathan, Photodegradation of an azo dye with reusable SrF_2-TiO_2 under UV light and Influence of operational parameters, Separation and Purification Technology, 101 (2012) 98–106.
26. B. Subash, B. Krishnakumar, V. Pandiyan, M. Swaminathan, M. Shanthi, An efficient nanostructured Ag_2S-ZnO for degradation of Acid Black 1 dye under day light illumination, Separation and Purification Technology, 96 (2012) 204–213.

ELECTROCHEMICAL STUDIES OF LANTHANIDES AND ACTINIDES IN RTIL MEDIUM CONTAINING EXTRACTANTS – A REVIEW

R. Rama
Assistant Professor, Department of Chemistry, School of Basic Sciences, Vels University (VISTAS), Chennai
E-mail: rama.sbs@velsuniv.ac.in

ABSTRACT

Over the past few decades, room temperature ionic liquids (RTILs) are being studied for various applications in the area of nuclear fuel reprocessing and waste management. RTILs have been explored as diluents, extractants and electrolytic medium. Several studies are reported to understand the electrochemical behavior of lanthanides (Lns) and actinides (Ans) in RTIL medium. Moreover, recently, electrochemical behavior of Lns and Ans in the presence of extractants present in the RTIL electrolytic medium is being investigated and it has been explained in this review.

Keywords: Actinides, Lanthanides, Room temperature ionic liquids, Extractant, Electrolytic medium.

1.0 INTRODUCTION

Room temperature ionic liquids (RTILs) which are being considered as “green solvents” have been investigated for several decades. They are composed fully of dissociated ions and their melting points are below 373 K.[1-2] The most commonly used ionic liquids(IL) cations are 1-alkyl-3-methylimidazolium, 1-alkylpyridinium, N-methyl-N-alkylpyrrolidinium, cholinium, phosphonium and ammonium ions etc. and the IL anions are halides, BF_4^-, PF_6^-, sulfonates, triflates, tosylates, phosphates and bis(trifluoromethanesulfonyl)imide (NTf_2^-) etc. In the past few decades, RTILs are explored for the nuclear fuel cycle application. Using RTILs as diluents, various studies on extraction of actinides and lanthanides are reported. [3-9] Similarly, in the recent years, functionalized ionic liquids (FILs) (or task specific ionic liquids (TSILs)) and the ionic liquids with strongly coordinating anion have been studied as extractants for the metal ion separation and mostly high metal ion extraction % was observed in RTIL medium compared to the conventional systems.[10-19]

The concept of using RTILs for non-aqueous reprocessing has evolved in the past few decades and several studies have been reported to understand the electrochemical behavior of actinides and fission products in RTIL electrolytic medium. Moreover, the extraction-electrodeposition (EX-EL) approach for the separation of metal ions using RTIL medium was explored in the recent years. In this approach, some of the attractive properties of RTILs namely the hydrophobicity and wide electrochemical window are exploited and RTILs can be used either as an extractant or as a diluent in conjunction with the molecular extractant for the liquid-liquid extraction of target metal ions from aqueous phase.[20]

In this review, the electrochemical studies of lanthanides (Lns) and actinides (Ans) ions in the presence of extractants dissolved in RTIL electrolytic medium is focused. The structure of RTILs used in these work are given in table 1.

Table-1: Structure of RTILs used in the electrochemical study of Ans and Lns in the presence of extractants

S. No	Name of ionic liquid	Structure of the ionic liquid
1	1-Alkyl-3-methylimidazolium bis(trifluoromethylsulfonyl)imide ($[C_n mim] [NTf_2]$)	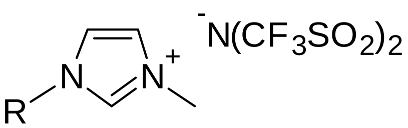 R: butyl/ hexyl
2	1-Alkyl-3-methylimidazolium bromide ($[C_8 mim] [Br]$)	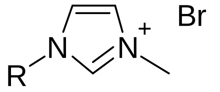 R: Octyl
3	1-Butyl-3-methylpyrrolidinium bis(trifluoromethylsulfonyl)imide ($[C_4 mpy][NTf_2]$)	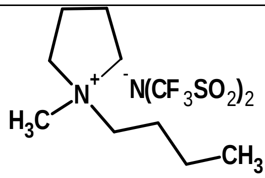

ISSN 2394 - 7780

4	1-octyl-1-methylpiperidinium octylphosphite (Pip18-OP)	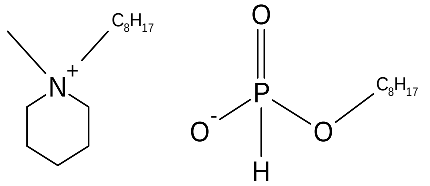
5	1-octyl-1-methylmorpholinium octylphosphite (Mor18-OP)	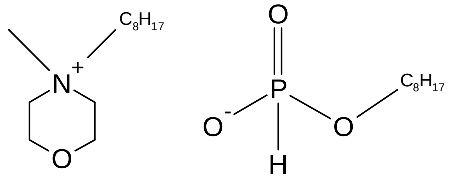
6	1-octyl-1-methylpyrrolidinium octylphosphite (Pyr18- OP).	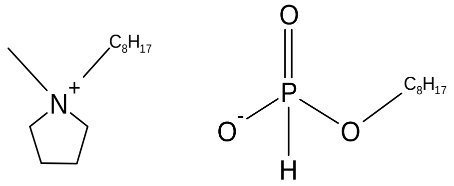
7	Triethyl-pentyl-phosphonium bis(trifluoromethyl-sulfonyl)amide ([P2225][NTf$_2$])	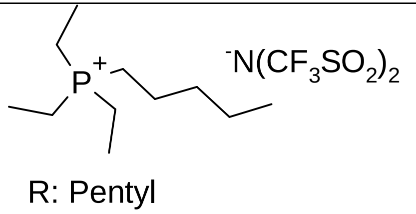

2.0 ELECTROCHEMICAL STUDIES OF LANTHANIDE IONS IN RTIL MEDIUM CONTAINING EXTRACTANTS

Several studies on the electrochemical behaviour of lanthanide ions in RTILs have been reported. In the recent past, some studies have been carried out to understand the electrochemical behaviour of lanthanide ions in RTIL electrolytic medium in the presence of extractants. Hussey *et al.*[21] made an investigation on electrochemistry and electronic absorption spectroscopy of Sm(III), Eu(III), and Yb(III) in RTILs, [C_4mPy][NTf_2]and [$BuMe_3$N[[NTf_2] and also in the RTIL medium containing N,N,N′,N′-tetraoctyl-3-oxo-pentane diamide (TODGA). When TODGA was added to solution containing Ln(III) ion in [C_4mPy][NTf_2], the reduction peak currents for Ln(III) ions decreased . Formation of Ln(III)-TODGA complex is associated with positive change in ΔG and the reduction potential of Ln(III) ion was shifted to more negative potential side in the presence of which in turns indicate that stability constant of Ln(III)-TODGA complex in [C_4mPy][NTf_2] is must be quite large. It was reported that TODGA forms 3:1 complexes with Sm(III) and Eu(III) but Yb(III) ion forms a 2:1 complex . Matsumiya *et al* [22] studied the extraction of Pr(III), Nd(III) and Dy(III) from aqueous phase and also carried out the electrodeposition of the Nd metal from the extracted IL phase, tri *n*-butyl phosphate (TBP) / [P2225][NTf_2] by applying the applied over potential of -3.2 V on the cathode with stirring the electrolyte at 500 rpm. The Nd deposit was analysed by XPS and found that middle layer is metallic state and the top surface is a part of the oxidation state.

Zarrougui *et al.*[23] synthesized the nonfluorinated ionic liquids, namely, 1-octyl-1-methylpiperidinium octylphosphite (Pip18-OP), 1-octyl-1 methylmorpholiniumoctylphosphite (Mor18-OP) and 1-octyl-1-methylpyrrolidinium octylphosphite (Pyr18- OP). Extraction of Nd(III) from nitric acid solutions (0-11M) using these ILs have been reported and Pip18-OP was found to be more efficient than other two IL extractants. Moreover, the cyclic voltammogram of Pip18-OP and Nd(III) complex in Pip18-OP after extraction was recorded. Electro deposition of Neodymium from Pip18-OP IL on copper substrate was carried out by the electrolysis at −2V. Nearly 83% Current efficiency and 48% of Neodymium deposit was obtained. SEM image of Nd deposit indicated that they are small crystallite rods (length : 3–70μm, Diameter: 0.5–30μm).

Rama *et al.* [24] reported the electrochemical behavior of Eu(III) in [C_4mpy][NTf_2] in the presence of HDEHP and HDGA by cyclic voltammetry, chronopotentiometry and chronoamperometry techniques. The addition of HDEHP or HDGA to the Eu(III)/[C_4mpy][NTf_2] solution lowered the cathodic peak current and shifted the cathodic peak potential cathodically due to the co-ordination of Eu(III) with ligands in the ionic liquid medium. In the presence of ligands, the diffusion coefficients and heterogeneous rate constants decreased in the order Eu(III) > (Eu(III) + HDEHP) > (Eu(III) + HDGA) in the ionic liquid. The stability constants (ln K_f) of Eu(III)-HDEHP and Eu(III)- HDGA complexes were found to be 5 and 5.65 respectively.

Similarly, the electrochemical behaviour of Eu(III) in [C_6mim][NTf_2] was studied in the presence of ligands such as tri-*n*-butyl phosphate (TBP) and *N,N*-dihexyloctanamide (DHOA) by cyclic voltammetry .[25] Peak current was lowered and the peak potential shifted cathodically in the presence of ligands, due to the co-ordination of Eu(III) with ligands in ionic liquid phase. The stability constants (ln Kf) of Eu(III) - (DHOA) and Eu(III) - (TBP) complexes in [C_6mim][NTf_2] were found to be 1.6 and 2.09 respectively. Moreover, Prashant *et al.* synthesized ILs by dissolving NTf_2 based rare earth elements (Nd, Dy, Gd and Pr) in trimethyl phosphate (TMP) system and reported the electrodeposition of Nd,Dy,Gd and Pr from IL.[26]

3.0 ELECTROCHEMICAL STUDIES OF ACTINIDE IONS IN RTIL MEDIUM CONTAINING EXTRACTANTS

Extraction of uranium (VI) using TBP in [C_4mim][NTf_2] and also direct electrodeposition as uranium oxide from IL phase was reported by Giridhar *et al.*[27] Uranyl ion in IL pahse undergoes a single step two electron reduction process. Electrodeposition of black coloured U(VI) oxide was obtained by the controlled potential electrolysis at −2.1V (versus Pd). Rama *et al* [28] reported the electrochemical behavior of U(VI) in [C_4mim][NTf_2] electrolytic medium in the presence of tri-*n*-butyl phosphate (TBP) and tri-*n*-octyl phosphate (TOP) ligands. Cathodic wave responsible for the reduction of U(VI) to U(V) shifted cathodically and the peak current lowered in the presence of ligands in [C_4mim][NTf_2] electrolytic medium. The stability constant (ln K_f) of Eu(III) –TBP and Eu(III)-TOP complexes were determined to be 1.6 and 2.09 respectively. The diffusion coefficient of U(VI) and the heterogeneous electron transfer rate constant in [C_4mim][NTf_2] is in the order U(VI) > U(VI) – TBP > U(VI) –TOP.

Electrochemical and extraction behaviour of Pu(IV) in N,N-octyl carbamoyl methyl (2-pyridyl-N-Oxide) sulfide (NOSCO)/ [C_4mim][NTf_2] have been reported by Kavitha *et al* [29] and it was observed that the reduction of Pu(IV) to Pu(III) is quasi reversible. Similarly, the electrochemical behaviour of Np(IV) extracted by carbomyl methyl phosphine oxide (CMPO) in [C_4mim][NTf_2] was studied by Kavitha *et al* [30] and the reduction of NpO^{2+} to NpO_2^{2+} was found to be quasi reversible.

The electrochemical investigation of Np(IV)-TODGA and Np(IV)-DGATSIL-complexes in [C_6mim][NTf_2] [31], Np(IV)- CMPO and Np(IV)-CMPO-TSIL in [C_4mim][NTf_2] [32] and U(VI)-TODGA and U(VI)-DGA TSIL complexes in [C_8mim][Br] was carried out by Sengupta *et al* [33]. The redox reactions of Np was found to be irreversible for Np-DGA-TSIL complex at 298 K but mostly the redox reactions of Np were classified as quasi—reversible. The order of the diffusion coefficients of the Np(IV) complexes at 298 K was found to be TODGA> [DGA-TSIL] and at other temperatures (308 K, 318 K, 328 K) it was in reverse order. Diffusion coffecient was found to be higher for Np(IV)- CMPO-TSIL complex than Np(IV) - CMPO complex at all the studied temperature. Due to the more negative reduction potential of Np(IV) - CMPO complex (-0.884 V) than Np(IV)- CMPO-TSIL complex (-0.778 V), Np(IV) complex with CMPO is believed to be more stable than that with CMPO-TSIL. Similarly, in the case of U(VI)-TODGA and U(VI)-DGA TSIL complexes in [C_8mim][Br], there was less shift in the cathodic peak potential towards less negative potential and marginal shifts of anodic peak potential of U(VI) ion upon complexation with DGA TSIL. Moreover, the reduction potential of U(VI) to U(V) for the U(VI)-DGA TSIL is slightly more than U(VI)-TODGA complex in [C_8mim][Br]. Difffusion coefficient(D) and Heterogeneous rate constant (ks) for the lanthanide and actinide metal ion complexes studied in RTIL electrolytic medium are provided in table 2.

4.0 CONCLUSION

RTILs are being explored for the nonaqueous reprocessing of spent nuclear fuel. There have been increasing research interest to understand the electrochemical behaviour of Lns and Ans in RTIL electrolytic medium in the presence of extractants. Actually, Extraction-electrodeposition (EX-EL) approach using RTIL for the separation of actinides and fission products can provide high separation factor for the target metal ion but few studies have been reported in this aspect and hence some more studies yet to be done to bring a robust technology based on RTIL medium.

Table-2: The diffusion coefficient (D) and heterogeneous rate constant (ks) for the reduction of metal complex in RTIL medium.

S. No	Metal complex/RTIL	T /K	Diffusion coefficient (D) $cm^2\ s^{-1}$	Heterogeneous rate constant (ks) $cm\ s^{-1}$	Ref.
	Eu(III) – HDEHP in [C_4mpy][NTf_2]	343	0.72×10^{-9}	7.2×10^{-5}	[24]
	Eu(III) – HDGA in [C_4mpy][NTf_2]	343	0.39×10^{-9}	2.5×10^{-5}	
	Eu(III) - TBP in [C_6mim][NTf_2]	343	0.83×10^{-7}	$0.13 \times 10\text{-}^{4}$	[25]

	Eu(III) – DHOA in $[C_6mim][NTf_2]$	343	0.22x 10^{-7}	1.04 x 10^{-4}	
	TMP+Pr$(NTf_2)_3$	298	1.14 x 10^{-9}	--	[26]
	TMP+Nd$(NTf_2)_3$	298	4.25 x 10^{-10}	--	
	TMP+Gd$(NTf_2)_3$	298	1.04 x 10^{-10}	--	
	TMP+Dy$(NTf_2)_3$	298	2.20 x 10^{-10}	--	
	U(VI) - TBP in $[C_4mim][NTf_2]$	353	5.4 x 10^{-7}	3.04 x 10^{-4}	[28]
.	U(VI) -TOP in $[C_4mim][NTf_2]$	353	3 x 10^{-7}	1.56 x 10^{-4}	
.	Np(IV)-TODGA in $[C_4mim][NTf_2]$	298	1.25 x 10^{-15}	1.08 x 10^{-3}	[31]
.	Np(IV)-DGA-TSIL in $[C_4mim][NTf_2]$	298	7.51 x 10^{-16}	1.09 x 10^{-5}	
.	Np(IV)-CMPO in $[C_4mim][NTf_2]$	298	5.2 x 10^{-13}	8.04 x 10^{-5}	[32]
.	Np(IV)-CMPO-TSIL in $[C_4mim][NTf_2]$	298	1.08 x 10^{-11}	1.27 x 10^{-3}	
.	U(VI) – TODGA In $[C_8mim][Br]$	298	1.18 x 10^{-10}	--	[33]
.	U(VI) - DGA-TSIL In $[C_8mim][Br]$	298	5.40 x 10^{-11}	--	
.	Pu(IV) + NOSCO in $[C_4mim][NTf_2]$	298	9.38 x 10^{-6}	3.5 x 10^{-4}	[29]

REFERENCES

1. Welton T. (1999). Temperature ionic liquids. Solvents for synthesis and catalysis. *Chemical Reviews,* 99, 2071–2084.

2. Natalia. P.V., & Seddon K.R. (2008). Applications of ionic liquids in the chemical industry, *Chemical Society Reviews,* 37, 123–150.

3. Xie Z.B., Kang H.T., Chen. Z.S., Zhang. S.H. & Le. Z.G. (2016). Liquid–liquid extraction of U (VI) using malonamide in room temperature ionic liquid. *Journal of Radioanalytical and Nuclear Chemistry,* 308, 573-578.

4. Rama. R., Alok Rout, Venkatesan .K.A., Antony. M.P., & Suresh .A. (2016). Comparison in the solvent extraction behavior of uranium (VI) in some trialkyl phosphates in ionic liquid, *Radiochimica Acta,* 104, 865-872

5. Billard. I., Ouadi. A., Jobin. E, Champion. J, Gaillard. C & Georg. S. (2011). Understanding the Extraction Mechanism in Ionic Liquids: $UO_2^{2+/}HNO_3/TBP/C_4mimTf_2N$ as a Case Study, *Solvent Extraction and Ion Exchange*, 29, 577-601.

6. Gaillard. D.C., Boltoeva .M., Billard. I., Georg. S., Mazan. V., Ouadi. A., Ternova. D., & Hennig. C. (2015). Insights into the Mechanism of Extraction of Uranium (VI) from Nitric Acid solution into an Ionic Liquid by using Tri-n- butyl phosphate, *ChemPhysChem.*, 6, 2653-2662.

7. Panja. S., Mohapatra. P.K., Tripathi. S.C., Gandhi. P.M. & Janardan. P. (2012). A highly efficient solvent system containing TODGA in room temperature ionic liquids for actinide extraction, *Separation and Purification Technology,* 96, 289-295.

8. Turanov. A.N., Karandashev. V.K. & Baulin. V.E. (2012). Extraction of lanthanides (III) with N, N′-bis (diphenylphosphinyl-methylcarbonyl) diaza-18-crown-6 in the presence of ionic liquids, *Solvent Extraction and Ion Exchange,* 30, 244-261.

9. Alok Rout, Venkatesan .K.A., Srinivasan. T.G. & Vasudeva Rao. P.R. (2012). Liquid–liquid extraction of Pu(IV), U(VI) and Am(III) using malonamide in room temperature ionic liquid as diluents, *Journal of Hazardous Materials,* 221, 62-67.

10. Alok Rout,. Venkatesan. K.A,. Srinivasan. T.G & Vasudeva Rao. P.R. (2012). Ionic liquid extractants in molecular diluents: Extraction behavior of europium (III) in quarternary ammonium-based ionic liquids*Separation and Purification Technology,* 95, 26-31.

11. Alok Rout, Venkatesan. K.A., Srinivasan. T.G. & Vasudeva Rao. P.R. (2012). Extraction behavior of actinides and fission products in amide functionalized ionic liquid, *Separation and Purification Technology,* 97,164-171.

12. Alok Rout, Venkatesan. K.A., Srinivasan. T.G. & Vasudeva Rao. P.R. (2010). Unusual extraction of plutonium (IV) from uranium (VI) and americium (III) using phosphonate based task specific ionic liquid, *Radiochimica Acta,* 98, 459-466.

13. Rama. R., Alok Rout, Venkatesan. K.A. & Antony. M.P. (2017). A novel phosphoramide task specific ionic liquid for the selective separation of plutonium (IV) from other actinides, *Separation and Purification Technology,* 172, 7-15.
14. Sengupta. A., Mohapatra. P.K.. Iqbal. M.,. Huskens. J & Verboom. W.A. (2013). Diglycolamide-functionalized task specific ionic liquid (TSIL) for actinide extraction: solvent extraction, thermodynamics and radiolytic stability studies, *Separation and Purification Technology,* 118, 264-270.
15. Mohapatra. P.K., Kandwal. P., Iqbal .M., Huskens. J., Murali . M.S. & Verboom. W.A. (2013). novel CMPO-functionalized task specific ionic liquid: synthesis, extraction and spectroscopic investigations of actinide and lanthanide complexes, *Dalton Transactions,* 42, 4343-4347.
16. Paramanik. M., Raut .D.R., Sengupta. A., Ghosh. S.K. & Mohapatra. P.K. (2016). A trialkyl phosphine oxide functionalized task specific ionic liquid for actinide ion complexation: extraction and spectroscopic studies, *RSC Advances,* 6, 19763-19767.
17. Vicente. J.A., Mlonka. A., Gunaratne. H.N., Swadzba Kwasny. M. & Nockemann. P. (2012). Phosphine oxide functionalised imidazolium ionic liquids as tuneable ligands for lanthanide complexation. *Chemical Communications*, 48, 6115-6117.
18. Rout. A., Venkatesan. K.A., Srinivasan. T.G. & Vasudeva Rao. P.R. (2013). Tuning the extractive properties of Purex solvent using room temperature ionic liquid, *Separation Science and Technology,* 8, 2576-2581.
19. Wang. J., Zhao. J., Feng. D., Kang. X., Sun. Y., Zhao. L.and Liang. H. (2016). Enhancing extraction ability by rational design of phosphoryl functionalized ionic liquids and mechanistic investigation on neodymium (III) extraction, *Journal of Rare Earths,* 34, 83-90.
20. Venkatesan. K.A., Srinivasan. T.G. & Vasudeva Rao. P.R. (2009). A review on the electrochemical applications of room temperature ionic liquids in nuclear fuel cycle. *Separation Science and Technology,* 10, 1_R1-1_R6.
21. Pan. Y.and Hussey. C.L. (2013). Electrochemical & Spectroscopic Investigation of Ln^{3+} (Ln= Sm, Eu, and Yb) Solvation in Bis (trifluoromethylsulfonyl) imide-Based Ionic Liquids and Coordination by N, N, N′, N′-Tetraoctyl-3-oxa-pentane Diamide (TODGA) and Chloride, *Inorganic chemistry*, 52, 3241-3252.
22. Matsumiya. M., Kikuchi. Y., Yamada .T. & Kawakami. S. (2014). Extraction of rare earth ions by tri-n-butylphosphate/phosphonium ionic liquids and the feasibility of recovery by direct electrodeposition, *Separation and Purification Technology*, 130, 91-101.
23. Zarrougui .R., Mdimagh. R., and Raouafi. N. (2017). Highly efficient and eco-friendly extraction of neodymium using, undiluted and non-fluorinated ionic liquids. Direct electrochemical metal separation, *Separation and Purification Technology*, 175, 87-98.
24. Rama .R., Alok Rout, Venkatesan .K. A. & Antony. M. P (2016). Voltammetric Studies on the Complexing Behavior of Eu (III) with Acidic Extractants in 1-Butyl-1-methylpyrrolidinium Bis (trifluoromethanesulfonyl) imide, *Journal of The Electrochemical Society,* 163, H1113-H1121.
25. Rama. R., Alok Rout, Venkatesan. K.A., Antony. M.P., & Vasudeva Rao. P.R. (2015). Electrochemical behavior of Eu (III) in imidazolium ionic liquid containing tri-n-butyl phosphate and N, N-dihexyloctanamide ligands, *Journal of Electroanalytical Chemistry*, 757, 36-43.
26. Bagri .P., Luo. H., Popovs. I., Thapaliya. B.P., DehaudtJ. & Dai. S. (2018). Trimethyl phosphate based neutral ligand room temperature ionic liquids for electrodeposition of rare earth elements, *Electrochemistry Communications*, 96, 88-92.
27. Giridhar. P., Venkatesan .K.A., Srinivasan. T.G. & Vasudeva Rao. P.R. (2008). Extraction of Uranium (VI) by 1.1 M Tri-n-butylphosphate/onic liquid and the feasibility of recovery by direct electrodeposition from organic phase, *Journal of Alloys and Compounds*, 448,104–108.
28. Rama .R., Alok Rout, Venkatesan. K.A. & Antony. M.P. (2016)., Effect of alkyl chain length of tri-n-alkyl phosphate extractants on the electrochemical behaviour of U (VI) in ionic liquid medium, *Journal of Electroanalytical Chemistry,* 771, 87-93.
29. Jayachandran .K., Gupta. R., Vats. B.G., & Kannan. S. (2018)., Extraction & electrochemical investigations of Pu (IV) employing green solvent system containing new bifunctional ligand and Bmim [NTf_2] ionic liquid, *Journal of Radioanalytical and Nuclear Chemistry*, 318, 1009-1014.

30. Jayachandran. K., Gupta. R., Sundararajan. M., Gupta. S.K., Mohapatra. M. & Mukerjee S.K. (2016). Redox and Photophysical Behaviour of Complexes of NpO2+ Ions with Carbomyl methyl phosphine oxide in 1-Hexyl-3-methylimidazolium bis (trifluoromethylsulfonyl) imide Ionic Liquid, *Electrochimica Acta*, 224, 269-277.

31. Sengupta. A., Murali. M.S., Mohapatra. P.K., Iqbal. M., Huskens. J. & Verboom. W. (2015).Extracted species of Np (IV) complex with diglycolamide functionalized task specific ionic liquid: diffusion, kinetics and thermodynamics by cyclic voltammetry, *Journal of Radioanalytical and Nuclear Chemistry*, 304, 563-570.

32. Sengupta. A., Murali .M.S., Mohapatra. P.K., Iqbal. M, Huskens. J & Verboom. W. (2015). Np (IV) complex with task-specific ionic liquid based on CMPO: first cyclic voltammetric study, MonatshChem. *Monatshefte für Chemie*, 146, 1815-1821.

33. Sengupta. A, Murali M.S., Mohapatra P.K, Iqbal M, Jurriaan Huskens & Willem Verboom, An insight into the complexation of UO_2^{2+} with diglycolamide-functionalized task specific ionic liquid , *Polyhedron*, 10.1016/j.poly.2015.09.070.

International Journal of Advance and Innovative Research
Volume 6, Issue 1 (VI): January - March, 2019

ISSN 2394 - 7780

ONE POT SYNTHESIS OF PROPARGYLAMINES DERIVATIVES USING ERBIUM LOADED COPPER OXIDE NANOPARTICLES

R. Sasikala[1], B. Subash[2] and S. Kutti Rani[3]
Department of Chemistry[1], Vels Institute of Science, Technology and Advanced Studies, Chennai
Department of Chemistry[2], St. Joseph's College of Engineering, Chennai
Department of Chemistry[3], B. S. Abdur Rahman University, Chennai
E-mail: sasiram.sbs@velsuniv.ac.in

ABSTRACT

The Erbium loaded CuO nanoparticles (Er-CuO NPs) were prepared by thermal decomposition method. The prepared Er-CuO NPs was used as catalyst for the synthesis of propargylamines via three-component coupling reaction of aldehydes, alkynes and amines under ultrasonication. One-pot operation, atom-economical nature, regioselectivity and good yields are the significant features of this protocol. The reusability of the prepared nanocatalyst was successfully examined six times without any appreciable loss in catalytic activity.

Keywords: Coupling reaction, Erbium loaded CuO nanoparticles, Reusability, Ultrasonication.

INTRODUCTION

The copper catalyzed coupling reaction has made a great impact on biological, industrial and synthetic applications [1]. To achieve this type of reaction, commercially available Cu(I) salts are used and Cu(I) species are generated in situ from Cu(II) salts in the homogeneous conditions [2]. Drawback of this catalytic system are low yield and high catalyst loading. Therefore, low cost, highly efficient and ecofriendly reaction protocols using CuO NPs were introduced.

Recent research in this area has concentrated on heterogeneous catalytic systems, which have several advantages, such as faster and simpler isolation of the reaction products by filtration, as well as recovery and recycling of the catalyst systems. Furthermore, Propargylamines are important intermediates for the synthesis of natural products and nitrogen containing biologically active compounds [3]. Recently, propargylamines are prepared by transition metal-catalyzed A^3coupling reactions of aldehydes, alkynes and amines. A^3coupling reactions is an alternative atom-economical method to synthesize propargylamines by catalytic C-H activation, where water is only the theoretical by-product [4]. The alkyne C-H bond can be activated by employing different transition metal catalysts such as gold complexes [5], silver [6], zinc [7], iron [8], indium [9], iridium [10], Mercury[11]. But among these the most employed catalyst was copper.

Currently, nanoparticles are considered as heterogeneous catalysts which have high surface-to-volume ratio, enhanced activity and selectivity. They could be a competitive alternative to traditional catalysts [208, 209]. Several heterogeneous systems such as Ag(I) [12], and Cu(I) [13], silica-immobilized CuI [14], Cu(0)-nanoparticles on montmorillonite [15], copper ferrite nanoparticles [16], CuNPs/MagSilica [17], Au-SBA [18], impregnated Copper on magnetite [19], Copper–zeolites [20], Fe_3O_4 nanoparticles [21], nano size Co_3O_4 [22] and Au (III) [23] have been developed for synthesis of propargylamines through A^3 coupling.

New research has been focused on finding new catalysts to improve the efficiency of these azide-alkyne cycloaddition and A^3 coupling reactions [24, 25]. As the above mentioned methods are not compatible with heat sensitive substrates and there is a need to develop an effective synthesis of propargylamines employing more eco-friendly catalyst. In this view, we desire to describe a heterogeneous Erbium loaded CuO-catalyzed for the synthesis of 1, 4-disubstituted-1, 2, 3-triazole and propargylamine derivatives under ultrasonication.

EXPERIMENTAL

All chemicals were obtained from Sigma-Aldrich Company and used as received. All the solvents and aldehydes were used after distillation. Melting points were measured on Guna melting point apparatus and are uncorrected. NMR spectra were obtained on a Bruker Avance 400 NMR Spectrometer (^{1}H NMR: 400 MHz; ^{13}C NMR: 100 MHz). Analytical TLC was carried out with Merck plates precoated with silica gel 60 F_{254} (0.25 mm thick).

General procedure for the synthesis of propargylamine derivatives (4a-j):

In a 25 mL glass vial, a mixture of benzaldehydes **1a-j** (1mmol), amine **2a, 5b** (1.2 mmol), phenylacetylene **3** (1.5 mmol) and Er-CuO NPs (10 mg) in 5mL toluene, were sonicated for 30 min. The progress of the reaction was monitored by TLC (20% ethyl acetate/hexane). After completion of the reaction, the catalyst was removed by centrifugation. The reaction mixture was extracted with ethyl acetate (3×10 mL). The combined organic phases were dried with Na_2SO_4, filtered, concentrated, and the residue was purified by flash chromatography on silica gel (elutant: hexane/ethyl acetate, 3:1, v/v).

RESULTS AND DISCUSSION

The catalytic activity of the Er-CuO NPs was examined in the synthesis of propargylamines, the reaction of benzaldehyde, morpholine and phenylacetylene were examined and the results are presented in Table 1. Among the various solvents and solvent/co-solvent mixtures, toluene was found to be the most effective medium for this transformation (Table 1, entry 7). After finding the best solvent, amount of catalyst (Table 1, entry 8-11) was optimized. The highest yield of propargylamines was achieved when 10 mg catalyst in toluene was used (Table 1, entry 7). The low yield was obtained when the bare CuO NPs used as catalyst (Table 1, entry 12) and it clearly demonstrates the effect of Er-CuO NPs in this reaction.

Table-1: Effect of solvent on A^3 coupling reaction.

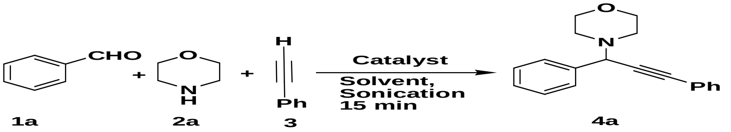

Entry	Catalyst (mg)	Solvent	Yield (%)[a]
1	Er-CuO (10)	Water	43
2	Er-CuO (10)	Ethanol	39
3	Er-CuO (10)	Methanol	47
4	Er-CuO (10)	DCM	38
5	Er-CuO (10)	DMF	30
6	Er-CuO (10)	CH_3CN	62
7	**Er-CuO (10)**	**Toluene**	**98**
8	Er-CuO (3)	Toluene	95
9	Er-CuO (7.5)	Toluene	96
10	Er-CuO (15)	Toluene	97
11	Er-CuO (30)	Toluene	96
12	CuO (10)	Toluene	68

[a] Isolated yield
[b] reaction time 1h

The scope of this Er-CuO NPs catalyzed A^3 coupling was further expanded with a variety of aldehydes and amines and these results were summarized in Table 2. The reactions proceeded well to obtain products in encouraging yields. Electron donating substituents like methyl, as well as methoxy group at para position (Table 2, entries 2,3 and 7,8) and electron withdrawing chlorine and bromine atom at the para position of aldehyde (Table 2, entries 4,5 and 9,10) did not induce appreciable changes in the reaction efficiency. In the presence of NO_2 group at para position of the aldehyde no product was isolated. (Table 2, entry 6).

Table-2: Substrate scope of different aldehydes and amines

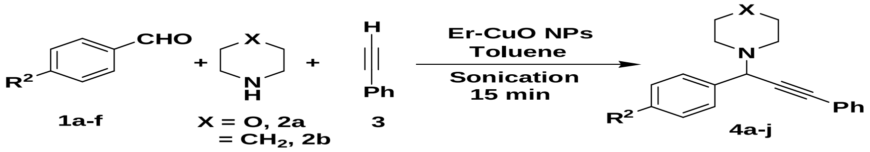

Entry	Aldehyde, R^2	Amine	Product	Yield[a] (%)
1	H, **1a**	**2a**	**4a**	96
2	CH_3, **1b**	**2a**	**4b**	88
3	OCH_3, **1c**	**2a**	**4c**	89
4	Br, **1d**	**2a**	**4d**	91
5	Cl, **1e**	**2a**	**4e**	90
6	NO_2, **1f**	**2a**	**4f**	-[b]
7	**1b**	**2b**	**4g**	94
8	**1c**	**2b**	**4h**	87
9	**1d**	**2b**	**4i**	90
10	**1e**	**2b**	**4j**	86

[a] Isolated yield.
[b] No reaction.

Proposed mechanism for the synthesis of Propargylamines

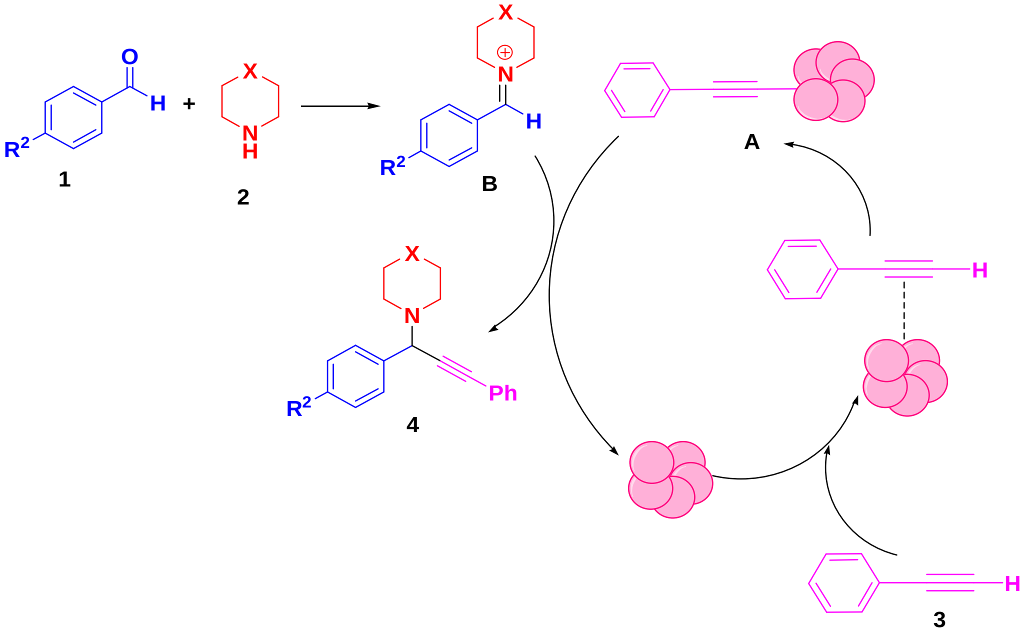

Scheme-1: Tentative mechanism of A^3 coupling reaction using Er-CuO nano catalyst.

A tentative mechanism (Scheme 1) is proposed for the probable sequence of events involving the activation of the C-H bond of alkyne (1) by Er-CuO NPs. The Cu-acetylide intermediate (A) generated by the reaction of acetylene and Er-CuO reacts with iminium ion (B), formed in situ by condensation of aldehyde with secondary amine to afford desired propargylamines (4), and the catalyst is generated.

Spectral data of one-pot synthesis of Propargylamines

4-(1,3-diphenylprop-2-yn-1-yl)morpholine (4a)(Fig.1a&b) [26] **:** Viscous liquid; ^{1}H NMR (400 MHZ, $CDCl_3$): δ_H 7.64-7.62 (m, 2H), 7.53-7.50 (m, 2H), 7.39-7.24 (m, 6H), 4.79 (s, 1H), 3.78-3.69 (m, 4H), 2.64-2.62 (m, 4H); ^{13}C NMR (100 MHz, $CDCl_3$): δc 137.8, 131.8, 128.6, 128.3, 128.28, 128.2, 127.8, 123.0, 88.5, 85.1, 67.2, 62.1, 49.9.

4-(3-phenyl)-1-(p-tolyl)prop-2-yn-1-yl)morpholine (4b) [27]**:** Viscous liquid; ^{1}H NMR (400 MHZ, $CDCl_3$): δ_H 7.32-7.30 (m, 4H), 7.23-7.21 (m, 3H), 7.17 (d, J = 8.0 Hz, 2H), 4.74 (s, 1H), 3.74-3.72 (m, 4H), 2.63-2.61 (m, 4H), 2.35 (s, 3H); ^{13}C NMR (100 MHz, $CDCl_3$): δc 137.5, 134.9, 131.8, 128.9, 128.6, 128.3, 128.2, 123.1, 88.3, 85.4, 67.2, 61.8, 49.9, 21.2.

4-(1-(4-methoxyphenyl)-3-phenylprop-2-yn-1-yl)morpholine (4c) [28]**:** Viscous liquid; ^{1}H NMR (400 MHZ, $CDCl_3$): δ_H 7.51-7.49 (m, 4H), 7.33-7.31(m, 3H), 6.91-6.89 (m, 2H), 4.73(s, 1H) 3.81 (s, 3H), 3.74-3.71 (m, 4H), 2.63-2.59 (m, 4H); ^{13}C NMR (100 MHz, $CDCl_3$): δc 171.1, 159.2, 131.8, 129.9, 129.7, 128.3, 123.0, 113.6, 88.3, 85.4, 67.2, 61.5, 55.3, 49.8.

4-(1-(4-bromophenyl)-3-phenylprop-2-yn-1-yl)morpholine (4d) [28]**:** Viscous liquid; ^{1}H NMR (400 MHZ, $CDCl_3$): δ_H 7.53-7.47 (m, 6H), 7.34-7.32 (m, 3H), 4.74 (s, 1H), 3.76-3.68 (m. 4H), 2.62-2.59 (m, 4H); ^{13}C NMR (100 MHz, $CDCl_3$): δc 137.0, 131.8, 131.4, 130.3, 128.5, 128.4, 122.7, 121.8, 88.9, 84.3, 67.1, 61.5, 49.8.

4-(1-(4-chlorophenyl)-3-phenylprop-2-yn-1-yl)morpholine (4e) [29]**:** Viscous liquid; ^{1}H NMR (400 MHZ, $CDCl_3$): δ_H 7.50 (d, J = 8.4 Hz, 2H), 7.44-7.41 (m, 2H), 7.26-7.24 (m, 5H), 4.67(s, 1H) 3.66-3.64 (m, 4H), 2.54-2.51 (m, 4H); ^{13}C NMR (100 MHz, $CDCl_3$): δc 136.5, 133.6, 131.8, 129.9, 128.4, 128.4, 122.7, 88.9, 84.4, 67.1, 61.4, 49.8.

1-(3-phenyl-1-(p-tolyl)prop-2-yn-1-yl)piperidine (4g) [30]**:** Viscous liquid; ^{1}H NMR (400 MHZ, $CDCl_3$): δ_H 7.51-7.49 (m, 4H), 7.31-7.30 (m, 3H), 7.17-7.15 (m, 2H), 4.75 (s, 1H), 2.60-2.52 (m, 4H), 2.35 (s, 3H) 1.62-1.53 (m, 4H), 1.44-1.42 (m, 2H); ^{13}C NMR (100 MHz, $CDCl_3$): δc 137.1, 135.6, 131.8, 128.8, 128.5, 128.3, 128.0, 123.5, 87.6, 86.4, 62.2, 50.7, 26.2, 24.5, 21.2.

1-(1-(4-methoxyphenyl)-3-phenylprop-2-yn-1-yl)piperidine (4h) [31] **:** Viscous liquid; ^{1}H NMR (400 MHZ, $CDCl_3$): δ_H 7.54-7.49 (m, 4H), 7.32-7.30 (m, 3H), 6.88 (d, J = 7.6 Hz, 2H), 4.78 (s, 1H), 3.80 (s, 3H), 2.59-2.57 (m, 4H), 1.65-1.54 (m, 4H), 1.44-1.42 (m, 2H); ^{13}C NMR (100 MHz, $CDCl_3$): δc 159.1 132.0, 131.8, 129.8, 128.3, 128.1, 114.3, 113.4, 87.7, 86.2, 61.7, 55.3, 50.5, 26.0, 24.4.

1-(1-(4-bromophenyl)-3-phenylprop-2-yn-1-yl)piperidine (4i) [32] **:** Viscous liquid; ^{1}H NMR (400 MHZ, $CDCl_3$): δ_H 7.53-7.48 (m, 6H), 7.45-7.32 (m, 3H), 4.73 (s, 1H), 2.54-2.51 (m, 4H), 1-62-1.57 (m, 4H), 1.45-1.44 (m, 2H); ^{13}C NMR (100 MHz, $CDCl_3$): δc 137.9, 132.5, 131.9, 131.2, 130.2, 128.5, 123.1, 121.4, 88.3, 85.3, 61.8, 50.7, 26.2, 24.4.

1-(1-(4-chlorophenyl)-3-phenylprop-2-yn-1-yl)piperidine (4j) [33] **:** Viscous liquid; ^{1}H NMR (400 MHZ, $CDCl_3$): δ_H 7.51 (d, J = 7.6 Hz, 2H), 7.44-7.42 (m, 2H), 7.26-7.23 (m, 5H), 4.69 (s, 1H), 2.49-2.43 (m, 4H), 1.55-1.49 (m, 4H), 1.38-1.34 (m, 2H); ^{13}C NMR (100 MHz, $CDCl_3$): δc 137.4, 133.3, 131.9, 129.9, 128.7, 128.3, 123.2, 121.6, 88.4, 85.5, 61.9, 50.8, 26.3, 24.5.

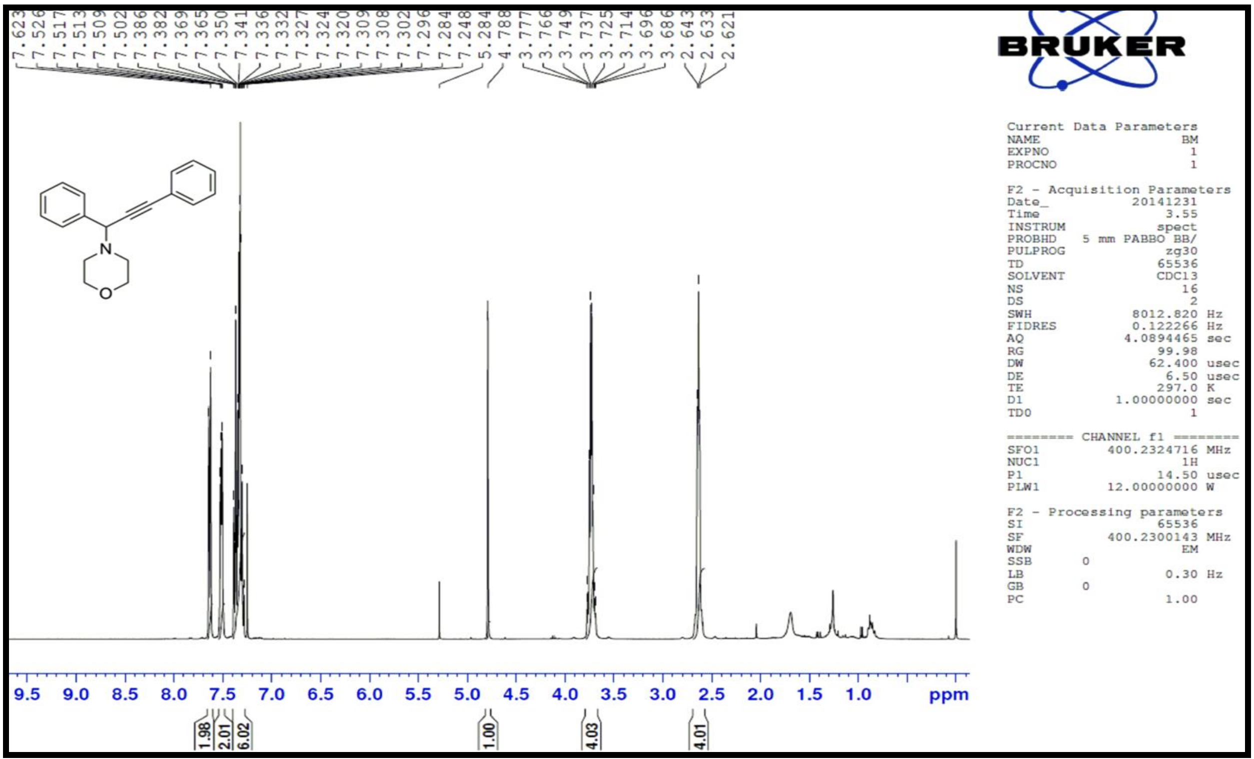

```
Current Data Parameters
NAME                     BM
EXPNO                     1
PROCNO                    1

F2 - Acquisition Parameters
Date_              20141231
Time                   3.55
INSTRUM               spect
PROBHD   5 mm PABBO BB/
PULPROG                zg30
TD                    65536
SOLVENT               CDC13
NS                       16
DS                        2
SWH                8012.820 Hz
FIDRES             0.122266 Hz
AQ                4.0894465 sec
RG                    99.98
DW                   62.400 usec
DE                     6.50 usec
TE                    297.0 K
D1               1.00000000 sec
TD0                       1

======== CHANNEL f1 ========
SFO1            400.2324716 MHz
NUC1                     1H
P1                    14.50 usec
PLW1            12.00000000 W

F2 - Processing parameters
SI                    65536
SF              400.2300143 MHz
WDW                      EM
SSB      0
LB                     0.30 Hz
GB       0
PC                     1.00
```

Fig-1a: ^{1}H NMR spectrum of compound 4a

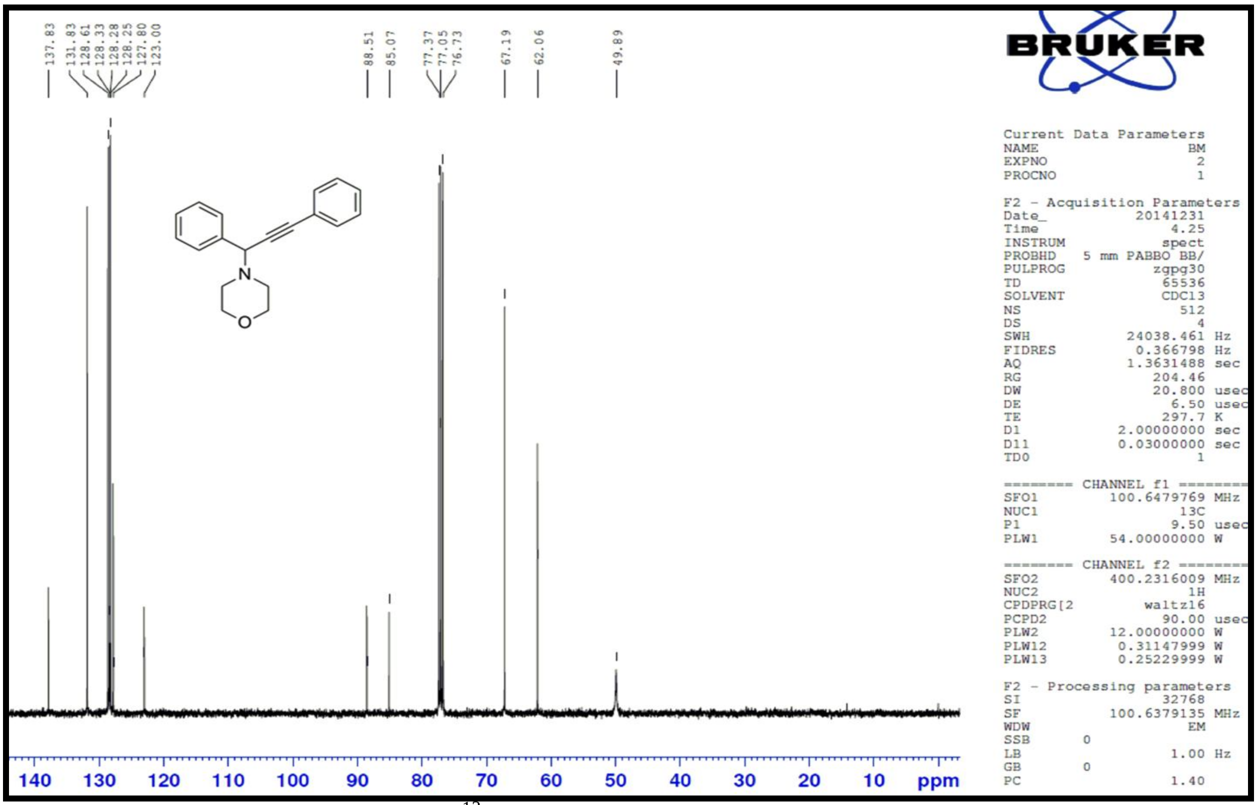

```
Current Data Parameters
NAME                     BM
EXPNO                     2
PROCNO                    1

F2 - Acquisition Parameters
Date_              20141231
Time                   4.25
INSTRUM               spect
PROBHD   5 mm PABBO BB/
PULPROG              zgpg30
TD                    65536
SOLVENT               CDC13
NS                      512
DS                        4
SWH               24038.461 Hz
FIDRES             0.366798 Hz
AQ                1.3631488 sec
RG                   204.46
DW                   20.800 usec
DE                     6.50 usec
TE                    297.7 K
D1               2.00000000 sec
D11              0.03000000 sec
TD0                       1

======== CHANNEL f1 ========
SFO1            100.6479769 MHz
NUC1                    13C
P1                     9.50 usec
PLW1            54.00000000 W

======== CHANNEL f2 ========
SFO2            400.2316009 MHz
NUC2                     1H
CPDPRG[2           waltz16
PCPD2                 90.00 usec
PLW2            12.00000000 W
PLW12            0.31147999 W
PLW13            0.25229999 W

F2 - Processing parameters
SI                    32768
SF              100.6379135 MHz
WDW                      EM
SSB      0
LB                     1.00 Hz
GB       0
PC                     1.40
```

Fig-1b: ^{13}C NMR spectrum of compound 4a

CONCLUSIONS

We have developed an efficient Er loaded CuO nanoparticles as heterogeneous catalyst for the synthesis of propargyl amine by A^3 coupling reaction of aldehyde, secondary amine and terminal alkynes under ultrasonic irradiation. In this method, the catalyst was collected easily by filtration and the reusability of the prepared nanocatalyst was successfully examined over six times and was found to be effective with only a very slight loss of catalytic activity. This protocol is a clean and safe process, and can be used to generate a diverse range of product in good to excellent yields.

RERERENCES

1. Perez-Balderas F, Ortega-Munoz M, Morales-Sanfrutos J, Hernández-Mateo F, Calvo-Flores F.G, Calvo-Asin J.A, Isac- Garcia J, Santoyo-Gonzalez F, “Multivalent Neoglycoconjugates by Regiospecific Cycloaddition of Alkynes and Azides Using Organic-Soluble Copper Catalysts”, Org. Lett., Vol. 5, pp. 1951-1954, 2003.
2. Xu L, Sithambaram S, Zhang Y, Chen C-h, Jin L, Joesten R, “Novel urchin-like CuO synthesized by a facile reflux method with efficient olefin epoxidation catalytic performance”, Chem. Mater.,Vol. 21, pp. 1253–9, 2009.
3. (a) E-S. Lee, H.-S. Yeom, J-H. Hwang and S. Shin, *Eur. J. Org.Chem*., 2007, 3503-3507; (b) B. Jiang and M. Xu, *Angew. Chem. Int. Ed*., 2004, **43**, 2543-2546.
4. Wei C.M, Li C.J, “Enantioselective direct-addition of terminal alkynes to imines catalyzed by copper (I) pybox complex in water and in toluene”, J. Am. Chem. Soc., Vol. 124, pp. 5638–5639, 2002.
5. Lo V.K.Y, Liu, Y.G, Wong M.K, Che C.-M, “Gold (III) salen complex-catalyzed synthesis of propargylamines via a three-component coupling reaction”, Org. Lett., Vol. 8, pp. 1529–1532, 2006.
6. Ji J.X, Au-Yeung T.T.L, Wu J, Yip C.W, Chan A.S.C, “Efficient synthesis of alkynyl a-amino acid derivatives by Ag (I)-catalyzed alkynylation of a-imino esters”, Adv. Synth. Catal., Vol. 346, pp 42–44, 2004.
7. Fischer C, Carreira E.M, “Zn-alkynylide additions to acyl iminiums”, Org. Lett., Vol. 6 pp. 1497–1499, 2004.
8. Chen W.W, Nguyen R.V, Li C.-J, “Iron-catalyzed three-component coupling of aldehyde, alkyne, and amine under neat conditions in air”, Tetrahedron Lett., Vol. 50, pp. 2895–2898, 2009.
9. Zhang Y.C, Li P.H, Wang M, Wang L, “Indium-catalyzed highly efficient threecomponent coupling of aldehyde, alkyne, and amine via C–H bond activation”, J. Org. Chem., Vol. 74, pp. 4364–4367, 2009.
10. Fischer C, Carreira E.M, “Direct addition of TMS-acetylene to aldimines catalyzed by a simple, commercially available Ir (I) complex”, Org. Lett., Vol. 3 pp. 4319–4321, 2001.
11. Li P.H, Wang L, “Mercurous chloride catalyzed Mannich condensation of terminal alkynes with secondary amines and aldehydes”, Chin. J. Chem., Vol. 23, pp. 1076–1080, 2005.
12. Li Z, Wei C, Chen L, Varma R.S. Li C.J, “Three component coupling of aldehyde, alkyne and ammine catalyst by silver in ionic liquid”, Tetrahedron Lett., Vol. 45, pp. 2443–2446, 2004.
13. Park S.B, Alper H, “An efficient synthesis of propargylamines *via* C–H activation catalyzed by copper(I) in ionic liquids”, Chem. Commun., pp. 1315–1317, 2005.
14. Likhar P.R, Roy S, Roy M, Subhas M.S, De M.L, Kantam R.L, “Silica-Immobilized CuI: An Efficient Reusable Catalyst for Three-Component Coupling Reaction of Aldehyde, Amine and Alkyne”, Synlett,, pp. 2301–2303, 2007.
15. Borah B.J, Borah S.J, Saikia L, Dutta D.K, “Efficient three-component coupling reactions catalyzed by CuO-nanoparticles stabilized on modified montmorillonite”, Catal. Sci. Technol., Vol. 4, pp. 1047–1054, 2014.
16. Kantam M.L, Yadav J, Laha S, Jha S, “Synthesis of Propargylamines by Three-Component Coupling of Aldehydes, Amines and Alkynes Catalyzed by Magnetically Separable Copper Ferrite Nanoparticles”, Synlett, Vol. 40, pp. 1791–1794, 2009.
17. Nador F, Volpe M. A, Alonso F, Feldhoff A, Kirschning A, Radivo G, “Copper nanoparticles supported on silica coated maghemite as versatile, magnetically recoverable and reusable catalyst for alkyne coupling and cycloaddition reactions”, Appl. Catal., A, Vol. 455, pp. 39–45, 2013.

18. Anand N, Ramudu P, Reddy K.H.P, Rao K.S.R, Jagadeesh B, Babu V.S.P, Burri D.R, “Gold nanoparticles immobilized on lipoic acid functionalized SBA-15: Synthesis, characterization and catalytic applications”, Appl. Catal., A, Vol. 45, pp. 119–126, 2013.
19. Tajbakhsh M, Farhang M, Baghbanian S.M, Hosseinzadeh R, Tajbakhsh M, “Nano magnetite supported metal ions as robust, efficient and recyclable catalysts for green synthesis of propargylamines and 1,4-disubstituted 1,2,3-triazoles in water”, New. J. Chem., Vol. 39, pp. 1827-1839, 2015.
20. Patil M.K, Keller M, Reddy B.M, Pale P.J, “Copper Zeolites as Green Catalysts for Multicomponent Reactions of Aldehydes, Terminal Alkynes and Amines: An Efficient and Green Synthesis of Propargylamines”, Eur. J. Org. Chem.,) 4440-4445, 2008.
21. Sreedhar B, Suresh Kumar A, Reddy P.S, “Magnetically separable Fe_3O_4 nanoparticles: an efficient catalyst for the synthesis of propargylamines”, Tetrahedron Lett., Vol. 51, pp. 1891-1895, 2010.
22. Bhatte K.D, Sawant D.N, Deshmukh K.M, Bhanage B.M, “Nanosize Co_3O_4 as a novel, robust, efficient and recyclable catalyst for A^3-coupling reaction of propargylamines”, Catal. Commun., Vol.16, pp. 114–119, 2011.
23. Price G.A, Brisdon A.K, Flower K.R, Pritchard R.G, Quayle P, “Solvent effects in gold-catalysed A^3-coupling reactions”, Tetrahedron Lett. Vol. 55, pp. 151–154, 2014.
24. Sasikala, R., Kutti Rani, S., Easwaramoorthy, D., Karthikeyan, K., 2015. Lanthanum loaded CuO nanoparticles: synthesis and characterization of a recyclable catalyst for the synthesis of 1, 4-disubstituted 1,2,3-triazoles and propargylamines. RSC Adv. 5, 56507–56517.
25. Sasikala, R., Kutti Rani, S., Easwaramoorthy, D., Karthikeyan, K., 2017. Synthesis, Characterization and Recyclable Cerium Loaded CuO Nanocatalyst for the Synthesis of 1, 4- Disubstituted 1,2, 3-Triazoles and Propargylamines. Silicon. DOI 10.1007/s12633-017-9576-3.
26. Chang L.L, Yang J, Wei Y, Ying J.Y, “Semiconductor-Gold Nanocomposite Catalysts for the Efficient Three-Component Coupling of Aldehyde, Amine and Alkyne in Water”, Adv. Synth. Catal., Vol. 351, pp. 2887–2896. 2009.
27. Li P, Wang L, “A highly efficient three-component coupling of aldehyde, terminal alkyne, and amine via C–H activation catalyzed by reusable immobilized copper in organic–inorganic hybrid materials under solvent-free reaction conditions”, Tetrahedron., Vol. 63, pp. 5455–5459, 2007.
28. Namitharan K, Pitchumani K, “Nickel-Catalyzed Solvent-Free Three-Component Coupling of Aldehyde, Alkyne and Amine”, Eur. J. Org. Chem., pp. 411–415. 2010.
29. Lim J, Park K, Byeun A, Lee S, “Copper-catalyzed decarboxylative coupling reactions for the synthesis of propargyl amines”, Tetrahedron Lett., Vol. 55, pp. 4875–4878, 2014.
30. Eagalapatia N.P, Rajacka A, Murthy Y.L.N, “Nano-size ZnS: A novel, efficient and recyclable catalyst for A^3-coupling reaction of propargylamines”, J. Mol. Catal. A: Chem., Vol. 381, pp 126–131, 2014.
31. Samai S, Nandi G. C, Singh M. S, “An efficient and facile one-pot synthesis of propargylamines by three-component coupling of aldehydes, amines, and alkynes via C–H activation catalyzed by $NiCl_2$”, Tetrahedron Lett., Vol. 51, pp. 5555–5558, 2010.
32. Satyanarayana K.V.V, Atchuta Ramaiah P, Murty Y.L.N, Ravi Chandra M, Pammi S.V.N, “Recyclable ZnO nano particles: Economical and green catalyst for the synthesis of A^3 coupling of propargylamines under solvent free conditions”, Catal. Commun., Vol. 25, pp. 50–53, 2012.
33. Wei C, Li C.J, “A Highly Efficient Three-Component Coupling of Aldehyde, Alkyne, and Amines via C−H Activation Catalyzed by Gold in Water”, J. Am. Chem. Soc., Vol. 125, pp. 9584–9585, 2003.

International Journal of Advance and Innovative Research
Volume 6, Issue 1 (VI): January - March, 2019

ISSN 2394 - 7780

AN EFFICIENT ENANTIOSELECTIVE CARBONYL REDUCTION BY CHIRAL SPIROBORATE ESTERS

D. Gavaskar and V. Sriraman
Department of Chemistry, School of Basic Sciences, Vels (VISTAS), Chennai
E-mail: ragharaghunathan@yahoo.com

ABSTRACT

The Assymmetric reduction of different prochiral ketones using chiral boranes to give enantiopure secondary alcohols in good enantiomeric yields. The structures and relative stereochemistry of cycloadducts were confirmed by, ^{1}H and ^{13}C NMR spectroscopy and mass spectrometry.

Keywords: Assymmetric synthesis, prochiral ketone, chiral borane, enantiopure

INTRODUCTION

Asymmetric catalysis is a combination of asymmetric synthesis, where a chiral molecule is used to govern an enantioselective transformation, and catalysis. In catalysis an addition of a small amount of a foreign material called "catalyst" speeds up a chemical process by decreasing the transition state energy, thus increasing the rate of the reaction without being consumed itself during the transformation. This process seems ideal for the preparation of chiral molecules since it only requires a very small amount of chiral catalyst to transform an achiral molecule into an enantioenriched chiral product. Noyori reported pioneering work in the field of catalytic asymmetric transformations in the mid 60s.[1] Although the observed enantioselectivity was poor, it opened up a new field in organic synthesis that became the focus of many research groups during the last decades. The most common asymmetric catalytic methods involve a transition metal, which once bonded to a chiral ligand, become the chiral catalyst. As mentioned earlier, in 2001 the Nobel Prize in Chemistry was awarded to Dr William S. Knowles, Professor Ryoji Noyori, and Professor K. Barry Sharpless for *"their development of catalytic asymmetric synthesis"*. Knowles and Noyori received half the Prize for: *"their work on chirally catalysed hydrogenation reactions"* and Sharpless was rewarded with the other half of the Prize for: *``his work on chirally catalysed oxidation reactions"*. This was the final recognition for a process which has had a remarkable impact on the chemical industry and especially the pharmaceutical industry where catalytic systems are used to prepare an enantiopure drugs on large-scale.

The chemistry of boron and, in particular, organoboron chemistry, is extremely diverse and ubiquitous in modern day chemistry.[2] During the 20th century, chemists unveiled a vast array of reactions involving boron reagents which demonstrated their utility in organic synthesis. There has been a significant amount of interest in the field of asymmetric synthesis in recent years, due in part to the increasing demand for enantiomerically pure compounds from the pharmaceutical industry.[3] Synthesising such compounds has been achieved using a variety of methodologies. These range from using 'chiral pool' substrates as enantioselective reagents,[4] chiral auxiliaries[5] and chiral reagents[6] through to kinetic resolution[7] and asymmetric catalysis.[8] Most notable was the 1979 Nobel Prize for Chemistry, awarded to H. C. Brown and Georg Wittig *for their development of the use of boron- and phosphoruscontaining compounds, respectively, into important reagents in organic synthesis*.[9] To this day, H. C Brown is best known for his work on hydroboration and organoboron chemistry. Hydroboration methodology became of particular interest to synthetic chemists as it allowed the regioselective addition of a boron containing species to the least substituted carbon in olefinic species (*anti*-Markovnikov addition). Therefore, the functionalisation of the boron-bearing substituent led to *anti*-Markovnikov-type products, which were previously challenging to obtain. The subsequent transformation of carbon-boron bonds into C-C, C-N, C-O, C-X bonds and homologations.

There has been growing interest in the application of electron-deficient boron species for symmetric synthesis.[10] The proliferation of boron-based synthesis dates back to 1956 with seminal work published by Herbert C. Brown *et al.* for which he later received the Nobel Prize.[11] In this paper, a novel technique for the conversion of olefins into trialkylboranes and through to their corresponding alcohols was described Trost *et al* has reported a concise synthesis of pyrrolopiperazines *via* Palladium-catalyzed a) asymmetric annulation between 5-bromopyrrole-2-carboxylate esters and vinyl aziridines [33]; b) AAA (asymmetric allylic alkylation) reactions of pyrroles and *N*-alkoxyamides (hydroxamic esters).[34] Recently Chang-Woo *et al* reported the concise synthesis of the natural product containing pyrrolopiperazine skeleton by a) tandem cross-metathesis/intramolecular aza-conjugate addition of acrolein with pyrrole derivatives [35], b) by the direct lactamization of azido amide *via* a Staudinger-type reductive cyclization [36] and c) by organocatalytic aza-Michael addition using pyrroles.[37] It is significant to note that all the reports mentioned above has only bicyclic core of pyrrolopiperazine skeleton.

In continuation of our investigations in the field of asymmetric synthesis , we herein report a facile asymmetric reduction of prochiral ketones using chiral boranes. Initially, a novel air- and moisture-stable crystalline enantiopure L-valine spiroborate esters, were conveniently prepared from ethylene glycol, and readily available enantiopure L-valine amino alcohols according to the method reported by Huskens and Reetz.[35] Literature procedure of commercially available L-valine, **1** was protected using $SOCl_2$ and ethanol under 0 °C gave protected L-valine ester **2** in 70% yield. and then protected L-valine ester **2** was converted into the diphenyl valinol **3** in 68% yield by treatment with phenylmagnesium bromide in THF. Separately L-valine, **1** was reduced using LAH to give valinol **4** in 76% yields (Scheme 1).

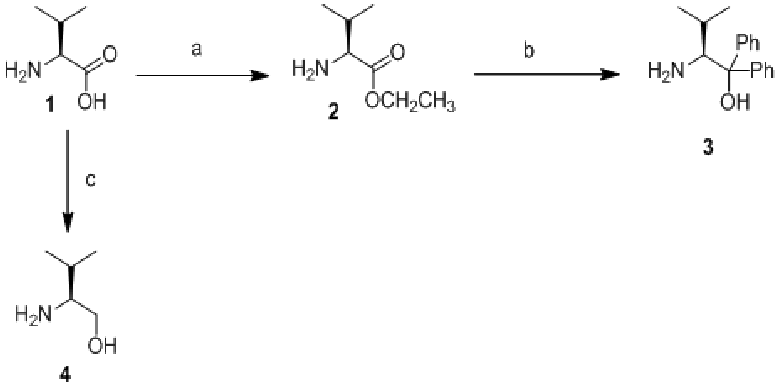

Synthesis of Valerine **(4)**

Scheme-1: Reagents and conditions:(a) $SOCl_2$, EtOH, 0 °C, 12 h, 70%; (a) PhMgBr, THF, rt, 24h, 68%; (c) LAH, dry THF, 0 °C to rt, 12 h, 76%.

The ^{1}H-NMR spectrum of valinol **4** displayed a two different doublet at δ 0.91 and 0.93 ppm for the two different methyl protons and a doublet of doublet at δ 3.64 ppm for $-CH_2OH$. The ^{13}C NMR spectrum of valinol **4** displayed the two different methyl carbons at δ 19.2 and 18.4 ppm and signals at δ 64.7 ppm for $-CH_2OH$ carbons. The spiroborates **5** and **6** in 68% and 85% yields respectively, were prepared as shown in Scheme 1 by gently heating isopropyl borate with the corresponding glycol in toluene until a clear solution, followed by the slow addition of the valinol **3** and **4** in toluene (Scheme 2). No further purification was attempted. The ^{1}H-NMR spectrum of spiroborates **5** displayed a two different doublet at δ 0.88 and 0.94 ppm for the two different methyl protons and a sharp singlet at δ 6.31 ppm for quantized $-N-H_2$(Scheme 2).

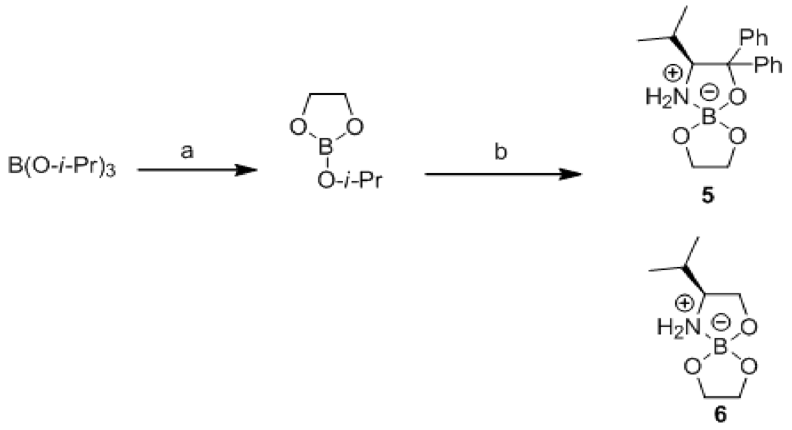

Scheme 2: Synthesis of Chiral Boranes **5** and **6**

Scheme 2: Reagents and conditions: (a) Ethylene glycol, toluene, reflux, 3 h; (b) valinol **3** and **4**, toluene, rt, overnight, 68% and 85%.

Initially, we studied the asymmetric borane reduction of acetophenone was carried out with BH_3–SMe_2 (1.6 equiv) and 10 mol % of the catalyst 5 and 6 at room temperature, obtaining the (R)-1-phenyl ethanol in quantitative yield and with 88% ee, as indicated in Scheme 3. Based on these results, other prochiral ketones were reduced enantioselectively in different solvents and the results are presented in Table 1. Modest to high enantioselectivities were achieved for all the substrates in THF. The selectivity decreases to 48% ee for the reduction of acetophenone in TBME (entry 4), but is comparable in dioxane (51% ee, entry 3). Reduction of other substrates gave similar results to that of acetophenone (entries 4–6) .(Scheme 3)

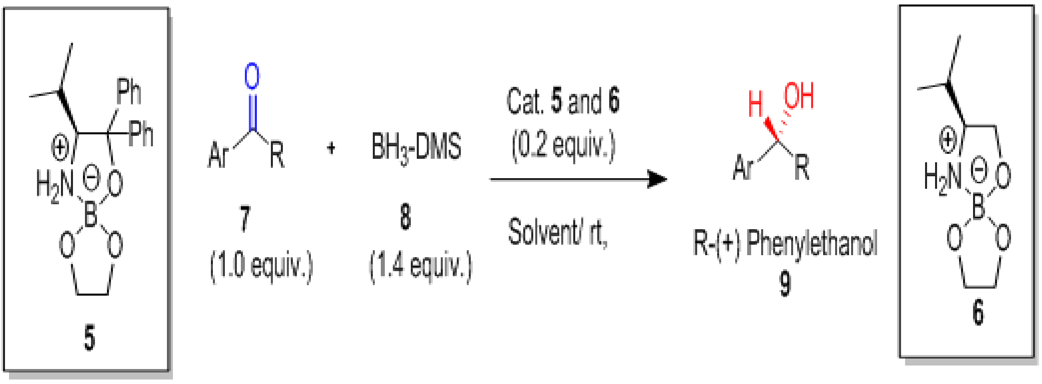

Scheme-3: Assymetric boran reduction of Ketone compound and it derivative

GENERAL PROCEDURE

Optimized procedure for the asymmetric borane reduction

Borane-DMS complex (1.4 equiv.) was added to solution of valine boran complex catalyst (0.2 equiv.) in dry THF (1.5mL) and stired at rt , under nitrogen for 15 min. A solution of acetophenone (1.0 equiv.) in dry THF(1 mL) was added to the reaction mixture for 1h. The solution was stirred at rt over 1h, then cooled to 0c and quenched with methanol (2mL). After stirring for 1h at rt the solvents were removed under vaccum. The residue was dissolved in DCM (40mL), washed with a saturated solution of ammonium chloride (25mL) and dried with sodium sulfate .The solvents were removed under vaccum to gave the final product as a yellow oil.

1. **Valinol: (4)-** Yield : 76%, Color: yellow oil, ^{1}H NMR (300 MHz, $CDCl_3$) : δ 0.9 (d, 3H, J=6Hz), 0.92 (d, 3H, J=6Hz), 1.51-1.60 (septet, 1H), 2.7 (bs, 2H), 3.3 (t, 1H, J=10.5Hz), 3.64 (dd, 2H, J=9Hz), ^{13}C NMR (125 MHz, $CDCl_3$) : δ 19.2(2C), 30.9, 58.3, 64.4
2. **Spiroborates (5):** Yield: 68%, Color: white crystal solid, ^{1}H NMR (300 MHz, $CDCl_3$): δ 0.9 (d, 3H, J=18Hz), 0.91 (d, 3H, J=18Hz), 1.51-1.60 (septet, 1H), 3.35(4H, d, J=3.3Hz), 6.03 (s, 1H), 7.18 (q, 2H, J=9Hz), 7.82 (q, 4H, J=6Hz), 7.41 (bs, 2H), 7.50 (d, 2H, J=9Hz), 7.65 (d, 2H, J=9Hz).
3. **R)-1-phenylethanol (7a):** Yield: 82%, Color: yellow oil, $[\alpha]_D^{34}$+42.01(*c* 0.1, $CHCl_3$)^{1}H NMR (300 MHz, DCl_3): δ 1.39(d, 3H, J=6.0Hz),δ 4.78(q,1H, J=6.3Hz),δ 5.19(s, 1H, bs),δ 7.10-7.21(m, 1H),δ 7.23-7.27(m, 4H),^{13}C NMR (125 MHz, $CDCl_3$): δ 24.1, 69.3, 124.3, 126.4, 127.4, 144.7.

Table-1: Enantioselective reduction of aromatic ketones with spiroborate 5 and 6

Entry	Prochiral Ketone	Catalyst	Solvent	Yield (%)	$[\alpha]_\lambda^T$	ee%c
1	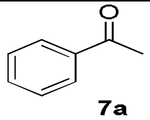 7a	5	THF	90	24.6	56
2	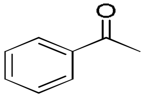 7a	6	THF	82	40	91
3	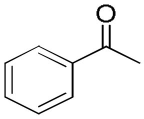 7a	6	Dioxane	80	22.4	51
4	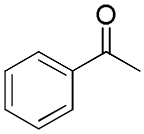 7a	6	TBME	76	21	48
5	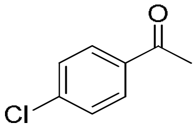 7b	6	THF	73	38	85

6	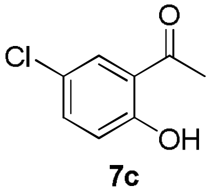 **7c**	6	THF	84	-	-
7	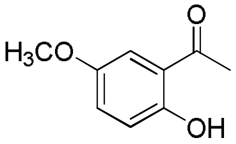 **7d**	6	THF	77	-	-
8	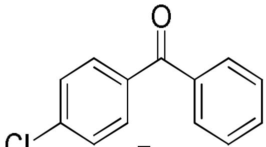 **7e**	6	THF	72	-	-

CONCLUSION

A facile and efficient method for the reduction of aralkyl-, and halogenated aromatic ketones in the presence of up to 20 mol % catalysts **5** and **6** with outstanding enantioselectivities has been established.

ACKNOWLEDGEMENTS

D.G and V.S thanks Vels University for support and encouragement.

REFERENCES

1. Nozaki, H., Moriuti, S., Takaya, H., Noyori, R. *Tetrahedron Lett.* 1966, 5239.
2. Muetterties, E. L., *The Chemistry of Boron and Its Compounds* (John Wiley & Sons Inc., New York, 1967).
3. Crudden, C. M., Glasspoole B. W., Lata, C. J., *Chem. Commun.*, 2009, 6704-6716.
4. Brown, H. C. *Hydroboration* (W. A. Benamin, Inc., New York, 1962).
5. Miyaura, N., Yamada. K., Suzuki, A. *Tetrahedron Lett.*, 1979, 36, 3437-3440.
6. Fernández, E., Hooper, M. W., Knight. F. I., Brown, J. M. *Chem. Commun.*,1997, 173-174.
7. Stymiest, J. L., Bagutski, V., French, R. M., Aggarwal, V. K. *Nature*, 2008, 456, 778-782.
8. Brown, H. C., Lane, C. F. *J. Am. Chem. Soc.*, 1970, 92, 6660-6661.
9. The Nobel Prize in Chemistry 1979. Last accessed on Janruary 2015: http://www.nobelprize.org/nobel_prizes/chemistry/laureates/1979/
10. Cotton, F. A.; Wilkinson, G.; Murillo, C. A.; Bochmann, M., *Advanced Inorganic Chemistry*. John Wiley and Sons: New York, 1999; p 131-174.
11. Brown, H. C.; Subba Rao, B. C., *J. Am. Chem. Soc.* 1956, 78, 5694-5695.
12. Corey, E. J.; Helal, C. J. Angew. Chem., Int. Ed. 1998, 37, 1986.
13. Smith, K.; Pelter, A., *Comprehensive Organic Synthesis*. Pergamon Press: Oxford, 1991; Vol. 8, p 703-731.
14. Brown, H. C.; Ramachandran, P. V., *Pure Appl. Chem.* 1994, 66, 201.
15. Ishihara, K., *Lewis Acids in Organic Synthesis*. Wiley-VCH: Weinheim, 2000; Vol. 1.
16. Matteson, D. S., *Chem. Rev.* 1989, 89, 1535.
17. Imai, T.; Tamura, T.; Yamamuro, A.; Sato, T.; Wollmann, T. A.; Kennedy, R. M.; Masamune, S., *J. Am. Chem. Soc.* 1986, 108, 7402-7404.
18. Seyden-Penne, J. Reductions by the Alumino- and Borohydrides in Organic Synthesis; Wiley-VCH: New York, 1997.

19. Daverio, P.; Zanda, M. Tetrahedron: Asymmetry 2001, 12, 2225.
20. Hirao, A.; Itsuno, S.; Nakahama, S.; Yamazaki, N. J. Chem. Soc., Chem. Commun. 1981, 315.
21. Itsuno, S.; Hirao, A.; Nakahama, S.; Yamazaki, N. J. Chem. Soc., Perkin Trans. 1 1983, 1673.
22. Itsuno, S.; Wakasugi, T.; Ito, K.; Hirao, A.; Nakahama, S. Bull. Chem. Soc. Jpn. 1985, 58, 1669.
23. Itsuno, S.; Nakano, M.; Miyazaki, K.; Masuda, H.; Ito, K.; Hirao, A.; Nakahama, S. J. Chem. Soc., Perkin Trans. 1 1985, 2039.
24. Itsuno, S.; Nakano, M.; Ito, K.; Hirao, A.; Ohwa, M.; Kanda, N.; Nakahama, S. J. Chem. Soc., Perkin Trans. 1 1987, 2615.
25. Itsuno, S.; Sakurai, Y.; Ito, K.; Hirao, A.; Nakahama, S. Bull. Chem. Soc. Jpn. 1987, 60, 395.
26. Brunel, J. M.; Paradigon, O.; fature, B.; Buono, G. J. Chem. Soc., Chem. Commun., 1992, 287.
27. Chiodi, O.; Fotiadu, F.; Sylvestre, M.; Buono, G. Tetrahedron Lett. 1996, 37, 39.
28. Corey, E. J.; Bakshi, R. K.; Shibata, S. J. Am. Chem. Soc., 1987, 109, 5551.
29. Huskens, J.; Reetz, M. T. Eur. J. Org. Chem. 1999, 1775.
30. Jones, S.; Atherton, J. C. C. Tetrahedron: Asymmetry 2000, 11, 4543.

International Journal of Advance and Innovative Research
Volume 6, Issue 1 (VI): January - March, 2019
ISSN 2394 - 7780

GREEN SYNTHESIS OF COPPER NANOPARTICLES SYNTHESISED USING MIMOSA PUDICA

D. Malathy and Meyyappan Revathi
Assistant Professor, School of Basic Sciences, Department of Chemistry, VISTAS, Chennai
E-mail: dm.malathy@gmail.com

ABSTRACT

The methods like Bio-green are advantages over physical and chemical methods due to eco-friendly and cost effective synthesis of nanoparticles. In current study, ethanolic extract of Mimosa pudica was used for the synthesis of copper nanoparticles. The formation of copper nanoparticle was confirmed by UV-Visible spectroscopy. Fourier Transform Infra red Spectroscopy(FTIR) revealed the possible involvement of photo-constituents in copper nanoparticles of crude extract.XRD is commonly used to determine the chemical composition and crystal structure of a material.Further Transmission Electron Microscopy(TEM) was used for the shape and morphology determination.

Keywords: Copper nanoparticles, FTIR, Mimosa Pudica, TEM, UV-Visible, XRD.

1. INTRODUCTION

Nanoparticles are very important in developing sustainable technologies for the future, for humanity and the environment. Synthesis of Nanoparticles by plants is a green chemistry approach that interconnects nanotechnology and plant biotechnology[1]. Plant extracts are used for the metal ions bio reduction to form nanoparticles. Recently, many studies have proven that the plant extracts act as a potential precursor for the synthesis of the nanomaterials in non-hazardous ways[2]. The plants are used successfully in the synthesis of several greener nanoparticles such as cobalt, copper, silver, gold, palladium, platinum, zinc oxide and magnetite[3-10]. In the present study we used copper nitrate for the biosynthesis. Copper Nanoparticles due to their excellent physical and chemical properties and low case of preparation have been of great interest[11,12]. Copper nanoparticles have wide applications as heat transfer systems, antimicrobial materials, super strong materials sensors and catalysts[13]. Copper nanoparticles are very reactive because of their high surface to volume ratio and can easily interact with other particles and increase their antimicrobial efficiency[14].

2. MATERIALS AND METHODS

2.1 Materials

Mimosa Pudica, the sample for the biosynthesis of the copper nanoparticles was purchased from the local supermarket. Copper nitrate used in the present study were of high purity and analytical grade and purchased from Ranbaxy chemical company, Inc, India The solvent ethanol was re distilled before use. Double Distilled water was used for the synthesis.

2.2 Preparation of Sample

Fresh leaves of mimosa pudica were thoroughly washed under running tap water followed by washing it with double distilled water to remove surface impurities. They were crushed using a blender to get powder. The dried Pulverized plant material of 5 g was extracted in 100 ml of ethanol at 60^0 C for 2 hours. The extracts were filtered using Whatmann No.1 filter paper and the analysis was carried out immediately without storage for the bio synthesis of copper nanoparticles.

2.3 Phytochemical Screening-Qualitative Analysis

Fresh extract of mimosa pudica was used for phytochemical screening- Qualitative analysis. Preliminary phytochemical screening was carried out by standard phytochemical methods[15].

2.3.1 Test for Tannins

To 99.9 ml of distilled water 0.1ml of ferric chloride reagent was added. Test 1 ml of the sample taken and a few drops of 0.1% ferric chloride was added and observed for brownish green or blue, black coloration.

2.3.2 Test for Saponins

To 1 ml of extract 5 ml of distilled water was added and shaken vigorously. Observed for soaking appearance indicates the presence of saponins.

2.3.3 Test for Flavonoids

To 1 ml of extract 5 ml of dilute ammonia solution was added, followed by addition of concentrated sulphuric acid along the sides of the tube. Appearance of yellow colouration.

2.3.4 Test for Alkaloids

1 ml of sample was taken to that few drops of Dragendvoff's reagent was added and observed for orange red colour.

2.3.5 Test for Protein

1 ml of sample was taken to that few drops of Bradford reagent was added. The blue colour was observed.

2.3.6 Test for Steroids

1 ml of the filtrate was taken to that 10% concentration H_2SO_4 was added and observed for green colour.

2.3.7 Test for Anthroquinones

1 ml of sample was taken to that aqueous ammonia (shaking) was added and observed for change in colour of aqueous layer (Pink, Red or Violet).

2.4 Biosynthesis of Copper Nanoparticles

To 100 ml of ethanolic extract of mimosa pudica ,added 90 ml of 1mm of copper nitrate solution in 250 ml beaker. The formation of copper nanoparticles is confirmed by the color change from pink to brown when it is kept on a water bath at 80^0C. The formation of copper nanoparticles is inferred by visual observation followed by recording UV-Visible spectrum. The biosynthesized copper nanoparticles are characterized by FTIR, XRD and TEM studies.

2.5 CHARACTERIZATION OF COPPER NANOPARTICLE

2.5.1 Visual Inspection

The bio-reduction of the aqueous solution of copper nitrate using mimosa pudica extract was monitored and the appearance of brown color indicates the formation of copper nanoparticles.

2.5.2 UV-Visible Spectroscopy

The reduction of copper nitrate to copper was monitored by recording UV-Visible spectrum of the reaction mixture after diluting a small aliquot of the sample with deionised water. The measurements are recorded on Shimadzu dual beam spectrometer (model uv-1650pc) operated at resolution of 1nm.

2.5.3 Fourier Transform Infra-red (FTIR) Spectroscopy

FT-IR measurement was carried out for both the extract and copper nanoparticles to identify the possible bioactive molecules responsible for the reduction of the copper ions.FT – IR Spectra were recorded using a perkin Elmer 360 model IR double beam spectrophotometer The Spectra were collected from 4000 to 400 cm-1 with 4 cm-1 resolution over 40 scans All spectra were collected against the background spectra of KBr.

2.5.4 X-Ray Diffraction Studies

X-ray diffraction (XRD) measurement of the copper nanoparticles was carried out using powder x-ray diffractometer instrument (SEIFERT JSO DEBYEFLEX-2002) in the angle range of 100 -700 operated at a voltage of 40Kv and a current of 30mA with CuKα radiation in a θ-2θ configuration. The crystallite domain size was calculated by using Debye- Scherrer formula.

2.5.5 Transmission Electron Microscopy

TEM images were obtained with a field emission JEOL JEM-1400 120 KV instrument.

3 RESULTS AND DISCUSSION

3.1 Qualitative Pharmocognostic Evaluation of Extract

The results of qualitative phytochemical analysis of the mimosa pudica extract are shown in table-1 which indicate the presence of carbohydrates alkaloids, proteins, amino acids, tannins, phenolic, flavonoids and steroids.

Phyto constituents	Observation
Carbohydrates	+
Alkaoids	+
Protiens & aminoacids	+
Tannins & phenotics	+
Flavonoids	+
Triterpenoids	-
Steroids	+
Glycosides	-
Fixed oils	+
Gums	-
Mucilages & saponins	+

(+) Indicates the presence of chemical constituents

(-) Indicates the absence of chemical constituents

3.2 Visual Characterization

When the extract was mixed in the aqueous solution of copper nitrate,it started to change the color from pink to brown.The color change to brown indicates the reduction of copper nitrate and formation of copper nanoparticles. Fig 1 indicates the formation of nanoparticles.

Figure-1: Color change of reduced copper ion

3.3 UV-Visible Studies on Copper nanoparticles

UV-Visible absorbance spectroscopy has proved to be a very useful technique for studying metal nanoparticles because the peak positions and shapes are sensitive to particle size.The surface plasmon peak of CuNp has been reported to appear at around 570nm[16].

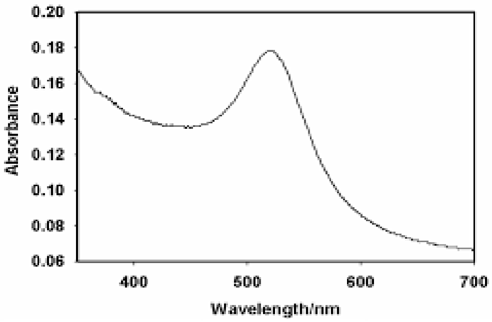

3.4 Fourier Transform Infra-Red Spectroscopy

FTIR spectroscopy was used to analyze the interaction between the metal and plant extract. The wavelength of light absorbed is characteristic of the chemical bond present in the chemicals by interpreting the infra-red absorption spectrum. The chemical bond in a molecule can be determined to further realize the role of plant extract in the formation of copper nano particles.The FTIR spectra for bio synthesis metals nano particles were studied. In figure 2 of copper nanoparticles, showed strong bands at 3436.5,1652.0, 1398.0,1066.0 and 743 cm^{-1} respectively, these intense bands corresponds to the strong stretching free hydroxyl O–H of alcohols and phenols, –C=C– alkenes, C–H rock alkanes, C–O strong stretching ethers, C–H strong bending alkene.

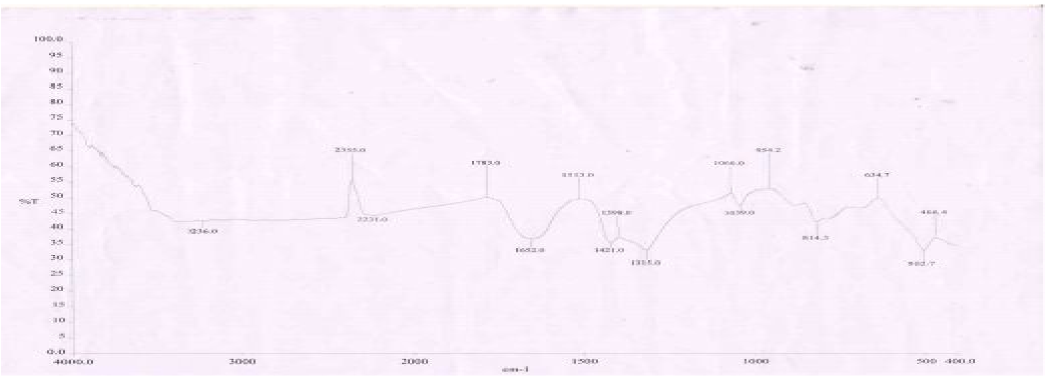

Figure-2: IR Spectra of biosynthesised copper nanoparticles

3.5 XRD Analysis

A number of Bragg reflections corresponding to (111), (200) and (220) sets of lattice planes are observed, which can be indexed to face-centered cubic copper[17]. The peaks match with the Joint Committee of powder Diffraction Standards, which further proves the formation of copper nanoparticles. Furthermore, the average diameter of the copper nanoparticles is calculated in the range 15-30nm by Scherrer's formula using FWHM obtained from the diffraction peaks:

$D= 0.89\lambda/\beta\cos\theta$

Where D is the mean grain size, λ is the wavelength of copper target, β is the FWHM of the diffraction peaks and θ is the diffraction angle. Thus XRD is commonly used to determine the chemical composition and crystal structure of a material.

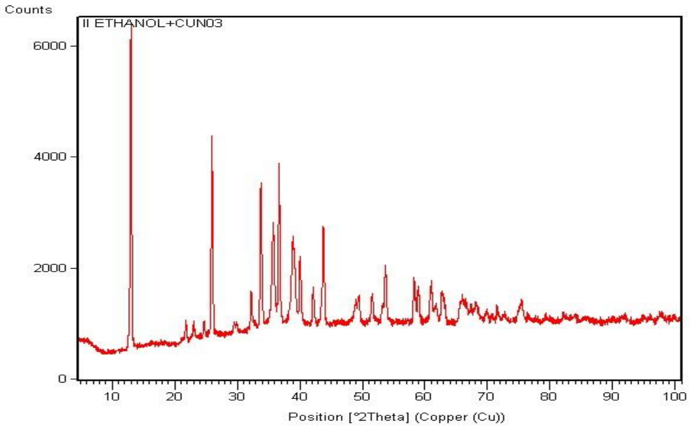

Figure-3: XRD Data for copper nanoparticles

3.6 Transmission Electron Microscopy

The size and morphology of the copper nanoparticles synthesized using mimosa pudica extract were analyzed with a transmission electron microscopy. The typical TEM microscopy and the size of distribution of copper nano particles obtained by mixing aqueous extract of plant in mimosa pudica medium were shown in the figure 4. The resultant particles essentially were very fine with the mean diameter of 20nm Further it was observed that morphology of the particles was spherical in size.

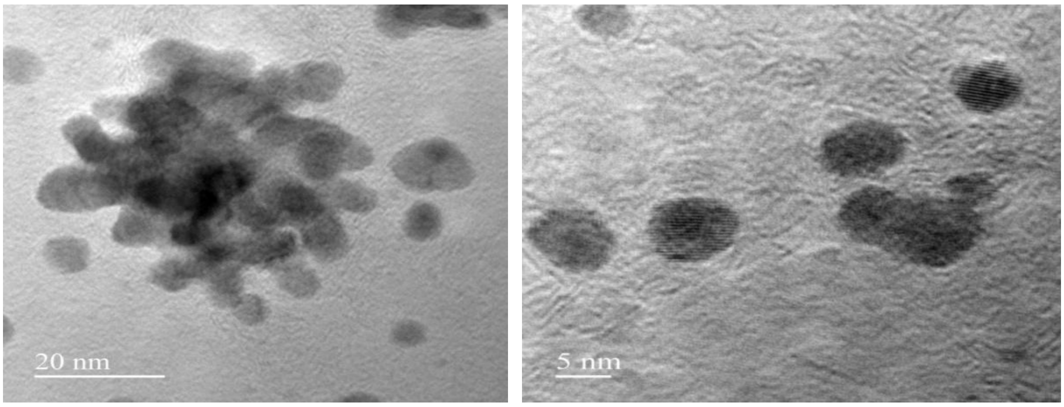

Figure-4: TEM image of copper particles

4. CONCLUSION

The present study deals with the extraction of copper nanoparticles from leaf extract of mimosa pudica which provides cost effective, easy and proficient way for synthesis of nanoparticles. The colour change of the solution confirmed the presence of copper nano particles. FTIR spectroscopy studies showed the change in the metal and the plant extract there by resulting in the formation of nanoparticles. XRD pattern is used to study the crystal structure of copper nanoparticles. The TEM image revealed that very stable copper nano particles with almost spherical size were observed with average size of 20nm in diameter.

5. ACKOWLEGEMENT

The authors are grateful to the management of VISTAS for their support to carry this work. We also thank the University of Madras for recording UV-Visible, FT-IR spectra and XRD and IIT-Madars for TEM.

6. REFERENCES

1. Shalini Thakkar, Santosh Wanjale and Prasad Panzade, Eco-Friendly Phyto-Synthesis Of Silver Nanoparticles Using Colchicum Autumnale And Its Characterization,International Journal of Advanced Research (2016), Volume 4, Issue 6, 1903-1915.
2. PalaniselvamKuppusamy,MashitahM.Yusoff,GaantyPragasManiam,Natanamurugaj Govindan,Biosynthesis of metallic nanoparticles using plant derivatives and their new avenues in pharmacological applications – An updated report,Saudi Pharmaceutical Journal, Volume 24, Issue 4, July 2016, Pages 473-484.
3. Kashif Ahmed, Iqbal Tariq , Solat Ullah Siddiqui and Muhammad Mudassir,Green synthesis of cobalt nanoparticles by using methanol extract of plant leaf as reducing agent,Pure Appl. Biol., 5(3): 453-457, September, 2016.
4. 4.R. Ramanathan, M.R. Field, A.P. O’Mullane, P.M.Smooker, S.K. Bhargava, V. BansalAqueous phase synthesis of copper nanoparticles: a link between heavy metal resistance and nanoparticle synthesis ability in bacterial systems,Nanoscale, 21 (2013), pp. 2300-2306.
5. K. Shameli, M. Ahmad, E.A.J. Al-Mulla, N.A.Ibrahim, P. Shabanzadeh, A. Rustaiyan, Y.AbdollahiGreen biosynthesis of silver nanoparticles using Callicarpa maingayi stem bark extraction,Molecules, 17 (2012), pp. 8506-8517.
6. Paz Elia, Raya Zach, Sharon Hazan,Sofiya Kolusheva, Ze’ev Porat, and Yehuda Zeiri,Green synthesis of gold nanoparticles using plant extracts as reducing agents, Int J Nanomedicine. 2014; 9: 4007–4021.
7. K. Amarnath, J. Kumar, T. Reddy, V. Mahesh, S.R. Ayyappan, J. Nellore,Synthesis and characterization of chitosan and grape polyphenols stabilized palladium nanoparticles and their antibacterial activity,Colloid Surf. B, 92 (2012), pp. 254-261.
8. K.N. Thakkar, S.S. Mhatre, Y.P. Rasesh, Biological synthesis of metallic nanoparticles, Nanomedicine, 6 (2010), pp. 257-262.
9. G. Sangeetha, S. Rajeshwari, R. Venckatesh,Green synthesis of zinc oxide nanoparticles by aloe barbadensis miller leaf extract: structure and optical properties, Mater. Res. Bull., 46 (2011), pp. 2560-2566.
10. Amedea B. Seabra,Paula S. Haddad, Antimicrobial Applications of Superparamagnetic Iron Oxide Nanoparticles,Nanostructures for Antimicrobial Therapy, 2017.
11. Yeshchenko, OA, Dmitruk IM, Dmytruk AM and Alexeenko AA. Influence of annealing conditions on size and optical properties of copper nanoparticles embedded in silica matrix. Mater. Sci. Eng., B 2007: 137 (1):247–54
12. Suresh, YS. Annapurna, G. Bhikshamma, and AK. Singh. Characterization of green synthesized copper nanoparticles: A novel approach. InternationaI Conference on Advanced Nanomaterials & Emerging Engineering 2013: 13 (9):63–67.
13. Varshney, RS. Bhadauria P, Gaur, M and R. Pasricha.. Characterization of copper nanoparticles synthesized by a novel microbiological method. JOM 2010: 62 (12):102–04.
14. Varshney, RS. Bhadauria, and MS. Gaur. A review: Biological synthesis of silver and copper nanoparticles. Nano Biomedicine Eng. 2012:4 (2):99–106.
15. V. Subha Priya, K. V. Rajeswari, M. Geetha, M. Flory Shobana, K. Mohammed Rafiq Khan and S. N. Suresh,Preliminary Phytochemical Screening and Antimicrobial Analysis of Mimosa pudica (Linn.),Journal of Pharmaceutical and Biological Research,JPBR, 2014, Vol.2(2): 160-164.
16. González JP, Covarrubias C, Cádiz M, Corral C Cuadra F, Fuentevilla I and Bittner M,Design of Antimicrobial Release Systems Based on Chitosan and Copper Nanoparticles for Localized Periodontal Therapy,Journal of Dentistry and Oral Disorders,Volume 2 Issue 7 - 2016.
17. Theivasanthi and M.Alagar, X-ray Diffraction studies of Copper Nanoparticles,Archive of Physics Research, 1, 112-117.

International Journal of Advance and Innovative Research
Volume 6, Issue 1 (VI): January - March, 2019

ISSN 2394 - 7780

ELECTROLYTIC CONDUCTANCE STUDY OF 3-NITRO BENZOIC ACID IN ETHANOL – WATER MIXED SOLVENT MEDIUM

Nithya. G and Sudha R
Department of Chemistry, Vels Institute of Science, Technology and Advanced Studies, Chennai
E-mail: nithyaranju@gmail.com

ABSTRACT

Electrolytic conductance of a solution is used to calculate equivalent conductance and specific conductance of a solution at different dilutions. Specific conductivity measurement for 3-nitrobenzoic acid in ethanol water mixed media containing 50%, 60%, 70%, 80%, 90% at room temperature were measured. With increasing electrolytic concentration it showed a sharp increase in the conductivity. By increasing the ethanol concentration, the electrolyte conductivity decreases. The nature of ion-solvent interactions and solvent-solvent interactions have been studied by using the conductivity measurement obtained in the system.

Keywords: Dissociation constant, mixed solvent medium, 3-nitro benzoic acid, electrolytic conductance, ionic interactions.

INTRODUCTION

Solvent blending or co solvency usually affects important characteristics of a solute in a solution like its solubility, stability and dissociation constants. During last few years the spot light of conductivity measurements has shifted to various mixed-solvent systems. In water-organic solvent and binary organic solvents media a numerous experimental and theoretical studies were devoted [1-4]. The ion-association can be controlled and solubility profile of a liquid mixture can be predicted by adding the organic solvent. The solvent added might change dielectric constant of the medium which leads to change in structure of the molecule. Although various mixed solvents are used, water and alcohol mixtures are of particular attention because of their wider application in both investigational and hypothetical part. Between aqueous and non aqueous solvent molecules these mixtures also draw attention to the particular type of interactions in the course of hydrogen bonding [5]. Systems similar to ethanol-water mixtures are identified by comparatively large dielectric constants. Ethanol is a extremely accepted solvent in forming uniform homogenous mixtures with water. These parameters have an immense opportunity to form a highly complex-hydrogen bonded configuration in the liquid condition.

Like water, alcohol is also a strong hydrogen-bonded self associated liquid. Although the intermolecular bonding of the liquid has a major consequence on the physiochemical properties alcohol will not form open structure like water. The information about the hydrophobic hydrocarbon chain in alcohols opposes the hydrophilic –OH group in its endeavor by a close understanding of the structure of alcohol –water mixtures is provided to drag the molecule in solution [6]. In binary liquid mixture the hydrogen bonding in hydroxyl group and solvent molecules takes place.

The current study compares the conductivity performance of 3–nitro benzoic acid at 303K. For knowing the theory behind the changes in structure of solvent the conductance behavior of such salts in mixed solvents must be known. The ion-ion and ion-solvent interactions in different conditions can be identified by using this study [7-15]. The limiting conductance of the electrolyte λ^o, the equilibrium constant (association constant) K_A , and the interpretation of the ion-size parameter is determination from the experimental data λ vs concentration C. The assessment of these parameters were based on the various versions of the inter ionic attraction assumption of charged spheres in a solvent field. The geometry and the size of the ions is identified by the limiting conductance λ^o in solution.

EXPERIMENTAL PROCEDURE

Measure the required percentage of ethanol and prepare the solution of 90%, 80% , 70% , 60% and 50% of ethanol using ethanol – water solvent mixture.Prepare 0.1 N 3-nitrobenzoic acid by weighing 0.33 g of 3-nitrobenzoic acid in the 90 % ethanol-water mixed solvent. Similarly prepare the concentrations of 0.05N, 0.025N, 0.0125N, 0.00625N by 90% ethanol-water mixed solvent. Using different solvent concentrations of ethanol water mixture (80% , 70% , 60% , 50%) repeat the same procedure for different concentration of 3-nitro benzoic acid. The conductance for the different concentrations of 3-nitro benzoic acid in different solvent mixtures were calculated. Repeat the measuring steps for every concentration (every time wash the conductivity cell by distiled water) and for different percentages and note down the reading. From the conductance, the equivalent conductance and specific conductance were measured.

RESULTS AND DISCUSSION

The table below shows the comparative analysis of equivalent conductance, specific conductance and dissociation contestant for varied nitro benzoic acid solution in ethanol water mixtures , also its shows the equivalent conductance of nitro benzoic acid solution in ethanol water mixtures in infinite dilution.

Table: Comparative analysis of k, λ , λ∞ and α for the varied nitrobenzoic acid solution in ethanol water mixtures

% of Ethanol	Concentration	K=(conduntance) x 10^{-3} $ohm^{-1}cm^{-1}$	$\lambda = 1000k/c$	$\alpha = \lambda/\lambda_\infty$	$Ka = c\alpha^2(1-\alpha)$	λ_∞
90	0.1	0.00013	1.3	0.075144	0.00061	17.3
	0.05	0.00012	2.4	0.13872	0.001118	
	0.025	0.00011	4.4	0.25433	0.002145	
	0.0125	0.00009	7.2	0.416184	0.003708	
	0.00625	0.00009	14.4	0.83236	0.025838	
80	0.1	0.00016	1.6	0.08083	0.000865	18.01
	0.05	0.00012	2.4	0.133259	0.001023	
	0.025	0.00011	4.4	0.24430	0.001974	
	0.0125	0.00010	8.0	0.44419	0.004437	
	0.00625	0.00009	14.4	0.7995	0.019925	
70	0.1	0.00017	1.7	0.08056	0.000705	21.1
	0.05	0.00014	2.8	0.13270	0.001014	
	0.025	0.00013	5.2	0.24644	0.002014	
	0.0125	0.00012	9.6	0.45497	0.004746	
	0.00625	0.00011	17.6	0.83412	0.026211	
60	0.1	0.00020	2.0	0.06493	0.00044	30.8
	0.05	0.00019	3.8	0.12337	0.00866	
	0.025	0.00018	7.2	0.23376	0.00177	
	0.0125	0.00017	13.6	0.4444	0.00442	
	0.00625	0.00016	25.6	0.83116	0.02552	
50	0.1	0.00032	5.6	0.08101	0.000713	39.5
	0.05	0.00028	10.4	0.14177	0.001169	
	0.025	0.00026	19.2	0.26329	0.002352	
	0.0125	0.00024	33.6	0.48607	0.005745	
	0.00625	0.00020	33.6	0.85063	0.030275	

From figure1, it is verified that with increasing concentration there is a pointed increase in specific conductivities of the investigated range in all concentrations. The specific conductivities of the solution increases with the increase in concentration with the number of ions per unit volume in the solution.

The affinity for ion formation is improved and the conductivity decreases with increasing ethanol content. The added ethanol will reduce the permittivity of the medium.

In each mixture the λo value depends on the medium. The λo values decreases with increasing the percentage of alcohol.

When the alcohol content is increased the conductance of the solution decreases for the intended ethanol-water mixed solvent system. The existance of ethanol reduces the dielectric constant of the solvent phase. The ion pairs obtained in the solution phase is due to the interaction produced. In solvent medium it leads to the reduction in the dielectric constant. It is thus seen that the greater part of the solutes are appreciably subjective by the existence of solutes.

Figure 1: Specific conductance vs concentration

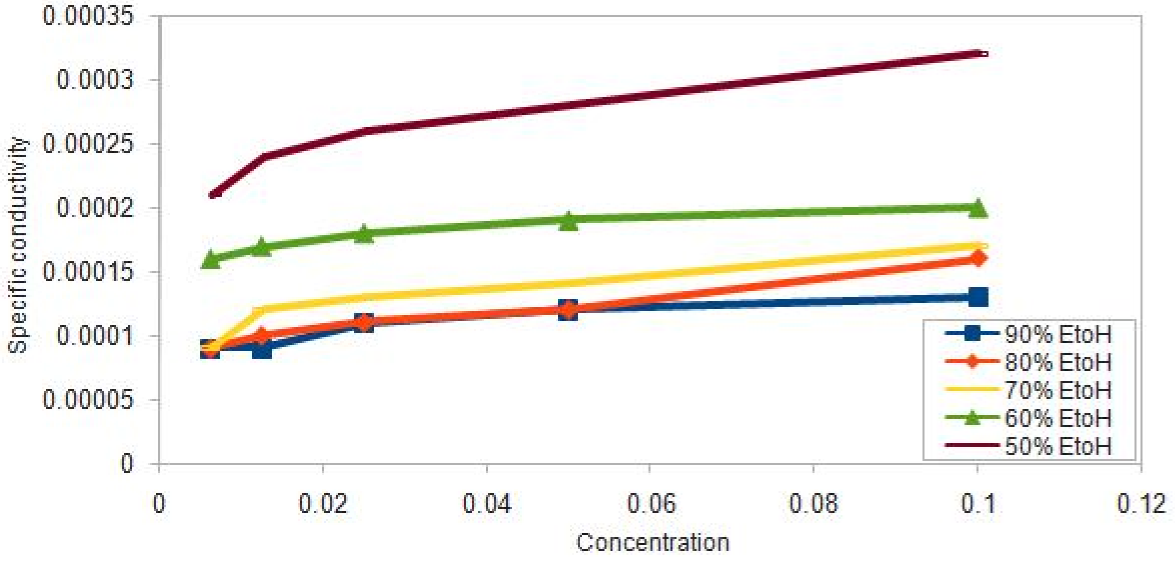

In figure 2, Equivalent conductance against square root of concentration (λ vs√c) plots is drawn to get the value of the equivalent conductance of 3-nitrobenzoic acid solution in ethanol water mixtures in infinite dilution for each of the water ethanol mixtures.

Figure 2: Equivalent conductance vs square root of concentration

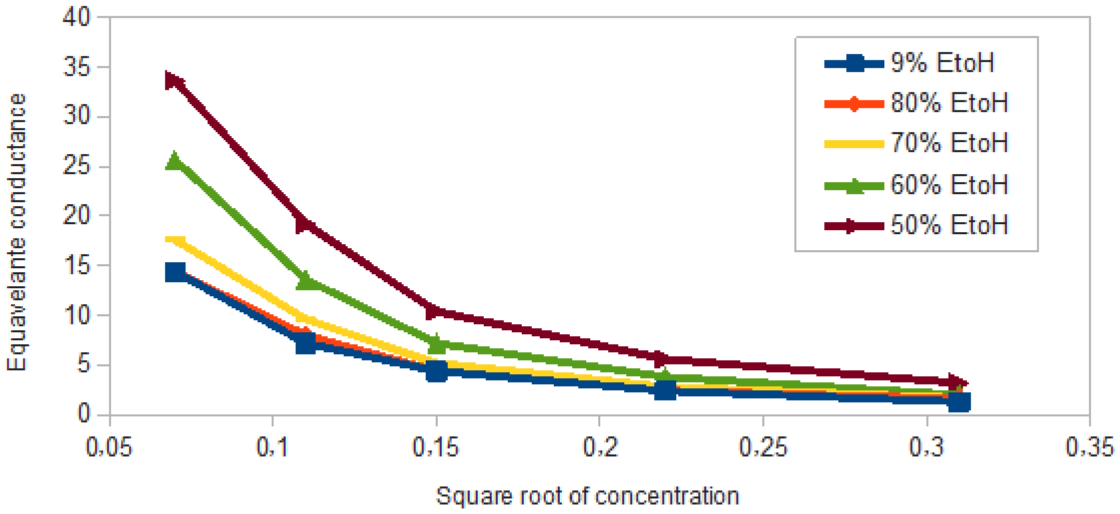

The change in decrease of ionic association is obtained with increase in ethanol content is the actual trend. In figure 2 the variation in the conductivity values of 3-nitrobenzoic acid is calculated. Between the solute and solvent molecules the equivalent conductance variation shows that there is an increased intermolecular interaction. When the percentage of mass in ethanol increases the limiting conductance $\lambda\infty$ decreases. In the solution phase the structural changes occurs as the ethanol starts dominating at advanced proportion of alcohol.

CONCLUSION

In the field of solution chemistry, the nature of intermolecular interactions has been studied widely by using conductivity which is one of the powerful medium. In a binary liquid mixture the solubility profile, extent of dissociation and the kinetics of a reaction were studied. The α value increases with the increase in concentration of 3-nitrobenzoic acid. This leads to the reality that at higher ethanol proportions strong intermolecular association of the ethanol solute molecules takes place.

REFERENCES

1. Radhika V & Manikyamba P. (2008), “Conductance and solvation behaviour of benzimidazolium dichloromate in Dimethyl sulphoxide – Water mixture”, Indian J. Chem., Vol.47.A, 1814- 1817.
2. Ishwara Bhat J & Sree latha TN.(2005), “Effect of Ethanol on the solvation behaviour of BI3 in acetonitrile, methanol and DMF as a function of temperature”, J. Mol. Liq., Vol.116.3, 175-180.
3. Dip Singh Gill, Anand H, Kumari A & Puri JK.(2004), “Study on the Comparative solvation behaviour of Na+ and Cu+ cations in acetonitrile + N,N dimethyl formamide mixtures at 298K”, Natur forsch, Vol.59.9, 615-620.
4. Ajaya Bhattarai , Deepak Sapkota , Netra P.Subedi , Manoj Khanal & Tulsi P.Niraula.(2011), “Conductance of Sodium Nitrate in Methanol Water Mixtures at different temperatures”, Nepal Journal of Science and Technology, Vol.12, 187-192.
5. Moazzem Hossen S.M , Md. Shahidul Silam , Mir Monir Hossain , Mahammed Enamul Hoque , & Gazi Akteruzzaman.(2012), “ Spectrophotometric Method for determination of dissociation constant of weak acid like 2,4- Dinitrophenol in 1-Propanol-water mixtures at 24.5±0.5ºC”,Der pharma Chemica, Vol.4.4, 1375- 1384.
6. Frank .F, Ives.D.J.G & Quart.Rev.(1996), “Temperature Dependence of Activation Volumes of Solvolysis Reactions in Light and Heavy Water “, Vol.20,1.
7. Kannappan V, Xaxier Jesu Raja S & Jaya Santhi R.(2003), “Ultrasonic study of induced dipole dipole intractions in binary mixtures”,Indian J Pure Appl Phys, Vol.41, 690.
8. Pandharinath S, Patil V U & Hasan Mehdi.(2001), “Intermolecular interaction in binary liquid mixture by ultrasonic measurements “,J Indian Chem Soc, Vol.78, 368.
9. Ali Anwar, Nain Anil Kumar, Sharma Vinod Kumar & Ahmad Shaki.(2001),” Theoretical Ultrasonic Velocities in Binary Liquid Mixture Containing Aniline and Anisole at Different Temperatures – A Comparative Study”, Acoust Lett, Vol.24, 9.
10. Kannappan V, Jaya Santhi R & Xaxier Jesu Raja S.(2003), “Ultrasonics investigation of induced dipole - induced dipole interactions in binary mixtures at 298K”, Phys Chem Liq., Vol.14, 133.
11. Kannappan V, Jaya Santhi R & E J P Malar.(2002),” Ultrasonic Studies on Charge Transfer Complexes of Cyclo Alkanones with Chloroform in n -Hexane Solutions”, Phys Chem Liq., Vol.40, 507.
12. Kannappan V & Jaya Santhi R.(2001),” Ultrasonic studies on dye stain removal by surfactants”, J Acoust Soc Ind., Vol.29, 192.
13. Deepali P, Gulwade Narwade M L & Wadodkar K N.(2004),” Ultrasonic behavior in study of molecular interactions of substituted azole in N,N-dimethyl formamide at different temperatures and concentrations”, Indian J Chem., Vol.43.A, 2102-2104.
14. Arul G & Palaniappan L.(2001), “Molecular interaction studies in the ternary mixture of cyclohexane + toluene + 2 – propanol”, Indian J Pure Appl Phys., Vol.39, 561 – 564.
15. A. Ali, S. Abida, S. Hyder & A.K. Nain.(2002), “Ultrasonic study and molecular interactions in binary liquid mixture”,Indian J. Phys., Vol.76.B .5, 661–667.

International Journal of Advance and Innovative Research
Volume 6, Issue 1 (VI): January - March, 2019
ISSN 2394 - 7780

SYNTHESIS AND CHARACTERISATION OF HAP@AL_2O_3 CORE-SHELL NANOPARTICLES FOR ANTIBACTERIAL ACTIVITY

Irusappan Ramesh, R. A Kalaivani, K. S. Meena

ABSTACT

The hydroxyapatite (HAp) NPs was synthesized by co-precipitation method and Al_2O_3 *coating by sol-gel process. HAp@*Al_2O_3 *core-shell nanostructure was synthesized and characterized by HR-Tem, XRD, and FTIR techniques. The antibacterial activity of HAp and HAp@*Al_2O_3 *core-shell NPs was tested using Escherichia coli (E.coli) and Staphylococcus aureus (S.aureus) as model strains of gram negative and gram positive bacteria, respectively.*

Moreover, HAp@Al_2O_3 *coatings are exhibit excellent antibacterial properties against Escherichia coli (E. coli) and Staphylococcus aureus (S.aureus). The results confirm that the* Al_2O_3 *coated HAp nanopowders exhibit large specific surface area and good antibacterial activities.*

1. INTRODUCTION

Hydroxyapatite (HAp) is a calcium phosphate based ceramic (Ca/P ratio of 1.66) with a chemical composition ($Ca_{10}(PO_4)_5(OH)_2$) similar to that of bone. HAp has been widely accepted in the biomedical industry for orthopedics, maxillofacial surgery and dental implants because of its biocompatibility and osseointegration[1]. HAp has achieved excellent results as bioceramics in bone-substituted operations and in teeth repair due to its unique mechanical properties and bioactivity[2-3].However its clinical applicability is restricted due to its poor mechanical strength [4]. Hence, there is a need to improve the mechanical properties of the HAp coatings without compromising the biocompatibility. Several research studies are being undertaken to overcome this limitation by preparing nanocomposites with reinforcing polymers, metal oxides and strong bioceramics [5-7]. Despite the advantages that HAp presents, the brittle nature, and low fracture toughness of HAp coating often result in rapid wear, and premature fracture of the coated layer. Inorganic metal oxide nanoparticles can be used as effective disinfectants in view of their non toxic profile, stability and antibacterial activities[8]. As a response to such need, many efforts have attempted to enhance the mechanical properties of HAp via the addition of secondary ceramic reinforcement materials such as Al_2O_3, ZrO_2, TiO_2[9-17]. Many studies has been reported metal oxides such as CuO[18], TiO_2[19], ZnO[20], CeO[21-22], coated HAp NPs was investigated antibacterial activity against many bacterial strains. With extensive application in many areas, however the use of HAP@Al_2O_3 Core-Shell nanoparticles towards antibacterial activity has not yet been investigated. Al_2O_3 has a variety of commercial and industrial uses and is one of the most important commercial ceramic materials[23]. Al_2O_3-NPs also have biological applications such as biosensors[24]. Bio filtration and drug delivery[25], antigen delivery for immunization purposes[26], and bactericides[27-29].The antimicrobial activity of nanoscale alumina has been reported against the bacillus subtilis, Escherichia coli and P. fluorescens [30]. Alumina coatings have been widely used for anti-wear and anticorrosion applications due to their high hardness, chemical inertness and high melting point, as well as to their high resistance to abrasion and erosion[31-32]. Although Al_2O_3 coatings are selected for their favourable mechanical properties, they do not meet the requirement of antibacterial behaviour, which has limited their application in microbiologically influenced corrosion, water treatment industry and environmental protection etc. Therefore, considerable efforts have been made to develop the antibacterial properties of Al_2O_3 coatings [33-34]. Al_2O_3 coatings could be prepared by techniques such as chemical vapour deposition (CVD), physical vapour deposition (PVD), sol–gel, plasma electrolytic oxidation (PEO) and plasma spray[35]. It was well known that alumina oxide nanoparticles exhibit antimicrobial properties. But, free radical scavenging property of the alumina particles may cause lowered antimicrobial activity and as a result even at higher concentration, the particles exhibit mild toxicity toward micro organisms. Only limited information is available on the antimicrobial properties of aluminium oxide nanoparticles (Al_2O_3 NPs). In this paper, Al_2O_3 coated HAp nanoparticles were synthesized and characterized by HR-TEM, XRD, and FTIR, techniques. The antibacterial activity of HAp@ Al_2O_3 core-shell nanoparticles were investigated against two major pathogenic strains E.Coli and S. aureus.

2. EXPERIMENTAL SECTION

2.1 Chemicals

Special grade reagents calciumnitrate tetrahydrate $Ca(NO_3)_24H_2O$ (Aldrich Chemicals Ltd., USA), diammonium hydrogen phosphate $(NH_4)_2HPO_4$ (Aldrich Chemicals Ltd., USA), Tetraethylorthosilicate (TEOS) (Sigma Chemicals, USA), Ethanol (SISCO Research Laboratories, India) was used for silica coating and ammonia

(25% aqueous solution) was used as catalysts. All other chemicals used were analytical grade and without further purification. Mill-Q water was used in all the preparations.

2.2. Preparation of HAp Nanoparticles

The HAp NPs was prepared by slight modification of the method described in the literature [36]. Briefly, 1 M of $Ca(NO_3)_{24}H_2O$ and 0.6 M of $(NH_4)_2HPO_4$ were dissolved in Milli-Q water separately. The pH of both aqueous solutions was brought to 11 by using 25% of NH_4OH solution. Under vigorous stirring the $Ca(NO_3)_2$ was added dropwise to $(NH_4)_2HPO_4$ solution over a period of 1 h to produce a milky white precipitate, which was then stirred for 1 h. Then the reflux process was employed at 100 ^{0}C for 1 h followed by aging for 24 h. Finally, the obtained product was then washed with distilled water, centrifuged and dried at 100 ^{0}C for 12 h and then calcined at 400 ^{0}C for 3 h.

2.3. Synthesis of Al_2O_3 NPs

Alumina NPs was synthesized by sol-gel method. In brief, 0.1 M $AlCl_3$ was added into 60 ml of ethanolic solution by adding a 28% NH_3 solution a gel was formed. The gel was let to maturate for 30 h at room temperature and then dried at 100 ^{0}C for 24 hours.

Synthesis of HAp@Al_2O_3 core-shell NPs.

50 mg of Al_2O_3 were dropped into Milli-Q water and homogenized for 10 min with an ultrasonic-homogenizer. Then, as prepared HAp NPs was added to Al_2O_3 suspension and stirred at RT for 2 h. The HAp@Al_2O_3 core-shell suspension was obtained in the same conditions described forward for the HAp. The suspension obtained was stirred for 24 h and the resulting precipitates were placed for 2 h in an oil bath set at 70 ^{0}C. The dried powder calcinated at 600 ^{0}C for 2 h.

2.4. Antibacterial activity

Agar well diffusion method

Agar well-diffusion method was followed to determine the antimicrobial activity. Nutrient agar (NA) plates were swabbed (sterile cotton swabs) with 8 hour old - broth culture of respective bacteria. Wells (10mm diameter and about 2 cm a part) were made in each of these plates using sterile cork borer. The plates were incubated at 37°C for 18-24 h for bacterial pathogens (100 µl) and spread evenly on the plate. After 20 minutes, the wells were filled with compound at 100, 200,300,400,500 and 600 µg/ml concentrations, The diameter of the inhibition zone (mm) was measured and the activity index was also calculated. Triplicates were maintained and the experiment was repeated thrice, for each replicates the readings were taken in three different fixed directions and the average values were recorded.

2.5. Characterization of NPs.

UV–visible spectra were recorded in a spectrophotometer (Perkin Elmer Lambda 35). High resolution transmission electron microscopy (HRTEM) photographs were taken using a JEOL JEM -3010 Electron microscope operating at 300 keV. The magnifying power used was 600 and 800k times. X-ray diffraction (XRD) patterns were taken from X'pert PRO PANalytical diffractometer operating with CuK (radiation (λ=1. 5406A°) source. Fourier transform infrared (FT-IR) spectra was measured on a FT-IR spectrometer (Bruker IFS 55, Fällanden, Switzerland) using the KBr pellet technique.

3. RESULT AND DISCUSSION

3.1. HR-TEM.

The transmission electron microscopic analysis was carried out to confirm the particle size, growth pattern and distribution of crystallites. The HR-TEM image of alumina coated HAp nanoparticle shown in Figure.(1a,b,&c). The image indicated that the as-synthesized HAp powders was mono-dispersive and had a smooth surface and a rod-like shape, and the particle of diameter in the range of 10-15 nm was observed. The crystalline structures of the HAp nanoparticle was further confirmed by selected-area electron diffraction (SAED) image investigations in (Fig-1b). The HR-TEM image of alumina coated HAp nanoparticle shown in (Fig.1c) clearly displays the core– shell structure image of alumina coated HAp particles, in which tinge shell is ascribed to alumina. A nearly well defined spherical morphology is observed and the HAp particles appear to be associated within Al_2O_3 shell. The boundary between the core HAp and the shell Al_2O_3 is very much distinct. The particle size diameter is nearly 15 nm. This image illustrates that particle has a thin capping of Al_2O_3 shell of thickness in the range ~20 nm. The observed sizes of the crystallites are comparable with those calculated from the XRD pattern.

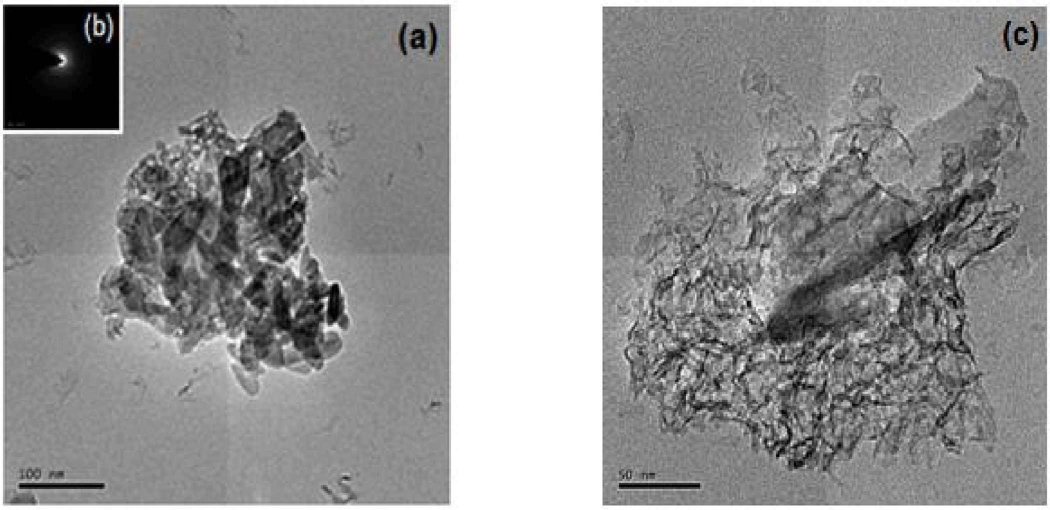

Fig-1: HR-TEM image of (a) HAp and (b) HAp@ Al_2O_3 core-shell NPs.

3.2. XRD Anasysis.

The XRD pattern of the as prepared pure HAp and HAp@Al_2O_3 core-shell nanoparticles calcined at 400 °C for 3 h is shown in the Fig. (1a & b).). After calcination, the powders reveal the crystallinity confirmation of $Ca_{10}(PO_4)_6(OH)_2$ (HAp), and can be well indexed to hexagonal crystal structure, ICDD(PDF Card file no. 9-432) [37].The scintillation detector present in the instrument moves through the required angle at specific counts and scans the sample with a start angle at 10^0 and a stop angle at 70^0.The output was obtained in the form of a graph with 2θ on x- axis and intensity on y-axis. From the result obtained, the average size of the nanoparticle was calculated using Scherer's formula,

$$D = 0.9\lambda / \beta \cos\theta$$

Where b, k and h is full width at half maximum (FWHM) of the intensity, incident wavelength (for Cu(ka), k = 1.54056 A °) and reflection angle, respectively. The diffracted peaks correspond to hexagonal system that confirms the phase pure hydroxyapatite formation in Fig.(1a) the peaks of HAp at 32^0 nm [38]. The peaks of HAp and Al_2O_3 become more distinct and also new additional peaks of Al_2O_3 at 23°, 50°, 53° and 66.5^0 are observed. These results indicate that the alumina reduces the crystallite size of HAp. Therefore, it is presumed that the introduction of alumina might affect crystalllinity of the HAp.

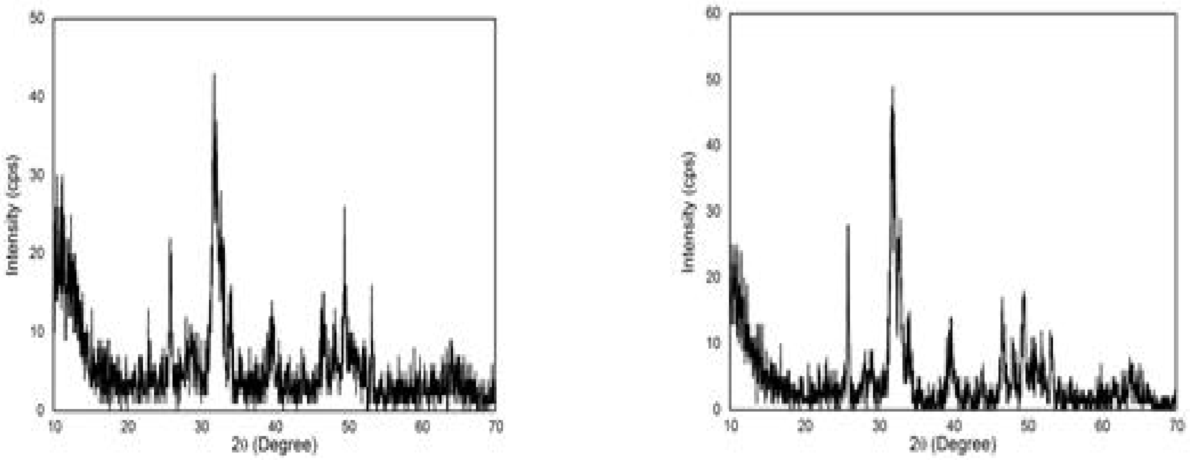

XRD patern of (a)HAp and (b)HAp@Al_2O_3 core-shell NPs

3.3. FTIR Analysis

Figure.(3a&b). shows the FTIR spectra of HAp and HAp@Al_2O_3 NPs respectively. The characteristic peaks for PO_4^{3-} appear at around 566, 1,036, and 601 cm-1[39-41]. The two additional peaks appearing at 884 and 724 cm^{-1} from Al_2O_3. The band at 2,932 cm-1 is assigned to C–H vibrations. The C–H could be attributed to the organic residues, which remained in HAp@Al_2O_3 Nps even after calcinations. The weak absorption band at 1,418.3 cm-1 stands for carbonate that might come from the atmosphere carbon dioxide during synthesis. The higher energy region peaks at 3,426 and 1,624 cm-1 are due to absorbed water and hydroxyl group of Al_2O_3 nanoparticles.[42]

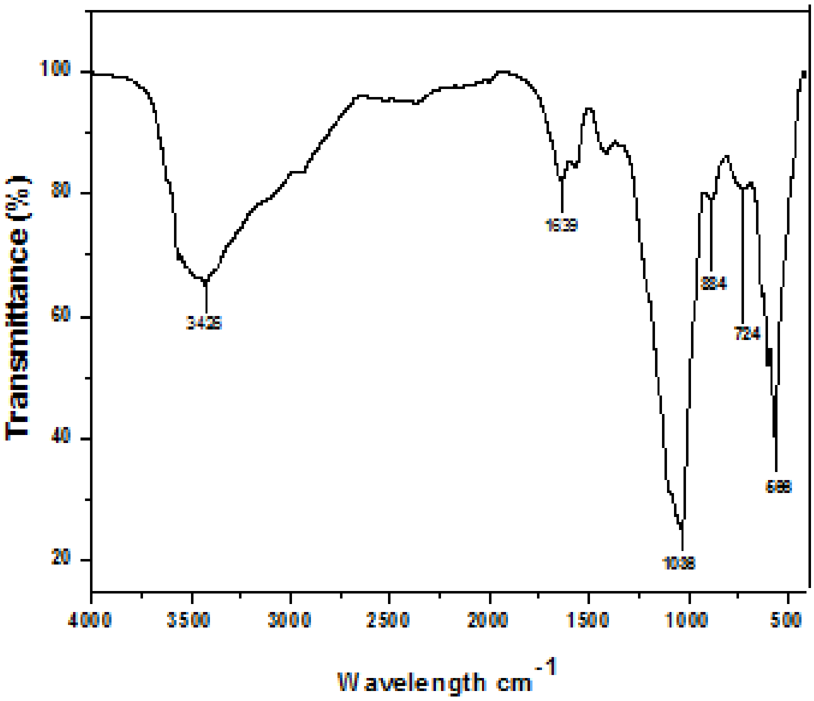

Fig-3: FTIR spectrum of HAp@Al_2O_3 core-shell NPs

3.4. Antibacterial activity

The antibacterial activity of pure HAp and HAp@Al_2O_3 core-shell NPs were investigated against two types of bacteria E.coli and S.aureus by agar diffusion method, and the results are shown in the Figure.4a&b. The structure of gram positive and gram negative cell was different compositions. The layer of peptidoglycan in gram positive bacteria is thicker than for gram negative bacteria which consequently decrease the penetrations of NPs to the cell wall of gram positive bacteria. According to these results, HAp without Al_2O_3 showed some cell reduction as well. This suggests that adhesion of microorganism cells to the particles of HAp may contribute to the overall reduction of cell number in liquid medium. The adhesion may facilitate contact of alumina ions with cells wall and thus enable their damaging effect to the cells.Metal ions in the crystal surface form strong bonds with thiole, imidazole, amino and carboxyl groups of microorganism membrane proteins, causing structural changes. A microorganism membrane with structural changes exhibits a significant increase in permeability, leaving the microorganism cells incapable of properly regulating transport through the plasma membrane and, finally, causing cell death. According to the results of the antibacterial activity, it can be concluded that Hap NPs is less susceptible to both E.coli and S.aureus strains than HAp@Al_2O_3 NPs.

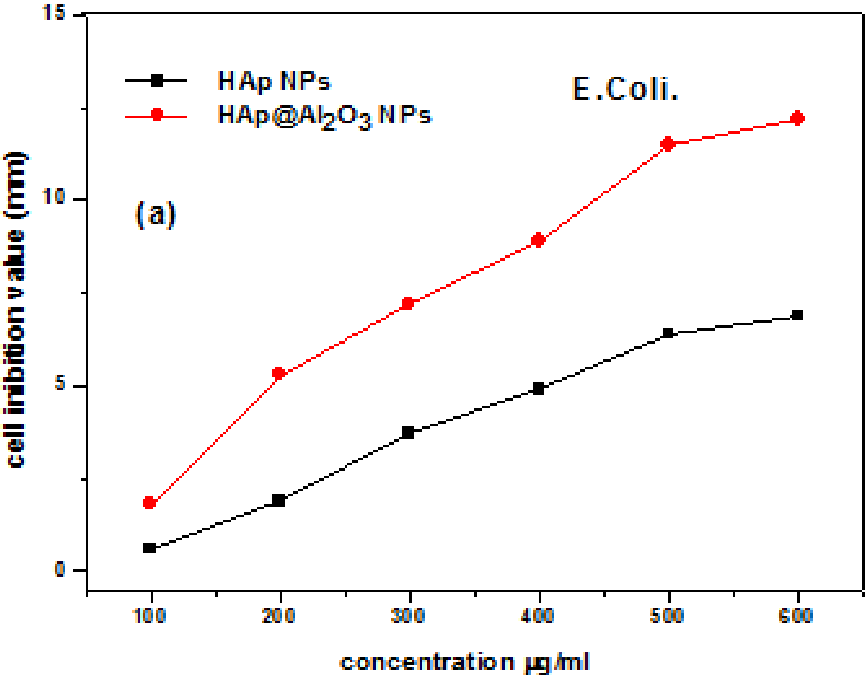

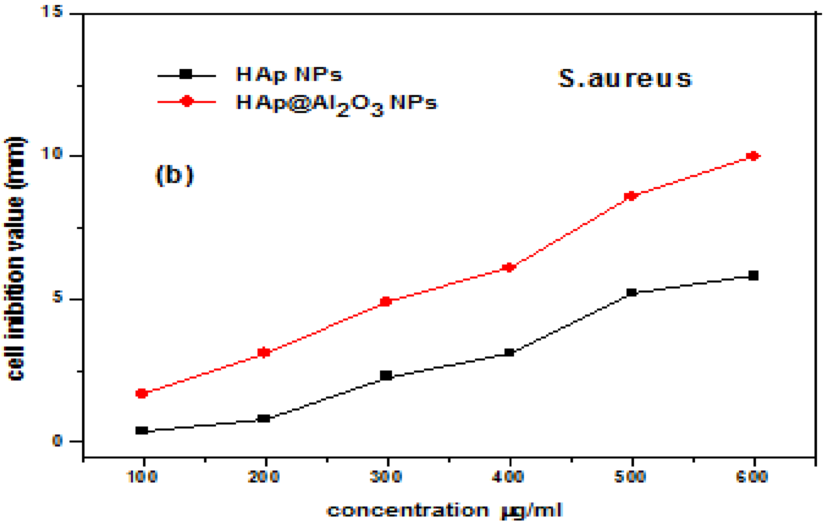

Fig: Inhibition curve of (a) E.Coli. and (b) S.aureus. in presence of HAp and HAp@Al_2O_3 core-shell NPs.

4. CONCUSION

HAp@Al_2O_3 core-shell nanostructure were synthesized and characterized by HR-Tem, XRD, and FTIR techniques. The antibacterial activity of HAp and HAp@Al_2O_3 core-shell NPs was tested using Escherichia coli (E. coli) and Staphylococcus aureus (S. aureus) as model strains of gram negative and gram positive bacteria, respectively. The results shown that Al_2O_3 coated HAp NPs exhibited excellent antibacterial activity when compared with the pure HAp Nps due to the Al_2O_3 shell not only prevent from aggregate which has increases the biocombatibility and create specific larger surface area of HAp core NPs. Thus it is concluded that the Al_2O_3 coated HAp core-shell Nps act as a good antibacterial agent, and its also suitable candidate for biomedical applications and water treatments.

REFERENCE

1. Q. Wang, G. Shirong, Z. Dekun, Wear 259 (2005) 952.
2. L. A. Capriotti, T. P. Beebe and J. P. Schneider, J. Am. Chem. Soc., 2007, 129, 5281 5287.
3. H. J. Zhou and J. Lee, Acta Biomater., 2011, 7, 2769–2781.
4. H. Zhou, J. Lee, Nanoscale hydroxyapatite particles for bone tissue engineering, Acta Biomater. 7 (2011) 2769-2781.
5. H. Itokawa, T. Hiraide, M. Moriya, M. Fujimoto, G. Nagashima, R. Suzuki, T. Fujimoto, A 12 month in vivo study on the response of bone to a hydroxyapatite polymethyl methacrylate cranioplasty composite, Biomater. 28 (2007) 4922-4927.
6. K.R. Mohamed, H.H. Beherei, G.T. EI Bassyouni, N. EI Mahallawy, Fabrication and mechanical evaluation of hydroxyapatite/oxide nano-composite materials, Mater. Sci. Eng., C 33 (2013) 4126-4132.
7. W. Kantana, P. Jarupoom, K. Pengpat, S. Eitssayeam, T. Tunkasiri, G. Rujijanagul, Properties of hydroxyapatite/zirconium oxide nanocomposites, Ceram. Int. 39 (2013) S379- S382.
8. Gordon T, Perlstein B, Houbara O, Felner I, Banin E, Margel S. Synthesis and characterization of zinc/iron oxide composite nanoparticles and their antibacterial properties. *Colloids and Surfaces A: Physicochemical and Engineering Aspects*. 2011; 374:1–8.
9. L. Fu, A.K. Khiam, P.L. Joo, J. Am. Ceram. Soc. 84 (4) (2002) 800.
10. K.H. Im, S.B. Lee, K.M. Kim, Y.K. Lee, Surf. Coat. Technol. 202 (2007) 1135.
11. J. Li, B. Fartash, L. Hermansson, Biomaterials 16 (1995) 417.
12. M. Inuzuka, S. Nakamura, S. Kishi, K. Yoshida, K. Hashimoto, Y. Toda, K. Yamashita, Solid State Ionics 172 (2004) 509.
13. D. Singh, M.D.L.C. Lorenzo-Martin, F. Gutiérrez-Mora, J.L. Routbort, E.D. Case, Acta Biomater. 2 (2006) 669.
14. Z. Evis, R.H. Doremus, J. Mater. Sci. 42 (2007) 2426.

15. S. Gautier, E. Champion, D.B. Assollant, J. Euro. Ceram. Soc. 17 (1997) 1361.
16. Z. Evis, R.H. Doremus, Mater. Lett. 59 (2005) 3824.
17. L.P. He, M. Yui-Wing, Z.Z. Chen, Mater. Sci. Eng. A 367 (2004) 51.
18. V. Stani'c, S. Dimitrijevi'c, J. Anti'c-Stankovi'c et al., "Synthesis, characterization and antimicrobial activity of copper and zincdoped hydroxyapatite nanopowders," *Applied Surface Science*, vol. 256, no. 20, pp. 6083–6089, 2010.
19. M. Wakamura, "Photocatalysis by calcium hydroxyapatite modified by Ti (IV)," *Fujitsu Scientific and Technical Journal*, vol. 41, no. 2, pp. 181–190, 2005.
20. X. Chen, Q. L. Tang, Y. J. Zhu, C. L. Zhu, and X. P. Feng, "Synthesis and antibacterial property of zinc loaded hydroxyapatite nanorods," *Materials Letters*, vol. 89, pp. 233–235, 2012.
21. Z. Feng, Y. Liao, and M. Ye, "Synthesis and structure of ceriumsubstituted hydroxyapatite," *Journal of Materials Science: Materials in Medicine*, vol. 16, no. 5, pp. 417–421, 2005.
22. Y. Lin, Z. Yang, and J. Cheng, "Preparation, characterization and antibacterial property of ceriumsubstituted hydroxyapatite nanoparticles," *Journal of Rare Earths*, vol. 25, no. 4, pp. 452– 456, 2007.
23. Uyeda R (1991) Studies of ultrafine particles in Japan: crystallography. Methods of preparation and technological applications. Prog Mater Sci 35:96
24. Liu X, Luo L, Ding Y, Xu Y (2011) Amperometric biosensors based on alumina nanoparticles-chitosan-horseradish peroxidase nanobiocomposites for the determination of phenolic compounds. Analyst 136:696–701
25. Monteiro-Riviere NA, Oldenburg SJ, Inman AO (2010) Interactions of aluminum nanoparticles with human epidermal keratinocytes. J Appl Toxicol 30:276–285
26. Skwarczynski M, Toth I (2011) Peptide-based subunit nanovaccines. Curr Drug Deliv 8:282–289
27. Sadiq MI, Chowdhury B, Chandrasekaran N, Mukherjeem A (2009) Antimicrobial sensitivity of Escherichia coli to alumina nanoparticles. Nanomedicine 5:282–286
28. Ansari MA, Khan HM, Khan AA, Pal R, Cameotra SS (2013) Antibacterial potential of Al2O3 nanoparticles against multi drug resistance strains of Staphylococcus aureus isolated from skin exudates. J Nanopart Res
29. Ansari MA, Khan HM, Khan AA, Cameotra SS, Saquib Q, Musarrat J (2014b) Interaction of Al2O3 nanoparticles with Escherichia coli and their cell envelope biomolecules. J Appl Microbiol 116(4):772–783
30. Balasubramanyam A, Sailaja N, Mahboob M, Rahman MF, Hussain SM, Grover P (2010) In vitro mutagenicity assessment of aluminium oxide nanomaterials using the Salmonella microsome assay. Toxicol In Vitro 24:1871–1876.
31. H. Mindivan, C. Tekmen, B. Dikici, Y. Tsunekawa and M. Gavgali, Mater. Des., 2009, 30, 4516–4520.
32. A. Rico, P. Poza and J. Rodr´ıguez, Vacuum, 2013, 88, 149–154.
33. M. Pisarek, A. Roguska, A. Kudelski, M. Andrzejczuk, M. Janik-Czachor and K. J. Kurzydłowski, Mater. Chem. Phys., 2013, 139, 55–65.
34. C. Fajardo, M. L. Sacca, G. Costa, M. Nande and M. Martin, Sci. Total Environ., 2014, 473–474, 254–261.
35. F. Guidi, G. Moretti, G. Carta, M. Natali, G. Rossetto, Z. Pierino, G. Salmaso and V. Rigato, Electrochim. Acta, 2005, 50, 4609–4614.
36. Bouyer E, Gitzhofer F, Boulos MI. Morphological study of hydroxyapatite nanocrystal suspension. J Mater Sci Mater Med 2000; 11: 523-31.
37. Y. Zhang, L. Zhou, D. Li, N. Xue, X. Xu, J. Li, Chem. Phys. Lett. 376, 493–497 (2003)
38. Y.X. Pang, X. Bao, Influence of temperature, ripening time and calcination on the morphology and crystallinity of hydroxyapatite nanoparticles, J. Eur. Ceram. Soc. 23 (2003) 1697-1704.
39. K. Lin, J. Chang, R. Cheng, M. Ruan, Mater. Lett. 61, 1683–1687 (2007)

40. Y. Sun, G. Guo, Z. Wang, H. Guo, Ceram. Int. 32, 951–954 (2006)
41. H. Chen, B.H. Clarkson, K. Sun, J.F. Mansfield, J. Colloid Interface Sci. 288, 97–103 (2005)
42. Socrates, G. Infrared and Raman Characteristic Group Frequencies - Tables and Charts. 3. John Wiley & Sons Ltd; West Sussex, England: 2001.

International Journal of Advance and Innovative Research
Volume 6, Issue 1 (VI): January - March, 2019

ISSN 2394 - 7780

SYNTHESIS AND CHARACTERIZATION OF TITANATE NANOFIBER USING HYDROTHERMAL METHOD

M. Alexander, R. A. Kalaivani, U. Senthilkumar, M. Elumalai, and R. Ganesamoorthy
Department of Chemistry, Vels Institute of Science, Technology & Advanced Studies, Chennai
E-mail: chemalexander@gmail.com

ABSTRACT

In this work, we develop simple and one-step hydrothermal preparation of commercial titanet nanofiber (TNF) using 10 M NaOH. The bulk TiO_2 *used as the precursor at 180°C. The hydrochloric acid used for neutralizing and forming agent for large scale production of TNF. The preparation conditions are much milder and simpler than those of conventional methods. The prepared TNF length is ranges from 1-2 µm and diameter of the nanofiber is 50-70 nm, which is characterized by FT-IR, XRD and SEM and EDX pattern.*

Keywords: Titanium dioxide. Titanate Nanofiber

INTRODUCTION

Titanate nanofiber (TNF) has three crystalline polymorphs such as rutile, anatase, andbrookite. Each phase has various physical properties, such as the refractive index, chemical reactivity, and photochemical reactivity. Consequently, it is important to develop preparation methods in which the crystalline form as well as the size and shape of the TiO_2 nanocrystals can be controlled. Among three polymorphs of TiO_2, the rutile phase crystalline materials have exhibits excellent physical properties. that has made it the most widely used white pigment on the world market as a result of its exceptional high refractive index, scattering efficiency, opacity, chemical inertness, and photo catalytic properties. But unlike anatase, the synthesis of rutile TiO_2 nanocrystals is much more difficult because most of the methods adopted for the synthesis of TiO_2 produce the kinetically controlled anatase, at low temperatures.(Thiele, 1998; Patton, 1973)

TiO_2 possesses interesting catalytic properties, optical, dielectric and that result in industrial applications such as pigments, dye-sensitized solar cells, (Ramakrishna, 2001) filters for catalyst supports, and photocatalysis.(McFarland, 2003; Anderson, 2002; Regan, 1991) As a pure component or combined with other elements, TiO_2 has been associated with improved sensitivity to humidity (Yen, 1989) and enhanced mechanical properties (Matsumoto, 2000) and catalytic activity, (Asahi 2001) and it has used in membrane for separations of reaction mixture.(Chemseddine, 1990) Being nontoxic, TiO_2 promises to create chemical and biological hybrid nanocomposites that can be introduced into cells that can further be used to initiate intracellular processes.(Thiele, 1998)1Moreover, TiO_2 has been recognized to make hydroxyapatite titania composites to provide biocompatible materials.(Kim, 2005; Xu, 2004) To get desirable applications from nonmaterial, due to reactive organic groups have to be attached to the surface of the inorganic nanocrystals.

EXPERIMENTAL SECTION

Chemicals required

The titanium dioxide (TiO_2) was purchased from sigma Aldrich chemicals. The sodium hydroxide (NaOH) and Hydrochloric acid (HCL) was getting from SRL chemicals.

Preparation of Titanate nanofiber

The titanium dioxide (TiO_2) is taken 0.200 g, which is dissolved in 10 M NaOH aqueous solution. The above dispersed mixture of the solution stir for 1 h, the mixture poured in sealed autoclave and then keep in muffle furnace 24 h at maintain at 180^{o}C. After then the reaction mixture washed with water and neutralized with 0.1M HCl. The TiO_2 is converted into titanate naanofiber which is finally washed with ethanol. The formed TNF dried at 100^{o}C for 12 h.

RESULT AND DISCUSSION

The FT-IR spectrum of TNF

The FTIR spectrum of TNF is shown in figure 1. As seen from this figure, the range of 3000–3650 cm^{-1} is strong peak is observed which is attributed to the stretching vibration of –OH. In particular, the content of water adsorbed in titania nanofiber. The strong band in the 753-491 cm^{-1} is associated with the characteristic vibration modes of TiO_2. The absorptions at 1647 cm-1 may be related to hydroxyl groups of molecular water.

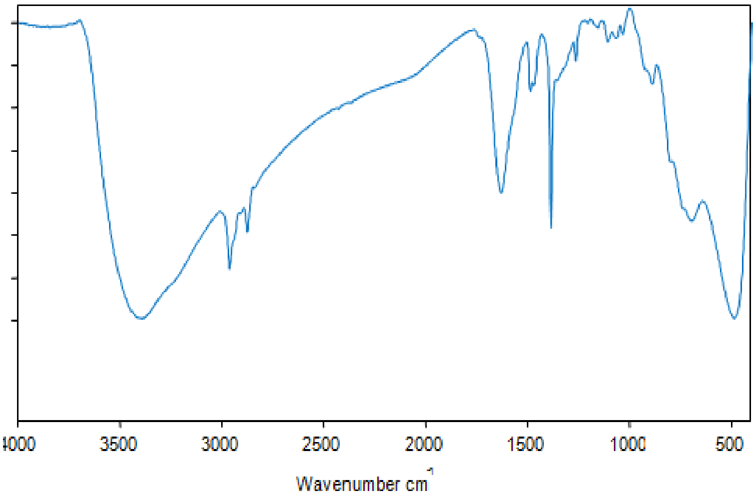

Figure-1: FTIR spectrum of titanium dioxide nanofiber in hydrothermal method

The XRD analysis of TNF

The crystal structure of the TNF sample is determined by XRD analysis as shown in Fig. 2. All the diffraction peaks can be well indexed to anatase phase of TiO_2 (JCPDS 71- 1169). No peaks of impurities were detected in the XRD patterns, indicating the high purity of the products. The strong and sharp peaks also confirm the well crystallization of the synthesized products. The X-Ray diffraction peak of TNF was appeared at 25.00, 27.59, and 48.00 with corresponding 101, 103, and 200 crystal lattice plane. The XRD pattern was shows broad peak, which is indicate TNF has size 50 nm.

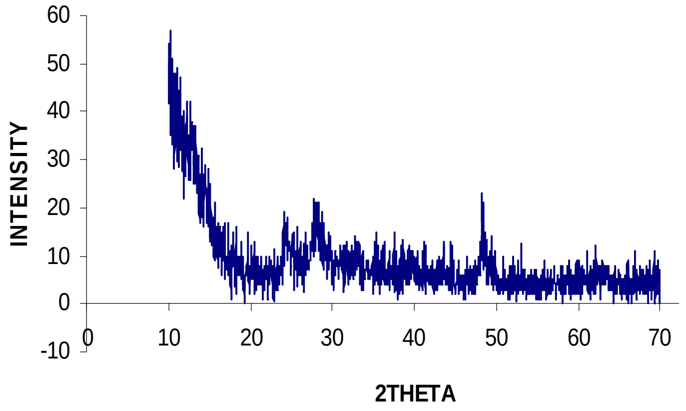

Figure-2: XRD pattern of titanium dioxide nanofiber in hydrothermal method

The SEM image and EDX pattern of TNT

The structure of TNF is further confirmed by their corresponding SEM images. A typical SEM image is shown in Figure 3. It indicates that the TNF length is 1-2 µm. These observations are in good agreement with the fiber structure; the diameter of the TNF is in the range of 50-60 nm, as shown in Figure 3. Further observation shows that the as-prepared TiO_2 fiber have rough external surfaces, the corresponding energy dispersive X-ray pattern was shows in Figure 3, which was contain Ti, O elements, the Ti element is indicated higher intensity peak at 4.5 and 5.0 KeV and also the oxygen element is indicated at 0.5 KeV.

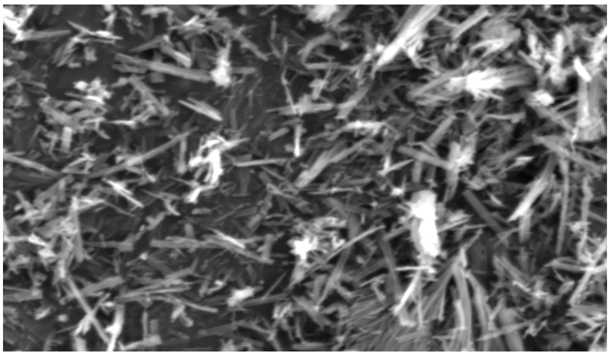

Figure-3: the SEM images of titanium dioxide nanofiber in hydrothermal method

CONCLUSION

We successfully develop the hydrothermal preparation of TNF using 10 M NaOH. The bulk TiO_2 is used as the precursor at 180°C. The preparation conditions are much milder and simpler. The TNF has length 1-2 µm. The SEM image observations are good agreement with the fiber structure and the diameter of the TNF is in the range of 50-60 nm. This types of nonmaterial used for reactive organic groups can be attached to the surface.

REFERENCES

[1] Thiele E. S, French R. H, (1998) “Light-Scattering Properties of Representative, Morphological Rutile Titania Particles Studied Using a Finite-Element Method”, J. Am. Ceram. Soc. 81, 469-479.

[2] Patton, T. C. Pigment Handbook; Wiley: New York, 1973.

[3] Ramakrishna G, Ghosh H. N, (2001) “Emission from the Charge Transfer State of Xanthene Dye-Sensitized TiO2 Nanoparticles: A New Approach to Determining Back Electron Transfer Rate and Verifying the Marcus Inverted Regime”, J. Phys. Chem. B 105, 7000-7008.

[4] McFarland, E. W Tang, J. (2003) “A photovoltaic device structure based on internal electron emission”, Nature 421, 616-618.

[5] Anderson M O, sterlund L, Ljungstrom S, Palmqvist A, (2002) “Preparation of Nanosize Anatase and Rutile TiO2 by Hydrothermal Treatment of Microemulsions and Their Activity for Photocatalytic Wet Oxidation of Phenol”, J. Phys. Chem. B 106, 10674-10679.

[6] Regan B. O, Gra¨tzel M. A, (1991) “low-cost, high-efficiency solar cell based on dye-sensitized colloidal TiO2 films”, Nature 353, 737-740.

[7] Yen Y. C, Tseung T. T, Chang D. A, (1989) “Electrical Properties of Porous Titania Ceramic Humidity Sensors”, J. Am. Ceram. Soc. 72, 1472-1475.

[8] Matsumoto T, Murakami Y, Takasu Y, (2000) Chem. Lett. 29, 348-349.

[9] Asahi R, Morikawa T, Ohwaki T, Aoki K, Taga Y, (2001) “Visible-Light Photocatalysis in Nitrogen-Doped Titanium Oxides”, Science 293, 269-271.

[10] Chemseddine, A Boehm, H. P. (1990) “A study of the primary step in the photochemical degradation of acetic acid and chloroacetic acids on a TiO2 photocatalyst”, J. Mol. Catal. 60, 295-311.

[11] Paunesku T, Rajh T, Wiederrecht G, Maser J, Vogt T, Stojicevic N, Protic M, Lai B, Oryhon J, Thurnauer M, Woloschak G, (2003) “Biology of TiO2–oligonucleotide nanocomposites”, Nat. Mater. 2, 343-346.

[12] Kim H.W, Kim H.E, Salih V, Knowels J. C, (2005) “Fluor-hydroxyapatite sol-gel coating on titanium substrate for hard tissue implants”, J. Biomed. Mater. Res. 72, 1-8.

[13] Xu C, Xu K, Gu G, Zheng R, Liu H, Zhang X, Guo Z, Xu B, (2004) “Dopamine as A Robust Anchor to Immobilize Functional Molecules on the Iron Oxide Shell of Magnetic Nanoparticles”, J. Am. Chem. Soc. 126, 9938-9939.

[14] Dimitrijevic N. M, Saponjic Z. V, Rabatic B. M, Rajh T, (2005) “Assembly and Charge Transfer in Hybrid TiO_2 Architectures Using Biotin−Avidin as a Connector”, J. Am. Chem. Soc. 127, 1344-1345.

[15] Niederberger M, GarnweitnerG, Krumeich F, Nesper R, Co¨lfen H, Antonietti M,. Tailoring (2004) “The Surface and Solubility Properties of Nanocrystalline Titania by a Nonaqueous In Situ Functionalization Process”, Chem. Mater. 16, 1202-1208.

[16] Rajh T, Chen L. X, Lukas K, Liu, T Thurnauer, M. C Tiede, D. M. (2002) “Surface Restructuring of Nanoparticles: An Efficient Route for Ligand−Metal Oxide Crosstalk”, J. Phys. Chem. B 106,

International Journal of Advance and Innovative Research
Volume 6, Issue 1 (VI): January - March, 2019

ISSN 2394 - 7780

REMOVAL OF HEAVY METALS BY ADSORPTION TECHNIQUE USING ACTIVATED CARBON– AN OVERVIEW

Meyyappan Revathi, D. Malathy, M. Elumalai and Subash Chandra Bose Raghu
Vels Institute of Science, Technology and Advanced Studies, Chennai

ABSTRACT

Modernization of the world requires huge number of heavy metals for decorative and protective purposes. Metal finishing industries utilizes those heavy metals during their processes. The untreated effluent from these industries having toxic heavy metals contaminates surface water resources as well as the ground water resources. Enormous researchers studying the removal of heavy metals from the effluents by using various techniques; among these adsorption process is one of the foremost efficient and cheap method for the removal of heavy metals. Variety of materials have been used as biosorbent for the removal of heavy metals which includes activated carbon, clay, vegetable wastes, fruit peels and rice husk etc., This review presents an overview of the efficiency of activated carbon prepared from various sources for the removal of heavy metals from metal finishing effluents. Furthermore, surface modified activated carbon prepared from biomaterials for the removal of heavy metals is reviewed as biosorbents.

Keywords: Heavy metal, Biosorbents, metal finishing effluents

INTRODUCTION

The contamination of waste water by heavy metal ions is a worldwide environmental problem due to their incremental accumulation in the food chain and continued persistence in the ecosystem [1]. Heavy metals differ widely in their chemical properties. There are more than 20 heavy metals, but some are of particular concern to human health: lead (Pb), cadmium (Cd), mercury (Hg), inorganic arsenic (As), copper (Cu), nickel (Ni) and zinc (Zn) according to the U.S. Agency for Toxic Substances and Disease Registry. They are highly toxic and can cause damaging effects even at very low concentrations. They tend to accumulate in the food chain and in the body and can be stored in soft and hard tissues. Consequently they tend to reach the environment from a vast array of anthropogenic sources as well as natural geochemical processes.

The heavy metals like lead, copper, cadmium, zinc and nickel are the most common pollutants found in industrial effluents. For instance, lead is extremely toxic and can damage the nervous system, kidneys, and reproductive system, particularly in children [2].

Exposure to some heavy metals, such as mercury and lead, may also cause development of autoimmunity, in which a person’s immune system attacks its own cells. This can lead to joint diseases such as rheumatoid arthritis, and diseases of the kidneys, circulatory system, nervous system, and damaging of the fetal brain.

REMOVAL OF HEAVY METAL POLLUTION

Today removal of heavy metals from water is being a challenging task and it can be achieved by different methods. The existing methods for the waste water treatment has its own disadvantages like uneconomical, it consumes lot of space, commercially they are unattractive and disposal problems. Table: 1 comprises the overall advantages and disadvantages of various treatment techniques. Hence there is a requirement of some other technique which can overcome all these problems in an appropriate manner.

Table-1: Comparison of technologies to heavy metal removal from wastewater

Method	Advantages	Disadvantages
Chemical precipitation	• Simple • Inexpensive • Most of the metals can be removed	• Large amount of sludge produced • Disposal problems
Ion exchange	• High regeneration of materials • Metal selective	• High cost • Less number of metal ions removed
Electrochemical methods	• Metal selective • Non consumption of chemicals • Pure metals can be achieved	• High capital cost • High running cost

Adsorption using activated carbon	• Most of metals can be removed • High efficiency (99%)	• Cost of activated carbon • No regeneration • Performance depends upon adsorbent
Using natural zeolite	• Most of the metals removed • Relatively less costly materials	• Low efficiency

Source: Farooq et al 2010 [3].

Adsorption is the widely used physical treatment method for heavy metal ion removal. In this technique, the heavy metal ions are transferred from waste water to the adsorbent surface. Basically, adsorption is a mass transfer process by which a substance is transferred from the liquid phase to the surface of a solid, and becomes bound by physical and/or chemical interactions. In general, there are three main steps involved in pollutant sorption onto solid sorbent: (i) the transport of the pollutant from the bulk solution to the sorbent surface; (ii) adsorption on the particle surface; and (iii) transport within the sorbent particle. Technical applicability and cost-effectiveness are the key factors that play major roles in the selection of the most suitable adsorbent to treat inorganic effluent.

There are number of successful systems which has been studied and developed using this technique. However, in the present review reported the activated carbon prepared from various sources and surface modified activated carbon which has been utilized as an adsorbent.

This article reviewed the suitability of AC that used in adsorption technique for purification heavy metals from water/wastewater.

ACTIVATED CARBON (AC)

AC undoubtedly has been the most popular and widely used adsorbent in wastewater treatment throughout the world. In the treatment of wastewater, it is used for purification, decolourization, and the removal of toxic organics and heavy metal ions [4]. Commercial activated carbons are prepared from a variety of carbonaceous raw materials. The qualities and characteristics of activated carbons depend on the physical and chemical properties of the starting materials and the activation methods used. Presently, lignite, peat, wood and coconut shell are the main common precursors for commercial activated carbons [5].

ACTIVATED CARBON FROM VARIOUS NATURAL SOURCES

In recent years, researches are focused on the production of activated carbon from cheap material such as agricultural waste. Activated carbon production from agricultural waste has two advantages. First, waste material is converted to useful, value added adsorbents and secondly, the produced activated carbons are used for removing organic chemicals and metals from wastewater [6]. Rice husk [7], rice straw [8], hazelnut shells [9], coir pith [10], Moringa oleifera (MO) wood [11], cotton seed shell [12], palm shell [13], hydrothermal char (HTC), a by-product from biomass hydrothermal liquefaction [14], Macadamia nutshells [15], bamboo dust [16], Areca NutWaste [17], corncob [18] were used for activated carbon production. Because of cheap, easy availability and having high adsorption capacity activated carbon has been utilized in various fields for purification including water. Since AC having significant weak acidic ion exchange character, activated carbon is effectively removing contaminants like trace metals and to adsorbing pollutants from wastewater.

ACTIVATED CARBON FOR HEAVY METAL IONS REMOVAL

Because of its large surface area and very excellent porosity the AC removing the heavy metal ions by electrostatic attraction with various surface functional groups. AC is easily prepared from readily available carbonaceous precursors such as coconut shell [19], Silk Cotton Hull [20], Hazelnut shell [21], Palm shell [22, 23] and agricultural wastes [24].

M. Chaudhuri & S. N. B. Saminal was prepared activated carbon from coir pith (CCAC) for the removal of lead from aqueous solutions. It shows maximum lead adsorption occurred at pH 5 and equilibrium adsorption was attained in 2.5 h [25]. CCAC followed pseudo second-order kinetics for lead removal. The maximum adsorption capacity and some operational parameters of activated carbon for the removal of heavy metals reported in the literature are summarized in Table.3

Table.2. Removal of heavy metals using activated carbon and their optimal operational conditions

Adsorbent	Metal ions removed	Optimum pH	Contact time required (min)	Dosage (gL^{-1})	Initial concentration studied ($mg\ L^{-1}$)	Maximum adsorption capacity (Q_{max}) ($mg\ g^{-1}$)	References
Silk Cotton Hull Carbon	Pb(II)	5-10	90	2.4 2.8 3.0	20 30 40	NA	[20]
Carbon prepared from *Recinius Communis Linn*	Fe(III) Cu(II) Co(II)	3	20	250	20	1.569 1.194 1.762	[26]
Hazelnut shell activated carbon	Ni(II)	7	180	NA	NA	5.77	[21]
Coir pith carbon	Ni(II) ions	5	40	1.2	NA	62.5	[27]
Palm shell activated carbon	Cu(II) ions Ni(II) ions Pb(II) ions	5 5 5	75 75 30	1 1 1	Mixed metals of 2.0 Cu, 1.5 Pb and 0.8 Ni	1.581 0.130 1.337	[22]
Granular activated carbon	Ni(II) ions	4 -10	300	1.2	20	1.49	[28]
Peanut hull carbon	Ni(II) ions	4 – 10	90	0.09	20	53.65	
Rice hull activated carbon	Cu(II) Cd(II)	6.90	80	40	15 15	5.10×10^{-5} 6.76×10^{-6}	[29]

SURFACE MODIFIED ACTIVATED CARBON

Based on the type and nature of the targeted heavy metals ions, the surface of AC may be modified to enhance the affinity. As an inert porous carrier material having large specific surface area, AC is capable of attracting a variety of chemicals. Depending on the application, there are different methods to modify AC, which make the surface accessible to a variety of reactants. n general, the surface modification of AC is carried out after the activation of reactive sites. As shown in Figure 1, the modification can be categorized in three classes: chemical modification, physical modification and biological modification.

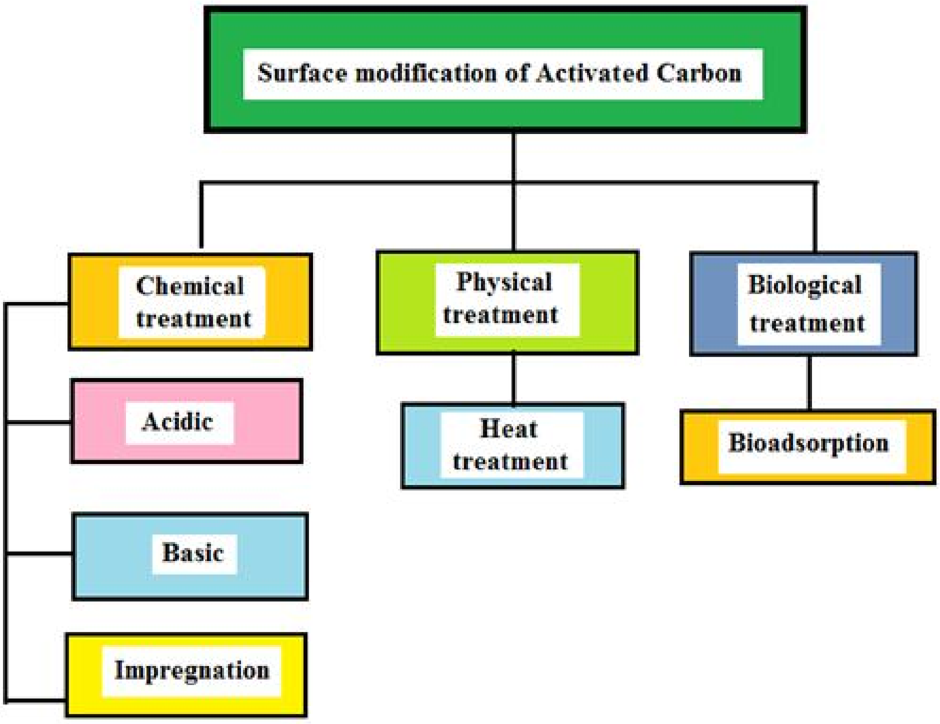

Fig-1: Various methods of modification of surface of AC

The chemical modification further divided into two broad groups, those resulting in acidic and basic surface. The third classification of chemical modification is the surface impregnation of AC with active metals and their oxides. The physical modification consists of mainly heat treatment. The biological modification is a relatively newer approach, wherein biological methods of environmental control can be used for water treatment and other applications. Depending on the chemical modification the AC surface can show acidic, basic or neutral behavior due to surface functional groups.

Various chemical and physical treatments have been performed for surface modifications of AC to increase the adsorption efficiency. Especially surfactants that used for surface modification can increase significantly the activated carbons' heavy metal adsorption capacity [30]. Edwin vasu 2008 intended at modifying the surface of an activated carbon prepared from coconut shells by oxidation with reagents like concentrated nitric acid, hydrogen peroxide and ammonium persulphate for the enhancement of copper adsorption. Activated carbon (AC) was modified by heat treatment where it was washed with deionized water and then heated to 450°C for 4 hrs showed maximum adsorption capacity for Ni - 400 mg/g, Zc - 344.82 mg/g, Pb - 294.11 mg/g, Cd - 178.5 mg/g and Cr - 60.9 mg/g [31].

Paola Rodríguez-Estupinan et al modified the surface of Granular Activated carbons with different oxidation treatments either HNO3, H2O2, or NaOCl (GACoxN, GACoxP, and GACoxCl)for the removal of Cd (II) from aqueous solution. The performances ranking was GACoxCl > GACoxP > GACoxN > GAC, likely due to the chemical surface properties of the adsorbents [32].

CONCLUSION

Over the past years, environmental regulations have become more rigorous, necessitating an improved quality of treated effluent. In recent years, a wide range of treatment technologies such as chemical precipitation, adsorption, membrane filtration, electrodialysis, and photocatalysis, have been developed for heavy metal removal from contaminated wastewater. It is apparent from the literature review of 100 articles (2000–2018) that: adsorption of heavy metals using activated carbon has been found as one of the most effective conventional method to treat inorganic effluent with a metal concentration higher than 500 mg/L; new activate carbon from different natural sources are the most frequently studied and widely applied for the treatment of the heavy metal-contaminated wastewater. Although many techniques can be employed for the treatment of wastewater loaded with heavy metals, it is imperative to note that the selection of the most suitable treatment for metal- contaminated wastewater depends on some basic parameters like pH, initial metal concentration, the treatment performance and cost of the treatment techniques compared to other technologies. Finally, technical applicability, plant simplicity and cost-effectiveness are the key factors that play major roles in the selection of the most suitable treatment system for inorganic effluent. All the factors mentioned above should be taken into consideration in selecting the most efficient and low-cost treatment in order to defend the environment.

REFERENCES

1. Shafiquzzaman Siddiquee, Kobun Rovina, Sujjat Al Azad, Laila Naher, Saallah Suryani and Pasicha Chaikaew. (2015), Heavy Metal Contaminants Removal from Wastewater Using the Potential Filamentous Fungi Biomass: A Review, Journal of Microbial & Biochemical Technology, 7(6), 384-393.

2. Mohammed Abdulrazzaq Assi, Mohd Noor Mohd Hezmee, Abd Wahid Haron, Mohd Yusof Mohd Sabri, and Mohd Ali Rajion. (2016), The detrimental effects of lead on human and animal health, Veterinary World. 9(6): 660–671.

3. MS Abdel-Raouf and ARM Abdul-Raheim. (2017), Removal of Heavy Metals from Industrial Waste Water by Biomass-Based Materials: A Review, Journal of Pollution Effects & Control, 5(1), 2-13.

4. U Farooq , JA Kozinski , MA Khan , Athar. (2010), Biosorption of heavy metal ions using wheat based biosorbents--a review of the recent literature, Bioresour Technol. 101(14), 5043-5053.

5. B. S. Patil, K. S. Kulkarni. (2012), Development of high surface area activated carbon from waste material, International Journal of Advanced Engineering Research and Studies, (1)2, 109-113.

6. M. Mokhlesur, Rahman, Mohd Adil, M. Alias, Yusof , B. Yunus, Kamaruzzaman and H. Rezaul, Ansary. (2014), Removal of Heavy Metal Ions with Acid Activated Carbons Derived from Oil Palm and Coconut Shells, Materials 7, 3634-3650.

7. Sneh Lata and S.R. Samadder. (2014), Removal of Heavy Metals Using Rice Husk: A Review, International Journal of Environmental Research and Development, (4) 2, 165-170.

8. Amandeep Kaur and Sangeeta Sharma. (2017), Removal of Heavy Metals from Waste Water by using Various Adsorbents- A Review, Indian Journal of Science and Technology, 10(34), 1-14.

9. Ali Sheibani, Masoud Reza Shishehbor and Hamed Alaei. (2012), Removal of Fe(III) ions from aqueous solution by hazelnut hull as an adsorbent, International Journal of Industrial Chemistry, (3) 4, 1-4.

10. K.Santhy and P.Selvapathy. (2004), Removal of Heavy Metals from Wastewater by Adsorption on Coir Pith Activated Carbon, Separation Science and Technology, (39) 14, 3331-3351.

11. K. Ravikumar, A.K. Sheeja. (2013), Heavy Metal Removal from Water using Moringa oleifera Seed Coagulant and Double Filtration, International Journal of Scientific & Engineering Research, (4) 5, 1-4.

12. D. S. Malik, C. K. Jain, Anuj K. Yadav. (2016), Removal of heavy metals, Appl Water Sci, 3, 1-24.

13. Nur Azreen Fuadi, Ahmmed Saadi Ibrahem, Kamariah Noor Ismail. (2014), Removal of heavy metals from simulated wastewater using physically and chemically modified Palmshell activated Carbon, Journal of Applied sciences, 14(12), 1294-1298.

14. June Fang, Bin Gao, Jianjun Chen, Andrew R. Zimmerman. (2015). Hydrochars derived from plant biomass under various conditions: Characterization and potential applications and impacts, Chemical Engineering Journal, 267, 253–259.

15. Lindiwe Hlungwane, Elvera Logie Viljoen and Vusumzi Emmanuel Pakade. (2017), Macadamia nut shells derived activated carbon and attapulgite clay combination for synergistic removal of Cr(VI) and Cr(III), Adsorption Science & Technology, 36(1–2), 713-731.

16. N. Kannan and T. Veemaraj. (2003), Removal of Lead(II) Ions by Adsorption onto Bamboo Dust and Commercial Activated Carbons -A Comparative Study, 6(2), 247-256.

17. Lalhmunsiama, Seung Mok Lee, Suk Soon Choi and Diwakar Tiwari. (2017), Simultaneous Removal of Hg(II) and Phenol Using Functionalized Activated Carbon Derived from Areca Nut Waste, Metals, 7, 248, 1-15.

18. C. Arunkumar, R. Perumal, S. Lakshmi Narayanan and J. Arunkumar. (2014), Use of Corn Cob as Low Cost Adsorbent for the Removal of Nickel (II) From Aqueous Solution, (5) 3, 325-330.

19. Dipa Das, Debi Prasad Samal, BC Meikap. (2015), Preparation of Activated Carbon from Green Coconut Shell and its Characterization, Journal of Chemical Engineering & Process Technology, (6) 5, 1-7.

20. R. Shanmugavalli, P.S. Syed Shabudeen, R. Venckatesh, K. Kadirvelu, S. Madhavakrishnan, S. Pattabhi. (2006), Uptake of Pb(II) ion from aqueous solution using silk cotton hull carbon: an agricultural waste biomass, E-Journal of Chemistry, 3(13), 218-229.

21. E. Demirbas, M. Kobya, S. Oncel, and S. Sencan. (2002), Removal of Ni(II) from aqueous solution by adsorption onto hazelnut shell activated carbon: equilibrium studies, Bioresour. Technol., 84, 291-293.

22. Y.B. Onundi, A.A. Mamun, M.F. Al Khatib, M.A. Al Saadi, and A,M, Suleyman. (2011), Heavy metals removal from synthetic wastewater by a novel nano-size composite adsorbent, Int. J. Environ. Sci. Tech., 8(4), 799-806.

23. G, Issabayeva, M.K. Aroua, M.N. Sulaiman. (2010), Study on palm shell activated carbon adsorption capacity to remove copper ions from aqueous solutions, Desalination, 262, 94 – 98.

24. M.H. Nasir, R. Nadeem, K. Akhtar, M.A. Hanif, and A.M. Khalid. (2007), Efficacy of modified distillation sludge of rose (Rosa centifolia) petals for lead and zinc removal from aqueous solutions, J. Hazard. Mater., 147, 1006-1014.

25. M. Chaudhuri and S. N. B. Saminal. (2011), Coconut coir activated carbon: an adsorbent for removal of lead from aqueous solution, WIT Transactions on Ecology and The Environment, 148, 95-104.

26. G. Karthikeyan, and S. Siva ilango. (2008), Equilibrium Sorption studies of Fe, Cu and Co ions in aqueous medium using activated Carbon prepared from *Recinius Communis Linn*, J. Appl. Sci. Environ. Management, 12 (2), 81 - 87.

27. Kadirvelu, K., Thamaraiselvi, K. and Namasivayam,C. (2001), “Adsorption of nickel(II) from aqueous solution onto activated carbon prepared from coir-pith”, Sep. Purif. Technol., 24, 497-505.

28. K. Periasamy and C. Namasivayam. (1995), Removal of nickel(II) from aqueous solution and nickel plating industry waste water using an agricultural waste: Peanut hulls, Waste Manage., 15 ,63-68.

29. M. Teker, M. Imamoglu, and O. Saltabas. (1999), Adsorption of copper and cadmium ions by activated carbon from rice hulls, Turkish J. Chem., 23, 185 - 191.

30. Chi Kyu Ahn, Donghee Park, Seung Han Woo, Jong Moon Park. (2008), Removal of Cationic Heavy Metal from Aqueous Solution by Activated Carbon Impregnated with Anionic Surfactants, Journal of hazardous materials, 164 (2-3), 1130-1136.

31. A. Edwin Vasu. ((2008), Surface Modification of Activated Carbon for Enhancement of Nickel(II) Adsorption, E-Journal of Chemistry, 5(4), 814-819.

32. Paola Rodríguez-Estupiñán, Alessandro Erto, Liliana Giraldo and Juan Carlos Moreno-Piraján. (2017), Adsorption of Cd (II) on Modified Granular Activated Carbons: Isotherm and Column Study, Molecules, 22, 2280-2297.

STUDIES ON ADSORPTION ISOTHERM OF DYES USING NANOPOROUS MATERIAL (ZEOLITE)

Perumal Andal and S. Tamijselvy
Department of Chemistry, Vels Institute of Science Technology and Advanced Studies, Chennai
E-mail: andalprithu.sbs@velsuniv.ac.in

ABSTRACT

The effluents of wastewater in some industries such as, textiles, leather, paper and plastics contain various kinds of synthetic dyes. Molecular sieves like aluminosilicate or aluminophosphate materials containing tiny pores of precise and uniform size, which are used as adsorbents, catalyst carriers, desiccants, and so on. In this work, to collect dyes used in leather industries and study the removal efficiency of Zeolite on removal of dyes, study the impact of pH, reaction time, temperature and concentration of adsorbent on the adsorption ability of Zeolite. The kinetic studies were carried out to evaluate the adsorption isotherm, i.e. Freundlich and Langmuir on the efficiency of Zeolite in adsorption of dyes.

INTRODUCTION

Water is one of the most important natural resources, essential for all forms of life. This natural resource is being contaminated every day by various anthropogenic activities such as rapid growth of population, urbanization and industrialization that ultimately make the environment polluted [1]. Ground water is the prime source of drinking water in urban and rural areas of our country. The quality of drinking water in Indian cities has been deteriorated in the recent years mainly due to growth of population and improper disposal of waste water from industries [2].

In the past few decades, uncontrolled urbanization has caused a serious pollution problem due to the disposal of sewage and industrial effluents to water bodies. In developing and underdeveloped countries, the industrial effluents are released directly or indirectly into natural water resources, mostly without proper treatment, thus posing a serious threat to the environment [3]. The release of pollutants differs from industry to industry. The waste from the pulp industry mainly contain carbohydrates, textile industry contain dyes, plating industry contain nickel and leather tanning wastes contain mainly chromium, zinc, copper, sulphides, carbonates, sodium and many other toxic organic compounds and inorganic compounds [4].One of the effects of rapid industrialization is water pollution, which threatens all forms of life. Tanning is one of the industrial processes that cause great deterioration of surface and ground water quality [5]. Industrialization and urbanization have resulted in several disadvantages, with the release of hazardous effluents being the utmost issue of concern. Several industries such as textiles, paper and pulp, plastic, food, pharmaceutical, cosmetics, leather, printing, jute industries etc., use dyes in numerous processes. Over 100,000 commercially available dyes exist and more than $7x10^5$ tonnes of dye are produced annually [6]. Wastewater from dyeing units is often rich in color due to the residues of dyes. In many cases, untreated or partially treated wastewater is allowed into water sources which affect the nature and its biota, due to contamination of the ground water, increase in water turbidity, decrease in the dissolved oxygen level and decrease in soil productivity.

Several health risks such as skin irritation, eye irritation, formation of blisters, disruption of hormones, cancer, etc., [7-8] are also reported to be caused by dyes. In few of the developing countries, several dyeing units are closed due to the impact of dyes in the environment. Removal of dyes from industrial effluents is mandatory, mainly owing to the toxic impacts of dyes on the environment.

Removal of dyes from effluents is a herculean task for industries. Industries are on the lookout of low cost adsorbents and one such available adsorbent is Clinoptilolite, a natural form of Zeolite. Naturally found in volcanic ashes, Clinoptilolite is a mineral comprising silica and alumina tetrahedral microporous complex with the formula $(Na,K,Ca)_{23}Al_3(Al,Si)_2Si_{13}O_{36}.12H_2O$. The microporous nature, high resistance and neutral basic structure of Clinoptilolite make it a potential adsorbent for wide range of pollutants. Natural and modified Clinoptilolite have been used for the adsorption of reactive dyes (Alver and Metin, [9],Azomethines [10], heavy metals, ammonium [11] etc.

DYE ADSORPTION

Dyes are important pollutants in wastewater, which are mainly discharged from textile, printing, food and leather industries. Various types of dyes including basic, acidic, reactive, and dispersive dyes are widely used. Dyes in waters affect the nature of the water, inhibiting sunlight penetration into the stream and reducing the photosynthetic reaction. Some dyes are also toxic and even carcinogenic. In the past years, some investigations using natural zeolites for dye adsorption have been reported.

Meshko et al. (2001)[12] investigated the adsorption of two basic dyes, MG-300 and MG-400 with components of (2-[[(4-methoxyphenyl) methylhydrazono]methyl]-1,3,3-trimethylindolium methosulfat and 2-[[4-[ethyl(2-hydroxyethyl) amino]phenyl]azo]-6-methoxy-3-methylbenzothiazoliumchloride), onto granular activated carbon and natural clinoptiolite. The influences of agitation, initial dye concentration and adsorbent mass were studied using batch reactor. The equilibrium studies showed that both dyes have higher adsorption capacity for the granular activated carbon than for the natural zeolite. Homogeneous diffusion model combined with external mass transfer resistance was proposed for the kinetic investigation. The adsorption capacities of two dyes on natural zeolite are 55.9 and 14.9 mg/g, respectively.

Armagan *et al.,* (2004) [13]conducted a comprehensive study on a Turkey clinoptillolite for adsorption of three reactive azo dyes (reactive black 5, reactive red 239, and reactive yellow 176) and compared the adsorption with a clay sample, sepiolite. The adsorption results indicated that both natural sepiolite and zeolite have limited adsorption capacities of the reactive dyes. After modification with quaternary amines (hexadecyltrimethylammonium bromide. HTAB), the adsorption was significantly improved. An electrostatic adsorption mechanism involving the formation of a bilayer of amine molecules on the clinoptilolite surface onto which anionic dye molecules adsorb was proposed. The adsorption data were fitted to the Langmuir isotherm and the modified zeolite produced adsorption capacities of 111, 89, and 61 mg/g for reactive red, yellow and black, respectively.

Karadag *et al.*, (2006)[14] also studied raw zeolite and surfactant modified zeolite for adsorption of basic red 46 (BR46) and reactive yellow 176 (RY176) and compared the effect of different surfactants of cetyl trimethy lammonium bromide (CTAB) and hexadecyl trimethyl ammonium bromide (HTAB) on dye adsorption. BR46 adsorption onto natural zeolite increased to minor extent with increasing pH, whereas pH did not significantly affect RY176 adsorption. The increase in ionic strength caused a decrease in adsorption of BR46 and an increase in adsorption of RY176. Adsorption of BR46 on natural zeolite ismorefavourable than RY176 on the CTAB and HTAB modified zeolites. They further investigated CTAB modified-natural zeolite for other reactive dye adsorption. The adsorption capacity of Reactive Red 239 was found to be two times higher than Reactive Blue 5 due to the hydrophilicity of the dye molecules. The pseudo-second-order model provided a very good fitting for the two anionic dyes. The calculated maximum adsorption capacity increased with increasing initial dye concentration, but there is no linear relationship with pH and temperature.Kinetic studies showed that adsorption of TBO on the clinoptilolite was fitted to the second-order adsorption model with two-step diffusion process. The activation energies for TBO adsorption on clinoptilolite for the first and second diffusion processes were 8.72 and 19.02 kJ/mol, respectively. The adsorption isotherm was well fitted to both isotherms.

LANGMUIR AND FREUNDLICH MODELS

The maximum adsorption capacity of clinoptilolite for TBO was 2.1×10^{-4} mol/g at solution pH of 11.0. An Australian natural clinoptiloite was tested for basic dye adsorption [15]. The natural zeolite presented maximal adsorption capacity of 2.8×10^{-5} and 7.9×10^{-5} mol/g at 50◦C for Rhodamine B and methylene blue, respectively. Kinetic studies indicated that the adsorption followed the pseudo-second-order kinetics and could be described as two-stage diffusion process. It has also found that the regenerated zeolites by high-temperature calcination and Fenton oxidation showed similar adsorption capacity but lower than the fresh sample. Only 60% capacity could be recovered by the two regeneration techniques Langmuir model and the adsorption capacity is 5×10^{-5} mol/g. In the binary system, malachite green and Pb^{2+} exhibit competitive adsorption on the natural zeolite. The adsorption is reduced to 90 and 80% of single component of Pb^{2+} and malachite green, respectively. However, the total adsorption is higher. In the binary system, Pb^{2+} exhibits relative higher affinity and selectivity to be adsorbed on zeolite.

The dynamic adsorption of malachite green and Pb^{2+} still follows the first-order kinetics. The results showed that natural zeolite was efficient to remove methylene blue from solution. The breakthrough data were fitted to Thomas model equations. From the above investigations, it is found that natural zeolites are effective for cationic dye adsorption due to the cation-exchange characteristic while they exhibit low capacity in anionic dyes. After surfactant modification, natural zeolites will be good adsorbents for anionic dye adsorption.

Dye

The Crimson red dye that are used in industries are procured from vendors in Chennai. The dye is widely used in industries like textile as well as leather. To impart red coloration, crimson red is used widely. The dye was treated for estimating the amount of decolorization on treatment with nano porous material, Zeolite. The molecular formula of the dye is $C_{28}H_{20}ClN_7Na_2O_{12}S_3$ and its structure is shown in Fig.1 Crimson is a strong, red color, inclining to purple. It originally meant the color of the kermes dye produced from a scale insect, Kermes vermilio, but the name is now sometimes also used as a generic term for slightly bluish-red colors that are between black and rose.

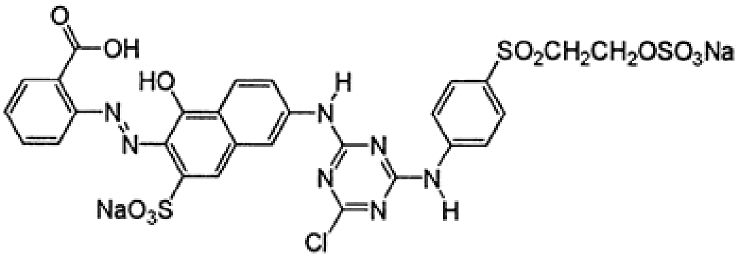

Zeolite

The adsorbent, Zeolite, was be procured from the company, Tree of Life, Chennai, Tamil Nadu. **Characterization of natural zeolite:**The composition and surface topography of the sample was analyzed using (SEM) Scanning Electron Microscope and Energy Dispersive X-ray Crystallography (EDAX).

ADSORPTION OF CRIMSON RED USING ZEOLITE

The Crimson Red dye solution prepared at the concentration of 100ppm was treated with Zeolite at different concentrations. Equal volumes of solution prepared were taken in different beakers. The concentrations of zeolite studied were 0.5, 1 and 1.5 percentages. The same was treated at different pH value of 5,7 and 9. Further, the impact of temperature was studied by conducting the experiments at different temperatures as 30, 37 and 45°C. The samples were taken every 30 minutes up to 90minutes, centrifuged and read under UV-spectrophotometer at 520nm to measure the amount of decolorization using the same formula.

Adsorption studies

The removal of dyes from synthetic solutions were studied at varying concentrations of Zeolite, pH, temperature and reaction time. The pH of the dye solution (100 mg/L) will be adjusted to varying pH (5, 7 and 9) using NaOH/HCl. To 100 ml of the pH altered solution, varying adsorbent concentrations (0.5, 1 and 1.5 g) and varying temperature (30, 37 and 45°C) and allowed to react at varying time intervals (30, 60 and 90 min).After the reaction period, the solutions are filtered and the filtrate were used for analysis through UV-Vis spectrophotometry to evaluate the percent of dye removed. The percent removal of dye from the synthetic solution will be calculated as

$$\%\ \text{removal} = \frac{(\text{Control absorbance} - \text{Test absorbance})}{\text{Control absorbance}} \times 100$$

Adsorption isotherms

The relationship between the adsorbent and adsorbate will be studied by Freundlich and Freundlich isotherms. The Freundlich isotherm, describing the homogenous adsorption is given by the linear form :

$$\frac{Ce}{Qe} = \frac{1}{QmKL} + \frac{Ce}{Qm}$$

where Q_e is the equilibrium amount of the dye exchanged by clinoptilolite (g/g), C_e is the equilibrium concentration of dye in the solution (g/L), Q_m (g/g) is the maximum uptake of dye exchanged and K_L is the Freundlich constant (L/g).The Freundlich constants Q_m and K_L are evaluated from the linear regression analysis of the plot C_e vs C_e/Q_e. R_L is the dimensionless separator which provides the essential features of Freundlich isotherm (Ho and McKay, 1999).

$$RL = \frac{1}{1 + KLCo}$$

Where Co is the initial concentration of the dye in the filtrate after treatment.

The Freundlich isotherm describes the heterogenic nature of adsorption process. The linear form of it is given by $\ln Qe = \ln KF + \frac{1}{n} \ln Ce$

Where K_F is Freundlich constant (L/g) and 1/n is the heterogeneity factor. The constants n and K_f can be evaluated from the linear regression analysis of the plot ln C_e vs ln Q_e.The regression coefficients (R^2) derived from the linear regression plots of the adsorption studies enable in assessing the best model that fits the experiment.

RESULTS

Zeolite characterization

The SEM studies on the surface size showed the size range of the zeolite varies from 26nm to 65nm. The SEM Images of the Zeolite is provided in Fig. 2. The EDAX revealed the presence of Carbon, Oxygen, Magnesium, Aluminium, Silica, Potassium, Calcium and Iron. However the major proportion lies with Carbon and Oxygen which revealed the presence of Silica oxide and Aluminium oxide as 14.8 % and 4 % respectively. The proportion of different metal recorded by weight and by composition is given in Table 1. The spectrum received through EDAX in characterization of Zeolite is provided in Fig. 3.

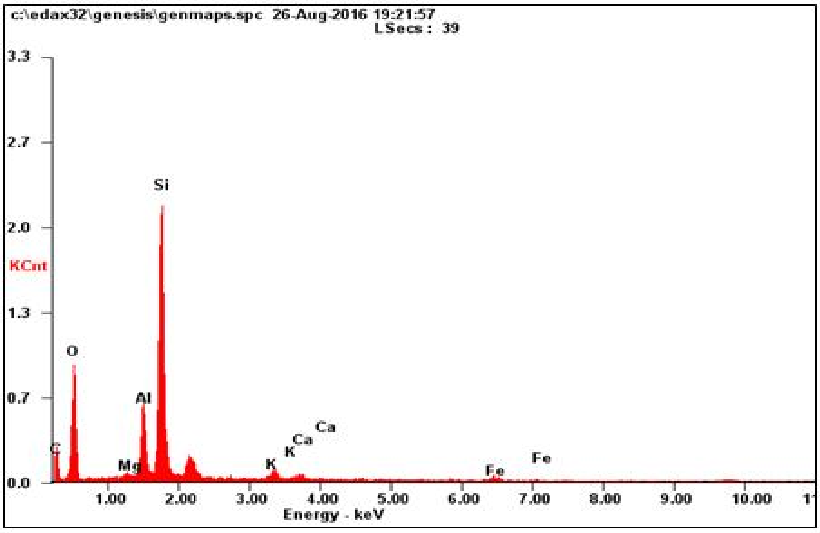

Fig-2: The Scanning Electron Microscope (SEM) image of Zeolite

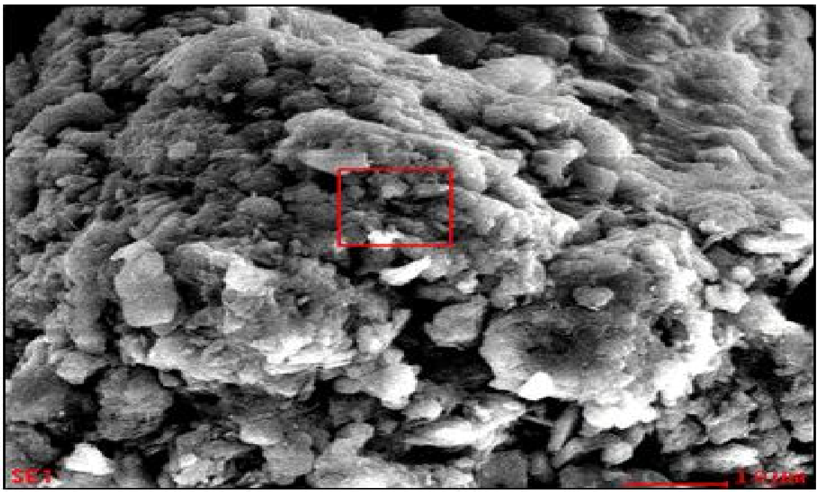

Fig-3: EDAX spectrum received for Zeolite

Element	Wt%	At%
CK	28.42	40.50
OK	36.19	38.72
MgK	00.51	00.36
AlK	06.36	04.04
SiK	24.33	14.83
KK	01.46	00.64
CaK	00.67	00.29
FeK	02.05	00.63
Matrix	Correction	ZAF

Table-1: Detection of compounds in Zeolite using EDAX

ADSORPTION OF CRIMSON RED AT THE TEMPERATURE OF 30°C

The dye Crimson Red was subjected to Adsorption using Zeolite at different factors. The set of experiment was conducted at 30°C. The factors include, different pH at 5, 7 and 9. The same was allowed to react with Zeolite at different concentration which includes 0.g, 1 and 1.5 g respectively. The zeolite was allowed to react with the solution prepared as said above for the time limit of 30, 60 and 90 minutes respectively.The result revealed maximum adsorption was at pH 5, with the zeolite concentration of 1.5g in the reaction time of 90 minutes. Nearly 92 % of the dye was adsorbed at the above said factors. This was closely followed by pH5, zeolite concentration of 1g but with the reaction time of 90 minutes and 60 minutes respectively. Both the set of experiments yielded the percent removal of 89 %. This was followed by pH5, zeolite concentration of 0.5g with the reaction time of 90 minutes. The different removal percentage recorded for Crimson red at 30°C using different factors is presented in Fig. 4.

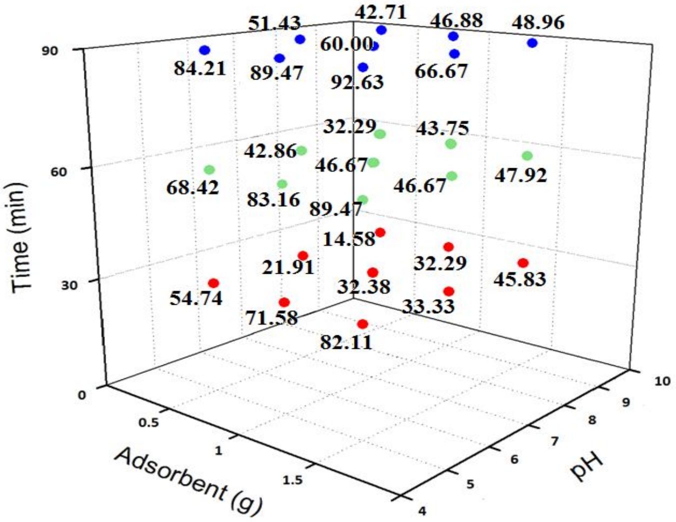

Fig.-4: Removal Percent of Crimson Red recorded using Zeolite at 30°C with different factors

ADSORPTION OF CRIMSON RED AT THE TEMPERATURE OF 37°C

The dye Crimson Red was subjected to Adsorption using Zeolite at different factors. The set of experiment was conducted at 37°C. The factors include, different pH at 5, 7 and 9. The same was allowed to react with Zeolite at different concentration which includes 0.g, 1 and 1.5 g respectively. The zeolite was allowed to react with the solution prepared as said above for the time limit of 30, 60 and 90 minutes respectively.The result revealed maximum adsorption was at pH 5, with the zeolite concentration of 1.5g in the reaction time of 90 minutes. Nearly 89 % of the dye was adsorbed at the above said factors. This was closely followed by pH5, zeolite concentration of 1g but with the reaction time of 90 minutes which revealed the adsorption percent up to 88.4. This was followed by pH5, zeolite concentration of 1.5g with the reaction time of 60 minutes. The different removal percentage recorded for Crimson red at the temperature of 37°C using different factors is presented in Fig. 5.

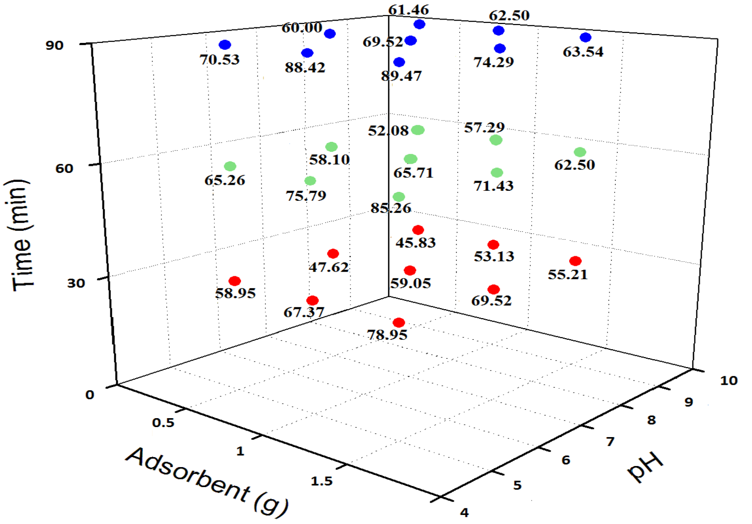

Fig-5: Removal Percent of Crimson Red recorded using Zeolite at 37°C with different factors

ADSORPTION OF CRIMSON RED AT THE TEMPERATURE OF 45°C

The dye Crimson Red was subjected to Adsorption using Zeolite at different factors. The set of experiment was conducted at 45°C. The factors include, different pH at 5, 7 and 9. The same was allowed to react with Zeolite at different concentration which includes 0.g, 1 and 1.5 g respectively. The zeolite was allowed to react with the solution prepared as said above for the time limit of 30, 60 and 90 minutes respectively.The result revealed maximum adsorption was at pH 5, with the zeolite concentration of 1.5g in the reaction time of 90 minutes. Nearly 76 % of the dye was adsorbed at the above said factors. This was closely followed by pH5, zeolite concentration of 1g but with the reaction time of 90 minutes which revealed the adsorption percent up to 74.7. This was followed by pH5, zeolite concentration of 1.5g with the reaction time of 60 minutes. The different removal percentage recorded for Crimson red at the temperature of 45°C using different factors is presented in Fig. 6.

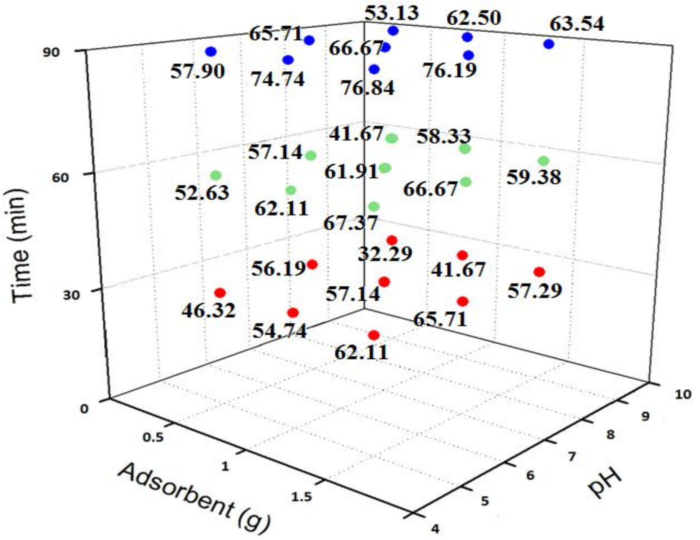

Fig-6: Removal Percent of Crimson Red recorded using Zeolite at 45°C with different factors

LANGMUIR ISOTHERM FOR CRIMSON RED DYE USING ZEOLITE AT 30°C

The dye Crimson Red was subjected to Adsorption using Zeolite at different factors. The set of experiment was conducted at 30°C. The factors include, different pH at 5, 7 and 9. The same was allowed to react with Zeolite at different concentration which includes 0.g, 1 and 1.5 g respectively. The zeolite was allowed to react with the solution prepared as said above for the time limit of 30, 60 and 90 minutes respectively. The Langmuir isotherm was applied for 27 set of experiments. The result indicated that all the tests conducted follows Langmuir isotherm favorably. Then, Kf and R2 value of the isotherm for individual reaction is provided in Table 2.

Table-2: Langmuir isotherm studies on Removal of Crimson Red using Zeolite at 30°C with different factors

Reaction Set	pH	Zeolite	Time	n	Kf	R2
1	5	0.5	30	2.53614	1.575858	0.96
2	5	0.5	60			
3	5	0.5	90			
4	5	1	30	4.426737	1.383339	0.973
5	5	1	60			
6	5	1	90			
7	5	1.5	30	7.251632	2.149854	0.9837
8	5	1.5	60			
9	5	1.5	90			
10	7	0.5	30	0.542299	352.3412	0.9808
11	7	0.5	60			
12	7	0.5	90			
13	7	1	30	0.858885	30.88282	0.9741
14	7	1	60			
15	7	1	90			
16	7	1.5	30	1.038637	15.09857	0.9658
17	7	1.5	60			
18	7	1.5	90			

19	9	0.5	30	0.36543	7319.52	0.9693
20	9	0.5	60			
21	9	0.5	90			
22	9	1	30	0.640492	122.0584	0.9972
23	9	1	60			
24	9	1	90			
25	9	1.5	30	0.898311	24.23748	0.9998
26	9	1.5	60			
27	9	1.5	90			

LANGMUIR ISOTHERM FOR CRIMSON RED DYE USING ZEOLITE AT 37^{O}C

The dye Crimson Red was subjected to Adsorption using Zeolite at different factors. The set of experiment was conducted at 37^{o}C. The factors include, different pH at 5, 7 and 9. The same was allowed to react with Zeolite at different concentration which includes 0.g, 1 and 1.5 g respectively. The zeolite was allowed to react with the solution prepared as said above for the time limit of 30, 60 and 90 minutes respectively. The Langmuir isotherm was applied for 27 set of experiments. The result indicated that all the tests conducted follows Langmuir isotherm favorably. The n, Kf and R2 value of the isotherm for individual reaction is provided in Table 3.

Table-3: Langmuir isotherm studies on Removal of Crimson Red using Zeolite at 37^{o}C with different factors

Reaction Set	pH	Zeolite	Time	n	Kf	R2
1	5	0.5	30	1.005328	2.771254	0.9947
2	5	0.5	60			
3	5	0.5	90			
4	5	1	30	3.963535	1.213732	0.9737
5	5	1	60			
6	5	1	90			
7	5	1.5	30	5.527916	1.738808	0.9868
8	5	1.5	60			
9	5	1.5	90			
10	7	0.5	30	1.152339	9.900646	0.9989
11	7	0.5	60			
12	7	0.5	90			
13	7	1	30	1.7963	2.944385	0.9963
14	7	1	60			
15	7	1	90			
16	7	1.5	30	2.575992	1.458779	0.999
17	7	1.5	60			
18	7	1.5	90			
19	9	0.5	30	1.176332	9.295217	0.9926
20	9	0.5	60			
21	9	0.5	90			
22	9	1	30	1.380262	5.695065	0.997
23	9	1	60			
24	9	1	90			
25	9	1.5	30	1.452855	4.950061	0.9996
26	9	1.5	60			
27	9	1.5	90			

LANGMUIR ISOTHERM FOR CRIMSON RED DYE USING ZEOLITE AT 45^{O}C

The dye Crimson Red was subjected to Adsorption using Zeolite at different factors. The set of experiment was conducted at 45^{o}C. The factors include, different pH at 5, 7 and 9. The same was allowed to react with Zeolite at different concentration which includes 0.g, 1 and 1.5 g respectively. The zeolite was allowed to react with the solution prepared as said above for the time limit of 30, 60 and 90 minutes respectively. The Langmuir isotherm was applied for 27 set of experiments. The result indicated that all the tests conducted follows Langmuir isotherm favorably. The n, Kf and R2 value of the isotherm for individual reaction is provided in Table 4.

Table-4: Langmuir isotherm studies on Removal of Crimson Red using Zeolite at 45^{o}C with different factors

Reaction Set	pH	Zeolite	Time	n	Kf	R2
1	5	0.5	30	1.087429	11.97594	0.9956
2	5	0.5	60			
3	5	0.5	90			
4	5	1	30	1.920492	2.590886	0.9873
5	5	1	60			
6	5	1	90			
7	5	1.5	30	2.359047	1.71738	0.9923
8	5	1.5	60			
9	5	1.5	90			
10	7	0.5	30	1.578034	4.002824	0.9997
11	7	0.5	60			
12	7	0.5	90			
13	7	1	30	1.63372	3.668196	0.9966
14	7	1	60			
15	7	1	90			
16	7	1.5	30	2.487562	1.557995	0.9996
17	7	1.5	60			
18	7	1.5	90			
19	9	0.5	30	0.748615	54.74576	0.985
20	9	0.5	60			
21	9	0.5	90			
22	9	1	30	1.066439	13.15234	0.995
23	9	1	60			
24	9	1	90			
25	9	1.5	30	1.538462	4.255873	0.999
26	9	1.5	60			
27	9	1.5	90			

FREUNDLICH ADSORPTION ISOTHERM FOR CRIMSON RED DYE USING ZEOLITE AT 30^{O}C

The dye Crimson Red was subjected to Adsorption using Zeolite at different factors. The set of experiment was conducted at 30^{o}C. The factors include, different pH at 5, 7 and 9. The same was allowed to react with Zeolite at different concentration which includes 0.g, 1 and 1.5 g respectively. The zeolite was allowed to react with the solution prepared as said above for the time limit of 30, 60 and 90 minutes respectively. The Freundlich isotherm was applied for 27 set of experiments. The result indicated that all the tests conducted follows Freundlich isotherm favorably. The n, Kf and R2 value of the isotherm for individual reaction is provided in Table 5.

Table-5: Freundlich isotherm studies on Removal of Crimson Red using Zeolite at 30^{o}C with different factors

Reaction Set	pH	Zeolite	Time	n	Kf	R2
1	5	0.5	30	2.53614	1.575858	0.96
2	5	0.5	60			
3	5	0.5	90			
4	5	1	30	4.426737	1.383339	0.973
5	5	1	60			
6	5	1	90			
7	5	1.5	30	7.251632	2.149854	0.9837
8	5	1.5	60			
9	5	1.5	90			
10	7	0.5	30	0.542299	352.3412	0.9808
11	7	0.5	60			
12	7	0.5	90			
13	7	1	30	0.858885	30.88282	0.9741
14	7	1	60			

15	7	1	90			
16	7	1.5	30	1.038637	15.09857	0.9658
17	7	1.5	60			
18	7	1.5	90			
19	9	0.5	30	0.36543	7319.52	0.9693
20	9	0.5	60			
21	9	0.5	90			
22	9	1	30	0.640492	122.0584	0.9972
23	9	1	60			
24	9	1	90			
25	9	1.5	30	0.898311	24.23748	0.9998
26	9	1.5	60			
27	9	1.5	90			

FREUNDLICH ADSORPTION ISOTHERM FOR CRIMSON RED DYE USING ZEOLITE AT 37^{O}C

The dye Crimson Red was subjected to Adsorption using Zeolite at different factors. The set of experiment was conducted at 37^{o}C. The factors include, different pH at 5, 7 and 9. The same was allowed to react with Zeolite at different concentration which includes 0.g, 1 and 1.5 g respectively. The zeolite was allowed to react with the solution prepared as said above for the time limit of 30, 60 and 90 minutes respectively. The Freundlich isotherm was applied for 27 set of experiments. The result indicated that all the tests conducted follows Freundlich isotherm favorably. The n, Kf and R2 value of the isotherm for individual reaction is provided in Table 6.

Table-6: Freundlich isotherm studies on Removal of Crimson Red using Zeolite at 37^{o}C with different factors

Reaction Set	pH	Zeolite	Time	n	Kf	R2
1	5	0.5	30	1.005328	2.771254	0.9947
2	5	0.5	60			
3	5	0.5	90			
4	5	1	30	3.963535	1.213732	0.9737
5	5	1	60			
6	5	1	90			
7	5	1.5	30	5.527916	1.738808	0.9868
8	5	1.5	60			
9	5	1.5	90			
10	7	0.5	30	1.152339	9.900646	0.9989
11	7	0.5	60			
12	7	0.5	90			
13	7	1	30	1.7963	2.944385	0.9963
14	7	1	60			
15	7	1	90			
16	7	1.5	30	2.575992	1.458779	0.999
17	7	1.5	60			
18	7	1.5	90			
19	9	0.5	30	1.176332	9.295217	0.9926
20	9	0.5	60			
21	9	0.5	90			
22	9	1	30	1.380262	5.695065	0.997
23	9	1	60			
24	9	1	90			
25	9	1.5	30	1.452855	4.950061	0.9996
26	9	1.5	60			
27	9	1.5	90			

FREUNDLICH ADSORPTION ISOTHERM FOR CRIMSON RED DYE USING ZEOLITE AT 45°C

The dye Crimson Red was subjected to Adsorption using Zeolite at different factors. The set of experiment was conducted at 45°C. The factors include, different pH at 5, 7 and 9. The same was allowed to react with Zeolite at different concentration which includes 0.g, 1 and 1.5 g respectively. The zeolite was allowed to react with the solution prepared as said above for the time limit of 30, 60 and 90 minutes respectively. The Freundlich isotherm was applied for 27 set of experiments. The result indicated that all the tests conducted follows Freundlich isotherm favorably. The n, Kf and R2 value of the isotherm for individual reaction is provided in Table 7.

Table-7: Freundlich isotherm studies on Removal of Crimson Red using Zeolite at 45°C with different factors

Reaction Set	pH	Zeolite	Time	n	Kf	R2
1	5	0.5	30	n	Kf	R2
2	5	0.5	60	1.087429	11.97594	0.9956
3	5	0.5	90			
4	5	1	30			
5	5	1	60	1.920492	2.590886	0.9873
6	5	1	90			
7	5	1.5	30			
8	5	1.5	60	2.359047	1.71738	0.9923
9	5	1.5	90			
10	7	0.5	30			
11	7	0.5	60	1.578034	4.002824	0.9997
12	7	0.5	90			
13	7	1	30			
14	7	1	60	1.63372	3.668196	0.9966
15	7	1	90			
16	7	1.5	30			
17	7	1.5	60	2.487562	1.557995	0.9996
18	7	1.5	90			
19	9	0.5	30			
20	9	0.5	60	0.748615	54.74576	0.985
21	9	0.5	90			
22	9	1	30			
23	9	1	60	1.066439	13.15234	0.995
24	9	1	90			
25	9	1.5	30			
26	9	1.5	60			
27	9	1.5	90			

Nowadays, the world is facing water crisis due to lacking of clean drinking water. With the fast development of various industries, a huge quantity of wastewater has been produced from industrial processes and was discharged into soils and water systems. Wastewater usually contains many pollutants such as cationic and anionic ions, oil and organics, which have poisonous and toxic effects on ecosystems. Removal of these contaminants requires cost effective technologies and a variety of techniques have been developed in the past decades in dealing with wastewater treatment.

Currently, adsorption is believed to be a simple and effective technique for water and wastewater treatment and the success of the technique largely depends on the development of an efficient adsorbent. Activated carbon [16], clay minerals [17]), biomaterials [18], zeolites [19], and some industrial solid wastes [20] have been widely used as adsorbents for adsorption of ions and organics in wastewater treatment.

Since the original discovery of zeolitic minerals in a volcanogenic sedimentary rock, zeolitic tuffs have been found in many areas of the world. In the past decades, natural zeolites have found a variety of applications in adsorption, catalysis, building industry, agriculture, soil remediation, and energy [21-22]. It has been estimated that the world natural zeolite consumption is 3.98Mt and will reach 5.5Mt in 2010 [23].Natural zeolites are hydrated aluminosilicate minerals of a porous structure with valuable physicochemical properties, such as cation exchange, molecular sieving, catalysis and sorption. The use of natural zeolites for environmental applications is gaining new research interests mainly due to their properties and significant worldwide occurrence. Application of natural zeolites for water and wastewater treatment has been realised and is still a promising technique in environmental cleaning processes. In the past decades, utilisation of natural zeolites has been focussed on ammonium and heavy metal removal due to the nature of ion exchange and some review papers have been appeared [24-25]. Apart from the presence of cations in water, anions and organic compounds are widely presented in wastewater. In recent years, natural zeolite and its modified forms have also been reported for removal of anions and organics from water systems. However, no such a review has been found.

PROPERTIES OF NATURAL ZEOLITE

There are many natural zeolites identified in the world. Clinoptilolite, mordenite, phillipsite, chabazite, stilbite, analcime and laumontite are very common forms whereas offretite, paulingite, barrerite and mazzite, are much rarer. Among the zeolites, clinoptilolite is the most abundant natural zeolite and is widely used in the world. In zeolite structure, three relatively independent components are found: the aluminosilicate framework, exchangeable cations, and zeolitic water.

The primary building block of zeolite framework is the tetrahedron, the centre of which is occupied by a silicon or aluminium atom, with four atoms of oxygen at the vertices. Substitution of Si^{4+} by Al^{3+} defines the negative charge of the framework, which is compensated by monovalent or divalent cations located together with water. The aluminosilicate framework is the most conserved and stable component and defines the structure type. The water molecules can be present in voids of large cavities and bonded between framework ions and exchangeable ions via aqueous bridges. The water can also serve as bridges between exchangeable cations.

The ion-exchange behaviour of natural zeolite depends on several factors, including the framework structure, ion size and shape, charge density of the anionic framework, ionic charge and conconcentration of the external electrolyte solution [26]. Due to the formation environment, natural zeolite has varying chemical composition and cation-exchange capacity (CEC).

Dye removal/separation techniques Wastewater effluents contain synthetic dyes which may cause a potential hazard to the environment. Due to the environmental and health concerns associated with the wastewater effluents, different separation techniques have been used in the removal of dyes from aqueous solutions. The dye removal techniques are Physical, Chemical and Biological methods. Adsorption: Adsorption is used as top quality treatment procedures for the removal of dissolved organic pollutants like dyes from industrial waste water. Adsorption is defined as concentration of materials on the surface of solid bodies. Adsorption is a surface phenomenon which deals primarily with the utilization of surface forces. When a solution having absorbable solute, also called as adsorbate, comes into contact with a solid, called as adsorbent, with highly porous surface structure liquid-solid intermolecular forces of attraction causes the solute to be concentrated at the solid surface. Adsorption is one of the unit operations in the chemical engineering processes used for the separation of industrial wastewater pollutants. Adsorbents are mainly derived from sources such as zeolites, charcoal, clays, ores, and other waste resources. Adsorbents prepared from waste resources used include coconut shell, rice husk, petroleum wastes, tannin-rich materials, sawdust, fertilizer wastes, fly ash, sugar industry wastes, blast furnace slag, chitosan and seafood processing wastes, seaweed and algae, peat moss, scrap tyres, fruit wastes, etc. [27]. Dye removal by adsorption: While searching for cheap and existed low cost adsorbents used for the removal of dyes from waste water. Activated rice husk used as cheap adsorbent for dye removal from waste water [28]. Hamdaoui (2006)[29] stated that maximum adsorption of methylene blue, basic dye, onto cedar sawdust and crushed brick was 60 and 40 mg L-1, respectively.

Adsorption is a process that occurs when a gas or liquid solute accumulates on the surface of a solid or a liquid, forming a molecular or atomic film [30, 31]. In other words, adsorption is the adhesion of atoms, ions, biomolecules or molecules of gas, liquid, or dissolved solids to a surface and this process creates a film of the adsorbate (the molecules or atoms being accumulated) on the surface of the adsorbent [32]. It is a surface phenomenon and a consequence of surface energy. The atoms on the surface of the adsorbent are not wholly surrounded by the other atoms and thus, can attract adsorbates.

Adsorption takes place primarily on the walls of the pores or at specific sites inside the particle. As the pores are generally small, the internal surface area is greater than the external area. Separation occurs because differences in molecular weight, shape or polarity cause some molecules to be held more strongly on the surface than others. In many cases, the adsorbate is held strongly enough to allow complete removal of that component from the fluid.

It has been studied that more than 40 different types of Zeolites are available in the nature. However, researchers observed that linoptilolite is easily available and commonly used Zeolite, which is a heulandite mineral group. Because of its low cost, high surface area, and high ionexchange capability zeolites become adsorbents (attractive adsorbents). Zeolites are having different cavity structures since they are highly porous this is the reason sorption mechanism in Zeolites complex studied and observed that Zeolites removing trace elements also such as phenols, heavy metals, etc.

The constant Kf is an approximate indicator of adsorption capacity, while 1/n is a function of the strength of adsorption in the adsorption process. If n = 1 then the partition between the two phases are independent of the concentration. If value of 1/n is below one it indicates a normal adsorption. On the other hand, 1/n being above one indicates cooperative adsorption. The function has an asymptotic maximum as pressure increases without bound. As the temperature increases, the constants k and n change to reflect the empirical observation that the quantity adsorbed rises more slowly and higher pressures are required to saturate the surface. However, Kf and n are parameters characteristic of the sorbent-sorbate system, which must be determined by data fitting and whereas linear regression is generally used to determine the parameters of kinetic and isotherm models. Specifically, the linear least-squares method and the linearly transformed equations have been widely applied to correlate sorption data where 1/n is a heterogeneity parameter, the smaller 1/n, the greater the expected heterogeneity. This expression reduces to a linear adsorption isotherm when 1/n = 1. If n lies between one and ten, this indicates a favorable sorption process.

This study proves, that Zeolite can serve as a potential candidate for adsorption of Crimpson Red dye. The percent of reduction of dyes and the adsorption isotherm also proves, Zeolite as a potential candidate. Among the isotherm studies, Langmuir fits good when compared to Freundlich model.

CONCULSION

Crimson Red dye was treated with a Nanoporous material, Zeolite for its adsorption studies.The Zeolite was characterized using SEM and EDAX to know their size and chemical composition. The size range differed from 35nm to 185nm. The studies were conducted employing different factors like pH, Temperature, Concentration of Zeolite and time of reaction.Three different pH (5, 7 and 9), three different temperature (30, 37 and 45^{o}C), three different concentration of Zeolite (0.5, 1, 1.5 g) were reacted at three different time gap (30, 60 and 90 minutes).Among the study conducted, the treatment at 30oC with the pH value of 5 with the concentration of Zeolite at 1.5g allowing the reaction time of 90 minutes resulted in maximum adsorption. Nearly 92 % of the dye was adsorbed with the above said conditions.The raw data obtained using 81 sets of experiments were subjected to Langmuir and Freundlich adsorption isotherm studies.The study suggested Langmuir adsorption isotherm as a better one when compared with Freundlich.

REFERENCES

1. Vasseur L, Colutier C and Ansseau C. Effects of repeated sewage sludge application on plant community diversity and structure under agricultural field conditions on Podzolic soils in eastern Quebec *Agri. Ecosyst. Environ.* 2000; 81, 209-216.

2. Venkatasubramani R, Meenambal , T., Livingston P, Goldwyn, (2007), Ground water quality of palladam taluk, coimbatore district, Tamilnadu, Journal of Ecotoxicology and Environmental Monitoring, 17 (1): 85-90.

3. Akpan, U.G., B.H. Hameed. Parameters affecting the photocatalytic degradation of dyes using TiO2-based photocatalysts: A review. Journal of Hazardous Materials. 2009, 170, 520–529.

4. Nouri., M, Sepehr, S., Nasseri, M., Mazaheri A and Yaghmaian., K, (2005), Chromium Bioremoval From Tannery Industries Effluent by *Aspergillus Oryzae.*, Iran. J. Environ. Health. Sci. Eng, Vol. 2 : 273-279.

5. Raj, E.M., Sankaran, D.P., Sreenath, S.K., Kumarn, S., and Mohan, M.1996, Studies on treated effluent characteristics of a few tanneries of chromepet, Madras. Ind. J. Environ.Prot.6:252-254.

6. McMullan, G., C. Meehan, A. Conneely, N. Kirby, T. Robinson, P. Nigam, I.M. Banat, R. Marchant, W.F. Smyth. Microbial decolourisation and degradation of textile dyes. Appl. Microbiol. Biotechnol. 2001, 56, 81–87.

7. ONeill, C., F.R. Hawkes, D.L. Hawkes, N.D. Lourenco, H.M. Pinheiro, W. Dele´e. Colour in textile effluents—sources, measurement, discharge consents and simulation: a review. J. Chem. Technol. Biotechnol. 1999, 74, 1009–1018.

8. Vandevivere, P.C., R. Bianchi, W. Verstraete. Treatment and reuse of wastewater from the textile wet-processing industry: review of emerging technologies. J. Chem. Technol. Biotechnol. 1998, 72, 289–302.

9. Alver, E. and A.U. Metin. Anionic dye removal from aqueous solutions using modified zeolite: Adsorption kinetics and isotherm studies. Chemical Engineering Journal. 2012, 200–202, 59–67.
10. Cobzaru, C., C. Cernatescu and A. Marinoiu. Modified clinoptilolite used for removing azomethines from wastewaters. II. Adsorption of azomethines from wastewaters on clinoptilolite. Revue Roumaine de Chimie. 2014, 59(11-12), 1089-1096.
11. Huang, H., X. Xiao, B. Yan and L. Yang. Ammonium removal from aqueous solutions by using natural Chinese (Chende) zeolite as adsorbent. Journal of Hazardous Materials. 2010, 175, 247–252.
12. Meshko V (2001) Adsorption of basic dyes on granular activated carbon and natural zeolite. Water Res 35: 3357-3366.
13. Armagan, B., M. Turan, O. Ozdemir and M.S. Celik. Color Removal of Reactive Dyes from Water by Clinoptilolite. Journal of Environmental Science and Health Part A-Toxic/Hazardous Substances & Environmental Engineering. 2004, A39(5), 1251–1261.
14. Karadag, D.; Tok, S.; Akgul, E.; Ulucan, K.; Evden, H.; Kaya, M. A. Combining adsorption and coagulation for the treatment of azo and anthraquinone dyes from aqueous solution. *Ind. Eng. Chem. Res.* **2006**, *45*, 3969.
15. Wang, S. B., Z.H. Zhu, Characterisation and environmental application of an Australian natural zeolite for basic dye removal from aqueous solution, Journal of Hazardous Materials 136 (2006) 946–952.
16. Pollard, S.J.T., G.D. Fowler, C.J. Sollars, R. Perry, Low-cost adsorbents for waste and waste-water treatment—a review, Science of the Total Environment 116 (1992) 31–52.
17. de Aguiar, M.R.M.P., A.C. Novaes, A.W.S. Guarino, Removal of heavy metals from wastewaters by aluminosilicate, Quimica Nova 25 (2002) 1145–1154.
18. Crini, G. Recent developments in polysaccharide-based materials used as adsorbents in wastewater treatment, Progress in Polymer Science 30 (2005) 38–70.
19. Babel, S., T.A. Kurniawan, Low-cost adsorbents for heavy metals uptake from contaminated water: a review, Journal of Hazardous Materials 97 (2003) 219–243.
20. Wang, S.B., H.W.Wu, Environmental-benign utilisation of fly ash as low-cost adsorbents, Journal of Hazardous Materials 136 (2006) 482–501.
21. Bish, D.L., D.W. Ming, Applications of natural zeolites in water and wastewater treatment, Natural Zeolites: Occurrence, Properties, Applications 45 (2001) 519–550.
22. Tsitsishvili, G.V., T.G. Andronikashvili, G.N. Kirov, L.D. Filizova, Natural Zeolites, E. Horwood, New York, 1992.
23. Ozaydin, S., G. Kocar, A. Hepbasli, Natural zeolites in energy applications, Energy Sources Part A: Recovery Utilization and Environmental Effects 28 (2006) 1425–1431.
24. Kesraouiouki, S., C.R. Cheeseman, R. Perry, Natural zeolite utilization in pollution-control—a review of applications to metals effluents, Journal of Chemical Technology and Biotechnology 59 (1994) 121–126.
25. Caputo, D., F. Pepe, Experiments and data processing of ion exchange equilibria involving Italian natural zeolites: a review, Microporous and Mesoporous Materials 105 (2007) 222–231.
26. Kallo, D. Applications of natural zeolites in water and wastewater treatment, in: D.L. Bish, D.W.Ming (Eds.), Natural Zeolites: Occurrence, Properties, Applications (2001) 519–550.
27. Cameselle C, Gouveia S, Akretche DE, Belhadj B (2013) Advances in electrokinetic remediation for the removal of organic contaminants in soil. In: Rashed MN (ed.), Soils, Organic Pollutants-Monitoring, Risk and Treatment.
28. Vinod GK, Alok M, Rajeev J, Megha M, Shalini S (2006) Adsorption of Safranin-T from wastewater using waste materials- activated carbon and activated rice husks. Journal of Colloid and Interface Science 303: 80-86.
29. Hamdaoui O (2006) Batch study of liquid-phase adsorption of methylene blue using cedar sawdust and crushed brick. Journal of Hazardous Materials 135: 264-273.

30. Saad S., AIsa K.Md., Bahari R.,(2010) ‘Chemically modified sugarcane bagasse as a potentially lowcost biosorbent for dye removal’, *Desalination 264 ;123-128.*

31. Nageswara Rao M,. Chakrapani Ch., Suresh Babu Ch., Kaza Somasekhara Rao,P.Haritha ,I.T.Phucho,Kaza Rajesh,K.Emmanuel (2011), ‘Equilibrium and kinetic studies of methylene blue and rhodamineb onto prepared activated kaza’s carbons’, *International of applied biology and pharmaceutical technology.*

32. Wanchanthuek R. and Thapol A. (2011), ‘The kinetic study of Methylene Blue Adsorption over MgO from PVA Template preparation, *Journal of Environmental Science and Technology 4(5);552-559.*

International Journal of Advance and Innovative Research
Volume 6, Issue 1 (VI): January - March, 2019
ISSN 2394 - 7780

SYNTHESIS AND SPECTRAL CHARACTERISATION OF D-A BASED CYANO-STILBENE DERIVATIVES, FOR ORGANIC SOLAR CELL APPLICATIONS

R. Ganesamoorthy[1] **and P. Sakthivel**[2]
Assistant Professor[1], Department of Chemistry, School of Basic Sciences, VISTAS, Chennai
Professor[2], Department of Nanoscience and Technology, Bharathiar University, Coimbatore
E-mail: chemgmoorthy@gmail.com

ABSTRACT

1, 2-diphenylethene is called as stilbene. We synthesized ten donor acceptor based (D-A) cyano-stilbene derivatives and the structure was confirmed by ^{1}H-NMR, GC-MS, FT-IR. The absorption was calculated by UV-Visible spectrometer. From the UV-Vis study the stilbenes are having broad and strong absorption in the UV-Visible region. The strong and broad absorption in the UV-Visible region is the desired property for the high power conversion efficiency (PCE) organic photovoltaic (OPV).

Keywords: Acceptor, cyano-stilbene, donor, organic photovoltaic, and power conversion efficiency.

1. INTRODUCTION

In Greek colourful and shinning compounds are called as ‘stilbos’. The stilbene name was derived from the Greek word ‘stilbos’. Stilbene derivatives can be easily prepared by some conventional and eco-friendly methods. They are thermally and chemically stable, and possess absorption and fluorescence properties. The stilbene are mainly present in two isomeric forms namely trans-stilbene (E) and cis-stilbene (Z). In the above two forms trans form is more stable than compared with cis form because of steric factor and high energy in the later isomer. The two isomers are in equilibrium at room temperature but at high temperature or exposed to light the trans form is predominant because of the stability and energy difference. The energy of cis form higher than the trans form. The stilbenes are having same chemical properties but different physical properties like melting point, boiling point and refractive index and etc. They are insoluble in water but soluble in most of the common organic solvents [1].

Stilbenes are widely used in the manufacture of industrial dyes, dye lasers, optical brighteners, phosphor materials, scintillator and other materials. Donor– acceptor (D–π–A) dyestuff and colorants represent a vast majority of organic chromogens. Some of these compounds are also used as sources of dye laser radiation [2–3]. They are playing an increasingly prominent role in the area of photophysical, photochemical, biophysical and biomedical investigations. Un-substituted Stilbenes are less reactive but if any hydroxyl or some other functional group present in the stilbene it is highly reactive. Stilbenoids (hydroxylated derivatives of stilbene) are produced by plants are used as an important antibiotic material in their life time. The stilbene derivatives have also medical and biological activities, such as anti-microbial, antifungal, insecticidal and anti-inflammatory [4–5].

Stilbenes can be synthesized by many methods in that most important methods are given as follows, Aldol-type condensation, Wittig–Horner reaction, Perkin reaction, Negishi–Stille reactions and Heck reaction. In the above mentioned methods Aldol-type condensation between an aromatic aldehyde with active methylarene compound is most common because of economically benign, simple and easy way of preparation in short span of time [6-10]. The Aldol condensation type of stilbene synthesis involves the formation of carbanion and addition to the carbonyl group. The strong or weak base like Sodium hydroxide, pyridine or piperidine initiates the reaction by deprotonation of active methylarene. The carbanion then adds to carbon atoms of the carbonyl group of the aldehyde. The yield of the Aldol type stilbene synthesis is moderate. [11-14]

Broad and strong absorption band in visible and near infrared region to match the solar spectrum for increasing short circuit current (Jsc) [15]. A broad class of dyestuff and colorants are based on electron donor-acceptor (D-π-A) chromogens were synthesized by M. Asiri [16]. The stilbene dyes have a very wide absorption in UV-Visible range (200-600 nm). Due to the broad absorption in UV- Visible region stilbenes can be used as an efficient dye for organic photovoltaic. This observation leads us to synthesis stilbene dyes for the applications in organic photovoltaic.

2. MATERIALS AND METHODS

2.1 Materials

Thiophene-2-carboxaldehyde, Furfural, 4-hydroxybenzaldehyde, 4-bromobenzaldehyde, 5-bromothiophenecarboxaldehyde, Vanillin, 5-bromothiopheneacetonitrile, 4- hydroxyphenylacetonitrile, 4-

fluorophenylacetonitrile, 4-nitrophenylacetonitrile, Potassium tert-butoxide and Ethanol were purchased from Sd-Fine chem. Ltd. All the solvents were distilled prior to usage.

General scheme for the synthesis of stilbene

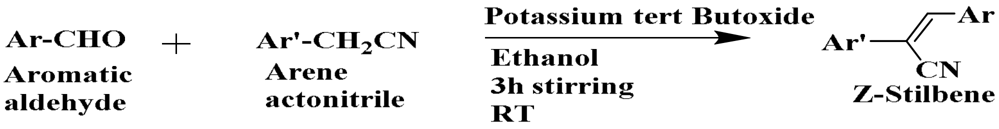

Table-1: Consolidated data for the stilbene synthesis:

Ar	Ar'	E- Stilbenes	Yield %	m.p ^{0}C	Colour	Stilbenes
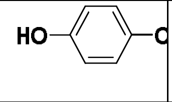	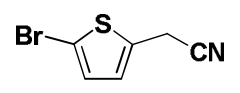	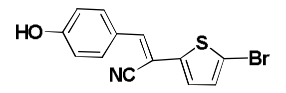	95	170	Brown	S-1
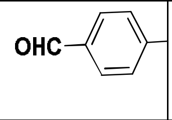	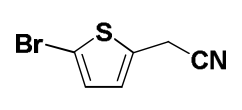	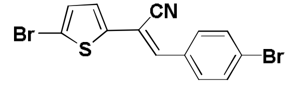	87	220	Golden yellow	S-2
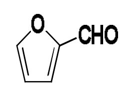	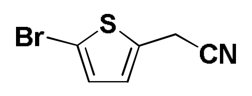	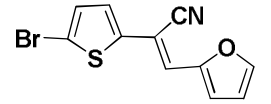	83	90	Greenish yellow	S-3
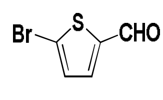	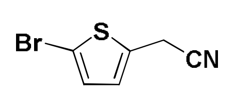	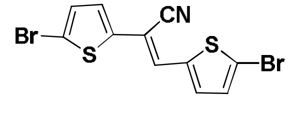	90	110	Light Yellow	S-4
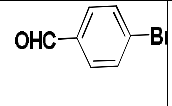	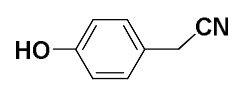	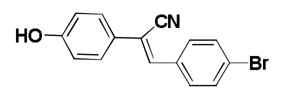	97	190	Light Yellow	S-5
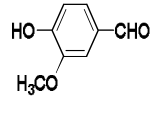	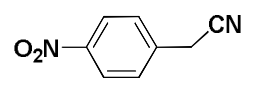	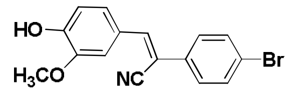	55	190	Reddish brown	S-6
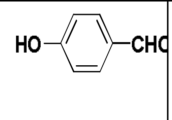	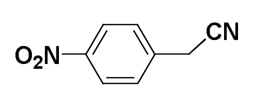	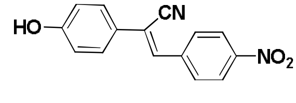	58	217	Dark yellow	S-7
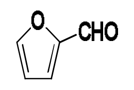	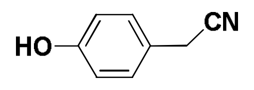	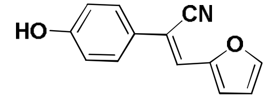	63	140	Yellow	S-8
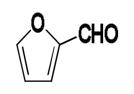	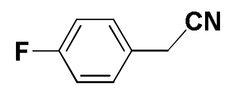	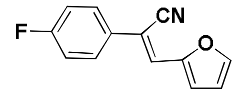	90	84	Brownish yellow	S-9
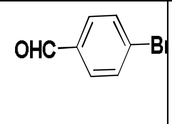	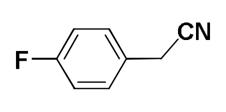	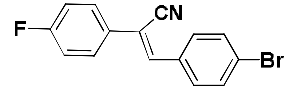	88	86	Light yellow	S-10

2.2 Methodology

Cyanostilbene Synthesis

Aryl acetonitrile (20 mmol) was dissolved in 20 mL of ethanol and taken in a three neck flask. To this 10 mmol of alcoholic potassium tert-butoxide was added and stirred for half an hour. An alcoholic solution of aromatic aldehyde (20 mmol) was added drop wise into the above solution. Within a few minutes formation of coloured product was started. The reaction mixture was again stirred for 3 h at room temperature. Progress was monitored by TLC. The reaction mixture was then poured into crushed ice and neutralized with sufficient amount of water. The precipitated product was filtered by using a Buckner funnel. The filtered stilbene was washed with water and ethanol for several times to eliminate the sodium hydroxide and unreacted reactants present in the mixture respectively. The product was further purified by recrystallization in ethanol. Melting point of the stilbene checked. The product formation was further confirmed by the GC-MS, UV-Visible, FT-IR and ^{1}H-NMR spectra's. The consolidated data for the synthesized cyano-stilbenes were summarized in Table **1**.

1. Spectral characterization of (E)-2-(5-bromothiophen-2-yl)-3-(4-hydroxyphenyl)acrylonitrile
Brown color stilbene. FT-IR (KBr, cm^{-1}): 3303($\nu_{O\text{-}H}$), 2945(Ar $\nu_{C\text{-}H}$), 2270 ($\nu_{C\text{-}N}$), 1487, 1429 (Ar $\nu_{C=C}$), 615 ($\nu_{C\text{-}Br}$),cm^{-1}. ^{1}H-NMR [400 MHz, $CDCl_3$, δ=7.26 ppm, s]: 7.7 (2H, d), 7.3 (1H, d), 7.3 (IH, d), 7.2 (1H, s), 7.0 (1H, q), 6.9 (2H, d) was shown in Fig 1. M. F: $C_{13}H_9ONS$, calculated mass- 305, observed mass- 306. Yield: 95%, m.p-170 ^{0}C. The absorption spectra of S-1 was shown in Fig. 2.

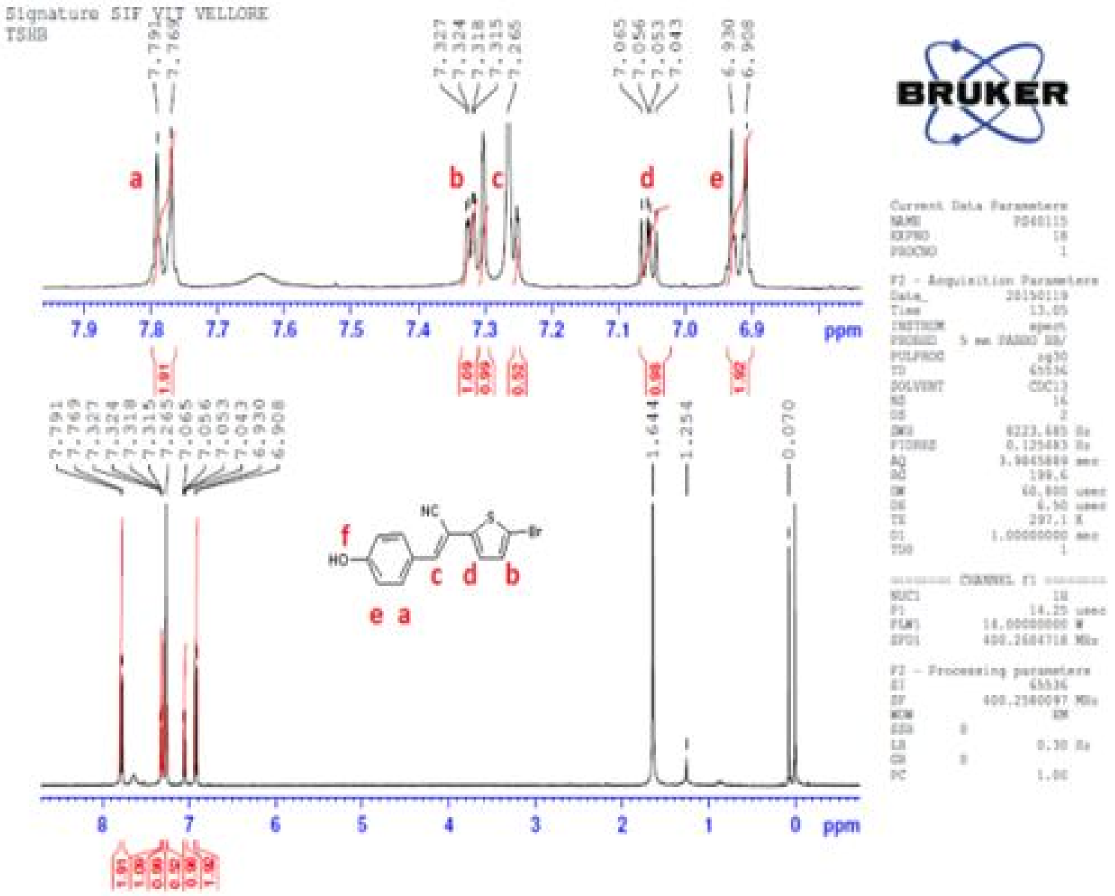

Fig-1: ^{1}H-NMR spectra of (E)-2-(5-bromothiophen-2-yl)-3-(4-hydroxyphenyl)acrylonitrile.

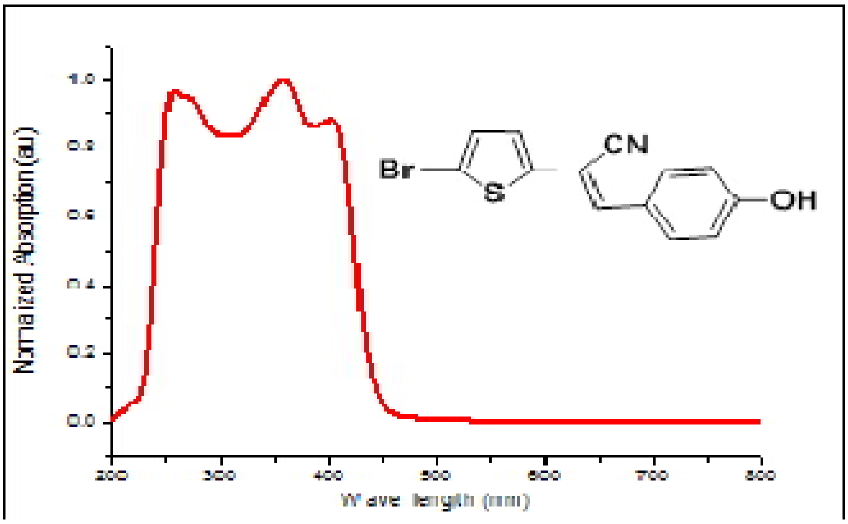

Fig-2: UV-Visible spectra of (E)-2-(5-bromothiophen-2-yl)-3-(4-hydroxyphenyl)acrylonitrile in chloroform.

2. Spectral characterization of (E)-3-(4-Bromophenyl)-2-(5-bromophen-2-yl)acrylonitrile
Golden yellow colour stilbene. FT-IR (KBr, cm^{-1}): 3034 (Ar $\nu_{C\text{-}H}$), 2223 ($\nu_{C\text{-}N}$), 1587, 1581, 1487 (Ar $\nu_{C=C}$), 810 ($\nu_{C\text{-}Br}$). ^{1}H-NMR [400 MHz, $CDCl_3$, δ=7.26 ppm, s]: 7.7 (2H, s), 7.5 (2H, d), 7.1 (2H, t), 7.0 (1H, d) was shown in Fig. 3. M. F: $C_{13}H_7Br_2NS$, calculated mass- 367, observed mass- 367.Yield: 87%, m.p- 220 ^{0}C. The absorption spectra of S-1 was shown in Fig. 4.

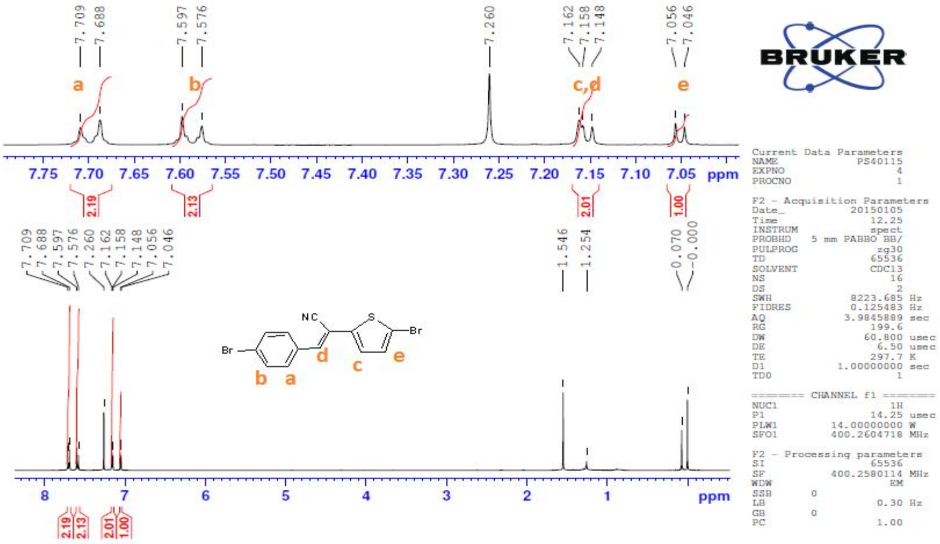

Fig-3: ^{1}H-NMR spectra of (E)-3-(4-Bromophenyl)-2-(5-bromophen-2-yl)acrylonitrile.

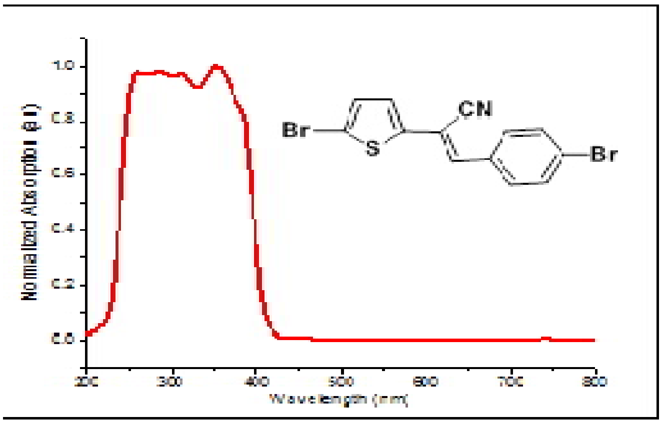

Fig-4: UV-Visible spectrum of (E)-3-(4-Bromophenyl)-2-(5-bromophen-2-yl)acrylonitrile in chloroform.

3. Spectral characterization of (E)-3-(4-Bromophenyl)-2-(5-bromophen-2-yl)acrylonitrile

Greenish yellow colour stilbene. FT-IR (KBr, cm^{-1}): 2945 (Ar $\nu_{\text{C-H}}$), 2227 (Ar $\nu_{\text{C-N}}$), 1487, 1429 (Ar $\nu_{\text{C=C}}$), 695 ($\nu_{\text{C-Br}}$). ^{1}H-NMR [400 MHz, $CDCl_3$, δ=7.26 ppm, s]: 7.6 (1H, d), 7.1 (2H, d), 7.0 (2H, t), 6.5 (1H, q) was shown in Fig. 5. M. F: $C_{13}H_7Br_2NS$, calculated mass- 278, observed mass- 279. Yield: 83%, m.p- 90 ^{0}C.

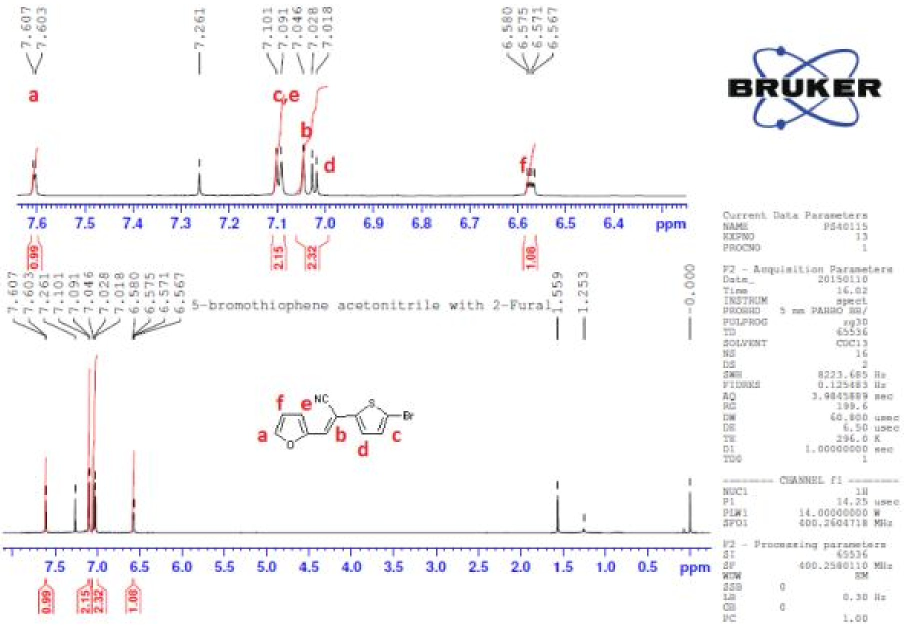

Fig-5: ^{1}H-NMR spectra of (E)-3-(4-Bromophenyl)-2-(5-bromophen-2-yl) acrylonitrile.

4. Spectral characterization of (E)-2,3-bis(5-bromothiophen-2-yl)acrylonitrile

Light yellow colour stilbene. FT-IR (KBr, cm^{-1}): 3305 (Ar $\nu_{C\text{-}H}$), 2231 ($\nu_{C\text{-}N}$), 1583, 1610, 1514 (Ar $\nu_{C=C}$), 821 ($\nu_{C\text{-}Br}$). ^{1}H-NMR [400 MHz, $CDCl_3$, δ=7.26 ppm, s]: 7.27 (2H, d), 7.1 (2H, t), 7.0 (1H, d) was shown in Fig. 6. M. F: $C_{11}H_5Br_2NS_2$, calculated mass- 372, observed mass- 373. Yield: 83%, m.p- 90 ^{0}C. The absorption spectra of S-1 was shown in Fig. 7.

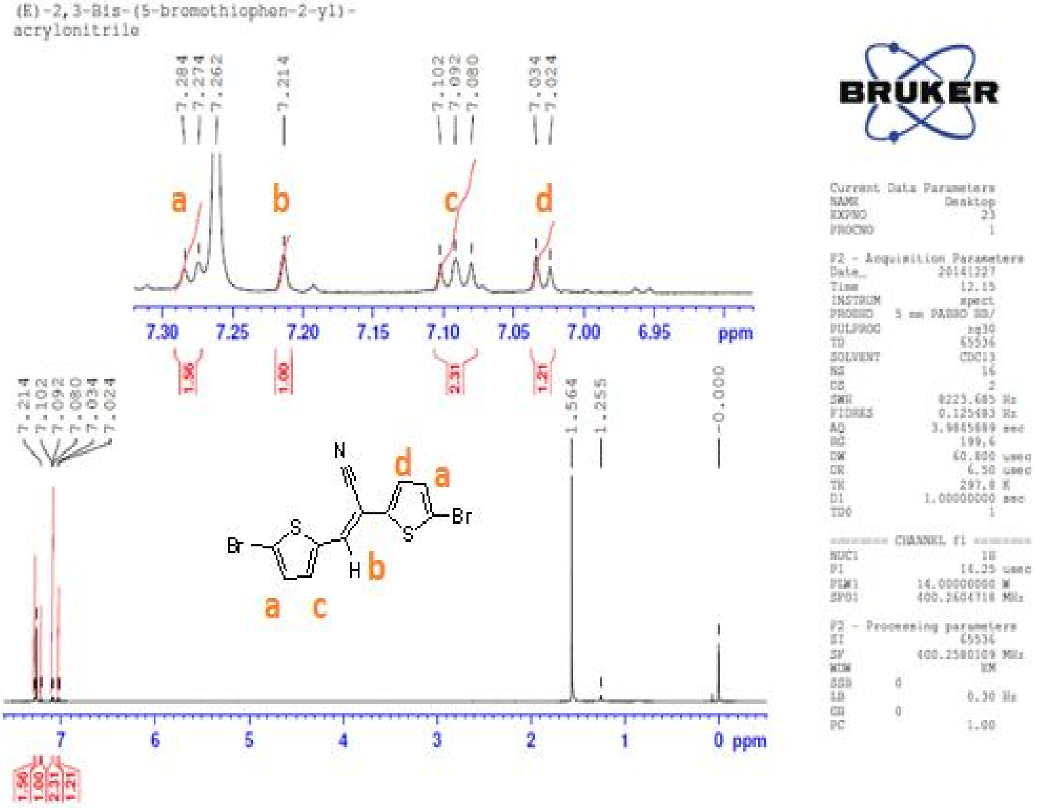

```
Current Data Parameters
NAME              Desktop
EXPNO                  23
PROCNO                  1

F2 - Acquisition Parameters
Date_            20141227
Time                12.15
INSTRUM             spect
PROBHD   5 mm PABBO BB/
PULPROG              zg30
TD                  65536
SOLVENT             CDCl3
NS                     16
DS                      2
SWH            8223.685 Hz
FIDRES         0.125483 Hz
AQ            3.9845889 sec
RG                  199.6
DW               60.800 usec
DE                 6.50 usec
TE                297.8 K
D1          1.00000000 sec
TD0                     1

======== CHANNEL f1 ========
NUC1                   1H
P1                14.25 usec
PLW1        14.00000000 W
SFO1       400.2604718 MHz

F2 - Processing parameters
SI                  65536
SF         400.2580109 MHz
WDW                    EM
SSB      0
LB                 0.30 Hz
GB       0
PC                   1.00
```

Fig-6: ^{1}H-NMR spectra of (E)-2,3-bis(5-bromothiophen-2-yl)acrylonitrile.

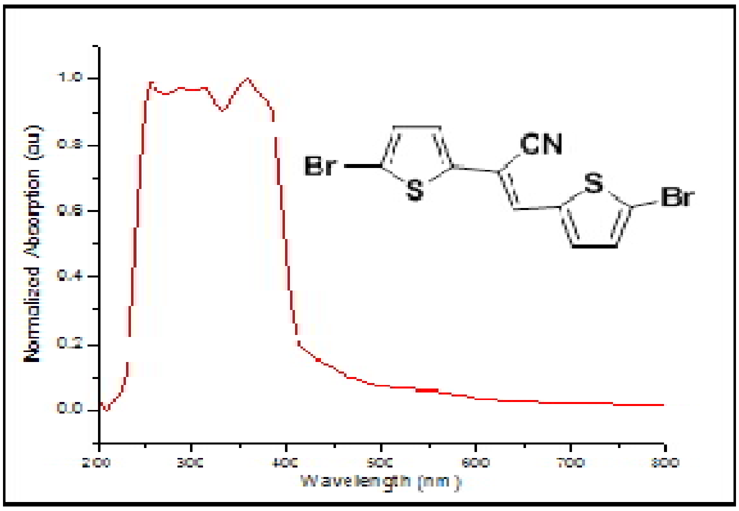

Fig-7: UV-Visible spectra of (E)-2,3-bis(5-bromothiophen-2-yl)acrylonitrile in chloroform.

5. Spectral characterization of (E)-3-(4-bromophenyl)-2-(4-hydroxyphenyl) acrylonitrile

Light yellow colour stilbene. FT-IR (KBr, cm^{-1}): 3379, 3338 ($\nu_{O\text{-}H}$), 3230 (Ar $\nu_{C\text{-}H}$), 2227 ($\nu_{C\text{-}N}$), 1610, 1583 ($\nu_{C=C}$), 821 ($\nu_{C\text{-}Br}$). ^{1}H-NMR [400 MHz, $CDCl_3$, δ=7.26 ppm, s]: 7.7 (2H, d), 7.5 (4H, t), 7.3 (1H, s), 6.9 (2H, d), 5.3 (1H, s) was shown in Fig. 8. M. F: $C_{15}H_{10}BrNO$, calculated mass- 298, observed mass- 299. Yield: 55%, m.p- 190 ^{0}C.

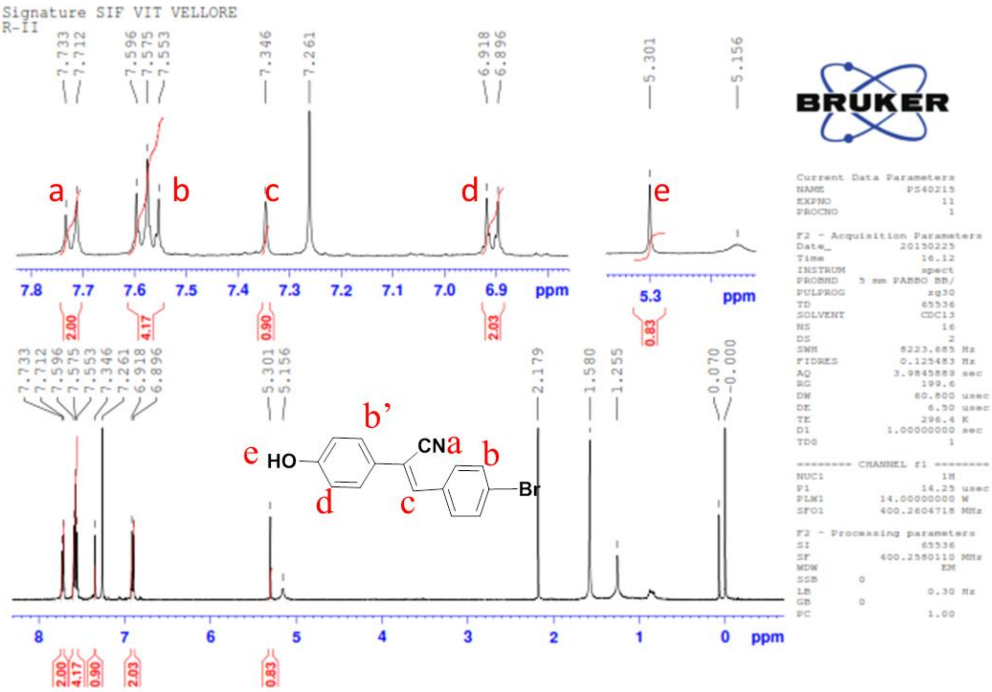

Fig-8: ^{1}H-NMR spectra of (E)-3-(4-bromophenyl)-2-(4-hydroxyphenyl) acrylonitrile.

6. Spectral characterization of (E)-3-(4-hydroxy-3-methoxyphenyl)-2-(4-nitrophenyl) acrylonitrile

Reddish brown colour stilbene. FT-IR (KBr, cm^{-1}): 3130 (ν_{O-H}), 3094 (Ar ν_{C-H}) 2227, (ν_{C-N}), 1610 (ν_{C-O-C}), 1570 ($\nu_{C=O}$), 1215 (ν_{N-O}) ^{1}H-NMR [400 MHz, $CDCl_3$, δ=7.26 ppm, s]: 8.3 (2H, q), 7.84 (2H, q), 7.80 (1H, s), 7.6 (1H, s), 7.3 (1H, q) , 7.0 (1H, d), 6.0 (1H, s), 4.0 (2H, s) was shown in Fig. 9. M. F: $C_{16}H_{12}N_2O_4$, calculated mass- 296, observed mass- 297. Yield: 55%, m.p- 190 ^{0}C.

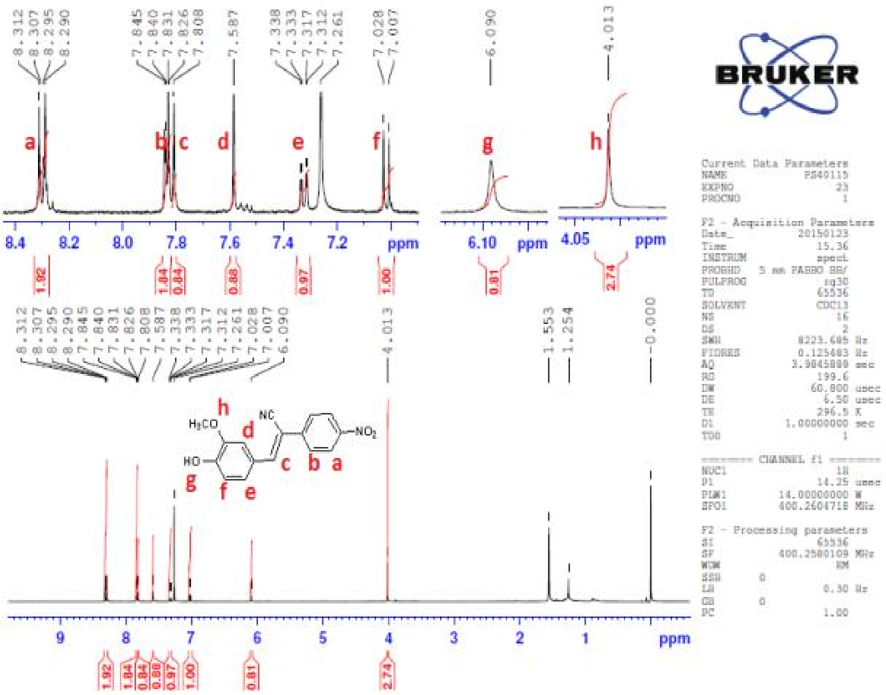

Fig-9: ^{1}H-NMR spectra of (E)-3-(4-hydroxy-3-methoxyphenyl)-2-(4-nitrophenyl) acrylonitrile.

7. Spectral characterization of (E)-2-(4-hydroxyphenyl)-3-(4-nitrophenyl)acrylonitrile

Yellow colour stilbene. FT-IR (KBr, cm^{-1}): 3404 (ν_{O-H}), 2214 (ν_{C-N}), 1585, (Ar $\nu_{C=C}$), 1512 ($\nu_{N=O}$). ^{1}H-NMR [400 MHz, $CDCl_3$, δ=7.26 ppm, s]: 8.3 (2H, d), 7.9 (2H, d), 7.8 (2H, d), 7.6 (1H, s), 6.9 (2H, d) was shown in Fig. 10. M. F: $C_{15}H_{10}N_2O_3$. Calculated mass-266, observed mass-267. Yield: 55%, m.p- 190 ^{0}C.

ISSN 2394 - 7780

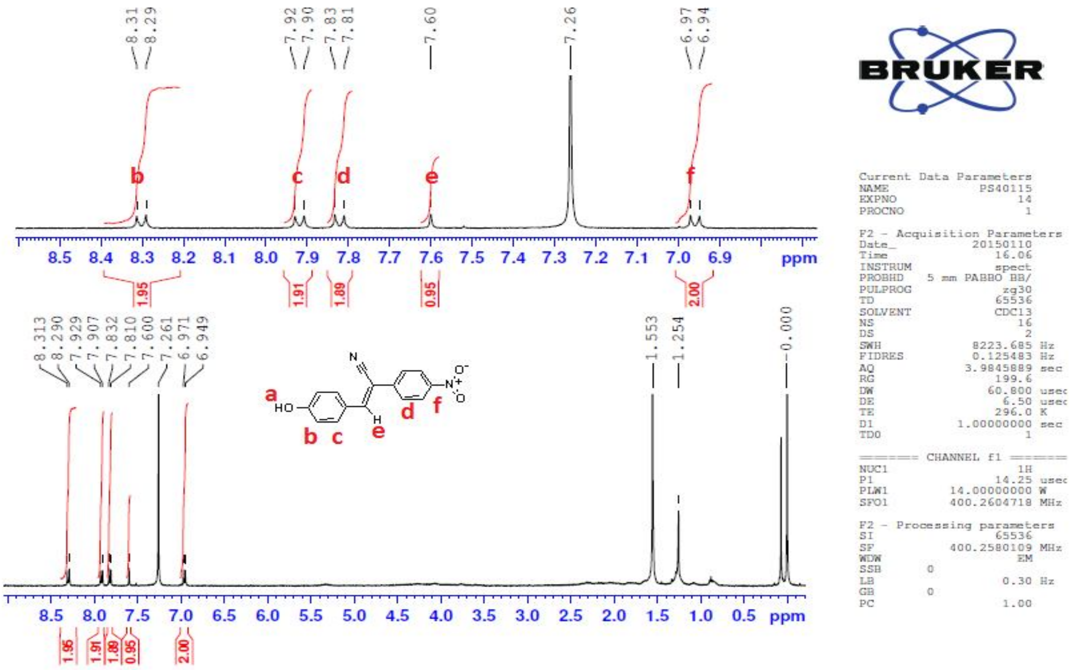

```
Current Data Parameters
NAME              PS40115
EXPNO                  14
PROCNO                  1

F2 - Acquisition Parameters
Date_            20150110
Time                16.06
INSTRUM             spect
PROBHD   5 mm PABBO BB/
PULPROG              zg30
TD                  65536
SOLVENT             CDC13
NS                     16
DS                      2
SWH              8223.685 Hz
FIDRES           0.125483 Hz
AQ              3.9845889 sec
RG                  199.6
DW                 60.800 usec
DE                   6.50 usec
TE                  296.0 K
D1             1.00000000 sec
TD0                     1

====== CHANNEL f1 ======
NUC1                   1H
P1                  14.25 usec
PLW1          14.00000000 W
SFO1          400.2604718 MHz

F2 - Processing parameters
SI                  65536
SF            400.2580109 MHz
WDW                    EM
SSB       0
LB                   0.30 Hz
GB        0
PC                   1.00
```

Fig-10: ^{1}H-NMR spectra of (E)-2-(4-hydroxyphenyl)-3-(4-nitrophenyl)acrylonitrile

8. Spectral characterization of (E)-3-(furan-2-yl)-2-(4-hydroxyphenyl) Acrylonitrile

Yellow colour stilbene. FT-IR (KBr, cm^{-1}): 3269 (Ar ν $_{C-H}$), 2227 (ν $_{C-N}$), 1614, 1591 (ν $_{C=O}$), 1514 (ν $_{C-Br}$). ^{1}H-NMR [400 MHz, CDCl$_3$, δ=7.26 ppm, s]: 7.8 (1H, d), 7.6 (1H, s), 7.5 (2H, d), 7.0 (1H, d), 6.7 (3H, m), 5.3 (1H, s). M. F: $C_{16}H_{12}N_2O_4$, calculated mass-296, observed mass-297.Yield: 55%, m.p-190 ^{0}C.

9. Spectral characterization of (E)-2-(4-fluorophenyl)-3-(furan-2-yl) acrylonitrile

Light yellow colour stilbene. FT-IR (KBr, cm^{-1}): 3156 (Ar ν $_{C-H}$), 2337 (ν $_{C-N}$), 748, 588 (ν $_{C-F}$). ^{1}H-NMR [400 MHz, CDCl$_3$, δ=7.26 ppm, s]: 7.8 (2H, d), 7.6 (H, s), 7.3 (2H, d), 7.1 (2H, d), 6.9 (1H, d) , 6.4 (1H, s). M. F: $C_{13}H_8FNO$, Calculated mass- 213, observed mass- 214.Yield: 55%, m.p- 190 ^{0}C.

10. Spectral characterization of (E)-2-(4-fluorophenyl)-3-(furan-2-yl) acrylonitrile

Light yellow colour stilbene. FT-IR (KBr, cm^{-1}): 3026 (Ar ν $_{C-H}$), 2216 (ν $_{C-N}$), 1834, (ν $_{C=C}$), 1512, (ν $_{C-N}$)1246, (ν $_{C-Br}$)1078 (ν $_{C-F}$). ^{1}H-NMR [400 MHz, CDCl$_3$, δ=7.26 ppm, s]: 7.9 (2H, d), 7.8 (1H, s), 7.6 (2H, d), 7.5 (2H, d), 7.01 (2H, d) , 6.4 (1H, s). M. F: $C_{15}H_9BrFN$, calculated mass- 300, observed mass- 302. Yield: 55%, m.p-190 ^{0}C.

3. RESULTS AND DISCUSSION

Cyano-stilbene are most widely used in organtic solar cell to construct a D-A acceptor system with broad absorption in the UV-vis region. In the paper we reported synthesis and studies of some of cyano-stilbene derivatives. From the FT-IR, we confirmed the functional groups such as –OH, -CN, -NO$_2$, and -C=C-. NMR spectroscopic techniques we used to confirm the product formation. The Gas chromatography with mass spectroscopy was used to find the product formation with yield.

4. CONCLUSION

We synthesized a donor- acceptor based cyano-stilbene derivatives from an aromatic aldehyde and aryl acetonitrile by an efficient Aldol condensation method using alcoholic alkali as a catalyst. We got moderate-good yields. The formation of the stilbene was confirmed by the ^{1}H-NMR, GC-MS, FT-I.R and melting point. Calculated mass clearly matched with the observed GC-Mass. ^{1}H-NMR also confirms the formation of product and its purity. UV-Visible absorption studies revealed that broad and stronger absorption of cyano-stilbenes. The strong and broad absorption is the desired property for the high PCE organic photovoltaic. From the electronic absorption studies it is clear our molecule could be a good harvester of solar radiations. In future we are planned to use this dyes as a good light harvester in organic solar cells.

REFERENCES

1. Block J. Wilson and Gisvold’s, (2004), Textbook of Organic Medicinal and Pharmaceutical Chemistry, 351 West Camden Street 530 Walnut Street, Baltimore, MD 21201 Philadelphia, PA 19106

2. Gutlich, P., Garcia, Y., and Woike, T, (2001), Photoswitchable coordination compounds, Coordination Chemistry Reviews, 839–879

3. Grabowski, R., Rotkiewicz, W., and Rettig, W. (2003), Structural Changes Accompanying Intramolecular Electron Transfer: Focus on Twisted Intramolecular Charge-Transfer States and Structures, Chemical Reviews, 103, 3899–4032.
4. Momotake, A. and Arai, T. (2004), Photochemistry and photophysics of stilbene dendrimers and related compounds, Journal of Photochemistry and Photobiology C: Photochemistry Reviews, 5, 1–25.
5. Ververidis, F., Trantas, E., Douglas, C., Vollmer, G., Kretzschmar, G., and Panopoulos, N. (2007), Biotechnology of flavonoids and other phenylpropanoid-derived natural products. Part I: Chemical diversity, impacts on plant biology and human health, Biotechnology Journal, 2, 1214–1234.
6. Cai, Y., Luo, Q., Sun, M., and Corke, H. (2004), Antioxidant activity and phenolic compounds of 112 traditional Chinese medicinal plants associated with anticancer. Life Sciences, 74, 2157–2184.
7. Wittig, G. and Werner H. Über. (1955), Triphenyl-phosphinmethylene als olefinbildende Reagenzien (II. Mitteil.[1])), Chemische Berichte, 88, 1654-1666.
8. Saiko, P., Szakmary, A., Jaeger, W., and Szekeres, T., (2008), Resveratrol and its analogs: defense against cancer, coronary disease and neurodegenerative maladies or just a fad? Mutation Research, 658(1-2), 68-94.
9. Lin, M. and Yao, C. S. (2006), Natural Oligostilbenes, Studies in Natural Products Chemistry, 33, 601–644.
10. Cravino, A., Neugebauer, H., Petr, A., Skabara, P. J., Spencer, H. J., McDouall, J. J. W., Dunsch, L., and Sariciftci, N. S., (2006), Spectroelectrochemistry of Poly(-ethylenedithiathiophene) the Sulfur Analogue of Poly(ethylenedioxythiophene), The Journal of Physical Chemistry B, 110, 2662- 2667.
11. Spencer, H. J., Skabara, P. J., Giles, M., McCulloch, I., Coles, S.J., and Hursthouse, M. B., (2005), The first direct experimental comparison between the hugely contrasting properties of PEDOT and the all-sulfur analogue PEDTT by analogy with well-defined EDTT–EDOT copolymers, Journal of Materials Chemistry, 15, 4783-4792.
12. Li, Y., (2012), Molecular Design of Photovoltaic Materials for Polymer Solar Cells: Toward Suitable Electronic Energy Levels and Broad Absorption, Accounts of Chemical Research, 45, 723-733,
13. Kwon, J. H., An, J.Y., Jang, H., Choi, S., Chung, D. S., Lee, M. J., Cha, H. J., Park, J. H., Park, C. E., Kim, Y. H., (2011), Development of a New Conjugated Polymer Containing Dialkoxynaphthalene for Efficient Polymer Solar Cells and Organic Thin Film Transistors, Journal of Polymer Science Part A: Polymer Chemistry, 49, 1119–1128
14. Kim, K. H.; Kang, H., Nam, S. Y., Jung, J., Kim, P. S., Cho, C. H., Lee, C., Yoon, S. C., Kim, B., (2011), Facile synthesis of o-xylenyl fullerene multiadducts for high open circuit voltage and efficient polymer solar cells, Chemistry of Materials, 23, 5090-5095.
15. Yingping Z., Bo P., Bo L., Li, Y., He, Y., Zhou, K., Pan, C. (2010), Conjugated copolymers of cyanosubstituted poly(p-phenylene vinylene) with phenylene ethynylene and thienylene vinylene moieties: Synthesis, optical, and electrochemical properties, Journal of applied polymer Science, 115, 1480-1488.
16. Asiri A. M., (2003), Synthesis and absorption spectral properties of bis-methine dyes exemplified by 2,5-bis-arylidene-1-dicyanomethylene-cyclopentanes, Bulletin of Korean Chemical Society, 24 (4), 426-430.

International Journal of Advance and Innovative Research
Volume 6, Issue 1 (VI): January - March, 2019
ISSN 2394 - 7780

SYNTHESIS OF AMLODIPINE BESYLATE

R. Govinda Rao and S. Suriyabalachandran
Department of Chemistry, Vels Institute of Science, Technology & Advanced Studies, Chennai
E-mail: govind.sbs@velsuniv.ac.in; govindchem2005@gmail.com

1. INTRODUCTION

Hypertension and dyslipidemia are the most commonly co-occurring cardiovascular risk factors. Coronary artery disease (CAD) is the leading cause of morbidity and mortality worldwide accounting for in excess of 930,000 deaths. It is a multi-factorial disease, emphasis is to treat overall cardiovascular risk rather than single risk factors in isolation. The third National Health and Nutrition Examination Survey (NHANES) estimated that more than 64% of patients with hypertension have dyslipidemia; conversely, approximately 47% of patients with dyslipidemia have hypertension. Antihypertensive and lipid lowering medications substantially reduce the risk of CAD, stroke and death in patients with cardiovascular risk factors. The fixed dose combination which contains the antihypertensive agent Amlodipine and the statin, Atorvastatin, is the first combination of its kind designed to treat two risk factors for cardiovascular disease (CVD). The pharmacokinetic and pharmacodynamic properties of Amlodipine and Atorvastatin make them well suited for combination in a single pill to manage cardiovascular risk. The half-lives of both agents facilitate once daily dosing and both can be administered at any time of day with or without food. Each drug has no adverse effects on the other's efficacy or tolerability [1].

Amlodipine Besylate is a white to off-white crystalline powder with a molecular weight of 567.1. It is slightly soluble in water and sparingly soluble in ethanol. Atorvastatin calcium is a white to off-white crystalline powder and it has a molecular weight of 1209.42. It is insoluble in aqueous solutions of pH 4 and below, it is very slightly soluble in distilled water, pH 7.4 phosphate buffer and acetonitrile. It is freely soluble in methanol [2]. Caduet® is indicated in patients for Hypertension, Coronary Artery Disease (CAD) like Angina, Prevention of Cardiovascular Disease and Hyperlipidemia [2]

The preparation of new combinations of drugs in pharmaceuticals encourages researchers to develop new and efficient methods for multi-quantification with separation procedures. HPLC is a dominant separation technique, especially in pharmaceutical analysis [3]. Literature survey indicated that several analytical methods have been described for the determination of Amlodipine Besylate, Atorvastatin Calcium alone [4-5] or in combination with other compounds [6-7]. Several method were reported for simultaneous determination of Amlodipine Besylate and Atorvastatin Calcium such as Spectrophotometry [8-10], HPTLC [11] Spectrofluorimetry, HPLC Coupled with Fluorescence Detection [12] Capillary Electrophoresis HPLC Coupled with UV Detection [13-17], HPLC–MS–MS [18- 20] and RP-UPLC [21-22].

MATERIALS AND METHODS

2.1 Materials

Amlodipine Besylate (ADB) and Microcrystalline Cellulose (MCC) were procured from Yarrow Pharmaceuticals, Mumbai, India. Magnesium Stearate, Lactose was procured from Vijlac Pharmaceuticals, Hyderabad, India. Crospovidone was purchased from DMV Fronterra excipients, Cuddalore, India. Talc and Sodium Saccharine was procured from Navdeep fine chemicals, Mumbai, India. All other chemicals and reagents used were of laboratory or analytical grade.

2.2 Instrumentation

Analysis was performed on a chromatographic system of WATERS 2695 separation module connected to WATERS 2487 UV/ VIS detector. The system equipped by Empower PC program. The chromatographic separation was achieved on Phenomenex kinetex 2.6 µm C18 100A (100x 4.6 mm).

2.3 Chemicals and reagents

All reagents used were of analytical grade or HPLC grade. Potassium dihydrogen phosphate and ortho-phosphoric acid were supplied by (Merck, Darmstadt, Germany), Acetonitrile and Methanol HPLC grade were supplied by (Fischer scientific, U.K.) and Distilled water was obtained from Milli-RO and Milli-Q systems (Millipore, Bedford, MA). Amlodipine Besylate and Atorvastatin Calcium working standard powders were kindly supplied by Egyptian international pharmaceutical industries company (EIPICO) (10th Ramadan, Egypt), and were used without further purification

2.4 Preparation of magnetic Fe_3O_4 nanoparticles

20 µl of drugs sample solutions were monitored at fixed wavelength (lambda =240 nm for Amlodipine Besylate and Atorvastatin Calcium). Liquid chromatography was performed on Phenomenex kinetex 2.6 µm C18 100A

(100x 4.6 mm) and the mobile phase consisted of Potassium dihydrogen phosphate (pH 5.5, 0.03M) - Acetonitrile (65:35 V/V) which pumped at a flow rate equals to 1.2 ml/min at 40 °C.

Potassium dihydrogen phosphate (pH 5.5, 0.03M) was prepared by dissolving 4.08 g of Potassium dihydrogen phosphate in approximately 950 ml distilled water. The pH was adjusted to 5.5 with sodium hydroxide then water was added to 1000 ml.

Mobile phase was filtered through a 0.45 µl Nylon membrane filter (Millipore, Milford, MA, USA) under vacuum and degassed by ultrasonication (Cole Palmer, Vernon Hills, USA) before usage. Mixture of acetonitrile and distilled water (50:50 V/V) was prepared to be used as diluents.

2.5 Preparation of stock standard solutions

Stock standard solutions containing 1 mg/ml of Amlodipine (as Besylate) (actual weight =103.6 mg) and 1 mg/ml of Atorvastatin (as Calcium) (actual weight =105.2 mg) were prepared by dissolving 100 mg of each in 40 ml methanol in 100 ml volumetric flask respectively. It was sonicated for 5 minutes and the final volume of solutions was made up to 100 ml with diluent to get stock standard solutions.

2.6 Preparation of calibration plot (working standard solutions)

To construct calibration plots, the stock standard solutions were diluted with diluent to prepare working solutions in the concentration ranges (5.18-15.54 and 5.26-15.78 µg/ml) for Amlodipine Besylate and Atorvastatin Calcium respectively. Each solution (n=5) was injected in triplicate and chromatographed under the mentioned conditions above. Linear relationships were obtained when average drug standard peak area were plotted against the corresponding concentrations for each drug. Regression equation was computed.

2.7 Sample preparation

A composite of ten Caduet® 10/10 tablets was prepared by grinding it to a fine, uniform size powder, triturated using mortar and pestle. After calculating the average tablet weight, amounts of powder equivalent to one tablet was accurately weighed and transferred to 100 ml volumetric flasks then completed with diluent up to 100 ml. The solutions were solicited for 15 min and the solutions were then filtered through 0.45 µm Nylon membrane filters (Millipore, Milford, MA, USA). Aliquots of appropriate volume (10 ml) were transferred to 100 ml calibrated flasks and diluted to volume with diluent to obtain the mentioned concentration above (10 µg/ml). The diluted solutions were analyzed under optimized chromatographic conditions and chromatogram.

3. RESULT AND DISCUSSION

3.1 FTIR study

In order to further study whether Amlodipine undergoes a polymorphic change during preparation of FDTs and to test for possible intermolecular interactions between Amlodipine and excipients, FTIR was used. The FTIR spectra of pure Amlodipine, Amlodipine with urea and joint spectrum of Amlodipine and Amlodipine with urea (A, B and C) are depicted in (figure 1). All the principal IR peaks of Amlodipine were present in all formulations (F1, F2 and F3). This clearly indicates that there is no interaction between Amlodipine and excipients

Fast disintegrating tablets of Amlodipine were prepared by direct compression method employing crospovidone and sodium starch glycolate as super-disintegrants in different ratio. A total of three formulations were designed. The flow properties of the powder mixture are significant for the uniformity of mass of the tablets. The flow of the powder mixture were analyzed before compression to tablets. The values of pre-compression parameters evaluated were within prescribed limits and indicated a good free flowing property. Low Hausner`s ratio (≤1.25), compressibility index (≤20.16) and angle of repose (≤36.89) values indicated a fairly good flow ability of powder mixture depicts post-compression parameters of Amlodipine FDTs. As the tablet powder blend was free flowing, tablets produced were of uniform weight with acceptable weight variation in the range from 136 mg to 140 mg due to uniform die fill. Hardness (3.4-3.7 kg/cm^2) and friability loss (0.7-0.87 %) indicated that tablets had a fine mechanical resistance. Drug content was found to be high (≥97.6 %) in all the tablet formulations. Uniform distribution of the active agent was assessed by UV, the content of Amlodipine was found inside the 98.1% of the theoretical value.

The most important parameter that needs to be optimized in the development of fast disintegrating tablets is the disintegration time of tablets. In this present study, it was observed that the disintegration time of the tablets had a significant effect with the type of super-disintegrate. However, disintegration time decreased when the combination of disintegrates was used in the tablets. This indicates that combination of super disintegrates had a positive effect on the disintegration of the tablets, which may be due to its rapid capillary activity and hydration with little tendency to gel formation. Thus, these results suggest that the disintegration time can be increased by using single disintegrate.

Wetting time is an important criteria for understanding the capacity of disintegrates to swell in presence of little amount of water and were found to be in the range of 26-28 seconds.

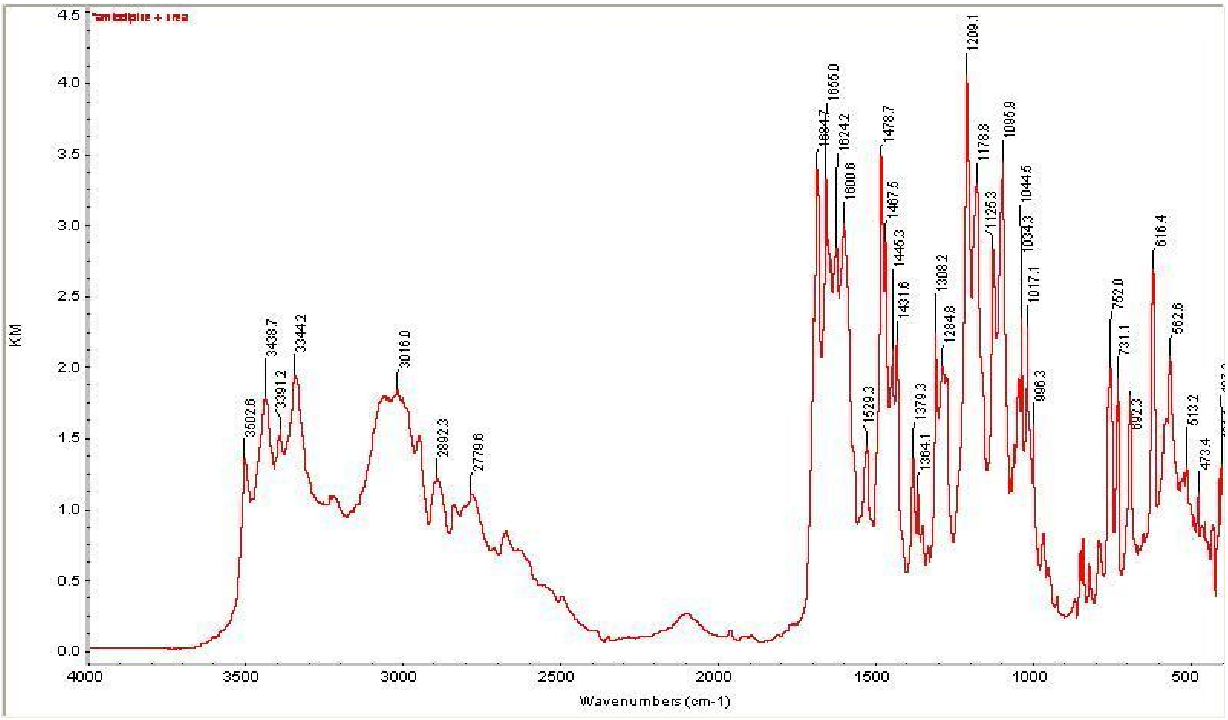

Fig-1: FTIR Spectrum of Amlodipine drug (A), Amlodipine with urea (B)

3.2 In vitro Drug Release Studies

The dissolution profile of the formulations range from77.84-87.55% (table 4). The dissolution rate was found to be comparatively less for the formulation containing sodium starchglycolate. The maximum increase in the dissolution rate was observed with the combination of crospovidone and sodium starch glycolate among the three formulations.

The order of the dissolution rate with various super disintegrants was found to be combination of disintegrants >crospovidone > Sodium starchglycolate. Combination of superdisintegrants was found to be better than using alone and the formulation containing crospovidone and sodium starch glycolate was found to be showing the maximum dissolution after 30 minutes of dissolution study. Many factors contributed to faster release rate such as decrease in particle size, decrease in agglomeration of particles increase wettability and decrease in crystallinity of the drug.

CONCLUSION

The present investigation of this study was undertaken with an aim to formulate and characterize fast disintegrating tablets of Amlodipine using direct compression method with the addition of super-disintegrating agents. FTIR study reveals that there is no drug-excipients interaction between Amlodipine and excipients. It is observed that the formulation F3 containing crospovidone and Sodium Starch Glycolate was found to be promising showing disintegration time of 10.12 second, wetting time of 26.2 second and highest dissolution rate (87.55%) in 30 min when compared to formulations (F1) and (F2). It was concluded that combination ofsuperdisintegrants showed better disintegrating time, wetting time and dissolution property than the formulation of single disintegrant containing tablets.

REFERENCES

1. Go, M. L., Wu, X., & Liu, X. L. (2005). Chalcones: an update on cytotoxic and chemoprotective properties. *Current Medicinal Chemistry*, *12*(4), 483-499.

2. Awasthi S. K., Mishra N., Kumar B., Sharma M., Bhattacharya A., Mishra L. C. &Bhasin V. K. (2009). Potent antimalarial activity of newly synthesized substituted chalconeanalogs*in vitro*.*Medicinal Chemistry Research, 18(6),* 407-420.

3. Aponte J. C., Verástegui M., Málaga E., Zimic M., Quiliano M., Vaisberg A. J., & Hammond G. B. (2008). Synthesis, cytotoxicity, and anti-Trypanosomacruzi activity of new chalcones.*Journal of Medicinal Chemistry*, *51*(19), 6230-6234.

4. Alam M. S. (2012). Biological Potentials of Chalcones A Review.*International Journal of Pharmaceutical & Biological Archive, 3*(6).

5. Nasir Abbas Bukhari S., Jasamai M., Jantan I., & Ahmad W. (2013).Review of methods and various catalysts used for chalcone synthesis.*Mini-Reviews in Organic Chemistry, 10(1),* 73-83.

6. Ducki, S. Anti-cancer Agents Med. Chem. 2009, 9, 336.

7. Flynn, B. L.; Hamel, H.; Jung, M. K. J. Med. Chem. 2002, 45, 2670; (b) Flynn, B. L.; Flynn, G. P.; Hamel, E.; Jung, M. K. Bioorg. Med. Chem. Lett. 2001, 11, 2341; (c) Romagnoli, R.; Baraldi, P. G.; Carrion, M. D.; Cara, C. L.; Cruz-Lopez, O.; Preti, D.; Tolomeo, M.; Grimaudo, S.; Di Cristina, A.; Zonta, N.; Balzarini, J.; Brancale, A.; Sarkar, T.; Hamel, E. Bioorg.Med. Chem. 2008, 16, 5367.

8. Morrison and Boyd, Organic Chemistry, sixth edition, 2004, 971-990, 997-820.

9. Alam M. S. (2012). Biological Potentials of Chalcones A Review.*International Journal of Pharmaceutical & Biological Archive*, *3*(6).

10. Rao, S. R.; Ravishankar, G. A. Biotecnol. Adv.2002, 20, 101-152.

11. Cowan, M. M. Clin. Microbiol.Rev.1999, 20, 564-582.

12. Alcaraz, L.E.; Blanco, S.E.; Puig, O.N.; Tomas, F.; Ferretti, F.H. Antibacterial activity of flavonoids against methicillin-resistant *Staphylococcus aureus*strains. *J. Theor. Biol.* 2000, *205*, 231–240.

13. Echeverria, C.; Santibañez, J.F.; Donoso-Tauda, O.; Escobar, C.A.; Ramirez-Tagle, R. Structural antitumoral activity relationships of synthetic chalcones. *Int. J. Mol. Sci.* 2009, *10*, 221–231.

14. Dhar D.N., The Chemistry of Chalcones and Related Compounds; John Wiley and Sons: New York, 1981. (b) Stoyanov E.V., Champavier Y., Simon A., Basly J-P., Bioorg.Med. Chem. Lett., 12: 2685 (2002); (c) Saravanamurugan S., Palanichamy M. Arabindoo B., Murugesan V., Catal.Commun., 6: 399 (2005); (d) Ballesteros J.F., Sanz M.J., Ubeda A., Miranda M.A. Iborra S., Paya M., Alcaraz M.J., J. Med. Chem., 38: 2794 (1995); (e) Tran T-D., Park H., Kim H.P., Ecker G.F. Thai K-M., Bioorg. Med. Chem. Lett., 19: 1650 (2009); (f) Casiraghi G., Casnati G., Dradi E., Messori R., Sartori G., Tetrahedron, 35: 2061 (1979); (g) Macquarrie D.J., Nazih R., Sebti S., Green Chem., 4: 56 (2002); (h) Barros A.I.R.N.A., Silva A.M.S., Alkorta I., Elguero J., Tetrahedron, 60: 6513 (2004); (i) Detsi A., Majdalani M., Kontogiorgis C. A., Dimitra H-L., Kefalas P., Bioorg. Med. Chem., 17: 8083 (2009); (j) Climent M.J., Corma A., Iborra S., Primo J., J. Catal., 151: 60 (1995); (k) orenz M., Kabir M.S., Cook J.M., Tetrahedron Lett., 51: 1095 (2010).

15. Sagreraa G.J., Seoane G.A., J. Braz. Chem. Soc., 16: 851 (2005); (b) Choudary B.M., Ranganath K.V.S., Yadav J., Kantam M.L., Tetrahedron Lett., 46: 1369 (2005); (c) Lee J.I., Jung M.G., Bull. Kor. Chem. Soc., 28: 859 (2007); (d) Dauzonne D., Monneret C., Synthesis 11: 1305 (1997); (e) Wang X., Cheng S., Catal. Commun.,7: 689 (2006); (f) Chaturvedi R., Patil P.N. Mulchandani N.B., Indian J. Chem., 31B: 340 (1992); (g) Wang L., Liu X., Dong Z., Fu X., Feng X., Angew. Chemie Int. Ed., 47: 8670 (2008).

16. G Yoon; BY Kang; SH Cheon, *Arch. Pharm. Res.*, 2007, 30(3), 313-316.

17. HD Durst; GW Gokel, Experimental Organic Chemistry., 2nd Edition, McGraw-Hill Publishing Company, New York, 1987, 428-430.

18. S Sebti; A Solhi; R Tahir; S Boulaajaj; JA Mayoral; JM Fraile; A Kossir; H Oumimoun, *Tetrahedron Lett.*, 2001, 42, 7953-7955.

19. K Watanabe; AImazawa, *Bull. Chem. Soc. Jpn.*, 1982, 55, 3208-3211.

20. MS Cheng; RS Li; G Kenyon, *Chin ChemLett*., 2000, 11(10), 851-854.

21. P Salehi; MM Khodaei; MA Zolfigol; A Keyvan, *MonatsheftefuerChemie.*, 2002, 133, 1291-1295.

22. F Fringuelli; F Pizzo; C Vittoriani; L Vaccacio, *Chem. Commun.*, 2004, 130, 2756-2757.

International Journal of Advance and Innovative Research
Volume 6, Issue 1 (VI): January - March, 2019

ISSN 2394 - 7780

ACOUSTICAL STUDIES ON MOLECULAR INTERACTION OF 4,4'-DIBROMO BENZILIC ACID WITH VARIOUS SOLVENTS AT DIFFERENT CONCENTRATIONS USING ULTRASONIC TECHNIQUE

R. Sudha, G. Nithya and Charles K. Kanakam
Department of Chemistry, School of Engineering, Vels University, Chennai

ABSTRACT

The ultrasonic velocity, density and viscosity have been measured for the binary mixtures of 4,4'-dibromo benzilic acid with polar and non-polar solvents at 298K. The experimental data have been used to calculate the Density (ρ) and acoustical parameters namely, ultrasonic velocity (U), adiabatic compressibility (β), apparent molar volume (Ø), acoustic impedance (Z), intermolecular free length (L_f), relative association (R_A). The excess values of some of the above parameters have also been evaluated. The above study is useful to discuss the nature and extent of solute – solvent interactions occurring in different solvents and in different concentrations at 298K.

Keywords: Ultrasonic velocity; Density; Excess parameters; Intermolecular hydrogen bonding

INTRODUCTION

The study of molecular interaction plays a vital role in the development of molecular science. Different acoustical properties like adiabatic compressibility, intermolecular free length and apparent volume can be studied by using flexible ultrasonic at 298 K. Also, ultrasonic studies were used to know the molecular interactions and structural behaviour of molecules and their mixtures. Late advancements have discovered utilization of ultrasonic studies in medication, building and farming [1-4]. In industry and biologic processes has been recognized practical application of mixed solvents, rather than single solvent, world, as they provide a wide choice of solvent mixtures with appropriate properties [5, 6]. Ultrasonic speed together with thickness and consistency information outfit abundance of data about the association between particles, dipoles, hydrogen bonding, multi-polar and dispersive forces [7-10]. We focus in this paper the results of ultrasonic studies of binary mixture of 4,4'-dibromo benzilic acid with solvents of different polarities. As a result, significant interaction through hydrogen bonding between unlike molecules in these binary mixtures is expected.

EXPERIMENTAL PROCEDURE

4,4'-dibromo benzilic acid was synthesised by benzoin condensation followed by oxidation with Conc.HNO_3. Then benzil formed was treated with aq. KOH. The driving force for the reaction is provided by the formation of a stable potassium benzilate, which was acidified. Solvents like ethanol, acetonitrile, chloroform and 1, 4-Dioxane (s. d. fine, India, AR) were dried over molecular sieves. All the binary mixtures were prepared by mass in a dry box and were kept in special air tight bottles. Solutions of benzilic acid in the concentration range of 0.000938-0.03 mole% with different solvents were prepared at room temperature. The densities of pure liquids and binary mixtures were measured using a simple capillary pycnometer of bulb capacity 8 x 10-6m3 with a graduated stem width of 5 x 10-8m3 divisions (Systronies India, Ltd.,). The marks on the capillary were calibrated using known densities of double distilled water. The accuracy of the density measurement was found to be 0.001 gm/cc. The viscosities of the binary mixtures were determined using an Ostwald Viscometer (Sigma Chemicals Instruments). The ultrasonic velocities of pure solvent and the binary mixtures were measured using a single crystal variable path interferometer at 2 MHz (Mittal Enterprises, New Delhi). The accuracy in ultrasonic velocity was found to be + 0.05%. The temperature of the test liquids and their binary mixtures was maintained to an accuracy of ±0.02 in an electrically controlled thermostatic water bath. From the measured values of density ρ, ultrasonic velocity u, the adiabatic compressibility b or Ks, intermolecular free length Lf, relative association RA and acoustic impedance Z, have been calculated using the standard relations.

$$\rho = (M\,\rho_w / M_w) \quad (1)$$

$$U = \nu\,\lambda \text{ ms}^{-1} \quad (2)$$

$$K = [1 / U^2 \rho] \text{ Kg}^{-1}\text{Ms}^2 \quad (3)$$

$$Z = U\rho \text{ Kg}^{-2}\text{ S}^{-1} \quad (4)$$

where K is a temperature-dependent constant (93.875+0.375 x T) x 10-8, T is the absolute temperature, Z is the acoustic impedance, b or Ks the adiabatic compressibility, Lf the intermolecular free length, RA is the relative association, and ro, r, u° and u are the densities and ultrasonic velocities of the solvent and solution respectively.

RESULT AND DISCUSSIONS

In the case of DBBA, there is an initial increase in the density for polar solvents like ethanol and acetonitrile in the range from 0.000938-0.001875 mole fraction%. The graph (Fig. 1) shows, from 0.00375-0.0075 mole fraction%, there is a sudden decrease in the density with increase in concentration by the mixing of solute to solvent which leads to breaking of inter molecular interaction between solvent molecules. The increase in density is observed at 0.015 mole fraction %, which may be due to the cluster formation between solute and solvent (Table 1). For non polar solvents, there is an initial decrease in density observed in the range from 0.000938-0.001875 mole fraction%, due to increase in volume of the solution by the addition of DBBA.

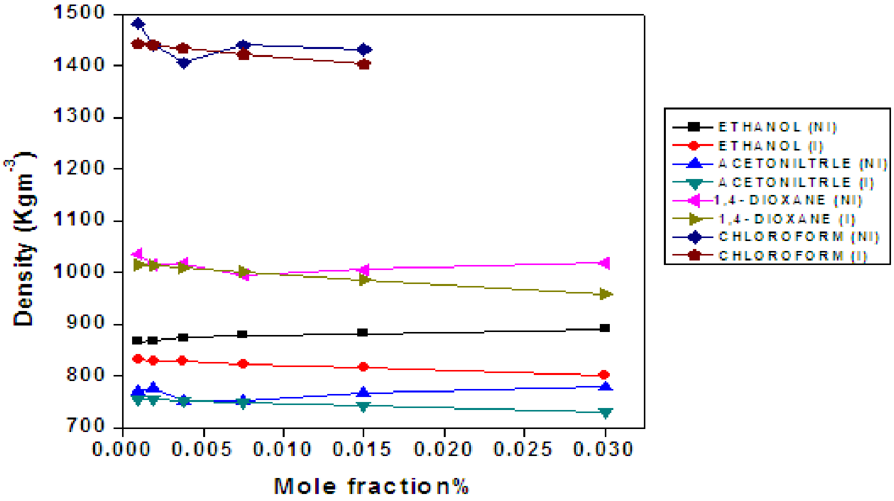

Figure-1: Density versus concentration graph for DBBA in different solvents

Fig. 2 shows the plots of ultrasonic velocity versus mole fraction. The ultrasonic velocity of DBBA increases with increase in concentration and maximum is observed at 0.001875 mole fraction% concentration followed by decrease in velocity for polar solvents like ethanol and acetonitrile. The increase in velocity due to the interaction between solute and solvent molecule is becoming more dominant and vice versa. In the case of non polar solvent, a decrease in velocity is observed at higher concentration, may be due to weak solvent- solute interaction.

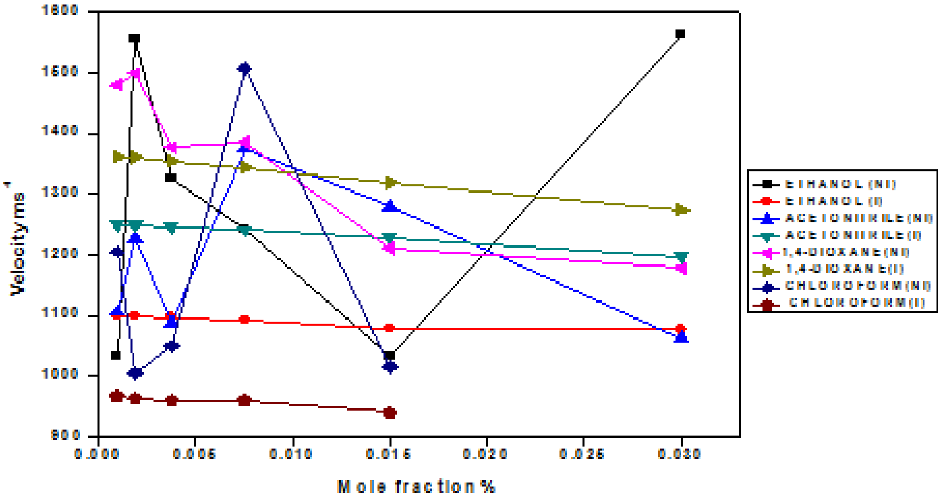

Figure-2: Velocity versus concentration graph for DBBA in different solvents

There is a high value of adiabatic compressibility for polar solvent observed at 0.000938 mole fraction%, which shows that there is no change in the hydrogen bonding at low concentration. The low value of adiabatic compressibility is observed for polar solvent at 0.001875 mole fraction%. Beyond this there is an increase in the adiabatic compressibility, which is due to the change in the arrangement of the solvent molecules around the solute molecules. This results in weakening of the solute/solvent interactions with more compressible solution. Beyond 0.0075 mole fraction% concentration for acetonitrile there is an increase in adiabatic compressibility, showing the change in the conformation of the solute in solution. This leads to the weaker intermolecular interaction. The initial decrease in adiabatic compressibility with increase in concentration indicates the breakdown of the network formed by the solvent molecules (Fig. 3).

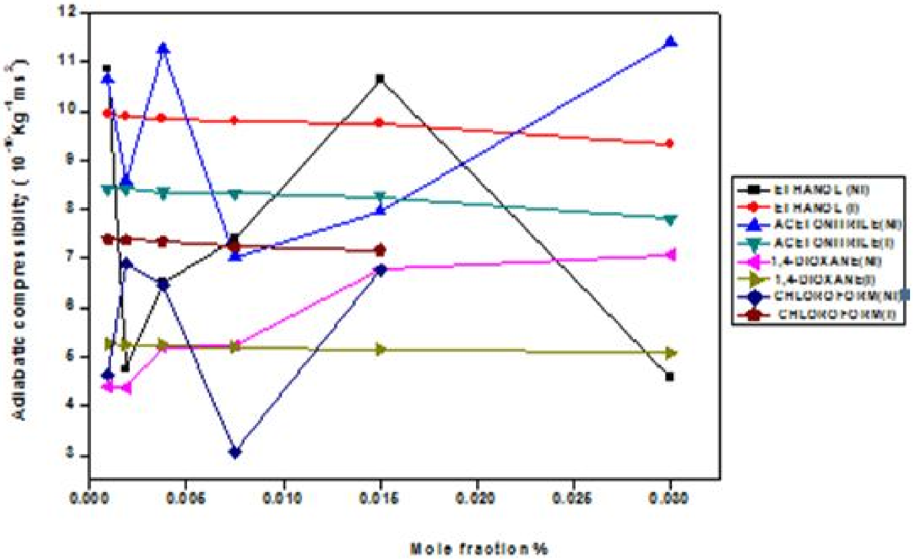

Figure-3: Adiabatic compressibility versus concentration graph for DBBA in different solvents

For polar solvent at low concentration in the range of 0.000938-0.001875 mole fraction%, there is a decrease in intermolecular free length showing the formation of tightly held aggregate. This is due to the strong forces acting between solute and solvent molecules. Beyond 0.001875 mole fraction% there is an increase in free length due to decrease in the degree of association among solvent molecules (Fig. 4).

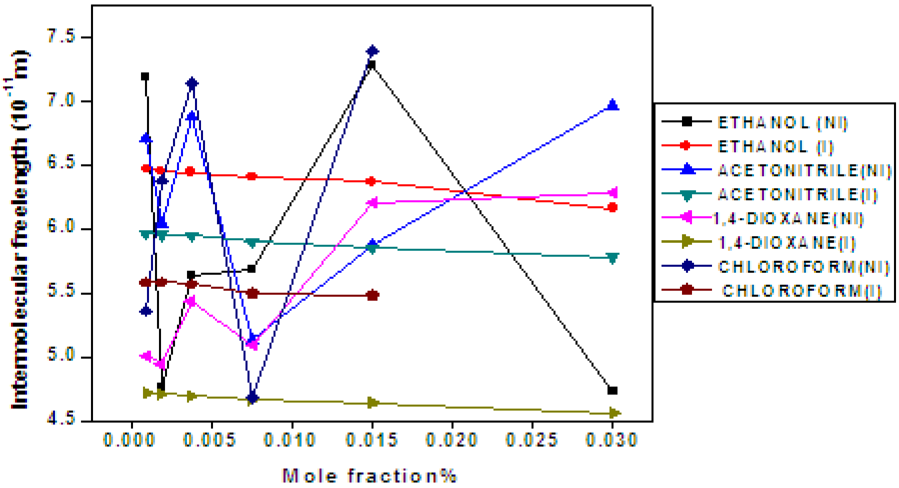

Figure-4: Intermolecular free length versus concentration graph for DBBA in different solvents

For polar solvent at 0.001875 mole fraction% concentration, a minimum relative association value is observed. The maximum value is reached at 0.03 mole fraction% (Fig. 5).

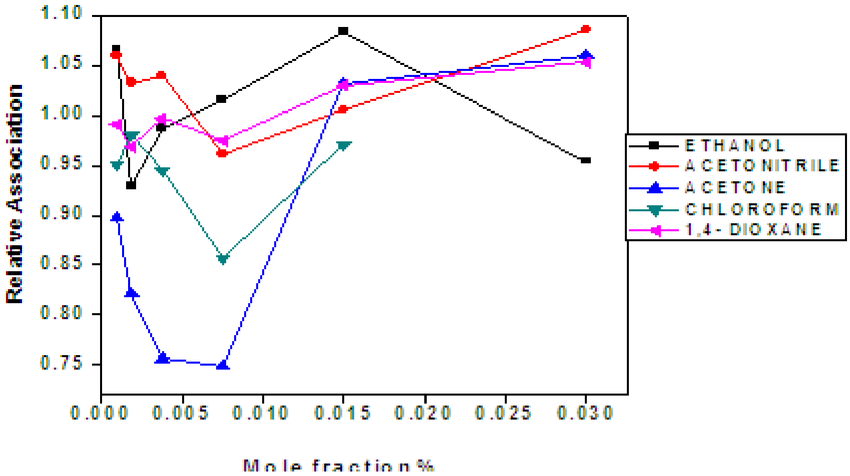

Figure-5: Relative Association versus concentration graph for DBBA in different solvents

Table-1: Variation of ultrasonic parameters for binary mixtures of DBBA with various solvents at different concentration (Mole fraction %)

Solvents	Concentration for various ultrasonic parameters					
	0.000938	**0.001875**	**0.00375**	**0.0075**	**0.015**	**0.03**
Non-Ideal(NI)	**Density Kgm^{-3}**					
Ethanol	867	868	874	870	882	892
Acetonitrile	769	776	751	750	766	778
Chloroform	1483	1440	1407	1440	1432	-
1,4-dioxane	1035	1016	1017	996	1006	1019
Non-Ideal(NI)	**Velocity ms^{-1}**					
Ethanol	1031.2	1556.8	1327.2	1240.8	1032.5	1562.9
Acetonitrile	1105.6	1226	1087.2	1374.8	1279	1061.6
Chloroform	1205	1004	1048	1506.4	1015.2	-
1,4-dioxane	1480.5	1409.6	1376.5	1385	1210.2	1177.2
Non-Ideal(NI)	**Adiabatic compressibility $Kg^{-1}ms^{2}$**					
Ethanol	10.8466	4.7535	6.4955	7.3894	10.644	4.5958
Acetonitrile	10.6458	8.5678	11.2562	7.0450	7.9805	11.456
Chloroform	4.6457	6.8934	6.4736	3.0623	7.7846	-
1,4-dioxane	4.4134	4.3578	5.1974	5.2345	6.7912	7.0823
	Intermolecular freelength 10^{-11} m					
Ethanol	7.1860	4.7599	5.6385	5.6841	7.2168	4.7321
Acetonitrile	6.7024	6.0422	6.8834	5.1301	5.8744	6.9666
Chloroform	6.1495	7.3806	7.1407	4.6819	7.4008	-
1,4-dioxane	5.0052	4.9414	5.4365	5.0992	6.2083	6.2825
Non-Ideal(NI)	**Relative Association (R_A)**					
Ethanol	1.0651	0.9294	0.9869	1.0151	1.0829	0.9538
Acetonitrile	1.0588	1.0321	1.0398	0.9616	1.0047	1.0858
Chloroform	0.9498	0.9801	0.9441	0.8562	0.9711	-
1,4-dioxane	0.9904	0.9681	0.9971	0.9745	1.0296	1.0525
Excess Velocity ms^{-1}						
Ethanol	-68.15	457.59	230.72	149.46	-45.49	486.67
Acetonitrile	-144.69	-22.49	-157.93	133.70	50.42	-136.26
Chloroform	239.95	41.01	88.13	546.25	75.32	-
1,4-dioxane	118.12	139.56	22.15	40.82	-108.7	-96.55
Excess Density Kgm^{-3}						
Ethanol	35.98	37.97	45.91	54.73	65.25	89.70
Acetonitrile	12.90	20.15	-2.29	1.36	48.62	23.3
Chloroform	40.61	0.378	-27.04	16.26	29.15	-
1,4-dioxane	19.14	2.156	7.07	-5.85	19.303	60.82
Excess adiabatic compressibility $Kg^{-1}ms^{2}$						
Ethanol	-9.7845	-5.1278	-3.3571	-2.4067	-9.4274	-4.7424
Acetonitrile	-8.300	0.1604	-8.2335	-1.2876	-0.2771	-7.6850
Chloroform	-2.7471	-0.4913	-0.8770	-4.1771	-0.4014	-
1,4-dioxane	-0.8588	-0.8780	-0.0478	0.0369	1.6222	2.0065
Excess Intermolecular free length 10^{-11} m						
Ethanol	0.7162	-1.6966	-0.8022	-0.7211	0.9101	-1.4284
Acetonitrile	0.7395	0.0872	0.9382	-0.7735	0.0210	1.1839
Chloroform	0.5616	`1.7975	1.5731	-0.8198	1.9132	-
1,4-dioxane	0.2889	0.23348	0.7409	0.4302	1.5743	1.7265

1.2. EXCESS FUNCTIONS

For all concentrations excess volumes are negative, due to the apparent existence of interactions between solute and solvent. As the polarity of the solvent increases there is an increase in the rate of disruption of intermolecular interaction between solvent molecules. This results in an increase in the negative excess volume and a decrease in the excess density of the solution.

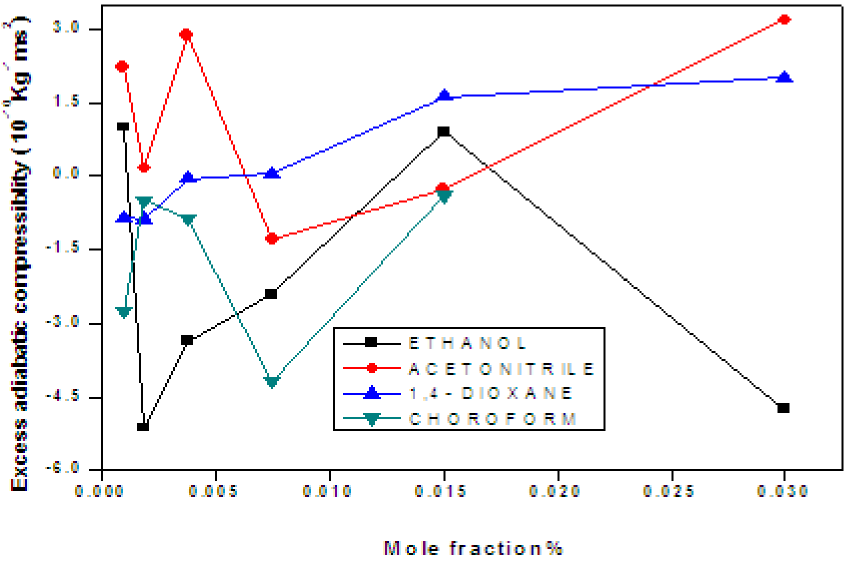

Figure-6: Excess adiabatic compressibility versus concentration DBBA in different solvents

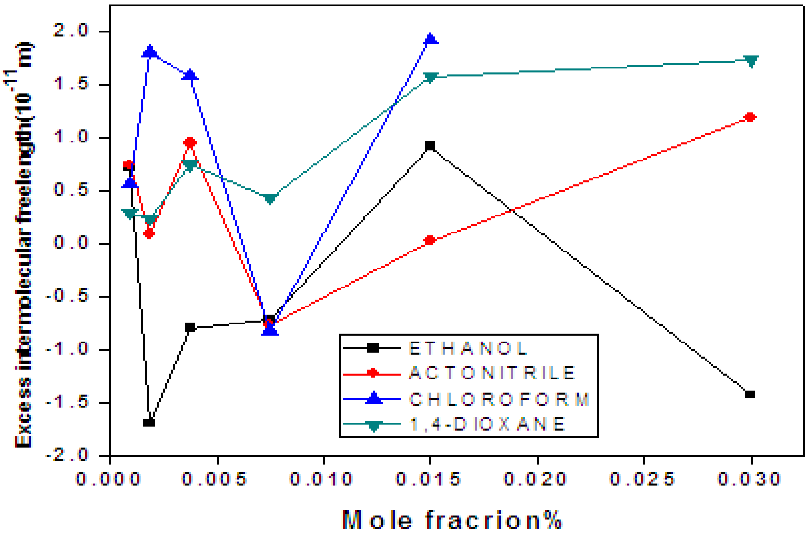

Figure-7: Excess intermolecular freelength versus concentration DBBA in different solvents

REFERENCES

1. Megremis, S., Chatziioannou, M., and Tritou L., J. (2010). Ultrasound in Medicine January 29, 145-147.
2. Golamari Siva Reddy and MalluMaheswara Reddy, (2013). Densities and viscosities of binary mixtures of methyl ethyl ketone with ethyl benzene at 303.15, 308.15, 313.15 K and atmospheric pressure, Journal of Chemical and Pharmaceutical Research, 5(11), 644-648.
3. Golamari Siva Reddy., and Mallu Maheswara Reddy, (2014).Thermodynamic properties of binary liquid mixture of toluene with benzene, Int J Pharm Bio Sci Jan; 5(1), (B) 1064 – 1073.
4. Golamari Siva Reddy, Mallu Maheswara Reddy,.Swathi Chowdary, V., and Golamari Krishna Reddy, (2013). Physical and Transport Properties of Binary Liquid Mixtures, Asian Journal of Biochemical and Pharmaceutical Research, 4(3), 64-73.
5. Kudrivavtsev, B.B. (1956). Sov. Phys. Acoust. 2, 36.
6. Ramanujappa, T., Bhavani, J.A., Rajagopal, E., and Manohara Murthy, N. (2000). Indian J. Pure Appl. Phys. 38, 301.
7. Vodamalar, R., Mani, D., and Balakrishanan, R. (2011). Res. J. Chem.Sci., 1, 9,79-82.
8. Thirumanan, S., Sardha Devi, S. (2009). Arch. Appl.Sci.Rers., 1, 2, 128-141.
9. Ali, A., Tiwari, K., Nain, A.K., and Charkravarthy, V. (2000). Ind.J.Phy. 74B, 5, 351-355.
10. Devadss, D., Thairiyaraja,M., and Palaniappau, L. (2003). Ind.J. Phy. 77B, 6, 669-672.

International Journal of Advance and Innovative Research
Volume 6, Issue 1 (VI): January - March, 2019
ISSN 2394 - 7780

AMPEROMETRIC DETERMINATION OF GLUCOSE USING GREEN SYNTHESIZED NANOPOROUS NICKEL OXIDE

S. Meenakshi[1] and M. Revathi[2]
Assistant Professor[1] and Associate Professor[2], Department of Chemistry, Vels Institute of Science, Technology and Advanced Studies, Chennai
E-mail: meenakshivanitha@gmail.com

ABSTRACT

We have developed green synthesized nanoporous nickle oxide nanoparticles (NpNiONPs) by simple chemical precipitation method. Structure and morphology of the NpNiONPs was investigated by SEM and XRD analysis. The modified NpNiONPs was successfully employed as a sensor of glucose in alkaline medium and the electrochemical oxidation of glucose was investigated by cyclic voltammetry and amperometric techniques. The NpNiONPs modified electrode exhibited high electrocatalytic activity, low detection limit, good reproducibility, better selectivity and sensitivity towards the oxidation of glucose. The proposed method can be applied for the determination of glucose in blood samples.

Keywords: Amperometric technique, Blood samples, Chiriyanankai leaves, *Glucose detection, Nanoporous nickle oxide.*

INTRODUCTION

Diabetes is a metabolic diseases resulting from insulin deficiency in blood and diverse organs particularly eyes, heart, kidney, and blood vessels [1]. For that reason, the sensitive diagnosis of unusual glucose levels in blood is very significant for appropriate treatment to decrease the above mentioned problems. Various analytical methods have been applied to detect the glucose concentration such as fluorescent, optical, electronic, capacitive, transdermal and electrochemical methods [2–7]. Among these, the electrochemical sensing approaches have drawn so much attention due to their acceptable sensitivity, selectivity, simple instrumentation, long stability, rapid response and flexibility.

Green synthesized nanoporous nickle oxide nanoparticles (NpNiONPs) have been a great deal of regard due to their high biocompatibility, magnetic property, displaying no hemolytic activity or genotoxicity, better interaction with desired bioactive molecules [8, 9] as well as their potential for providing the control of electrochemical processes [10]. In fact, the biological recognition elements can be attached to the surface of these nanoparticles to develop the various catalytic and affinity sensors. Furthermore, they can be retained and removed with a magnet without affecting the transducer surface, thus creating possibilities for regeneration and reuse. The advantages of the propsed method of synthesis includes: i) It is totally a green chemical route which does not involve any hazardous chemicals and ii) the oxidation of non-enzymatic glucose can be achieved.

In this study, we have developed to evaluate the electrocatalytic activity of the sensor against the oxidation of non-enzymatic glucose by green synthesized nanoporous nickle oxide nanoparticles. Non-enzyme glucose sensors are highly resistant to poisoning by chloride ions and are able to overcome interference from uric acid and ascorbic acid were studied by amperometric techniques. Additionally, the designed sensor is demonstrated by measuring the glucose concentration in blood samples at trace level.

EXPERIMENTAL

Chemicals

Chiriyanankai leaves were collected form Vels Institute of Science, Technology and Advanced Studies, Pallavaram, Chennai. Nickel nitrate and sodium hydroxide were received from CDH chemicals Pvt. Ltd., Chennai. Ethanol, nitric acid and acetone were bought from SRL Pvt. Ltd., Chennai. All other chemicals were obtained from analytical grade and used without any purification. High quality double distilled water was used throughout the experiment.

Preparation of NpNiONPs

Chiriyanankai leaves were collected, dried (at room temperature for 4 days) and powdered (mixing grinder). 10 g of powdered sample was mixed with 100 mL of ethanol and water followed by heated at 60 ^oC for 2 hours to obtain a green colour solution. After, the reaction mixture was filtered using whatmann filter paper and the filtrate was collected and stored with refrigerator. About 5 mL of collected extract was mixed with 45 mL of 1 M aqueous nickel nitrate and the mixture was stirred followed by heated at 80 ^oC for 60 minutes. After that, the colour of the reaction was changed to brown colour which formation of nanoporous nickel oxide nanoparticles.

Instrumentation

Morphological investigations were observed by field emission scanning electron microscope (JEOL-JSM-6360), USA. XRD pattern of the samples were recorded with JSO DEBYE FLEX 2002 Seifert difractometer. Voltammetric techniques were carried out using CH instrument (model 660C electrochemical work station), USA. A three-electrode system with a single compartment cell including GCE as working electrode, platinum wire as counter electrode and standard calomel electrode (SCE) as reference electrode were employed for the electrochemical measurements.

Preparation of NpNiONPs /GCE

The NpNiONPs modified electrode was developed with the following procedures. GCE surface was cleaned by alumina paste (0.5-micron powder) and washed with DD water followed by 1:1 v/v ratio of nitric acid and acetone and rinsed with DD water. Approximately, 5 mg of NpNiONPs was dispersed in 5 mL of ethanol which was sonicated for two minutes. The colloid suspension of NpNiONPs (5 µL) was dropped on the GCE surface and allowed to dry at RT.

RESULTS AND DISCUSSION

Characterizations

Morphology of the green synthesized NpNiONPs was confirmed by scanning electron microscopy at a resolution of 20 kV. Average size of the nanoporous nickel oxide was calculated to be 0.5 µm [11] (**Fig. 1A**). From XRD pattern, the main diffraction peaks were observed at 2θ, 37.11˚, 43.52˚, 63.22˚, 75.56˚ and 79.52˚ corresponding to the NpNiONPs [12]. All diffracttion peaks can be indexed to the pure NiO crystalline phase, no impure peaks are observed.

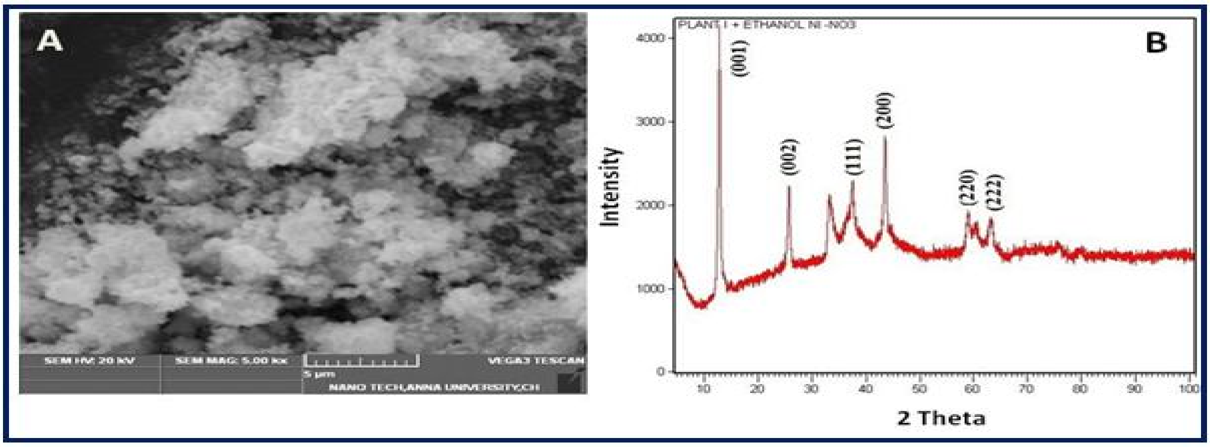

Figure-1: (A) SEM image of NpNiONPs ar a resolution of 20.0 kV. (B) XRD pattern of NpNiONPs.

VOLTAMMETRIC STUDIES

Electrohemical oxidation of NpNiONPs/GCE

The electrocatalytic activity of bare GCE, NiO/GCE and NpNiONPs/GCE were investigated by using cyclic voltammetry method in the presence of 0.1 M NaOH at a scan rate of 0.05Vs^{-1}. As can be seen from the result (**Fig. 2**), the bare GCE and NiO/GCE exhibits a poor electrocatalytic behavior towards the oxidation of glucose. The NpNiONPs shows a better peak current response and has an oxidative peak potential at + 0.45 V vs. Ag/AgCl indicating the enhanced catalytic properties of porous NiO electrode toward oxidation of glucose.

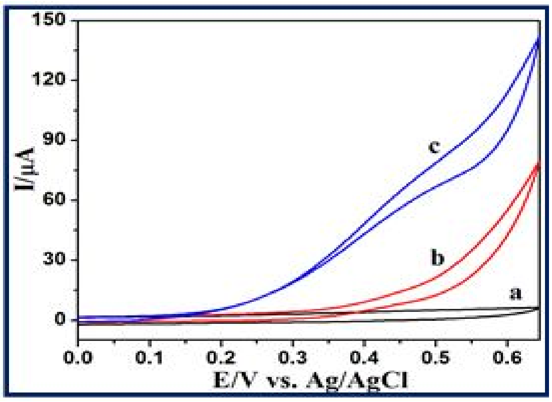

Figure-2: Cyclic voltammograms of a) bare GCE, b) NiO/GCE and c) NpNiONPs/GCE in the presence of 0.1 M NaOH at a scan rate of 50 mV/s.

Effect of scan rate on NpNiONPs/GCE

Effect of scan rate dependence of the electrocatalytic response of NpNiONPs/GCE towards glucose oxidation has been investigated and the results are shown in **Figure 3**. A cyclic voltammogram was recorded in 0.1 M NaOH at various scan rates (0.02 to 0.1 Vs^{-1}) as shown in **Fig. 3A**. While increasing the scan rate, the oxidative peak current of glucose is increased and the anodic peak potential was shifted in positive direction. A plot of oxidative peak current and a square root of scan rate exhibits a linear relationship (**Fig. 3B**), indicating the oxidation of glucose at NpNiONPs/GCE is diffusion controlled electron transfer process.

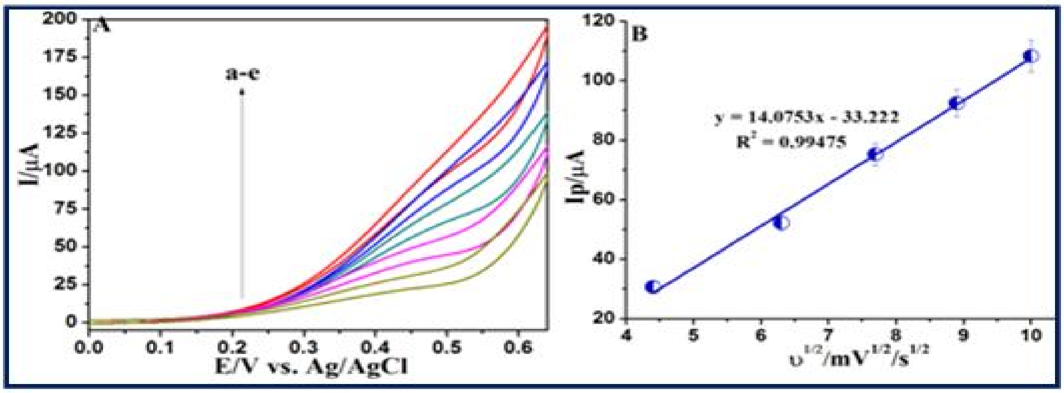

Figure-3: (A) CV of NpNiONPs/GCE in 0.1 mM glucose at various scan rates (0.02 to 0.1 Vs^1) in the presence of 0.1 M NaOH (pH 7.0). (B) Plot of I_p vs. $\upsilon^{1/2}$.

Amperometry detection of glucose at NpNiONPs/GCE

Amperometry method can easily measure the current response for each addition of glucose with respective time under stirring condition. The typical steady-state catalytic current-time response of NpNiONPs/GCE under constant stirring for step-wise injection of 50 μM of 1 mM glucose (50 s) was observed in 0.1 M NaOH at an applied potential of + 0.45 V vs. Ag/AgCl. **Figure 4A** clearly shows that the oxidative current increases by increasing the concentration of glucose and its linear ranges from 0 – 1.8 μM for glucose. A linear calibration plot was obtained, with a correlation coefficient of 0.9922, which demonstrates a better relationship between oxidation peak current and concentration. Limit of detection was calculated in the graph of glucose and was found to be 80 nM based on signal-to-noise ratio (S/N = 3) with the sensitivity of 1.470 $\mu AnM^{-1}cm^{-2}$ (**Fig. 4B**). This result depicts that the NpNiONPs/GCE shows good electrochemical activity towards the oxidation of glucose.

Stability and reproducibility studies

Long-term stability of the prepared electrode (NpNiONPs/GCE) was tested and an immersed in 0.1 M NaOH at room temperature. After two weeks, the CV response has retained about 98.9 % response than the freshly prepared one. After one month, the stability of the electrode was tested again 50 cycles recording by CV experiment in 0.1 M NaOH about 95.2 % response was retained which shows the NpNiONPs/GCE has a better stability and reproducibility. At different time intervals, the CV method was carried out for the determination of glucose in 0.1 M NaOH. The peak current response was preserved the same with the relative standard deviation of 2.8 % for five determinations. This result proposes that the NpNiONPs/GCE shows a good stability and reproducibility towards the oxidation of glucose.

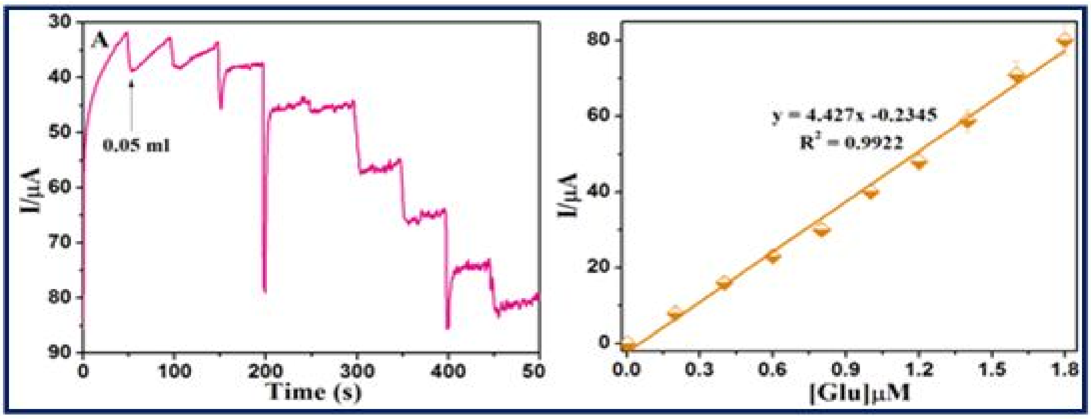

Figure-4: (A) Amperometric response of NpNiONPs/GCE at an applied potential + 0.45 V to subsequent addition of different concentrations of glucose in 0.1 M NaOH. (B) Calibration plot of I_p vs. conc. of glucose.

Analytical applications

In order to find out the accuracy of the sensor, the sensor was applied to real blood samples for determination of glucose. By employing standard addition method, glucose in human blood was determined on the modified sensor. Before measuring the current response, 0.05 mL of the samples (contains 4.4 – 6.4 mM glucose) were diluted by 10 mL phosphate buffer solution (pH 7.0) and then glucose solutions were added one after another to the system. All the measurements were carried out five times and the results are listed in **Table 1**. The calculated recovery and relative standard deviation (RSD) values from **Table 1** show that the prepared sensor possesses potential applications in determining certain concentration range of glucose.

Table-1: Determination of glucose in real samples

S. NO	Added (μM)	Found (μM)	Recovery (%)
1	0.1	0.96	96
2	0.5	0.464	92.8
3	1	1.06	106
4	5	4.62	92.4
5	10	10.16	101.6

4. CONCLUSION

NpNiONPs have been successfully prepared via green synthesized method using *Chiriyanankai* leaves. XRD and SEM results confirmed the presence of NpNiONPs. The electrochemical behavior of GCE coated with the NpNiONPs/GCE showed the highest electrocatalytic activity compared with other modified GCE. In this sensor, we obtained a wide linear range, high sensitivity and low detection limit of 80 nM. These great performances including high selectivity and sensitivity, easy fabrication and especially wide linear range, make NpNiONPs/GCE an excellent amperometric sensor for determining glucose concentration.

REFERENCE

1. Iqra H, Shariq R. M., Shahnaz A. M., Mudasar N., Khalid G.,& Bashir A. G. (2015). Type 2 diabetes mellitus: From a metabolic disorder to an inflammatory condition. World Journal of Diabetes, 6(4), 598-612.
2. Kelvin B., Mary K. B., Matthew D., Ning Z., Lim E., Kevin P. F., & Heather A. C. (2010) Fluorescent Nano-Optodes for Glucose Detection. Analytical Chemistry, 82(9), 3707–3713.
3. Lin L. H., Lo Y. L., Liao C. C., & Lin J. X. (2015). Optical detection of glucose concentration in samples with scattering particles. Applied Optics, 54(35), 10425-10431.
4. Xinyu X., Zhi Q., Yongming F., Binwei Y., Lili X., & Yan Z. (2016). Self-powered electronic-skin for detecting glucose level in body fluid basing on piezo-enzymatic-reaction coupling process. Nano Energy, 26, 148-156.
5. Ambran H., Sanjaya E., & Ramli R. (2018). Glucose Sensing Using Capacitive Biosensor Based on Polyvinylidene Fluoride Thin Film. Biosensors, 8, 1-20.
6. Joseph K., Samir M.,Robert A. G., Michael P., & Robert L. (200). Transdermal monitoring of glucose and other analytes using ultrasound. Nature Medicine, 6, 347–350.
7. Minmin L., Ru L., & Wei C. (2013). Graphene wrapped Cu_2O nanocubes: Non-enzymatic electrochemical sensors for the detection of glucose and hydrogen peroxide with enhanced stability. Biosensors and Bioelectronics, 45, 206-212.
8. Dumala N., Mangalampalli B., Chinde S., Kumari S. I., Mahoob M., Rahman M. F., & Grover P. (2017). Genotoxicity study of nickel oxide nanoparticles in female Wistar rats after acute oral exposure. Mutagenesis, 32(4), 417-427.
9. Muhammad I. D., & Aneela R. (2016). Recent Advances in the Synthesis and Stabilization of Nickel and Nickel Oxide Nanoparticles: A Green Adeptness. International Journal of Analytical Chemistry. 2016, 1-14.
10. Kien N., Nguyen D. H., Chu M. H., Dang T. T. L., Nguyen V. D., & Nguyen V. H. (2018). A comparative study on the electrochemical properties of nanoporous nickel oxide nanowires and nanosheets prepared by a hydrothermal method. RSC Advances, 8, 19449-19455.

11. Jeong M. G., Zhuo K., Cherevko S., & Chung C. H. (2012). Formation of nanoporous nickel oxides for supercapacitors prepared by electrodeposition with hydrogen evolution reaction and electrochemical dealloying. Korean Journal of Chemical Engineering, 29(12), 1802-1805.
12. Dhanaji D., Suryavanshi M. J., Dipali S. P., & Patil P. S. (2011). Nanoporous nickel oxide thin films and its improved electrochromic performance: Effect of thickness. Applied Surface Science 257(7), 2647-2656.

International Journal of Advance and Innovative Research
Volume 6, Issue 1 (VI): January - March, 2019

ISSN 2394 - 7780

CHRYSANTHEMUM INDICUM EXTRACT COATED COTTON BANDAGE FOR WOUND DRESSINGS

Sowmya S, Sanuja S, Arjun Kumar Gupta
Department of Chemistry, Vels Institute of Science, Technology and Advanced Studies, Chennai
E-mail: sowmi.sbs@velsuniv.ac.in

ABSTRACT

Objective: Wound dressing is the processes by which any loss in the tissue integrity is being repaired by a series of phases. Cotton bandage is a passive product type wound dressing. Though cotton bandage has several advantages as wound dressings, one of the major disadvantage is, the ease of microbial growth which can lead to cross infection. These disadvantages can be overcome by the introducing some substances with antibacterial properties.

Methods: Chrysanthemum indicum is a perennial plant which has been used in traditional Chinese medicine to treat several infectious diseases. Some of its medicinal properties include anti inflammatory, anti bacterial, anticancer etc. Chrysanthemum indicum flower extract was prepared and it showed antibacterial against gram positive and gram negative bacteria. The extract was coated on the cotton bandage by dip coating method.

Results: The zone of inhibition for coated cotton bandage (S.aureus) was found to be 13mm and for (E.coli) the zone of inhibition for coated bandage was 10mm. The percentage release of extract from the cotton bandage was found to be 70% at the end of 5 days.

Conclusions: Thus Chrysanthemum indicum flower extract coated cotton bandages will act as better wound dressings and will prevent cross infections.

Keywords: cotton bandage, wound dressings, Chrysanthemum indicum, antibacterial property.

INTRODUCTION

Wound is defined as any interruption in the continuous epithelial lining of the skin due to the thermal or physical damage. It can be segmented as acute and chronic wounds depending on the time span and nature of the healing process [1]. Wound healing process includes four phases. First phase is called coagulation or hemostasis phase which takes place immediately after injury. Second phase is the inflammatory phase during which swelling takes place. This phase occurs shortly after the injury. Third phase is the proliferation phase during which new tissues and blood vessels are formed. Fourth phase is the maturation phase during which remodeling of newly formed tissues takes place [2,3]. Earlier it was believed that open wounds heal faster than the closed wounds [4]. Later it was proved that closed wounds heal better than the open wounds as open wounds can catch microbial infections during the healing process[5]. The wound healing process can be promoted by covering the wounds by appropriate wound dressings[6]. Ideal wound dressings should provide and maintain moist environment, enhance epidermal migration, promote angiogenesis and connective tissue synthesis, allow gas exchange between wounded tissues and environment, maintain appropriate tissue temperature to improve the blood flow to the wound bed and enhances epidermal migration, provide protection against bacterial infection, should be non-adherent to the wound and easy to remove after healing, must provide debridement action to enhance leucocytes migration and support the accumulation of enzyme and must be sterile, non-toxic and non-allergic [7].

Gauze, lint, plasters and bandages are being used traditionally as secondary wound dressings to protect the wound from contaminants and for fast healing. Initially antibiotics and antimicrobial agents were being applied on the surface of the wounds and then later covered by secondary wound dressings [8].

In the current era, modern wound dressings are being designed in such a way that, it not only covers the wound but also facilitates the process of healing and keeps the wound away from infections[9]. Some of the biocompatible polymers are being used as modern wound dressing materials to facilitate the process of wound healing [10]. Modern wound dressings may either have antibacterial property by itself or the antibacterial property can be incorporated in to the traditional dressing materials [11]. Antibacterial property can be incorporated to the wound dressings by the addition of substances which poses antibacterial property. Silver nanoparticle incorporated cotton bandage is one of the example of modern wound dressing [12].

Chrysanthemum indicum is a perennial plant with a long history of being used in oriental traditional medicine for the treatment of several infectious dieses such as pneumonia, colitis, stomatitis cancer, fever and sore used to treat vertigo, peruses, and hypertensive symptoms [13]. Some of its medicinal properties include anti-inflammatory, anti bacterial, anti cancer etc [14].

Introduction of antibacterial property by the addition of herbal extracts is a greener approach and effective method. Addition of herbal extracts will give enhanced antibacterial property, as herbal extracts contains many compounds with antibacterial property.

MATERIALS AND METHODS

Chrysanthemum indicum flowers and cotton bandage dressing were purchased from the local market. The ethanol used for extraction was purchased from spectro chem India. The procured chemicals were used without any further purification.

Preparation 0f the *Chrysanthemum Indicum* Flower Extract

The purchased *Chrysanthemum indicum* flowers were shade dried. The dried flowers were soaked in 70% ethanol for 48h and it was refluxed for 4h at 50°C. After refluxing the extract was filtered [15]. The concentrated extract was used as a coating on the cotton bandage dressing.

Preparation of *Chrysanthemum Indicum* Flower Extract Coated Cotton Bandage Dressing

The concentrated extract was coated on the cotton bandage by dip coating method. The coated bandage was vacuum dried [16].

CHARACTERISATION TECHNIQUES

Sem Analysis

The surface morphologies of the uncoated cotton dressing and extract coated dressing were studied by the SEM analysis. The uncoated and extract coated cotton dressings were sputter coated with gold and analyzed under high resolution scanning electron microscope (FEI Quanta FEG 200-HRSEM) model with an accelerating voltage of 5-20 kV.

Functional Group Analysis

The functional groups present in the uncoated cotton dressing and extract coated dressing were analysed using AT-IR Perkin-Elmer spectrum UTAR TWO in the range of 4000 to 400 cm^{-1}.

In-Vitro Extract Release Studies

The rate of extract release from the cotton bandages were studied by the incubation of extract coated cotton bandages in the phosphate buffered saline (PBS) and ethanol mixture in the ratio of 2:1 at 37 °C for a period of 4 days. The bandages were immersed into the PBS and ethanol mixture and kept in a rotating incubator at 37 °C at 500 rpm. At regular intervals of time, the samples of aliquots were withdrawn and were replaced with the same amount of the buffer. The amount of extract released was determined using UV-Vis spectrophotometer (Perkin- Elmer) at a λ_{max} of 425 nm. The release studies were carried out in triplicates

Antibacterial Studies

The antibacterial activity of *Chrysanthemum indicum* extract and extract coated cotton dressings were studied by well diffusion assay[17].

Well Diffusion Assay

Nutrient agar was prepared and poured in the sterile Petri dishes and allowed to solidify. 24 hours growing bacterial cultures *Staphylococcus aureus* and *Escherichia coli* were swabbed on it. Then the flower extract and extract coated cotton dressings were placed on the plates using sterile forceps. Ampicillin was used as positive control. The plates were then incubated at 37ºC for 24hours. After incubation the inhibition diameter was measured.

RESULTS AND DISCUSSION

Surface Morphological Studies of the Extract Coated and Uncoated Cotton Dressings

The figure 1(a) and 1(b) shows the SEM images of the uncoated and extract coated cotton bandages respectively. The uncoated cotton bandage had smooth rod like structures whereas the extract coated bandage had ribbon like structures. The initial smooth surface of the uncoated bandage has become rough on extract coating. The extract coating had brought a change in morphology of the cotton bandage indicating adsorption of extract on the surface of the bandage.

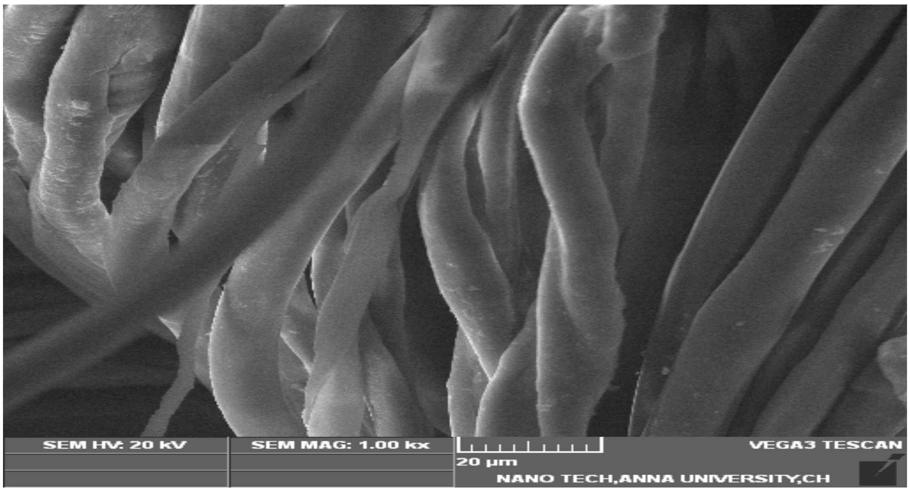

Figure-1(A): Sem Image of the Uncoated Cotton Bandage

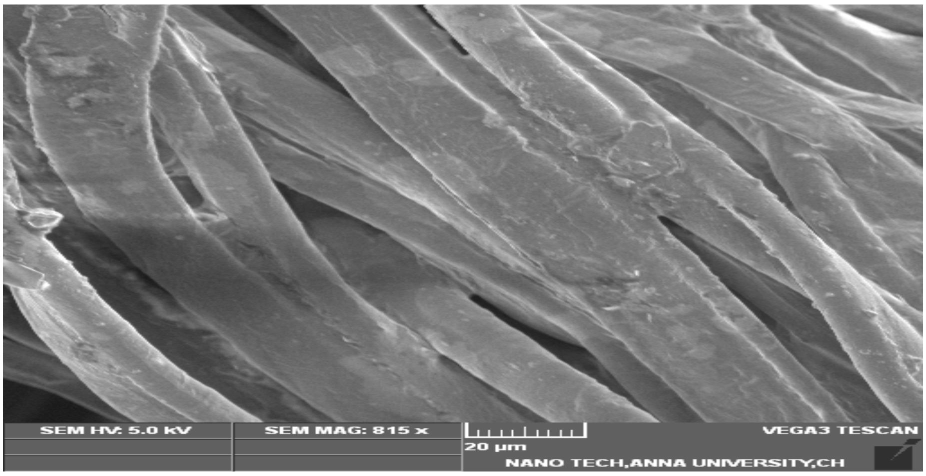

Figure-1(B): Sem Image of the Extract Coated Cotton Bandage

FUNCTIONAL GROUP ANALYSIS

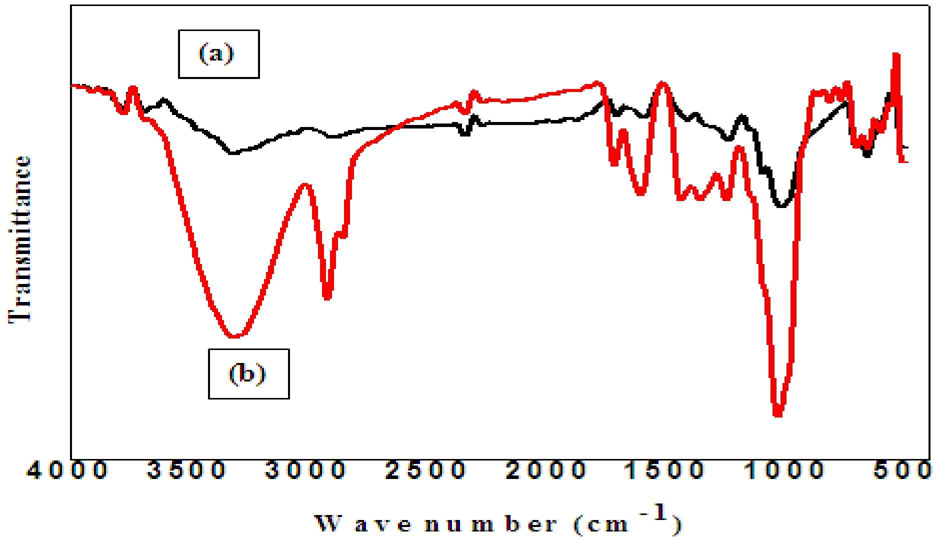

Figure-2(a): FT-IR of uncoated cotton bandage & 2(b) FT-IR of *Chrysanthemum indicum* extract coated cotton bandage.

The figure 2(a) and 2(b) shows the FT-IR of uncoated cotton bandage and extract coated cotton bandage. The peak at 3330 cm^{-1} and 2896 cm^{-1} are due to the hydroxyl group and C-H stretching vibrations respectively. The peak related to the carbonyl and OH stretching vibrations of the polysaccharide appeared around 1032 cm^{-1}. The presence of β-glycosidic linkages between monosaccharaides was confirmed by the peak at 894 cm^{-1}. The peaks due to the flavonoids, terpenoids and other natural products present in the extract appeared as small peaks in the range of 1400 cm^{-1} to 1000cm^{-1}.

IN-VITRO EXTRACT RELEASE STUDIES

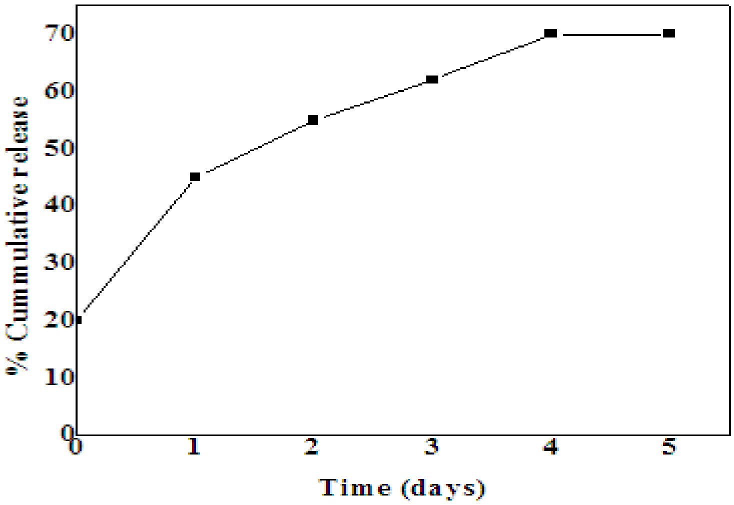

Figure-3: Extract release curve

The figure shows the cumulative release of extract from the cotton bandage. The release which occurred on the zeroth day and first day was due to the adsorbed extract which was present on the surface. So there was a burst release. Further release was due to the absorbed extract which was sustained release. The percentage release of extract from the cotton bandage was found to be 70% at the end of 5 days.

ANTIBACTERIAL STUDIES

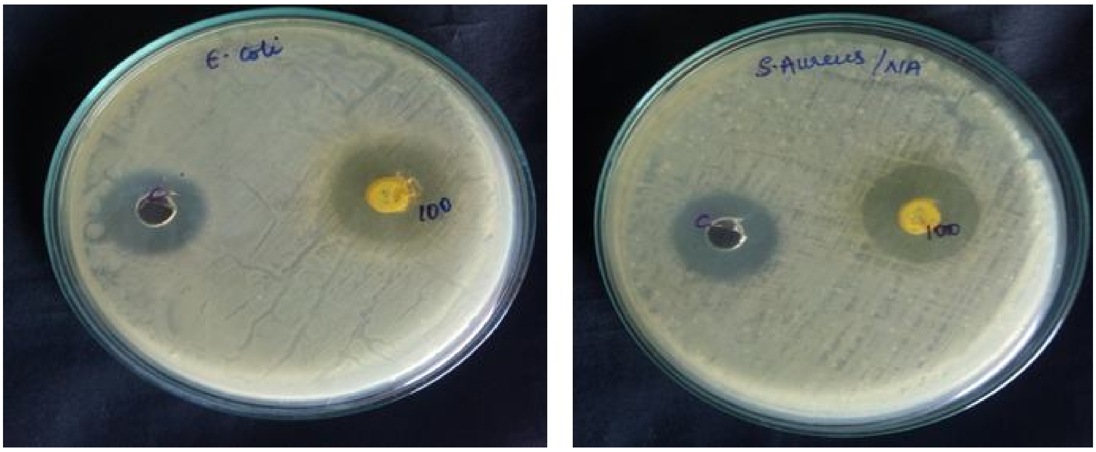

Figure-3(a): Antibacterial studies of the *Chrysanthemum indicum* flower extract

The extract had antibacterial activity and the zone of inhibition was found to be 20mm For both *Escherichia coli and Staphylococcus aureus*

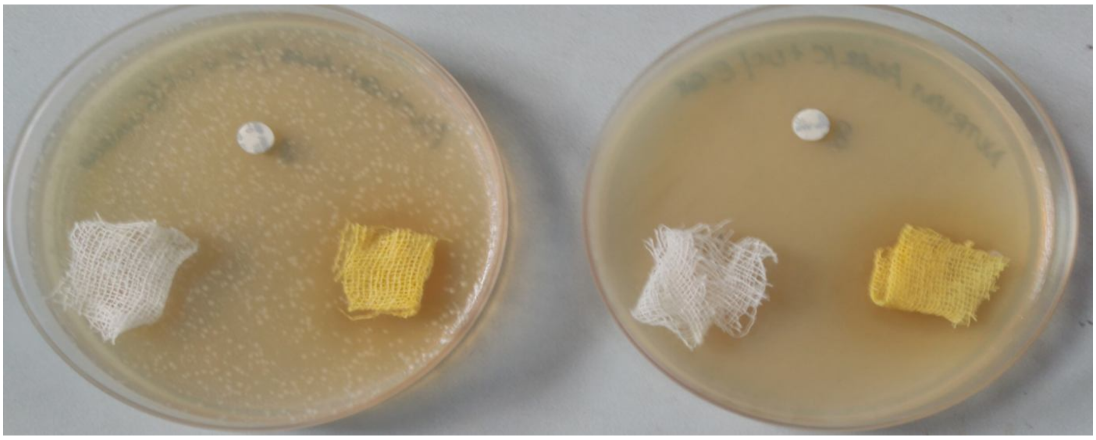

Figure-3(b): Antibacterial studies of the Uncoated and *Chrysanthemum indicum* flower extract coated cotton bandage

The zone of inhibition for coated cotton bandage (*S.aureus*) was found to be 13mm and for (*E.coli*) the zone of inhibition for coated bandage was 10mm. The uncoated cotton bandage did not show any activity.

SUMMARY AND CONCLUSIONS

Chrysanthemum indicum flowers extract was prepared with 70% ethanol. The prepared extract was coated on the cotton bandage by dip coating method. The SEM analysis of the uncoated cotton bandage had smooth rod like structures whereas the extract coated bandage had ribbon like structures. The extract coating had brought a change in morphology of the cotton bandage indicating adsorption of extract on the surface of the bandage. The percentage release of extract from the cotton bandage was found to be 70% at the end of 5 days. The antibacterial studies of the extract showed a zone of inhibition of 20mm against both gram positive and gram negative bacteria. The extract coated bandage showed 13mm zone of inhibition against Staphylococcus aureus and 10mm zone of inhibition against Escherichia coli. The antibacterial activity against both types of bacteria indicates the broad spectrum of secondary metabolite. Hence it can used as better wound dressing material as it can facilitate faster wound healing

REFERENCES

1. Szycher M and Lee SJ. Modern wound dressings: a systemic approach to wound healing. J Biomater Appl 1992; 7: 142-213.
2. Tarnuzzer RW, Schultz GS. Biochemical analysis of acute and chronic wound environments. Wound Repair Regen 1996; 4: 321-5
3. Hunt TK, Hopf H, Hussain Z. Physiology of wound healing. Adv Skin Wound Care 2000; 13: 6-11
4. Dowsett C, Newton H. Wound bed preparation: TIME in practice. Wounds UK 2005; 1: 58-70
5. Jayesh BS. The history of wound care. The journal of the American college of certified wound specialists 2011; 3: 65-6.
6. Sujatha S. Recent advances in topical wound care. Indian J Plast Surg 2012; 45: 379-87
7. Selvaraj Dhivya, Viswanadha vijaya Padma, Elango santhini, Wound dressings- a Review, Biomedicine, vol.5, pg 24-28, 2015
8. Boateng JS, Matthews KH, Stevens HNE, Eccleston GM. Wound Healing Dressings and Drug Delivery Systems: A Review. Indian J Pharml Sci 2008; 97: 2892-923
9. Degreef HJ. How to heal a wound fast. Dermatol Clin 1998; 16:365-75.
10. Rivera AE, Spencer JM. Clinical aspects of full-thickness wound healing. Clin Dermatol 2007; 25: 39-48.
11. Strecker-McGraw MK, Jones TR, Baer DG. Soft tissue wounds and principles of healing. Emerg Med Clin North Am 2007; 25: 1-22.
12. Chuh yean chen , Chen –Li Chiang, Preparation of cotton fibers with antibacterial silver nanoparticles, Materials Letters, vol.62, pg- 3607-3609, 2008.
13. Jiangsu new medical college: Dictionary of Chinese material medical science and technology. Shanghai: Press of Shanghai; 1993.
14. M. Ukiya, T. Akihisa, K. Yasukawa et al., “Constituents of Compositae plants. 2. Triterpene diols, triols, and their 3-O fatty acid esters from edible Chrysanthemum flower extract and their anti-inflammatory effects,” Journal of Agricultural and Food Chemistry, vol. 49, no. 7, pp. 3187–3197, 2001
15. Shyla .m. Haqq and poonam prakash, antibacterial activity of flower and stem extracts of *chrysanthemum coronarium,* international journal of pharma and bio sciences, 2015 6(4) :411 – 414.
16. Krishnaveni V**,** Anti-Bacterial Coating of Chrysanthemum Extract on Bamboo Fabric for Healthcare Applications, Journal of Textile Science & Engineering, 2016, 6: 267-269**.**
17. Ahmad I and Beg AZ, Antimicrobial and phytochemical studies on 45 Indian medicinal plants against multi-drug resistant human pathogens, Journal of Ethnopharmacol 2001, 74: 113- 123.

International Journal of Advance and Innovative Research
Volume 6, Issue 1 (VI): January - March, 2019

ISSN 2394 - 7780

PHYSICO-CHEMICAL STUDIES OF COPPER (II) COMPLEX OF CURCUMIN-SCHIFFS LIGAND

S. Tamijselvy, P. Andal and P. Indra Priyatharesini
Department of Chemistry, School of Basic Sciences, VISTAS, Chennai
E-mail: tamijselvy@gmail.com

ABSTRACT

The copper(II) complex of a Schiff base ligand, 1,7-bis(4-hydroxy-3-methoxyphenyl)-5-(2-phenylhydrazono)hepta-1,6-dien-3-one have been synthesized and characterized by IR, UV-Visible spectroscopy, mass spectroscopy and cyclic voltammetric studies. The Cu(II) ion is situated in a distorted square planar environment. The copper complex showed significant toxicity however the concentration required is found to be higher.

Keywords: Curcumin; Schiff base ligand; Copper complex; Voltammetric; Biological activities.

INTRODUCTION

The intention and synthesis of small molecules that bind to and cleave nucleic acids are quiet a major encounter for researchers. These synthetic nucleases have important applications as tools in molecular biology and as potential healing agents for the treatment of cancer and viral diseases. There has been ample interest in the rational design of unusual transition metal complexes which bind and cleave duplex DNA with high categorization or structure selectivity [1–3]. The characterization of DNA recognition by small transition metal complexes has been significantly supported by the DNA cleavage chemistry that is associated with redox active or photo activated metal complexes. Indeed, there is already a considerable literature involving the practical use of transition metal complexes as chemical nucleases [4–6].

Phenolic compounds from natural medicinal herbs and dietary plants comprising phenolic acids, flavonoids, tannins, stilbenes, curcuminoids, coumarins, quinones etc. play a vital role in cancer prevention and curing and several bioactivities [7]. Curcumin [1,7- bis(4-hydroxy-3-methoxyphenyl)-1,6-heptadiene-3,5-dione] is a polyphenol compound, a natural creation derived from the rhizome of curcuma longa [8]. It has been reported that curcumin possesses several biological activities and pharmacological effects including antioxidant [9], anti-inflammatory [10] and antimicrobial/antiviral [11], anticarcinogenic [12], anti-ischemic [13] and anti-HIV [14] etc. Furthermore, curcumin has been proven not to have toxic, genotoxic or teratogenic properties [15], so this safe phytonutrient has been widely applied in preclinical and clinical studies [16]. Much increasing interest in the medicinal uses of curcumin and wide prevalence of the spice, a facile method is applied to identifiy its activity. Recently, *Priyadarsini et al*. have reported that phenolic OH is mainly responsible for the activity of curcumin [17,18]. However, modifications in the β-diketone are less explored except where this moiety is modified with hydrazide [19] and cyclohexanone groups [20]. Preliminary studies in appending the β-carbonyl functionality in curcumin with known pharmacophore amine have shown to enhance its antioxidant potential [21].

Schiff bases are compunds resulting by the reaction of a primary amine and any carbonyl functional moiety, which coordinate to metal ions *via* the azomethine nitrogen. Schiff base chelating ligands containing O and N donor atoms show broad biological activity and are of special interest because of the variety of ways in which they are bonded to metal ions [22]. Transition metal complexes derived from Schiff base ligands are the most widely studied coordination compounds, as they are becoming progressively important as biochemical, analytical and antimicrobial reagents. Synthesis and characterization of new copper(II) complexes are important to develop models for copper proteins and to understand the factors affecting the distortions from regular coordination geometry observed in various copper(II) complexes [23, 24]

In the present study we discuss about the successful synthesize of new copper schiffs complex of curcumin derived from curcumin and phenylhydrazine. The complex is characterized using uv-visible, IR, mass and cyclic voltammetric studies (CV).

EXPERIMENTAL

UV-Visible spectrums were done using USB 2000+UV-Visible miniature spectrometer from Ocean Optics. IR spectrum was recorded using BRUKER optical Gmbh Spectrometer model TENSOR 27 in the spectral range 500-4000cm^{-1} with 1 cm^{-1} resolution. Mass spectrum was recorded using LCMS 2020 - SHIMADZU (JAPAN)

Cyclic voltammetric studies was carried in CHI 170 model (three electrode system) the working electrode was the so prepared metal complex, reference electrode as Ag/AgCl and platinum wire as counter electrode. The electrolyte used was aqueous solution of 6M KOH. Potential window was kept as +0.8 - 1.2 V. The CV was studied with scan rate of 10mV/sec.

Curcuma longa (turmeric) fresh root and organic turmeric powder were obtained from organic shop. Analar grade Phenylhydrazine hydrochloride, ethanol, chloroform, silica gel (Column & TLC) and Copper (II) chloride are obtained from SDfine India and used directly for the reaction.

The metal complex was mixed with conducting material (activated carbon), binder (Napheon) and made as paste using isopropanol. This mixture was than sonicated for 1hr. This paste was then coated on glassy carbon electrode, dried and used as working electrode for electrochemical measurements (Cyclic voltammetry).

Extraction of Curcumin from Curcuma longa

10 g of small slices of fresh rhizomes in 50 mL of ethanol was magnetically stirred and heated under reflux for 1 h. The mixture was suction-filtered and the filtrate was concentrated in hot-water bath maintained at 50°C. The reddish yellow oily residue was triturated with ethyl acetate to get crude product. TLC analysis (3% ethylacetate-97% hexane) showed the presence of three components. The crude material obtained was dissolved in a minimum amount of ethyl acetate and loaded into a column packed with 30 g of silica gel. The column was eluted with the same solvent. TLC analyses of the various fractions showed the presence of three components. The fractions containing the least polar color component were combined and the solvent was removed on water bath to give a yellow solid. Yield 76%, melting point 184-187 °C.

Extraction of Curcumin from Turmeric Powder

About 20g of organic turmeric powder was soaked in 50mL of ethanol for 48hrs. The solution was then filtered and distilled to get reddish yellow oily residue. Purification or isolation of curcumin was done as before and the yield is found to be 60%.

Preparation of Schiff's base ligand and its copper complex

Equimolar concentration of curcumin and phenyl hydrazine hydrochloride are mixed and stirred for an hour. About one equivalent of Copper (II) chloride (0.109 g, 0.81mmol) in minimum ethanol was added to the above mixture. The solution turned dark brown in colour. The reaction mixture was magnetically stirred under reflux for about 8 hrs. It was then cooled, concentrated in hot water bath and residue was washed with cold ethylacetate to remove any unreacted curcumin. Dark green powder of copper complex was then dried and used for further studies. Yeild is 26%. [M+] at m/z = 590

RESULTS AND DISCUSSION

Electronic Spectral Studies

The electronic spectra of curcumin and its copper complex were recorded in ethanol. Curcumin in ethanolic solution showed a broad characteristic UV-visible absorption at around 300-500 nm with maximum absorption band at wavelength 424 nm and shoulder near 360 and 460 nm, and a weak absorption band at 262 nm. The maximum absorption is due to the electronic dipole allowed π-π* type excitation of its extended conjugation system. Since there is electrostatic interaction between polar solvent (ethanol) and polar chromophores in curcumin molecule, this solvent tends to stabilize both the bonding electronic ground states and the π* excited states. This interaction causes the n-π* transition which occurs at lower energy than the π-π* transitions to move to higher energy and π-π* transition to move to lower energy. Thus, the π-π* and n-π* absorptions of curcumin move close to each other [25].

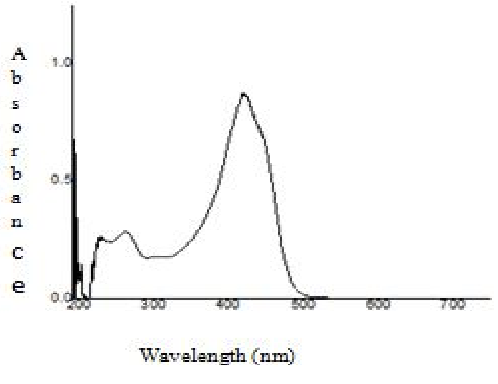

Fig-1: Absorption spectrum of copper curcumin schiffs complex in ethanol.

The electronic absorption spectrum of copper complex shows a predominant charge transfer bands around 434nm resulting in masking of the weaker d-d transition[26]. The intra-ligand π–π* entities in the complexes are observed in the 420 nm range with higher intensities comparable to their free ligands, which may be due to the presence of imine functions [27].

IR SPECTRAL STUDIES

IR spectrum of curcumin was discussed in detail [28]. In the IR spectrum of the copper complex(Fig. 2), the curcumin carbonyl is observed around 1601 cm^{-1} while the imine absorption is seen at 1510 cm^{-1} respectively. The shift in the absorption towards lower wavenumber when compared to curcumin and curcumin-schiffs ligand reflects the conjugation of copper to the curcumin-schiffs ligand. As observed in the ligand, the complex also shows the absorption due to phenolic O-H group but it is shifted to lower wavenumber (around 3450 cm^{-1}) due to hydrogen bonding. Apart from the phenolic O-H peak, we could see another distinct absorption around 3350 cm^{-1} due to–NH stretch present in the complex. A shift in the lower wavenumber is due to the same reason of hydrogen bonding between the carbonyl oxygen and the -NH present in the Schiff's ligand.

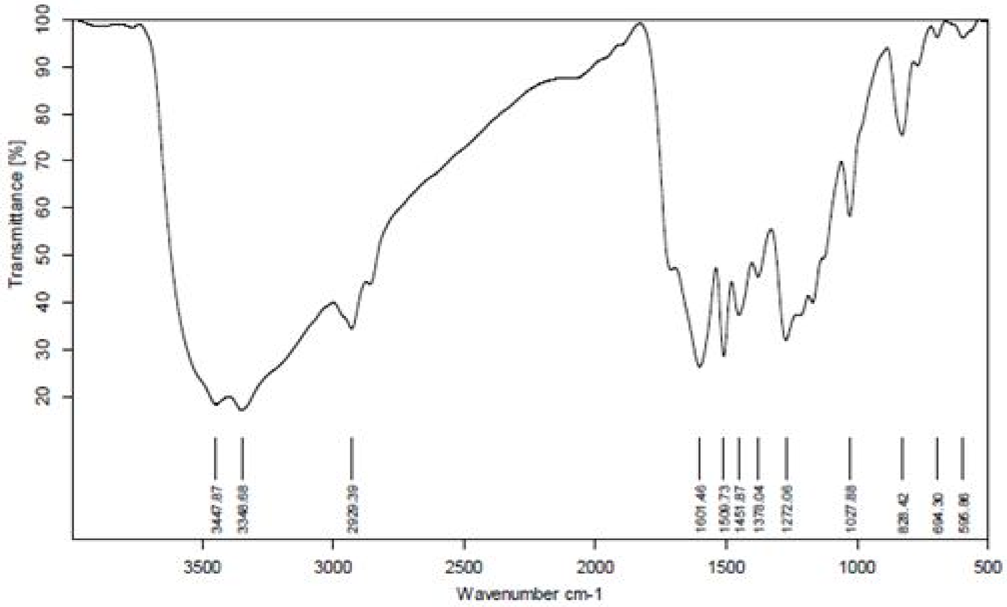

Fig-2: FT IR spectrum of copper curcumin schiffs complex

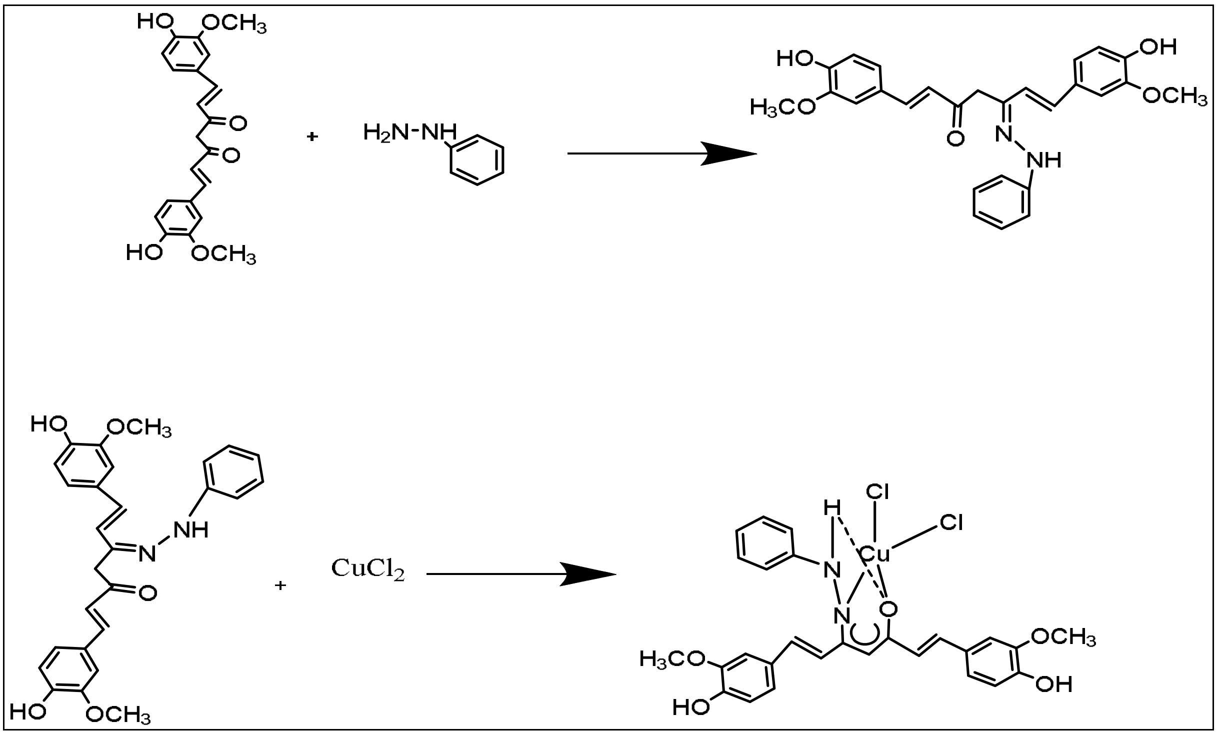

Scheme-I (**A**): Ethanol, stirred, 1hr; **B**) $CuCl_2$, ethanol, stirring & reflux, 8hrs

MASS SPECTRALSTUDIES

The LC-MS spectrum of copper complex was recorded at room temperature, the data for which were in good agreement with the proposed stoichiometry. The copper complex showed a molecular ion peak of [M+] ion at m/z = 590 which is equivalent to the molecular weight of the Cu(II) complex corresponding to the molecular formula$[CuC_{27}H_{24}N_2O_5Cl_2]^+$ (Fig 3). The base peak at m/z = 489 is attributed to $[C_{25}H_{18}N_2O_5Cu]^+$ species.

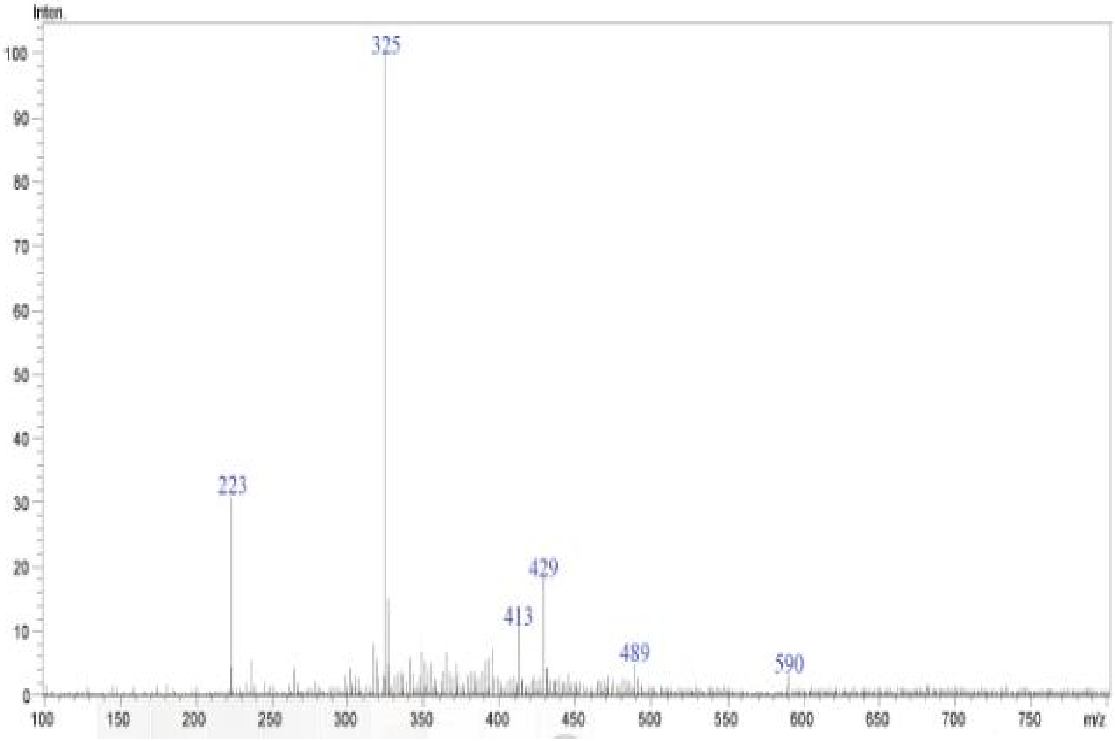

Fig-3: LC-MS spectrum of copper curcumin schiffs complex

CYCLIC VOLTAMMETRIC STUDIES

The electrochemical profile of curcumin shows a quasi-reversible peak centered at -0.84 V ascribed to the reduction of its carbonyl functions [29]. On Knoevenagel condensation, this peak is shifted to positive side and an additional peak is observed at -1.6 V due to reduction of azomethine functionality [30]. Analysis of the cyclic voltammetric profiles of copper conjugates indicates an irreversible electron transfer of Cu2+/Cu+ redox couple centered around +0.40 V. Also overlap of the peaks due to carbonyl and the azomethine functionality centering between -0.2 to -0.13 V were observed (Fig 4).

The redox potentials observed for the complex indicate a moderate strength for phenyl hydrazine to sustain these changes. It implies that greater deformation in the chelate rings of a coordinated phenyl hydrazine ligand induces substantial departure from square-planar geometry with more difficulty in stabilizing the Cu(I) state. The potentials of Cu(II)/Cu(I) couple of the present complex is notably shifted than expected may be due to the difference in the chemical environment and the chromophore around the Cu(II) ions.

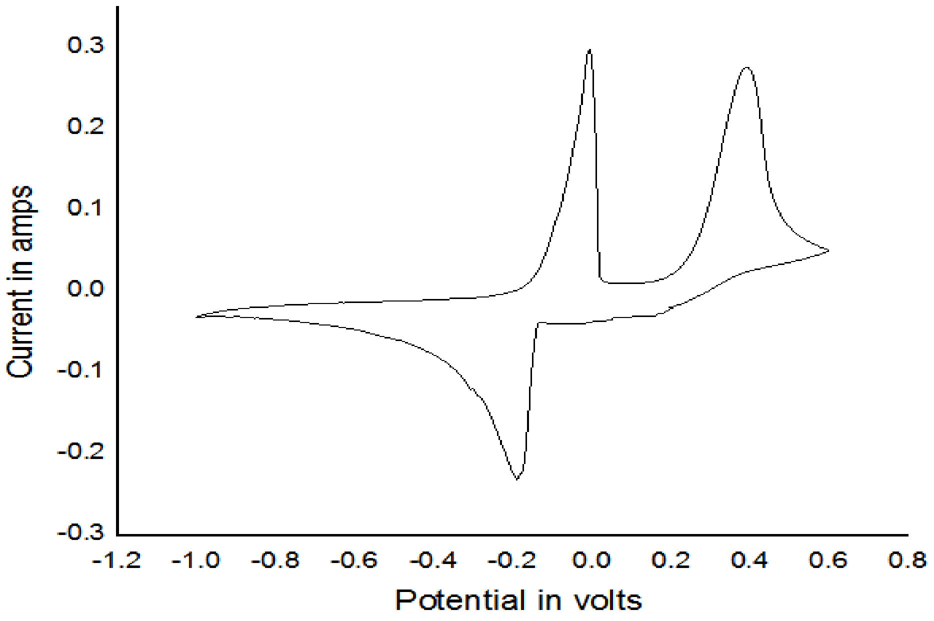

Fig-4: Cyclic voltammogram of copper curcumin complex coated on glassy carbon electrode at 300K

INVITRO ANTIBACTERIAL ACTIVITY

The antibacterial activity of the copper complex was studied because of the presence of imine group which facilitate the mechanism of transamination reaction [31]. The antibacterial data of the complex was assessed using inhibition zone diameter, (mm/µg sample), and in percent derived from zone of inhibition relative to the standard drug Ciprofloxacin which was used as positive control. The complex show moderate inhibition against the tested Gram-positive (S. aureus) and Gram-negative (P. aeruginosa) bacteria. The experimentally obtained highest antibacterial activity of Cu(II) complex is quite remarkable, which is in agreement with the earlier studies [32,33,34]. It is well known that the role of copper in biological systems is quite significant [33]. The enhanced activity of Cu(II) complex may be due to effective binding with DNA, leading to the significant antibacterial activity against all strains.

CONCLUSION

A successful extraction of curcumin from natural source has been achieved. Furthermore, the formation of Schiff's complex was achieved, though yield was very less. Instrumental studies reveal the formation of complex. The copper complex seems to form more distorted structure from planarity which makes it as applicable to biological systems, On the basis of its application; it could be interesting to further investigate the biological importance of this metal complex and also some more metal complexes of this type.

ACKNOWLEDGMENT

The authors thank VISTAS for providing facilities to perform the work.

CONFLICT OF INTEREST

The authors declare no conflict of interest.

REFERENCES

1. B.H. Geierstanger, M. Marksich, P.B. Dervan, D.E. Wemmer, *Science* **266** (1994) 646.
2. Y. Li, Y. Wu, J. Zhao, P. Yang, *J. Inorg. Biochem.* **101** (2007) 283.
3. F.Q. Liu, Q.X. Wang, K. Jiao, F.F. Jian, G.Y. Liu, R.X. Li, *Inorg. Chim. Acta* **359** (2006) 1524.
4. D.S. Sigman, A. Mazumder, D.M. Perrin, *Chem. Rev.* 93 (1993) 2295.
5. R. Vijayalakshmi, M. Kanthimathi, V. Subramanian, B. Unni Nair, *Biochem. Biophys. Res. Commun.* 271 (2000) 731.
6. S.T. Frey, H.J. Sun, N.N. Murthy, K.D. Karlin, *Inorg. Chim. Acta* 242 (1996) 329.
7. W. Y. Huang, Y. Z. Cai, Y. Zhang, Nutr. Cancer 2010, 62, 1.
8. P. Anand, A. B. Kunnumakkara, R. A. Newman, B. B. Aggarwal, Mol. Pharma. 2007, 4, 807.
9. C. M. Bitencourt, C. S. F.varo-Trindade, P. J. A. Sobral, R. A. Carvalho, Food Hydrocolloids 2014, 40, 145.
10. M. R. Bower, World J. Gastroentero. 2010, 16, 4152.
11. E. Krausz, B. L. Adler, V. Cabral, M. Navati, J. Doerner,R. A. Charafeddine, D. Chandra, H. Liang, L. Gunther, A. Clendaniel, S. Harper, J. M. Friedman, J. D. Nosanchuk, A. J. Friedman, Nanomedicine 2015, 11, 195.
12. B. B. Aggarwal, S. Shishodia, Biochem. Pharma. 2006, 71,1397.
13. P. K. Shukla, V. K. Khanna, M. M. Ali, M. Y. Khan, R. C.Srimal, Neurochem. Res. 2008, 33, 1036.
14. W. C. Jordan, C. R. Drew, J. Natl. Med. Assoc. 1996, 88, 333.
15. Z. Stanic´, Electrochemical Investigation of Some Biological Important Compounds Correlated to Curcumin. Curcumin: Biosynthesis, Medicinal Uses and Health Benefits, United States Nova Science Publishers, 2012.
16. K. M. Terlikowska, A. M. Witkowska, M. E. Zujko, B.Dobrzycka, S. J. Terlikowski, Int. J. Mol. Sci. 2014, 15, 21703.
17. K.I. Priyadarsini, D.K. Maity, G.H. Naik, M. Sudheer Kumar, M.K. Unnikrishnan, J.G. Satav, H. Mohan, *Free Rad. Biol. Med.*35 (2003) 475.
18. H.H. Tonneson, J.V. GreenHill, *Int. J. Pharm.* 87 (1992) 79.

19. J.S. Shim, D.H. Kim, H.J. Jung, J.H. Kim, D. Lim, S.K. Lee, K.W. Kim, J.W.Ahn, J.S. Yoo, J.R. Rho, J. Shim, H. Kwon, *J. Bioorg. Med. Chem.* 10 (2002) 2987.
20. (a) H. Ligeret, R. Barthelemy, J.P. Tillement, S. Labidall, D. Morin, *Free Rad. Biol. Med.* 36 (2004) 919; (b) H. Ligeret, S. Barthelassy, G.B. Doulakas, P.A. Carrupt, J.P. Tillement, S. Labidalle, D. Morin, *FEBS Lett.* 37 (2004) 569.
21. J. Annaraj, S. Srinivasan, K.M. Ponvel, PR. Athappan, *J. Inorg.Biochem.* 99 (2005) 669.
22. M. Melnik, M. Kabesova, M. Dunaj-Jurco, C.E. Holloway, *J. Coord. Chem.* **41** (1997) 35.
23. E.I. Solomon, M.J. Baldwin, M.D. Lowery, *Chem. Rev*. 92 (1992) 21.
24. N.F. Curtis, O.P. Gladkikh, M.M. Turnbull, *Aust. J. Chem*. 51 (1998)631.
25. James P. Annaraj, Kanagasabai M. Ponvel and PeriakaruppanAthappan., Transition metal chemistry 29; 722-727, 2004
26. Y.Nishida, Sc Kida, Coord.Chem.Rev, 27, 275 (1979).(b) A.B.P Lever, Inorganic Electronic Spectroscopy, 2 Elsevier, Amsterdam, 1984.
27. A.W. Addison, T. NageswaraRao and E. Sinn, Inorg. Chem., 23, 1957 (1984)
28. Dr. S. Tamijselvy, Dr. P.Andal, P. Indra Priyatharesini; Research Journal of Pharmacy and Technology;Vol:12No:3:March-:2019 (Accepted)
29. Dutta, S.; Murugkar, A.; Gandhe, N.; Padhye, S.; Metal Based Drugs 2001, 8, 183–188.
30. Sonawane, P. B.; Kumbhar, A.; Padhye, S. B.; Butcher, R. J. Synthesis, Trans. Met. Chem. 1994, 19, 277–282
31. N. Raman, R. Mahalakshmi, T. Arun, S. Packianathan, R. Rajkumar, B Biol. 138 (2014) 211–222.
32. T. Chandrasekar, N. Pravin, N. Raman, Inorg. Chem. Commun. 43 (2014) 45–50.
33. N. Shahabadi, M. Falsafi, N.H. Moghadam, B Biol. 122 (2013) 45–51.
34. H. Zafar, A. Kareem, A. Sherwani, O. Mohammad, M.A. Ansari, H.M. Khan, T.A. Khan, J. Photochem. Photobiol. B Biol. 142 (2015) 8–19.

International Journal of Advance and Innovative Research
Volume 6, Issue 1 (VI): January - March, 2019

ISSN 2394 - 7780

SYNTHESIS AND CHARACTERIZATION OF HIGHLY SOLUBLE ACRYLOYLOXYBENZYLIDENECYCLOHEXANONE BASED POLYMER

S. Tamijselvy, P. Indra Priyatharesini and P. Andal
Department of Chemistry, School of Basic Sciences, VISTAS, Chennai
E-mail: tamijselvy@gmail.com

ABSTRACT

A successful synthesize of acrylate-based polymers using 2,6 – bis (4- acryloyloxybenzylidene) cyclohexanone (BABCH) as cross-linker is achieved. The copolymerization using styrene and n-vinyl pyrilidone(NVP) with the cross-linker in presence of metal complex is found to be highly soluble. TGA analysis showed the high thermal stability of the material. SEM analysis helped to understand the morphology and size of the materials prepared by cross linker method.

INTRODUCTION

A non-linear optical (NLO) polymer material has several advantages over the predictable inorganic materials such as high-optical damage threshold, low dielectric constants, large optical nonlinearity, etc. Moreover, these polymer materials can be easily fabricated into a thin film and can be used in wave-guide form as required in several applications. There has been significant interest in recent years to synthesize a multifunctional macromolecule for potential usage in different polymer fields. For NLO applications, the polymers withphoto-cross-linkable[1] moieties were considered. Copolymerisation of NLO active materials with theflexible spacers such as methyleneunits leads to the production of side-chain polymers.More often the photo-cross-linked polymers wereprepared by the reaction of photosensitivemolecule with a polymer backbone.[2,3] The structures,which are used for altering the property of thepolymer containing NLO chromophore, were methylmethacrylate (MA),[4] poly(styrene-*co*-acrylic acid ester),[5]styrene-maleic anhydride,[6] etc. In addition to the previous examples, certain diblock binding units which are photosensitive were used to alter the physical, chemical, thermal stabilityof the polymer samples bearing the NLO active moiety. For instance, polystyrene-*block*-poly(2-cinnamoyl ethyl methacrylate),[7,8] poly(cinnamoyl ethyl methacrylate)-*block*-poly-(acrylic acid),[9] etc.

In accordance with the diblock moieties, we report on benzylidene polymers asthe target materialto achieve the above saidideas.The arylidene compounds was used as anti-inflammatory agents,[10] antimicrobial agents,[11]UV absorbing stabilizers,[12–14] and novel polyester synthesis,[15,16] etc. In this we discuss the synthesis and characterisation of Acrylate-based polymers ie., 2,6 – bis (4- acryloyloxybenzylidene) cyclohexanone (BABCH).

EXPERIMENTAL

Acrylic acid, Benzoyl chloride bought from Aldrich was used without further purification for the preparation of acryloyl chloride. Benzoyl peroxide, ethyl methyl ketone, Cyclohexanone, 2-Hydroxy Ethyl Acrylate , Triethylamine, Styrene, N-Vinyl-2-Pyrilidone, chloroform, benzene, tetrahydrofuran, dimethyl sulphoxide, dimethyl formamide, methanol, ethanol and acetone was purified as per literature.

The IR spectra of the monomer and copolymers were recorded using SHIMADZU FT-IR Spectrometer. ^{1}H NMR & ^{13}C NMR Spectra of the samples were run on a Bruker 320MHz Spectrophotometer at room temperature using CDCl3 and DMSO as solvents and TMS as internal standard. Thermo gravimetric analysis was carried out on Mettler TA 4000 thermal analyzer. Thermo grams were recorded with 5-10mg samples at a heating rate of 20 ^{O}C per minute in air.

Preparation of 2,6 –bis (4- hydroxybenzylidene) cyclohexanone (BHBCH)[17,18]

In a 500ml three-necked flask provided with a mechanical stirrer, 24.4 gm (0.2 mole) of p-hydroxy benzaldehyde and 100 ml of ethanol were stirred till the p-hydroxy benzaldehyde dissolves completely. To the reaction mixture 11.44 ml (0.1 mole) of cyclohexanone was added. The catalyst (HCl (g)) produced by the reaction of con H_2SO_4 and powdered NaCl was passed into the reaction mixture at room temperature. After 2h the contents of the flask were filtered. The military green precipitated is kept for drying in a dessicator. Yield: 92.5%; m.p: >350 ^{O}C. Elem. Anal. Calcd. for BHBCH C, 78.43%; H, 5.88%. Found: C, 78.48 %; H, 5.87%

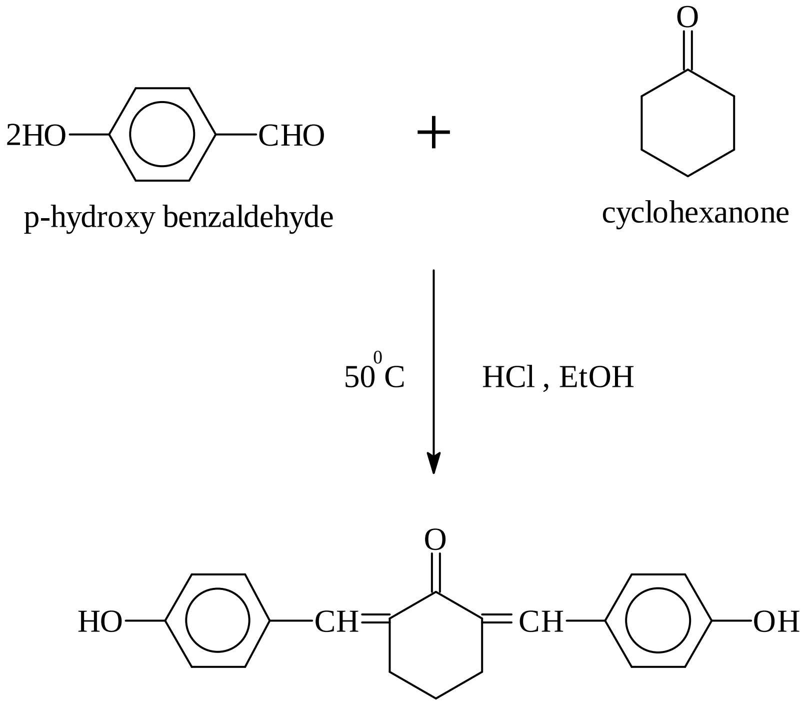

Scheme 1: Schematic representation of synthesis of 2,6 –bis (4- hydroxyl benzylidene) cyclohexanone (BHBCH)

Preparation of 2,6 – bis (4- acryloyloxybenzylidene) cyclohexanone (BABCH)

0.017moles (5.27g) of BHBCH, 0.04moles (5.6 ml) of triethyl amine and 250ml of ethylmethyl ketone (EMK) were taken in a three-necked bottom flask fitted with a mechanical stirrer. After thorough mixing, 0.036moles (2.9ml) of acryloyl chloride dissolved in 25ml of EMK taken in a pressure equalizer were added in drops at 0-5 ^{O}C for about half an hour. During the addition of the reagents, the round bottom flask was kept in an ice bath to maintain the required temperature. After the addition was over, stirring was continued for three more hours at room temperature. The reaction mixture was then filtered and the filtrate obtained was washed with 60 mL of distilled water in portions and the organic layer was dried in anhydrous sodium sulphate. The product was then obtained by evaporating the solvent. Yield: 53.8%; m.p: 143 ^{O}C. Elem. Anal. Calcd. for BABCH C, 75.36 %; H, 5.31%. Found: C, 75.40%; H, 5.29%

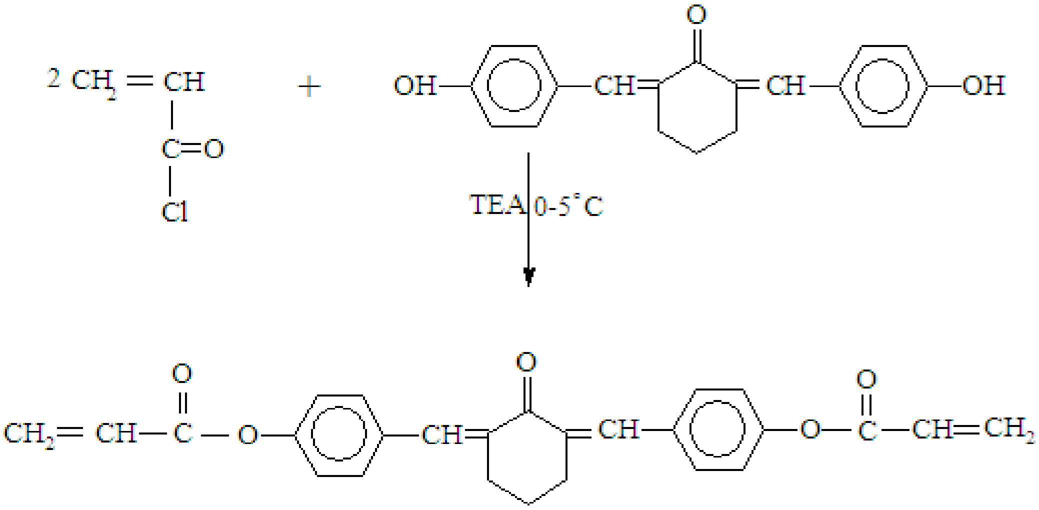

Scheme 1: Schematic representation of synthesis of 2,6 -bis (4- acryloyloxy benzylidene) cyclohexanone (BABCH)

Co-polymerization using Styrene

Co-polymerization was done using solution polymerization technique. BABCH, copper acetate and styrene were taken in different mole ratios in a polymerization tube containing EMK as a solvent and Benzophenone (BPO) (2% w/w) as initiator. The reaction medium was kept inert by passing nitrogen gas through the inlet of the polymerization tube. The polymerization was carried out at 70 ±1 ^{O}C. The solution was the precipitated in different solvents and found to be precipitated in methanol and the precipitate obtained was filtered in sintered crucible, washed with methanol and weighed till constancy was obtained.

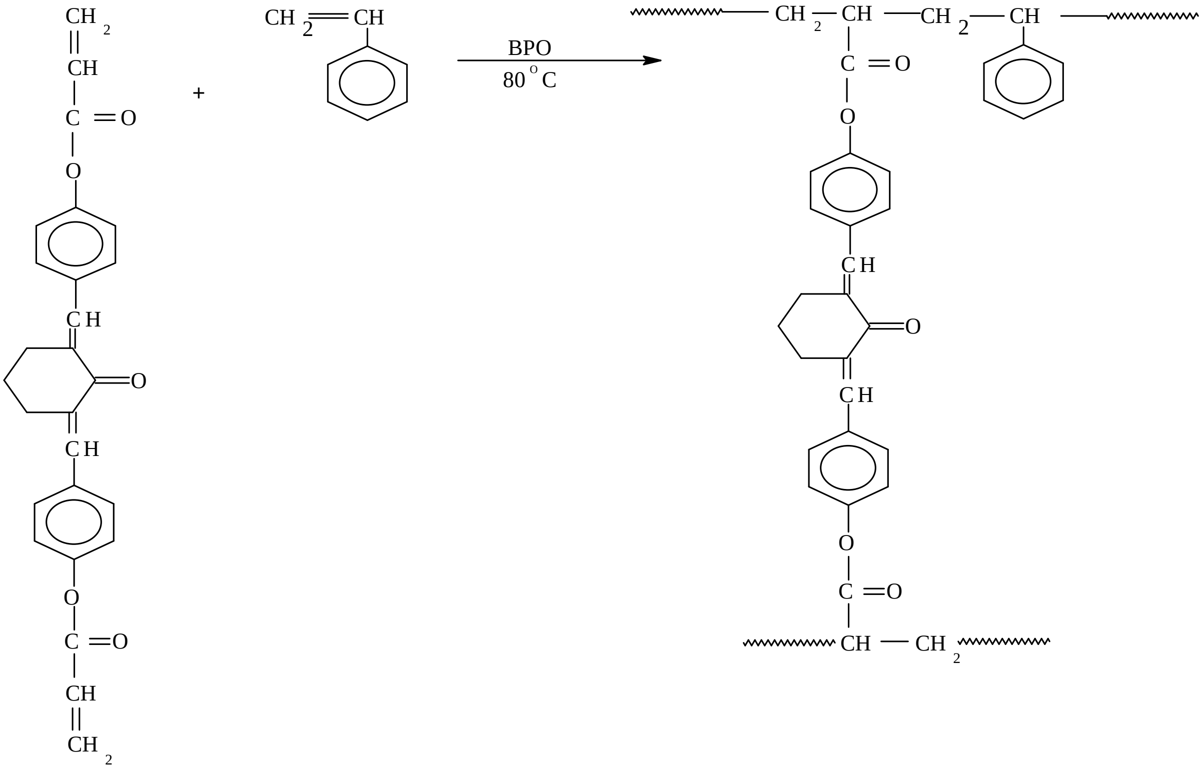

Scheme-3: Schematic representation of copolymerization of Styrene with BABCH.

Co-polymerization of BABCH and N-Vinyl Pyrilidone (NVP)

Co-polymerization was done using solution polymerization technique. BABCH, copper acetate and NVP were taken in different mole ratios in a polymerization tube containing EMK as a solvent and BPO (2% w/w) as initiator. The reaction medium was inert by passing nitrogen gas through the inlet of the polymerization tube. The polymerization was carried out at 70 ±1 ^{O}C. The solution was the precipitated in different solvents and found to be precipitated in methanol and the precipitate obtained was filtered in sintered crucible, washed with methanol and weighed till constancy was obtained.

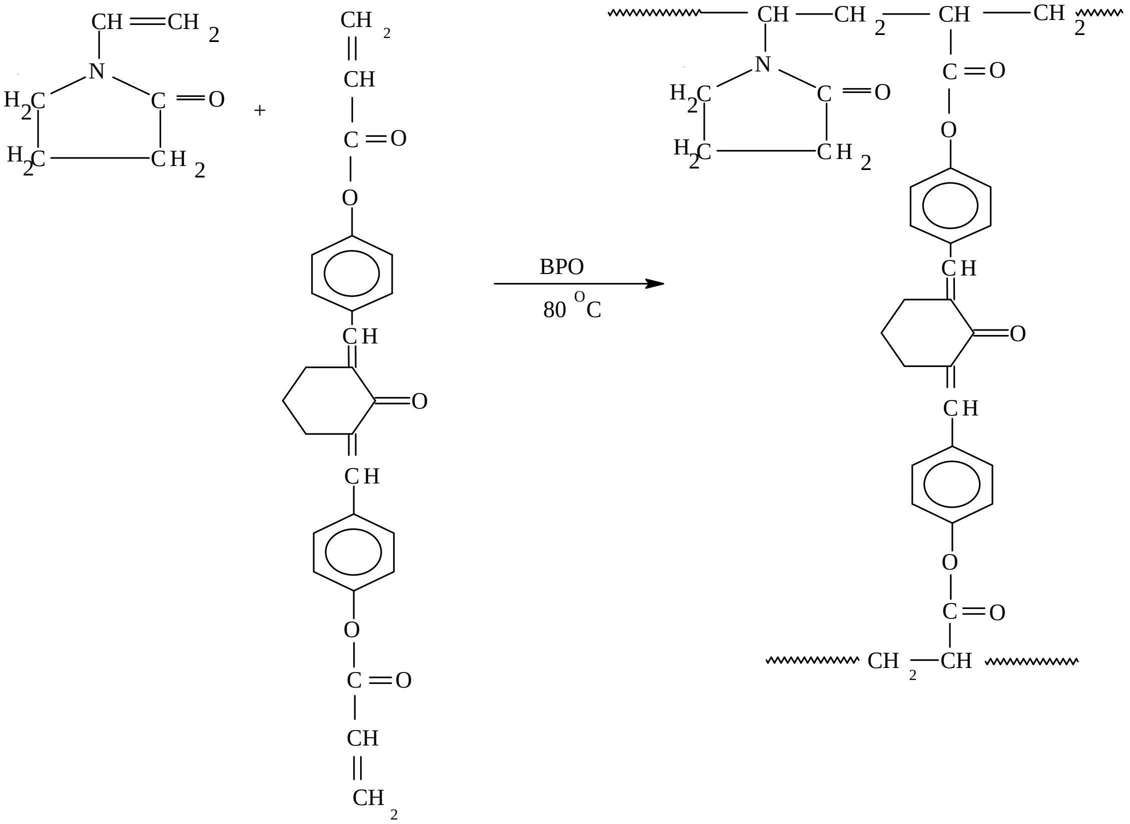

Scheme 4: Schematic representation of copolymerization of N-Vinyl Pyrilidone with BABCH

RESULT AND DISCUSSION

Solubility

The solubility of the monomer and the polymers were tested in several protic and aprotic solvents at room temperature. About 0.02g of the sample was taken in 10mL of the solvent and kept overnight. Their solubility's were noted and tabulated in table 1.

Table-1: Solubility data of monomer and co-polymers at 30 ^{O}C:

Name of compound	H_2O	MeOH	EtOH	CCl_4	$CHCl_3$	DMSO	DMF	Acetone	THF	Hexane	Benzene
BABCH	-	+	+	±	+	+	+	+	+	-	±
P(Styrene) with BABCH	-	-	-	-	-	Ξ	Ξ	-	Ξ	-	-
P(NVP) with BABCH	-	-	-	-	-	Ξ	Ξ	-	Ξ	-	-

- = Insoluble;

± = Sparingly soluble;

\+ = Soluble;

Ξ = Swelling of the sample

IR Spectroscopy

The IR spectra of various synthesized compounds were recorded and the values are tabluated. The key peaks for the identification of presence of both moieties in copolymerized product are seen. The fingerprint region spectra analysis shows marked changes between the starting material and the copolymerized polymer product.

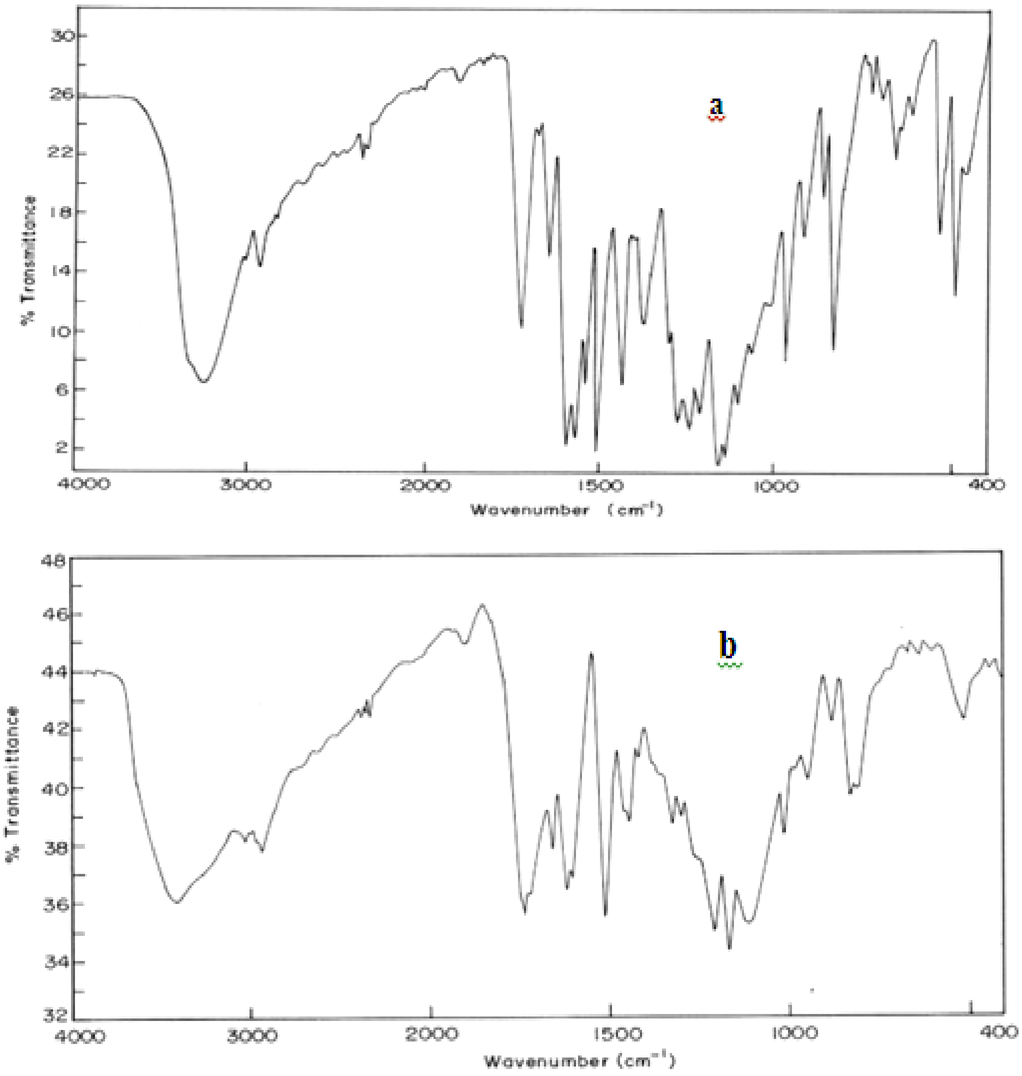

Figure-1: IR spectrum of **a**) poly(S-co-BABCH) ; **b**) poly(NVP-co-BABCH)

Table-2: IR spectral values of the synthesized compounds

Name of the compound	aromatic OH (cm^{-1})	aromatic CH (cm^{-1})	aliphatic CH (cm^{-1})	Ester C=O (cm^{-1})	C=O (cm^{-1})	Vinylic (cm^{-1})	O=C-O (cm^{-1})
BHBCH	3250	3032	2942	-	1658	1598	-
BABCH	-	3043	2925	1739	1656	1605	1204-1143
P (Styrene) with BABCH	3259	3053	2939	1739	1649	1596	1243-1163
P (NVP) with BABCH	3422	3038	2918	1734	1653	1609	1230-1166

^{1}H NMR ANALYSIS

Formation of Co-polymer was confirmed from the ^{1}HNMR data of the polymer.[19,20] ^{1}HNMR and ^{13}C NMR spectrum of the starting material were taken. From the chemical shift values of the ^{1}H-NMR, it was apparent that the copolymer chain contains both monomeric units. ^{1}H-NMR spectrum of P (Styrene) –co- BABCH clearly indicates that the methine (2*H*) protons of Styrene and BABCH units in the chain and the aromatic -OH (1*H*) protons of BABCH units were well separated from each other. Since the two sets of chemical shifts were distinctly separated, their integral values were taken conveniently for the accurate determination of mole fraction of monomeric units present in the copolymer chain. Similar observation was in the case of copolymer of N-Vinyl Pyrilidone. The values are tabulated in table 3. Figure 2 represents the ^{1}HNMR of the two copolymers.

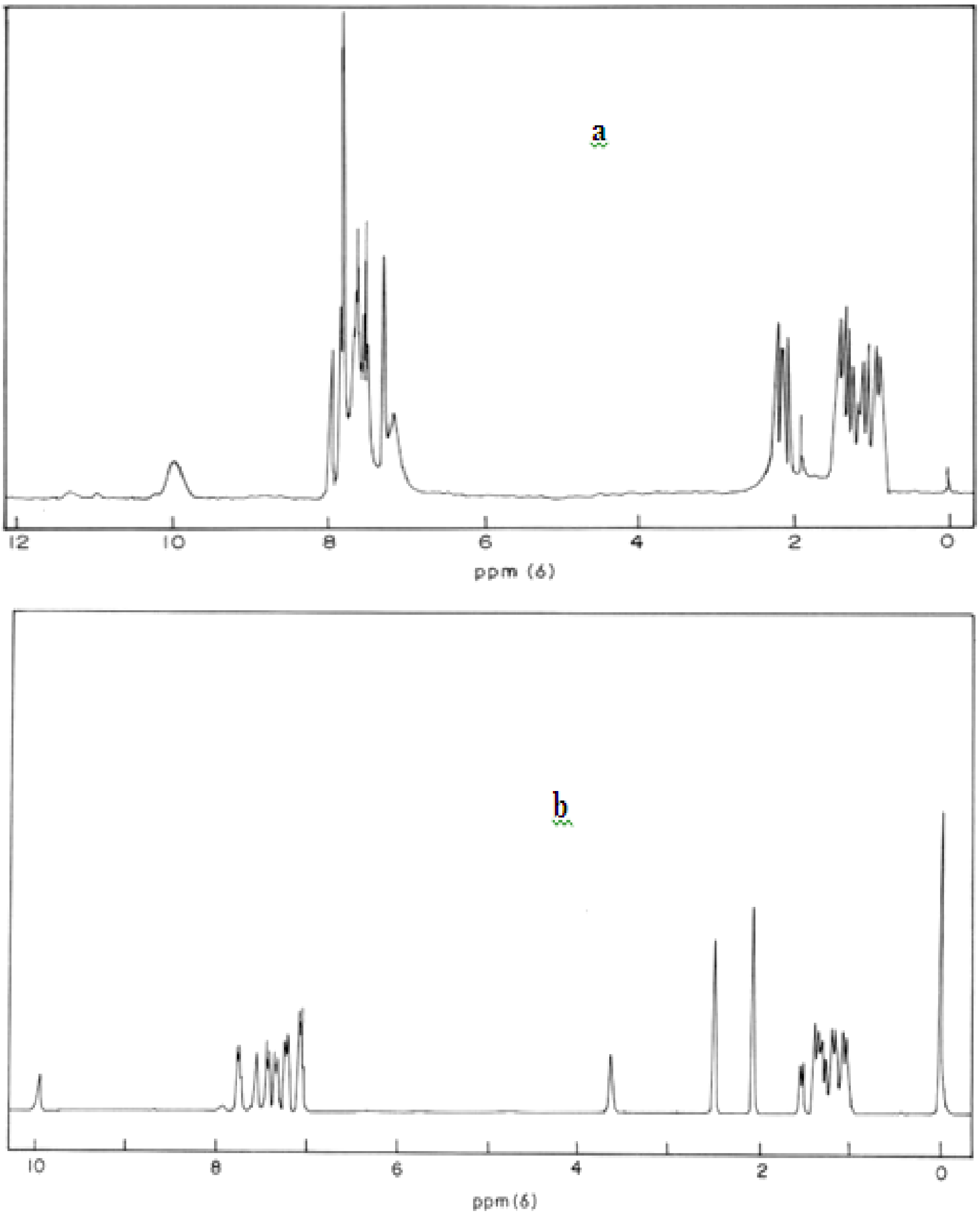

Figure-2: ^{1}H NMR spectrum of a) poly(S-co-BABCH) b) poly (NVP-co-BABCH) in DMSO

Table-3: ^{1}H NMR (δ, ppm) spectrum values of monomer and copolymer in CDCL3 / DMSO

Name of the compound	Phen-olic OH (1H)	-CH (1H)	vinyl type CH (1H)	vinyl type CH (1H)	Aromatic protons	polymerizable vinyl protons (4H)	polymerizable vinyl protons (2H)	cyclohexanone ring protons (6H)
BHBCH	10.2		7.2	7.4	7.5-7.8 (8H)			2.2
BABCH			7.4	7.6	7.0-7.8(10H)	6.4	6.2	2.1
P (Styrene) with BABCH		9.8 Styrene	7.9-7.0 (10+5H)			1.0-1.5	1.9	2.2
P (NVP) with BABCH		9.8 Vinyl Pyrilidone	7.0-8.0 (10H)			1.0-1.6	2.0	2.2

THERMAL DECOMPOSITION ANALYSIS

Thermo gravimetric analysis was used to study the thermal stability of poly(Styrene –co- BABCH) and poly(NVP –co- BABCH) in comparison with BABCH. All the polymer samples showed two-stage distinct weight loss. The TGA and DTG curves for the two co-polymer samples were shown in Figure 3. For poly (Styrene –co- BABCH) (50: 50), the first-stage decomposition was observed around 375°C and the second decomposition was revolved around 560°C. These two-stage decomposition mechanisms clearly indicate that the poly(Styrene –co- BABCH) has higher thermal stability than poly(BABCH)[21]. Similarly, the poly(NVP –co- BABCH) (50 : 50) shows two-stage decomposition around 365 and 470°C. The percentage decomposition at various temperatures was shown in the table 4.

Table-4: Thermal decomposition data of copolymer

Name of the polymer	IDT, ^{O}C	% Weight loss at different temperatures (^{O}C)								
		10%	20%	30%	40%	50%	60%	70%	80%	90%
P (Styrene) with BABCH	350	290	325	350	360	368	375	390	395	405
P (NVP) with BABCH	100	140	270	300	325	345	360	390	425	455

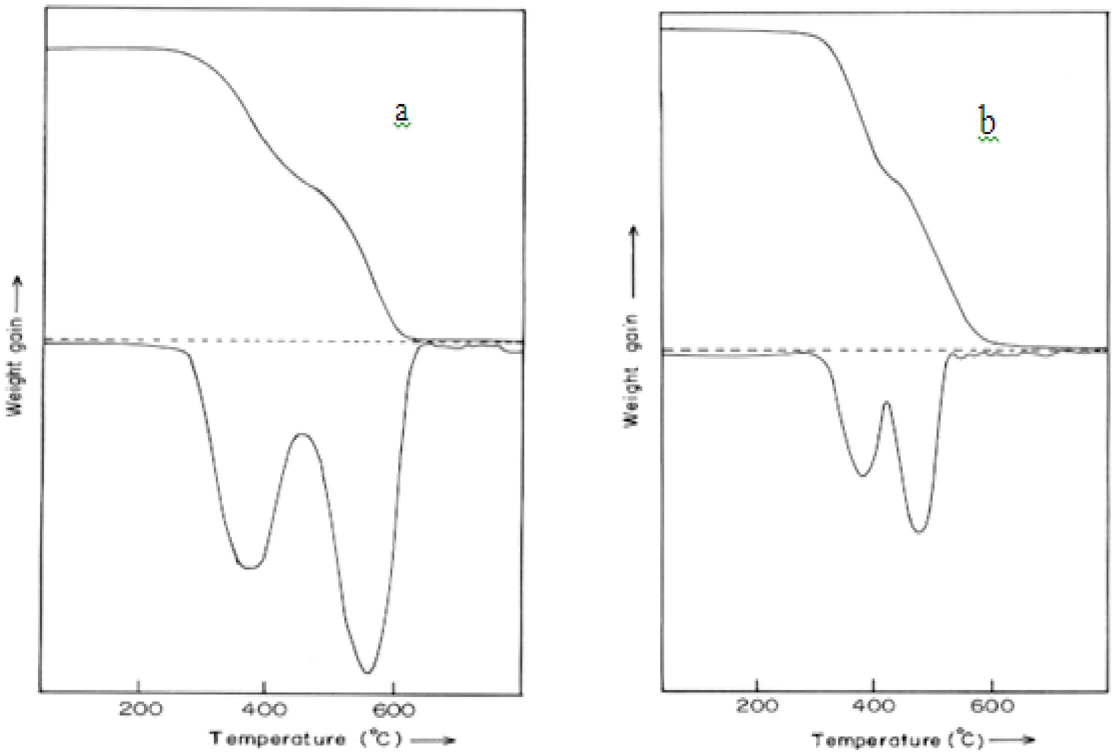

Figure-3: Thermal Analysis study of a) poly(Styrene-co-BABCH) b) poly (NVP-co-BABCH)

SCANNING ELECTRON MICROSCOPE (SEM)

Scanning Electron Microscope is the most widely used technique to study the shape, size, morphology, porosity and mechanism of formation of cross linked copolymer beads. SEM was used to determine the shape & size distribution of cross linked Styrene and NVP. SEM can also be used to observe the grain formation in suspension polymerization of Vinyl Chloride.

In the present work, the shape, size and morphology of the cross-linked copolymer beads are studied. The figures 1.(a) to 1.(b) show the cross linked Co-polymers beads of styrene. The low magnification electron micrographs show that the particles are spherical in shape and the surface is smooth and even. The agglomeration may be due to the small size of the particles. The higher magnification photographs concentrate on the surface of the cross linked beads, and is visible that it does possess some roughness (it is not perfectly smooth) due to this it is clear that the beads will possess low porosity in drying conditions.

The figures 1.(c) and 1.(d) show the cross-linked Co-polymers beads of NVP. These beads are of lower particle size when compared to the beads of cross-linked beads of styrene, due to which a higher magnification of the microscope is required to study the morphology of the beads. It is clear that there is an agglomeration of larger number of particles to form a coagulated mass of the cross linked polymer due to the smaller size of the beads. The higher magnification photograph of the beads suggests that the beads are spherical and are not smooth, but they possess corrugations on their surfaces, which increase the porosity of the beads in dry conditions.

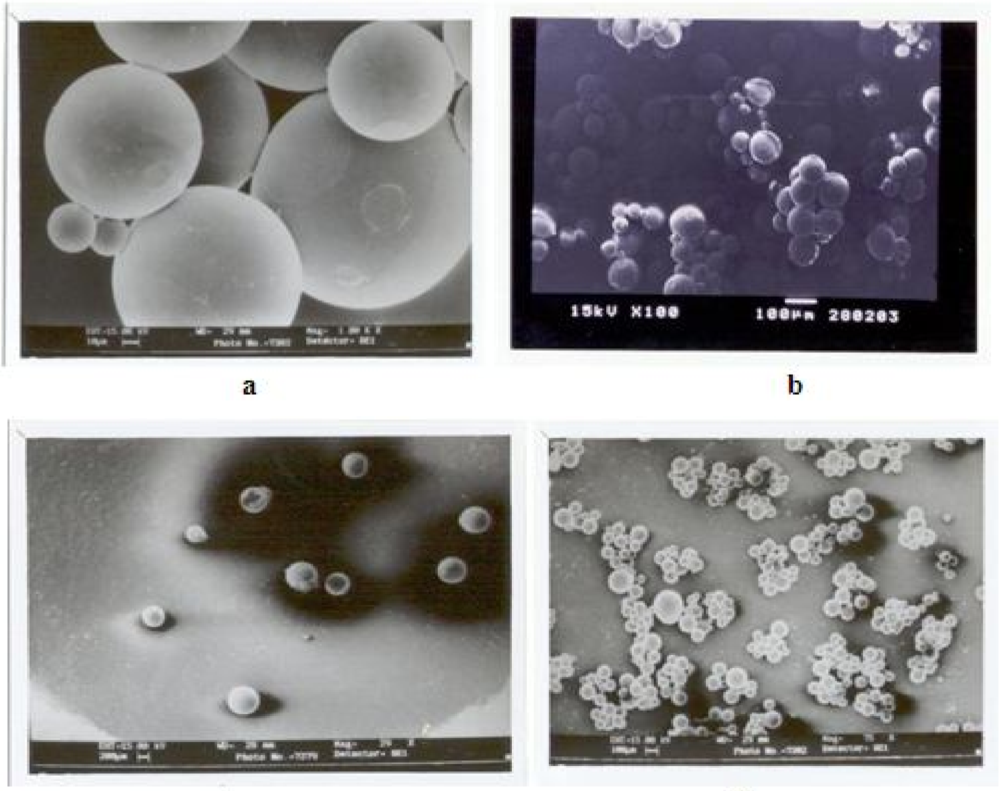

a b

c d

Figure-4: SEM Picture of a & b) poly (Styrene-co-BABCH) c & d) poly (NVP-co-BABCH)

REFERENCE

1. Belfield, K. D. Macromolecules 1998, 31, 2918.
2. Nishikubo, T.; Tisawa, T.; Saito, Y. MacromolChem 1985, 186, 1555.
3. Sierocka, M.; Lyk, B.; Paczkowsk, J.; Zakerzewski, A.; Wrzszczynski, A. PolymPhotochem 1984, 4, 207.
4. Katz, H. E.; Singer, K. D.; Sohn, J. E.; Dirk, C. W.; King, L. A.; Gordon, H. M. J Am ChemSoc 1987, 109, 6561.
5. Matsumoto, S.; Kubodera, K.; Kurihara, T.; Kaino, T. ApplPhys Lett 1987, 51, 1.
6. Hayden, L. M.; Sauter, G. F.; Ore, F. R.; Pasillas, P. L.; Hoover,J. M.; Lindsay, G. A.; Henry, R. A. J ApplPhys 1990, 68, 456.
7. Guo, A.; Liu, G.; Tao, J. Macromolecules 1996, 29, 2487.

8. Tao, J.; Guo, A.; Liu, G. Macromolecules 1990, 29, 1618.
9. Henselwood, F.; Liu, G. Macromolecules 1997, 30, 488.
10. Ramanan, P. N.; Rao, M. N. A. Indian J Pharm Sci 1989, 51,207.
11. Schraufstaffer, E.; Bernt, H. Nature 1949, 164, 456.
12. Arkesi, J. D.; Rauna, F. J.; Williams, J. L. R. Tech Pap Reg Tech ContSocPlastEng Mid-Hudson Sect 1970, Oct (15–16), 19 –23.
13. Mirza, M. S.; Navale, N. G.; Sadfule, D. S.; Kumbhar, C. G.; Panda, S. P. J MacromolSciChem 1990, A27 (1), 1–22.
14. Eh., Alaoui.;Mekki. EurPolym Mater 1992, 28 (6), 601–607.
15. Mohamed, A.; Abd-Alla; Maymouna M Kandeel; Kamal I Aly; Ahemed S Hammam. J MacromolSciChem 1990, A27 (5), 523–538.
16. Mikroyannidis, J. A. EurPolym Mater 1988, 24, 1093.
17. Kamal I.Aly, Liquid Crystalline Polymers, *J.Macrom.Sci.*,Mc Graw Hill,2000,93- 115.
18. Manish P.Patel,Ranjan G. Patel, Synthesis and Characterisation of Novel Polyesters, *J. Polym. Sci.* ,1999,240-244
19. S.Soundarajan and B.S.R.Reddy, *Polymer*, 34,1993, 2224.
20. Mohammed A. ABD – Alla , Maymouna M.Kandeel ,Kamal I. Aly, *J.Macromol. Sci. Chem.*,A 27 (5),1990,523-538.
21. A. Arun, B. S. R. Reddy, Journal of Applied Polymer Science, Vol. 92, 2494–2503 (2004)

International Journal of Advance and Innovative Research
Volume 6, Issue 1 (VI): January - March, 2019
ISSN 2394 - 7780

BACTERICIDAL ACTIVITY OF GREEN FACILE SYNTHESIS OF BIMETALLIC NANOPARTICLES (SILVER-COPPER) USING FRUITS WASTE MATERIALS

T. Somanathan[1], N. Kiruthika[2], Vijaya Ravinayagam[3, 4] and B. Rabindran Jermy[3]
Department of Chemistry[1], Vels Institute of Science, Technology & Advanced Studies (VISTAS), Chennai
Department of Nanoscience[2], Vels Institute of Science, Technology & Advanced Studies (VISTAS), Chennai
Department of Nano-Medicine Research[3], Institute for Research and Medical Consultations (IRMC), Imam Abdulrahman Bin Faisal University (IAU), Dammam, Saudi Arabia
Deanship of Scientific Research[4], Imam Abdulrahman Bin Faisal University (IAU), Dammam, Saudi Arabia
E-mail: soma_nano@yahoo.co.in

ABSTRACT

Nanotechnology has grown to play a prominent role in many biomedical applications owing to the predefined superstructures of doped nanoparticles. Bimetallic nanoparticles (BMP) are produced from the composite of two different metal nanoparticles behaving as one complete unit with regard to properties. In this experiment, green silver and copper nanoparticles were rapidly synthesized by using an aqueous solution of multiple fruit peel extract. Primary confirmation was signaled by a change in the color of the reaction mixture and particles characterization conducted by The X-ray diffraction (XRD) confirms the crystalline structure of bimetallic nanoparticles. Further, Transmission Electron Microscopy(TEM) confirms the morphology and uniform distribution of Cu-Ag core-shell nanoparticles. The bimetallic nanoparticles were effectively tested against the enteric group of bacteria. This primary investigation clarifies the phenomenon of antimicrobial activity against the tested pathogens.

Keywords: Bimetallic nanoparticles, Green synthesis, TEM, XRD, antimicrobial activity.

INTRODUCTION

Metal nanoparticles are of great importance in our day to day life because of their unique properties. Compared to bulk material, NP may possess much potential catalytic, optical, and electronic properties due to its high surface-to-volume ratio confinement of free electrons within finite domains as well as the changes in their electronic structure at very small sizes (Syed *et al*. 2017). Thus, Np has been continuously explored through the number of applications in the drug delivery system, biosensors, development of wound dressing materials as an antimicrobial agent, etc (Azmath *et al*. 2016; Shah *et al* 2015). Since there is a significant advantage in using metal particles as an antibacterial agent, it has also been used in bio-diagnostics or molecular diagnostic techniques that depend upon the size, shape, and composition of the nanoparticles (Belava *et al*. 2017).

There are number of research works stating that different nanoparticles possess antimicrobial potential, such as silver, gold, zinc, copper, magnesium, platinum etc (Alwan *et al*. 2019; Carroll *et al*. 2011). It has also been proven that silver and copper nanoparticles have the properties of microbe inactivation and heavy metal removal (Syed *et al*. 2016). Bimetallic Ag-Cu nano particles were reported to successfully prevent Cu nano particles from undergoing oxidation and, thus, enhance the antibacterial activities (Lee et al 2015). In this study, the Cu and Ag bimetallic nanoparticles were synthesized using multiple fruit peels extracts, wherein the phyto-components present in the peels act as reducing agents, leading to simultaneous reduction of two metal ions under the appropriate stabilized strategy to synthesize Cu-Ag bimetallic nanoparticles.

EXPERIMENTAL

Preparation of peel extract

The multiple fruit peels (pomegranate, orange, banana, apple), collected from the local fruit markets, were washed to remove dust particles and chopped into small segments. Further, 20 g of fruit peels were grounded using mortar and pestle to obtained aqueous extract which was filtered and estimated for the production of nanoparticles.

Synthesis of bimetallic nanoparticles (BMP)

According to our previous investigation procedure (Kiruthika & Somanathan, 2017; Kiruthika & Somanathan, 2016), BMP were synthesized utilizing the aqueous waste fruit peel extract was treated with a mixture of 0.1 mM silver nitrate and 0.1 mM copper nitrate (1:2 v/v). The colour changes in the reaction mixture which denotes the formation of nanoparticles. Further, the synthesized BMP were analyzed by various characterization techniques such as UV-Visible spectroscopy, XRD, FT-IR and TEM.

Antibacterial activity of bimetallic nanoparticles

Antibacterial activity of the nanoparticles solutions was examined with gram negative Enteric group of bacteria (E.coli and S. typhi) as per the procedure(Cho *et al*. 2005; Cioffi e*t al*. 2005).

RESULT AND DISCUSSION

UV-visible spectroscopy

The UV–Visible spectrum shown in Fig. 1 noticeable absorbance of bimetallic showed most extreme at 546 nm which further confirmed the formation of Cu nanoparticles. Surface plasma resonance groups demonstrating the arrangement of bimetallic nanoparticles (Sharma *et al*. 2017).

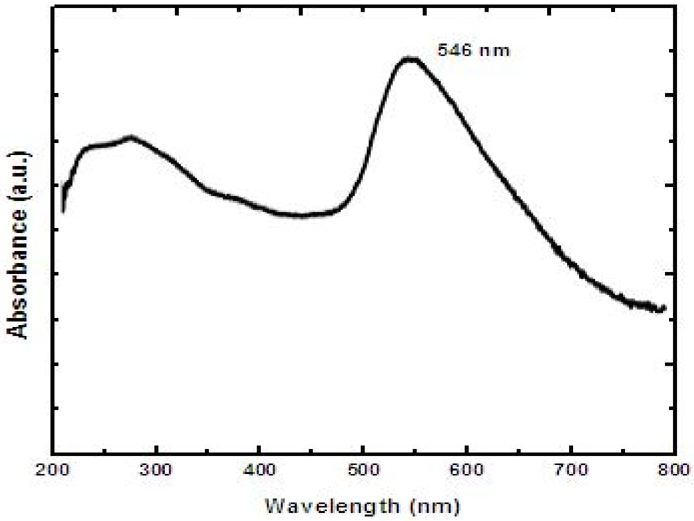

Fig-1: UV-Visible spectrum of BMP

XRD analysis

The XRD Peaks of (111), (200), (220) and (311) crystallographic planes of degree is suggested by Ag (111) peak broadening and the merger of Ag (200) and Cu (111) peaks (Fig. 2). However, there is no diffraction peaks of copper. Because of the lower concentration of copper precipated insufficient reaction (Hikmah et al. 2016). The SNP contain high atomic density facet as (111) in that are highly reactive, the chemical reaction is predicted to be incomplete. That is the reason the copper peaks are invisible.In addition to that, the silver peaks intensity are contributed by the invisible copper peaks is also contributed which are higher in strength and contains distinct crystalline morphology.

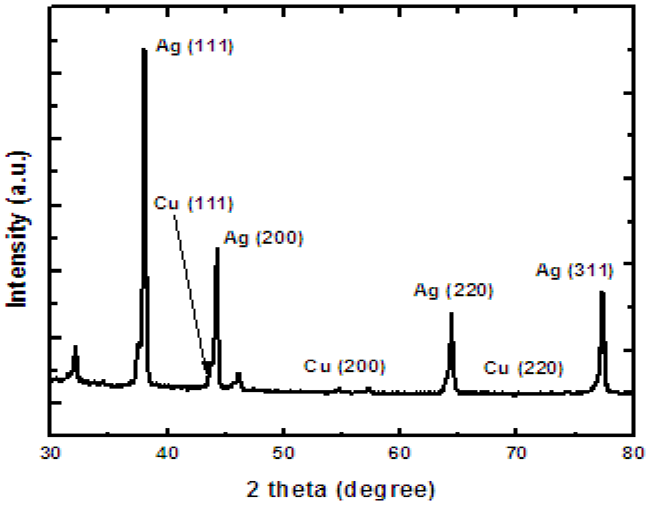

Fig-2: XRD Analysis of BMP

FTIR Analysis

The current investigation, extends of vibration happening at 3410 cm^{-1} relates to groups of NH extending (Balavandy et al. 2015) and 1658 cm^{-1} assigns to C=C extending groups, 673 cm^{-1} corresponds to groups of C-OH as refered in Fig. 3. The results of IR investigation of fruit peel intervened synthesised NP demonstrates that diverse useful hydroxyl, carboxyl and amide moitities are in charge of metal particles reduction to deliver the particles (Kathiravan, 2018).

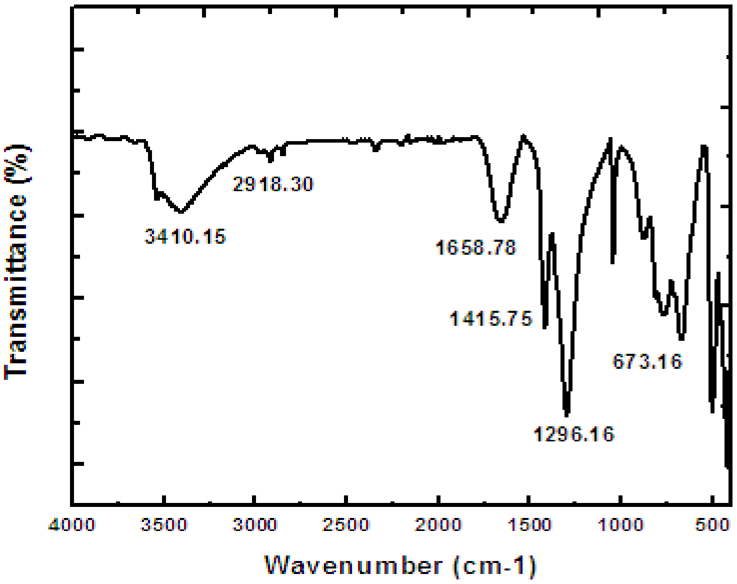

Fig-3: FTIR analysis of BMP

TEM Analysis

The TEM result reported the nanoparticles size is about 50 nm and also its used to find the morphology characteristic of synthesised nanoparticles like structure and arrangements (Fig. 4). Moreover the nanoparticles are not arranged separately it is confimed that core shell structure of copper and silver. The TEM-EDX spectrum of BMP revealed in Fig. 5 exhibits the occurrence of Cu and Ag elements with an approximate atomic ratio (Zhang *et al.* 2015)..

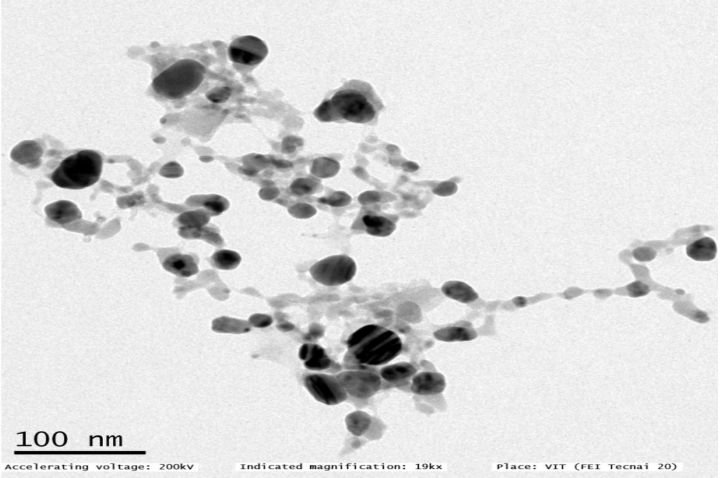

Fig-4: TEM analysis of BMP

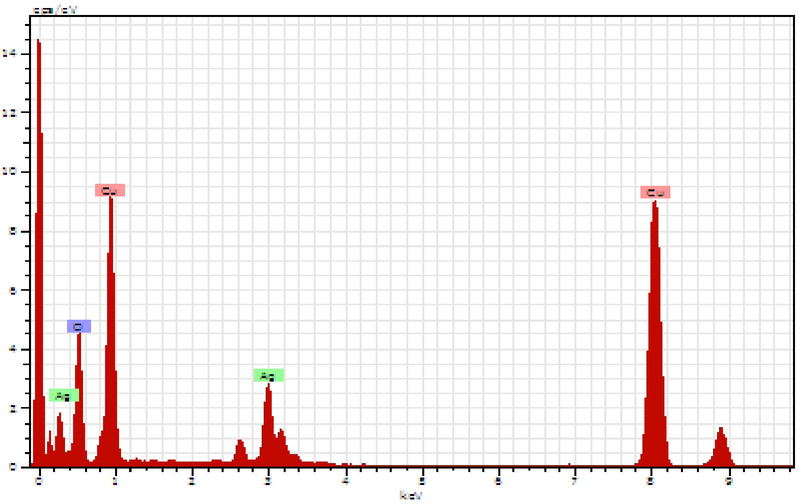

Fig-5: EDX analysis of BMP

Antibacterial activity

The synthesized BMP nanoparticles exhibited good antibacterial activity on enteric pathogens.The synthesised nanoparticles shown better synergist properties against taken bacteria (E.coli and S.aureus) which is shown in Fig.6. This results may attained by the bi metal ions will inhibit the metabolism of the bacteria which arrest the production of enteric toxin further leads the bacterial death and zone of inhibiton (Fig.6) level. The zone of inhibition of the MPE mediated BMP was shown in Table 1. The observed results evidently designates that the BMP displays high antibacterial activity against bacteria, even at lower concentrations.

Table 1: Antibacterial activity of MPE mediated BMP

Zone of Inhibition (mm)				
Organisms	**5µl of SNP**	**10µl of SNP**	**15µl of SNP**	**Control**
Salmonella	8	11.3	11.7	11
E.coli	9.2	12	14.4	9.8

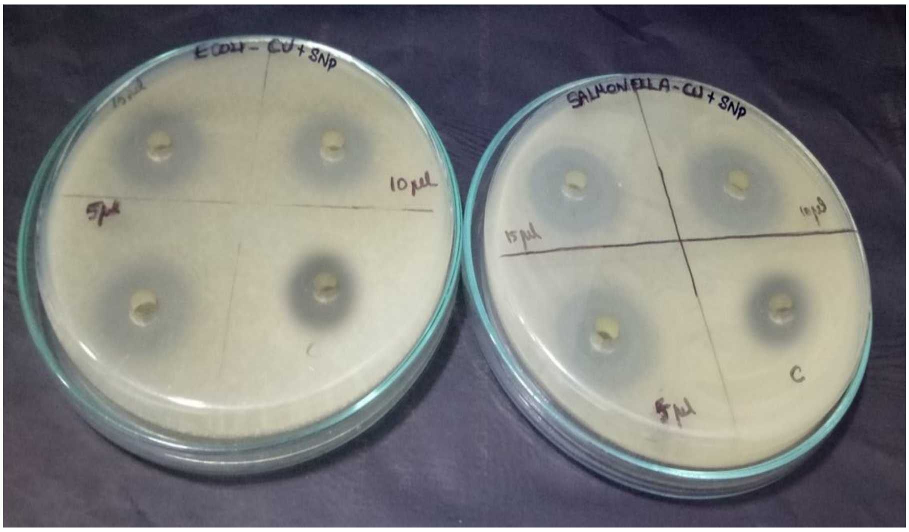

Fig-6: Antibacterial activity of MPE mediated BMP against *E.coli and Salmonella*

CONCLUSIONS

The present synthetic approach is a simple, cost effective and capable of synthesizing BMP utilizing multiple fruit peel extract (MPE). Production of plant-mediated BMP as one of the feasible alternates for combating drug-resistant pathogens and also BMP proves the extraordinary antimicrobial activity rather than mono metal nanoparticles. The results achieved in the existing study are sufficient for upcoming studies to include the use of synthesized nanoparticles along with routinely used antibiotics and sulpha drugs to observe their antimicrobial effects.

ACKNOWLEDGEMENTS

One of the authors, T. Somanathan would like to thank the Vels Institute of Science, Technology and Advanced Studies (VISTAS) for providing CENTRAL INSTRUMENTATION FACILITY.

REFERENCES

1. Syed, B., Bisht, N., Bhat, P. S., Karthik, R. N., Prasad, A., Dhananjaya, B. L., Satish, S., Prasad H., & Nagendra Prasad M. N. (2017) ‘Phytogenic synthesis of nanoparticles from Rhizophora mangle and their bactericidal potential with DNA damage activity’, *Nano-Structures & Nano-Objects*, 10: 112-115.
2. Azmath P., Baker S., Rakshith D., & Satish S. (2016) ‘Mycosynthesis of silver nanoparticles bearing antibacterial activity’, *Saudi Pharm J*, 24: 140-146.
3. Shah M., Fawcett D., Sharma S., Tripathy S. K., & Jai Poinern G. E. (2015) ‘Green Synthesis of Metallic Nanoparticles via Biological Entities’, *Materials*, 8: 7278-7308.
4. Belava V. N., Panyuta O. O., Yakovleva G. M., Pysmenna Y. M., & Volkogon M. V. (2017) ‘The Effect of Silver and Copper Nanoparticles on the Wheat—*Pseudocercosporella herpotrichoides* Pathosystem’, *Nanoscale Research Letters*, **12:** 250
5. Alwan H. A., Karam M. A., Hashim H. O., & Hussein F. H. (2019) ‘Synthesis and Antibacterial Activities of Silver Nanoparticles’, *Asian Journal of Chemistry,* 31: 56-60.

6. Carroll K. J., Reveles J. U., Shultz M. D., Khanna S. N. & Carpenter E. E. (2011) ‘Preparation of Elemental Cu and Ni Nanoparticles by the Polyol Method: An Experimental and Theoretical Approach’, *J. Phys. Chem. C,* 115: 2656-2664.

7. Syed B., Nagendra Prasad M. N., Dhananjaya B. L., Mohan Kumar K., Yallappa S., & Satish S. (2016) ‘Synthesis of silver nanoparticles by endosymbiont Pseudomonas fluorescens CA 417 and their bactericidal activity’, *Enzyme Microb.Technol*. 95: 128-136.

8. Lee C., Kim N. R., Koo J., Lee Y. J., & Lee H. M. (2015) ‘Cu-Ag core-shell nanoparticles with enhanced oxidation stability for printed electronics’, *Nanotechnology,* 26: 455601 (1-9).

9. Kiruthika N., & Somanathan T. (2017) ‘Green way genesis of silver nanoparticles using multiple fruit peels waste and its antimicrobial, anti-oxidant and anti-tumor cell line studies’, *IOP Conf. Series: Mater. Sci. Eng,* 191: 012009 (1-7)

10. Kiruthika N., & Somanathan T. (2016) ‘Biofabrication of Silver Nanoparticles from Fruits Waste Extract and their Application towards Antimicrobial Activity’, *Int. J. Pharma and Bio Sci,* 7: 7-11.

11. Cho K., Park J., Osaka T., & Park S. (2005) ‘The study of antimicrobial activity and preservative effects of nanosilver ingredient’, *Electrochim. Acta* 51: 956-960.

12. Cioffi N., Torsi L., Ditaranto N., Tantillo G., Ghibelli L., Sabbatini L., Bleve-Zacheo T., D’Alessio M., Zambonin P. G., & Traversa E. (2005) ‘Copper Nanoparticle/Polymer Composites with Antifungal and Bacteriostatic Properties’, *Chem. Mater.* 17: 5255–5262.

13. Sharma G., Kumar A., Sharma S., Ram Prakash Dwivedi M. N., ALOthman Z. A., Mola G. T. (2017) ‘Novel development of nanoparticles to bimetallic nanoparticles and their composites: a review’, *J. King Saud University-Sci*. (2017)https://doi.org/10.1016/j. jksus.2017.06.012

14. Hikmah N., Idrus N. F., Jai J., & Hadi A. (2016) ‘Synthesis and characterization of silver-copper core-shell nanoparticles using polyol method for antimicrobial agent’, *IOP Conf. Series: Earth and Environmental Science* 36: 012050 (1-7).

15. Balavandy S. K., Shameli K., & Abidin Z. Z. (2015) ‘Rapid and Green Synthesis of Silver Nanoparticles via Sodium Alginate Media’, *Int. J. Electrochem. Sci.*, 10: 486-497.

16. Kathiravan V. (2018) ‘Green synthesis of silver nanoparticles using different volumes of *Trichodesma indicum* leaf extract and their antibacterial and photocatalytic activities’, *Res Chem Intermed* 44: 4999-5012

17. Zhang Z., Ji Y., Li J., Zhong Z., & Su F. (2015) ‘Synergistic effect in bimetallic copper–silver (Cu_xAg) nanoparticles enhances silicon conversion in Rochow reaction’, *RSC Adv.* 5: 54364-54371

International Journal of Advance and Innovative Research
Volume 6, Issue 1 (VI): January - March, 2019

ISSN 2394 - 7780

CONTROLLED FABRICATION OF DOUBLE WALLED CARBON NANOTUBES (DWCNTs) BY CHEMICAL VAPOUR DEPOSITION (CVD)

T. N. Suresh[1] and T. Somanathan[2]
Department of Nanoscience[1], Vels Institute of Science, Technology &Advanced Studies (VISTAS), Chennai
Department of Chemistry[2], Vels Institute of Science, Technology & Advanced Studies (VISTAS), Chennai
E-mail: soma_nano@yahoo.co.in

ABSTRACT

Low temperature growth of double walled carbon nanotubes (DWCNTs) utilizing $NiMoAl_2O_3$ *catalyst by chemical vapour deposition (CVD) technique. The obtained* $NiMoAl_2O_3$ *catalyst and DWCNTs were described by x-ray diffraction (XRD), transmission electron microscope (TEM) and Raman spectroscopy. The TEM results suggested that the structure of the DWCNTs with diameter (3 – 8 nm) and also confirm the interlayer arrangement of graphene layer among the double walled carbon nanotubes is 0.35nm. Further, Raman spectroscopy shows the two typical regions (D-band and G-band) of DWCNTs. Therefore, efficient control of the catalyst nanoparticle diameter is vital to tailor CNTs properties*

Keywords: $NiMoAl_2O_3$ *catalyst; DWCNTs; XRD; TEM, CVD*

INTRODUCTION

Carbon nanotubes (CNTs), among which double walled ones (DWCNTs) are most promising, have now reached a high level of maturity. It has been exposed that DWCNTs can be modified by functionalizing so that the external wall of the tube is defectiveness; though, the internal wall is proposed to be exposed sacrificially by the external wall[1]. If the external of a DWCNT has been altered for enhancement, the internal tube is answerable for the electron transportation in a device such as solar cell junctions, supercapacitors, nanotransistors, or other semiconductor devices[2,3].

The numerous synthetic approaches have been established for the manufacture of carbon nanotubes including arc discharge, laser ablation, and chemical vapor depositions (CVDs)[4-7]. Therefore, CVD is one of the protuberant approaches for manufacturing high-yield DWCNTs with greater purity. In this work controlled synthesized of high purity DWCNTs were synthesized by CVD utilizing $NiMoAl_2O_3$ catalyst at low temperature.

EXPERIMENTAL

Preparation of Ni-Mo Al_2O_3 NPs

Nickel nitrate [$Ni(NO_3)_2.3H_2O$], ammonium molybdanate [$Mo(NH_3)_6.7H_2O$] were the source of Cu, Ni and Mo, respectively which has been utilized for the synthesis of metal substituted α-Alumina nanoparticles. α-Alumina nanoparticles (α-Al_2O_3) with size 20–30 nm act as a supporting material for the metal loading. All the chemicals and glasswares were purchased from SRL India and Schott Duran, respectively. The acetylene (99.9%) and nitrogen (99%) gases were involved as carbon source and carrier gas respectively.

Synthesis of DWCNTs using Ni-Mo substituted AL NPs

Ni and Mo, metal source (5:10 wt.%) were dissolved with 30 ml of double distilled water which is further substituted into 1 g of AL NPs taken in a 100ml beaker at room temperature. Then the resulting solid product were dried and calcined at 350 °C. The synthesis catalyst were utilized for the controlled fabrication of DWCNTs by CVD method with respect to our previous report[8-10].

CHARACTERIZATION OF CATALYST

X- Ray Diffraction (XRD)

Fig. 1 demonstrate the XRD pattern of NiMoAL NPs which clearly shows the three peaks for Ni substituted metal particles are observed at 2θ of 43.65, 52.12, 75.74 and corresponding planes of (111), (200) and (220) indicates FCC of Ni. (22). The other three peaks at 25.96, 36.93 and 54.12 and assigned the reflections of (111) (211) and (312) planes confirmed well the monoclinic MoO_2 [11].

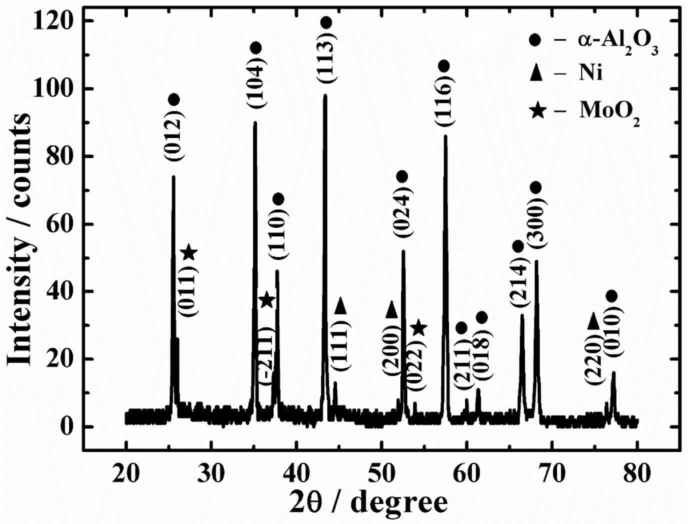

Fig-1: XRD pattern of NiMoAL NPs catalyst

Transmission Electron Microscope

The TEM image shown in Fig. 2 represents the Ni-Mo Al_2O_3 NPs on the surface AL phase. It confirms the presence of bi-metal in AL NPs support material[12]. It is also good agreement with XRD analysis.

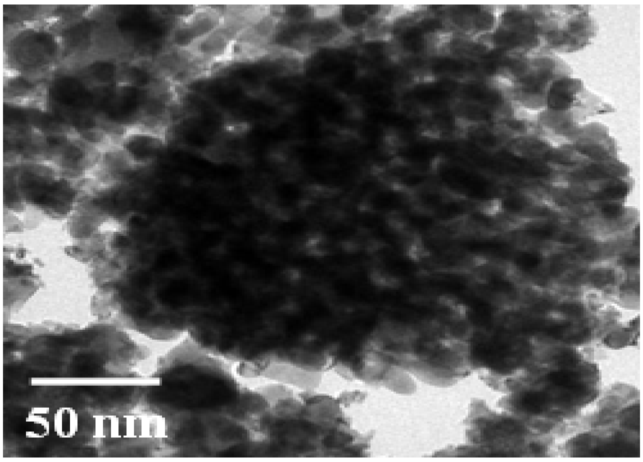

Fig-2: TEM image of NiMo AL nanoparticles

XRD of CNTs

Fig. 3 clearly demonstrates the XRD patterns of the carbon materials showed the graphitic carbon planes at 2θ ≈ 26.5° and 43.8° with reflections of (002) and (101) planes [9].

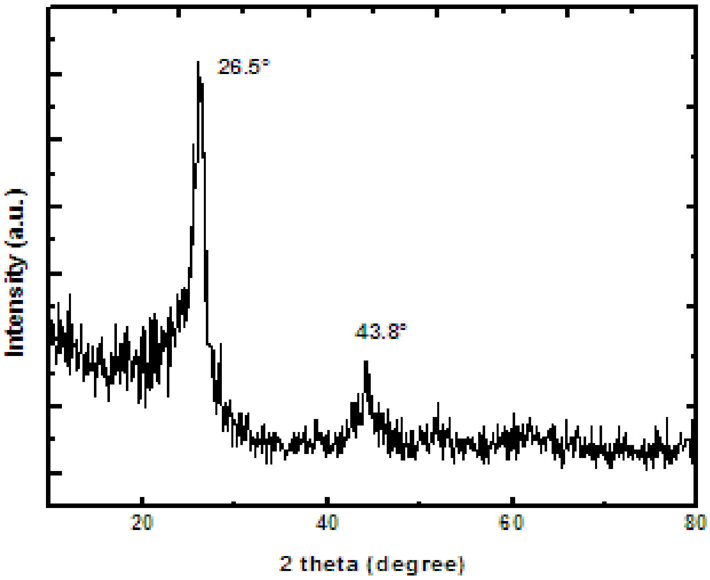

Fig-3: XRD of DWCNTs

TEM image of CNTs

Fig. 4 shows the TEM images of DWCNTs developed over NiMo Al nanoparticles at reaction time (10 min) with low temperature (450 °C) which clearly indicate the bundles of pure DWCNTs with the diameter in the range of 3 to 8 nm. The interlayer arrangement among the double walled carbon nanotubes[13] is 0.35nm which is clearly seen in the Fig. 4.

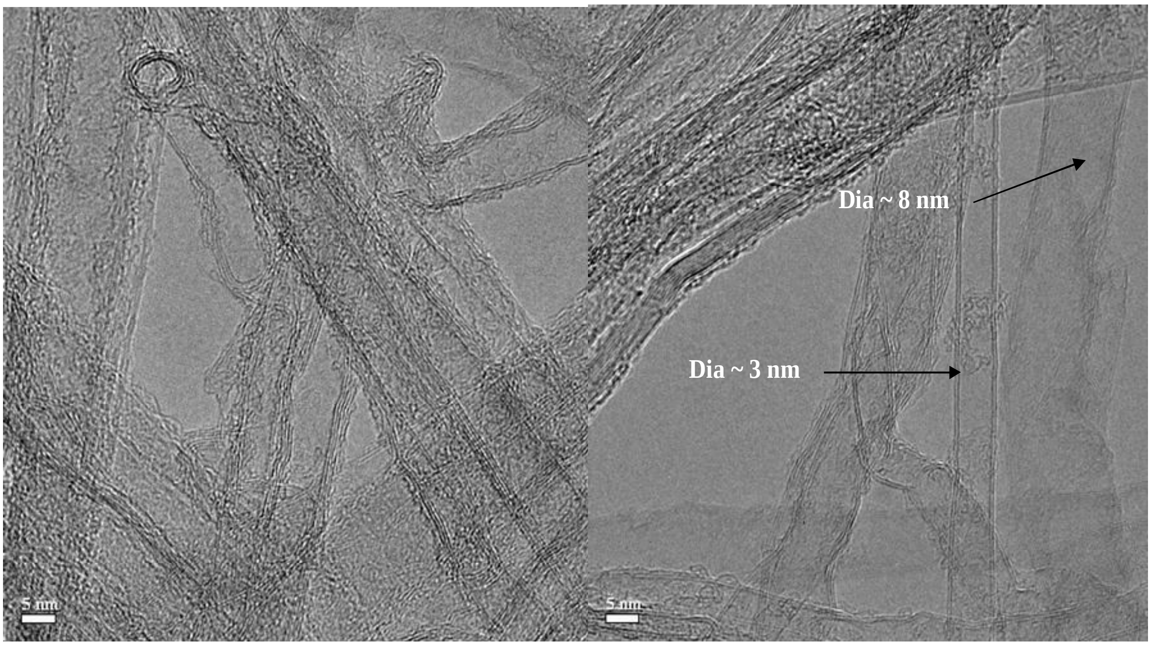

Fig-4: TEM images of DWCNTs

Raman spectrum of CNTs

Fig. 5 illustrate the Raman spectrum of DWCNTs which shows the two typical regions. In the low frequency radial breathing modes (RBM) originated from 100 – 250 cm^{-1}, in the sample[14,15]. The DWCNTs of the Raman spectrum also shows graphitic G-band at 1586 cm^{-1} and disorder D-band at 1370 cm^{-1} .

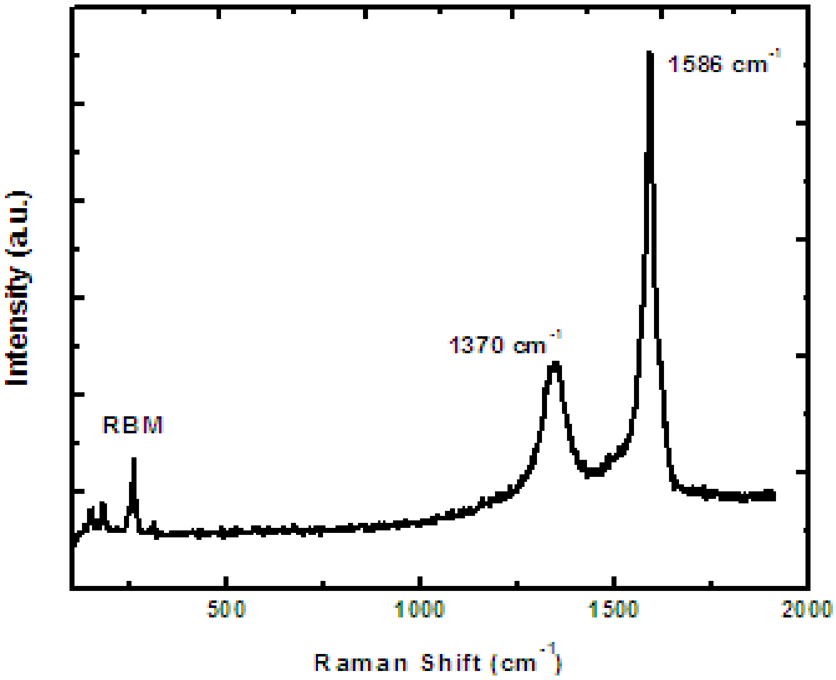

Fig-5: Raman spectrum of DWCNTs

CONCLUSION

The DWCNTs synthesized utilizing Ni-Mo Al_2O_3 NPs by CVD technique at low temperature (450 °C). A large scale production and economical method to development bundles of double walled carbon nanotubes was established. The smaller diameter of DWCNTs in the range of 3 to 8 nm. These tinny and elongated CNTs allows the production of elastic and wrinkled CNTs that can be utilized in many applications.

REFERENCES

1. Bulusheva, L.G et al. (2012) 'Bromination of Double-Walled Carbon Nanotubes', *Chem. Mater*. 24**:** 2708–2715.
2. Llinas, J.P. et al. (2017) 'Short-channel field-effect transistors with 9-atom and 13-atom wide graphene nanoribbons', *Nat. Commun*. 8: 633.
3. Chambers B. A. et al. (2018) 'Measuring the Density of States of the Inner and OuterWall of Double-Walled Carbon Nanotubes', *Nanomaterials* 8: 448
4. Bethune D.S. et al. (1993) 'Cobalt-catalysed growth of carbon nanotubes with single-atomic-layer walls', *Nature*. 363: 605-607.
5. Maser W.K. et al. (1998) 'Production of high-density single-walled nanotube material by a simple laser-ablation method', *Chem. Phys. Lett.* 292: 587-593.
6. Ren Z.F. et al. Synthesis of Large Arrays of Well-Aligned Carbon Nanotubes on Glass, *Science*. 282; 1998: 1105-1107.
7. Gan S. et al. Self-Oriented Regular Arrays of Carbon Nanotubes and Their Field Emission Properties, *Science* 283 (1999) 512-514.
8. Somanathan T and Pandurangan A, Helical shaped multiwalled carbon nanotubes synthesized by catalytic chemical vapour deposition (CCVD) technique, *Carbon*. 48; 2010: 3974.
9. Somanathan T, Gokulakrishnan N and Pandurangan A, Low temperature growth of double walled carbon nanotubes using FeMoMgo catalyst by chemical vapour deposition techniques, *J. Nanosci. Nanotech.* 14; 2014: 3272-3276.
10. Mohana Krishna V, Somanathan T and Gokulakrishnan N, Effective synthesis of well graphitized high yield bamboo-like multi-walled carbon nanotubes on copper loaded α-alumina nanoparticles', *Diamonds and Related Materials*, 50, 2014: 20-25.
11. Lobiak E.V. et al. Ni–Mo and Co–Mo alloy nanoparticles for catalytic chemical vapor deposition synthesis of carbon nanotubes, *Journal of Alloys and Compounds.* 621; 2015: 351–356.
12. Lobiak E.V. et al. One-step chemical vapor deposition synthesis and supercapacitor performance of nitrogen-doped porous carbon–carbon nanotube hybrids, *Beilstein J. Nanotechnol.* 8; 2017: 2669–2679.
13. Gohier A. et al. Growth kinetics of low temperature single-wall and few walled carbon nanotubes grown by plasma enhanced chemical vapor deposition, *Physica E*. 37; 2007: 34-39.
14. Ramesh P. et al. Purification and characterization of double-wall carbon nanotubes synthesized by catalytic chemical vapor deposition on mesoporous silica, *Chem. Phys. Lett.* 418; 2006: 408-412.
15. Osswald S, Flahaut E and Gogotsi Y. In Situ Raman Spectroscopy Study of Oxidation of Double- and Single-Wall Carbon Nanotubes, Chem. Mater. 18; 2006: 1525-1533.

International Journal of Advance and Innovative Research
Volume 6, Issue 1 (VI): January - March, 2019

ISSN 2394 - 7780

SYNTHESIS OF FUNCTIONALIZED NANO-SILICA AND ITS EFFECT ON THE PHYSICAL PROPERTIES OF SILICONE RUBBER

U. Senthilkumar
Associate Professor, Vels Institute of Science Technology & Advanced Studies (VISTAS), Chennai
E-mail: senthilkumar.sbs@velsuniv.ac.in

ABSTRACT

A novel method to synthesize hydrophobic functionalized nano-silica that is partially aggregated has been described. The nano-silica is found to have good storage and dispersion stability with the surface modification of the silanol groups with inert $Si[(CH_3)_3]$ groups. These silica particles are well characterized by means of TEM, IR and ^{29}Si NMR spectroscopy and TGA methods to establish the microstructure of the silica particles. Also, an attempt has been made to understand the role of the microstructure on the physical properties, as well as processability of the silicone rubber formulations.

INTRODUCTION

Silicone elastomers offer many interesting properties, such as high thermal stability, low surface tension, good weather and chemical resistance, good dielectric properties and inertness with low toxicity, and hence find an increasing use in many challenging applications [1-3]. However, the silicone elastomer prepared from polydimethylsiloxane (PDMS) shows poor mechanical properties that limit its use in many industrial applications [4]. In order to overcome this drawback, generally, reinforcing fillers such as fumed silica or colloidal silica are incorporated into the silicone matrix [5,6]. The silicone elastomers thus produced show improved mechanicals and find a variety of specialty applications in areas such as automotive, electrical and electronics, textile coatings and bio-medical devices [7].

The size, morphology and the nature of the silica filler dispersed in the PDMS matrix play a significant role on the final properties of the silicone elastomers [8,9]. Though the primary particle size of the silica fillers is in the nano-range, they have a high tendency to undergo aggregation during their dispersion in PDMS to form large micron-sized aggregates, leading to poor dispersion of fillers in the matrix. These aggregates are stable and very difficult to disaggregate, even under high shear. The other major issue with the nano-silica dispersed PDMS is increased hydrogen bonding between the hydroxyl groups on the surface of the filler over a period of time leading to increased viscosity and hardening of the silicone rubber. This behaviour adversely affects the processability of the liquid silicone rubber (LSR). In order to circumvent the creep hardening, the surface of the fillers is generally modified with hydrophobic groups by means of "hydrophobizing agents" during dispersion in the matrix. This process helps to reduce the filler-filler interaction and increases the filler-polymer interaction, resulting in improved processability and shelf stability of the LSR.

Generally, fumed nano-silica particles are the preferred filler for making silicone elastomers due to their reinforcing ability. These are produced by flame pyrolysis of silicon tetrachloride in the presence of oxygen and hydrogen [10,11]. Fumed silica consists of branched aggregates formed by the condensation of primary spherical particles with a surface covered by silanol groups. The aggregation of these particles in the matrix can be avoided to some extent by the surface treatment of the silica [10]. Colloidal silica particles are produced through sol-gel chemistry by hydrolysis of alkali metal silicates or silicon alkoxide to silicic acid, which rapidly condense to form silica particles [12]. These particles, unlike the earlier ones, are typically spherical in nature, varying from 15 nm to ~ 100 nm in size. The other type of silica, called precipitated silica, is made by acidification of cheaper sodium silicate to produce silicic acid that further condenses to precipitate out the silica. Though the precipitated silica is more cost-effective than the other types of silica, it shows weaker mechanical properties in silicone elastomers due to the structural difference of silica. Table 1 lists some of the physical characteristics of these silica particles.

Table-1: Physical characteristics of various silica particles

Form	BET Particle size	Appearance
Fumed silica	200-300 m2/g	0.1-1 micron Powder
Colloidal silica	100-260 m2/g	10-100 nm Solution
Precipitated silica	<200 m2/g	2-15 micron Powder

Although the use of sodium silicate as a precursor to generate silica particles is favourable from a cost standpoint, one of the significant problems associated with the use of sodium silicate is the contamination of silica with residual sodium silicate, which is undesirable in many applications. There are several common methods available for separating residual sodium silicate from silica. One such method is diluting the sodium silicate to the desired solid content and reacting with acid to make silica and an aqueous salt solution. The salt formed is typically removed either by washing or by adding an organic solvent to precipitate out the salt crystals. The multiple operations involved downstream make the process unattractive during large-scale operations. A better method to avoid sodium is the use of an ion exchange route [12]. Here, the sodium ions are exchanged with protons using an ion exchange resin (IER) to produce silica particles. Though the ion exchange resin is expensive, it can be readily regenerated using dilute acids and reused.

Generally, sodium silicate reacts with an acidic ion exchange resin to produce silicic acid, which further condenses to form nano-silica particles. The condensation reaction of silicic acid to form silica particles is strongly dependent on the pH of the solution. Initially, the pH of the solution is high and the silicic acid formed condenses to form larger oligomers that further condense to form silica particles. At higher pH, the silica particles are negatively charged, and this charge catalyses the further growth of the particles by condensing with silicic acid. The formation of aggregates is influenced by the critical coagulation concentration, particle concentration and particle charge, as well as the nature of the particle surface. During the aggregation stage, particles can form either spherical or fractal structures. As the concentration of particles is increased, the colloidal solution becomes more viscous, leading to gelation of the particles.

The focus of the present work was to develop a simple method to produce in-situ functionalized nano-silica sol solution using the cheaper sodium silicate route and generate silicone elastomers with properties similar to the commercially available functionalized silica particles. The main idea is to develop silica particles in nanometer range and in-situ functionalize them with hydrophobic groups in solvents, without any salt formation or gelation, and then evaluate the influence of microstructure of the functionalized silica particles on the physical properties of the silicone elastomer.

Although many articles are available on the synthesis of unfunctionalized nano-silica particles using the sodium silicate route, there are only a few reports available on hydrophobic functionalized nano-silica using sodium silicate. In some of these reported methods, silica particles are produced by passing sodium silicate through ion-exchange resin and subsequent surface modification using trimethylchlorosilane, after exchanging the aqueous solution with organic solvent. In the surface modification process, hydrochloric acid is the by-product and requires repeated washing with water. In the present study, we used ion-exchange resin to produce silica nano-particles, which are further hydrophobically functionalized with trimethylsilyl groups in the presence of base and polar solvent to produce stable functionalized nano-silica solution. The silica produced in this manner is stable with respect to time, without the formation of bigger secondary aggregates. The silica produced was further dispersed in high molecular weight polydimethylsiloxane to produce LSR formulations that are cured to obtain silicone elastomers. The property of the cured sheet was compared with one obtained using commercial hydrophobic functionalized colloidal silica of similar size.

EXPERIMENTAL

Materials

Vinyl-terminated linear polydimethylsiloxane (PDMS) (viscosity of 65 PaS), silanic hydrogen fluid (a crosslinker used for curing the material) and hexamethyldisilazane (HMDZ) were procured from Momentive Performance Material and used as received. Sodium silicate solution and ethyl alcohol were purchased from Aldrich. The acidic ion exchange resin, Thermax T-63, was received from Tulsion. Colloidal silica was received from Nalco and was further surface functionalized using HMDZ in aqueous alcoholic solution for property comparison.

Preparation of hydrophobic nano-silica particles

Hydrophobic nano-silica particles were prepared (Scheme l) by treating sodium silicate solution with acidic IER in demineralized water at room temperature. The pH was adjusted to 7-8 using an appropriate amount of IER. Under the basic pH, the silicic acid formed was allowed to condense to form silica particles. Additional IER was added for complete conversion of sodium silicate to silica. Ethanol was added to the solution, along with HMDZ, to functionalize the silica surface with hydrophobic groups. This reaction was carried out by increasing the temperature of the solution to 70[degrees]C, catalyzed by the addition of ammonia. The appearance of the hydrophobic nano silica solution thus produced by this sol-gel route was translucent and stable without any gelation.

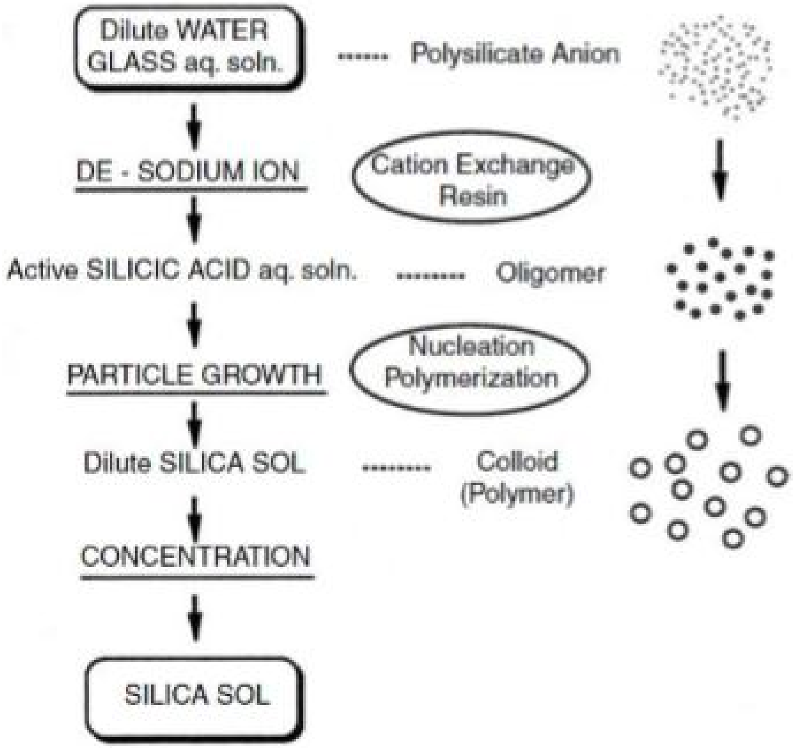

Scheme-1: Preparation of hydrophobic nano-silica particles

Dispersion of nano silica in PDMS and further curing for silicone elastomer

Silica dispersed PDMS was prepared by mixing the above prepared silica sol-gel solution with base polymer, vinyl terminated PDMS, using a planetary mixer. Water, ethanol and other volatiles in the mixture were stripped off at higher temperature under vacuum in the mixer. In this way, 17% of silica loaded LSR (coded as SS 17) was prepared. In order to cure the material, SS 17 was mixed with silanic hydrogen fluid (a crosslinker), platinum catalyst and an inhibitor using a hand blender. The blended mixture was placed in a mold and cured at 165[degrees]C for 10 minutes using a compression-molding machine to obtain a 2 mm thick silicone elastomer. Using the same procedure described here, 17 wt. % of colloidal silica filled PDMS (coded as CS 17) was produced and further cured using the compression molding machine.

Characterization

The hydrophobic nano-silica produced was characterized using a Fourier transform infrared (FTIR) spectrophotometer (Perkin Elmer), solid state 29Si NMR (400 MHz, Bruker) and thermogravimetric analysis (TGA) by heating the sample from 25[degrees]C to 700[degrees]C at a heating rate of 10[degrees]C per minute using a TGA 2950 (from TA instruments) for surface functionalization. The size and morphology of the functionalized silica particle was determined from transmission electron microscopy (TEM) using a Technai G2 TEM instrument. The silica dispersed LSR was characterized for rheology in dynamic frequency mode using an ARES II strain controlled rheometer. The cured silicone elastomer sheet was characterized for its tensile strength, elongation and modulus using an Instron 3356 instrument.

RESULTS AND DISCUSSION

Preparation of hydrophobic nano-silica sol solution

A new process for making in-situ functionalized nano silica particles is shown in scheme 2, avoiding the solvent exchange process and acid formation during the hydrophobic surface functionalization of silica. Initially, the sodium silicate solution was treated with a lesser equivalent of ion exchange resin to maintain the pH of the solution in the basic range. Under the basic condition, the particles were allowed to grow further. This process gives better control over the pH of the solution, which is important to get the particles in the desired nano range. The in-situ treatment of silica particles with hexamethylenedisilazane (HMDZ) under basic conditions, along with the addition of protic solvent such as ethyl alcohol, gave the hydrophobic silica nano particle sol-gel solution. Since the sodium silicate solution exhibits a high tendency to precipitate the silica particles, and the treated hydrophobic silica particles exhibit a high tendency to aggregate in an aqueous medium, an optimum ratio of water/ethyl alcohol is critical for stabilization of treated hydrophobic nano silica particle sol-gel solution. The appearance of the silica sol is a bluish translucent low viscosity homogenous solution.

The TEM image in Figure 1, obtained for the hydrophobic functionalized silica, clearly shows that the primary particle size is in the 10-20 nm range, with the particle partially aggregated/networked. The DLS of the silica solution also gives the average size of the aggregates in the range of 20-80 nm. The network structure and the high surface area of the hydrophobic nano particles is expected to facilitate better interaction of the filler with the polymer matrix, and hence better elastomer physical properties.

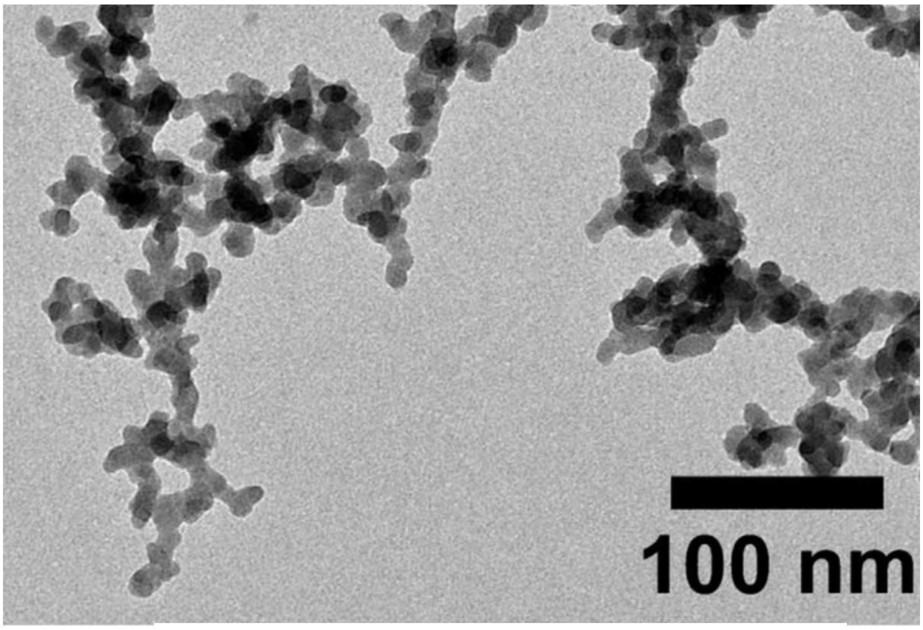

Fig-1: TEM image for the hydrophobic functionalized nano-silica

The hydrophobic functionalization of silica particles is well characterized using different analytical techniques such as FT-IR, ^{29}Si-NMR and TGA techniques. Figure 2 shows the FT-IR spectrum obtained for the functionalized nano silica particles. The spectrum shows a broad band at around 3,500 [cm^{-1}] due to uncapped Si-OH groups on the surface. It also shows a band at 2,969 [cm^{-1}] due to the C-H stretching vibration and a band at 1,254 [cm^{-1}] attributed to C-H bending vibration of the methyl group present in the hydrophobic -Si[(CH$_3$)$_3$] group on the filler surface.

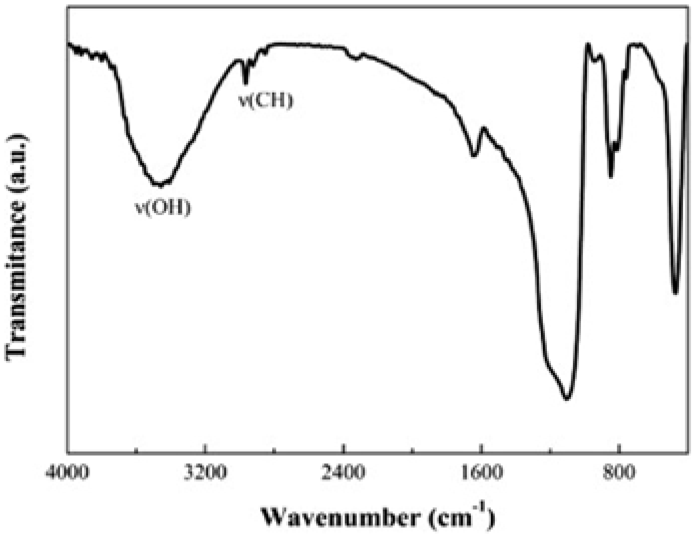

Fig-2: FTIR spectrum for the hydrophobic functionalized nano-silica

The solid state ^{29}Si-NMR (Figure 3) also confirms the incorporation of hydrophobic functional groups on the silica surface. Typically, in the case of particles with high surface area, it is not possible to cap all of the surface hydroxyl groups with a functionalization agent, and it is therefore expected to observe two signals, corresponding to capped and uncapped surfaces. The peak at -103 ppm corresponds to -Si[(OSi)$_3$](OH) ([Q$_3$]) uncapped and capped silanol group, indicating the partial conversion of hydrophilic surface to hydrophobic surface. The presence of silanol group on the surface is very much required to improve the filler-filler interaction, which in turn improves the mechanicals of the cured sheet. The peak at -112 ppm corresponds to the Si[(OSi)$_4$] ([Q$_4$]) structure.

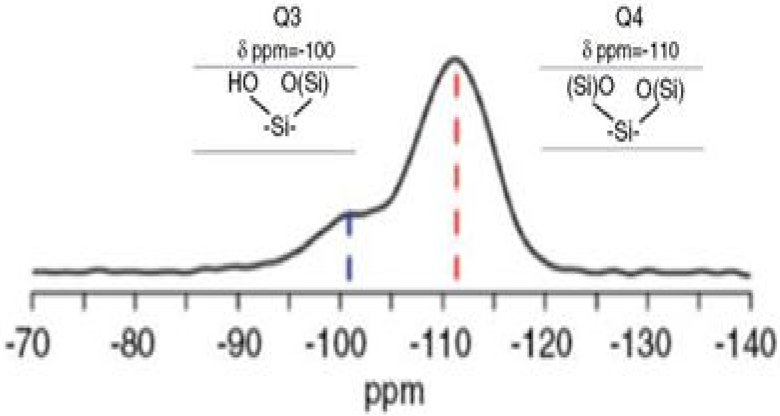

Fig-3: ^{29}Si-NMR spectrum for the hydrophobic functionalized nano-silica

The extent of capping with trimethylsilyl groups was measured using thermogravimetric analysis (TGA). The TGA curve obtained for the functionalized silica is shown in Figure 4. In TGA, the weight loss which occurred after 200[degrees]C, due to the degradation of the trimethylsilyl groups, can be attributed to the amount of hydrophobic capping on the filler surface. Like other analytical techniques, TGA also suggests the effective functionalization of the particle surface using HMDZ.

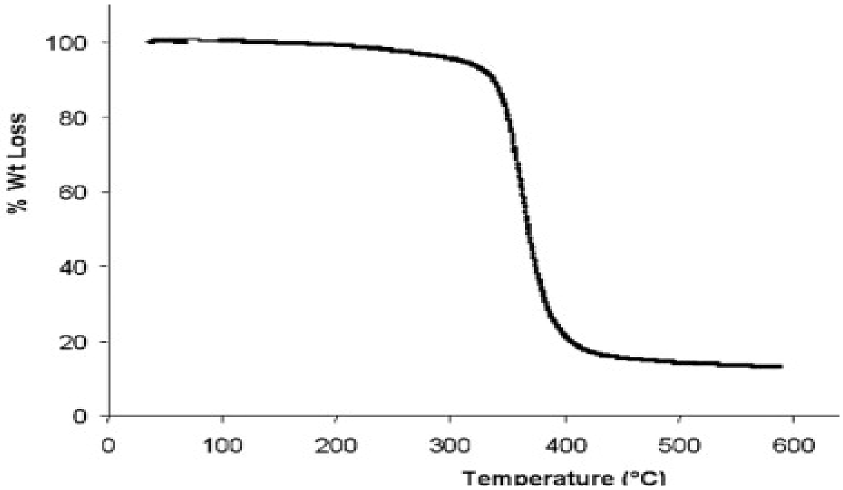

Fig-4: The TGA curve for the hydrophobic functionalized nano-silica

Dispersion of hydrophobic silica nano particle sol-gel in a PDMS matrix

Generally, in the aqueous sodium silicate route, silica nano particles were produced as spherical particles. These particles, because of the presence of hydroxyl groups on the surface, have a high tendency to aggregate due to the strong hydrogen bonding, yielding particles with larger agglomerates as a function of time, resulting in unusability of the silica nano particle solution. Also, since they are largely hydrophilic, they have poor interaction with the PDMS matrix, which is hydrophobic in nature. Hence, the dispersion of the unfunctionalized silica particles is very poor, with silica particles aggregating together to form large aggregates and poor dispersion. These in turn will result in poor physical properties of the silicone rubber.

In the current process, reacting the aqueous sodium silicate with acidic ion exchange resin produced silicic acid intermediates, which condense further to form the silica nano particles. The resultant nano-silica was in-situ functionalized by reacting with hexamethyldisilazane in the presence of ammonia and a mixture of solvents. The hexamethyldisilazane in the presence of a base forms trimethylsilanol, an intermediate, and reacts readily with hydroxyl groups on the surface of the particles to form hydrophobic trimethylsilyl capped silica nano particles. Thus the non-reactive alkylsilyl group on the surface of the silica avoids the unwanted secondary aggregation and produces silica sols that are stable with aging. The silica solution produced by this route was well dispersed uniformly in a PDMS matrix without any agglomeration of silica.

The frequency dependence of the viscosity (Eta) and storage modulus (G') for 17 wt. % loading of sol-gel silica dispersion in PDMS (SS 17) and commercial treated colloidal silica (CS 17) dispersion in PDMS revealed that with same loading and similar primary particle sizes of sol-gel silica and commercially-treated colloidal silica dispersion in PDMS, the viscosity behavior is similar under the wide frequency range ([10^{-1}] to [10^{3}] tad/s). Low viscosity indicates better flow, which will eventually help in the overall processing of the material.

Moreover, the storage modulus value (G') is higher with sol-gel silica compared to colloidal silica, indicating better mechanical performance of the polymer melt under shear. Thus, the novelty of the sol-gel silica lies in the fact that though it has a higher storage modules (G'), it has viscosity similar to colloidal silica. The rheological characteristics of the SS 17 show strong resemblance to a flocculated structure, and exhibit moduli with a strong frequency dependence with G" greater than G'.

Elastomer properties

The physical properties measured for the cured silicone elastomer are shown in Table 2. The results show similar mechanical properties for silicone elastomer produced using the in-situ functionalized silica (SS 17) and functionalized commercial silica (CS 17) at equal loading.

Table-2: Mechanical properties of the elastomer

Sample Name	Tensile Strength Mpa (SD)	Elongation % (SD)	Modulus Mpa (SD)	Hardness (durometer A)
SS 17	1.64 (0.09)	267 (32)	1.04 (0.02)	20
CS 17	1.63 (0.13)	356 (40)	0.96 (0.03)	16

CONCLUSIONS

The rheological study indicates good interaction between the filler polymer and good dispersion. As a model study, we have tried to compare the physical properties of a commercial silica with spherical dimensions vis-a-vis the partially aggregated/networked nano-silica of nearly similar particle size. At the loading levels specified, it seems that the viscosity of the modified silica is comparable to the viscosity of the colloidal silica system. Moreover, the modulus values and the tensile strength of the cured sheets indicate similar reinforcement by the fillers in comparison. A detailed evaluation at various loadings and varying surface modifications is in progress and will be published in a separate publication.

REFERENCES

1. Yilgor, I. & McGrath, J.E. (1988). Polysiloxane Containing Copolymers: A Survey of Recent Developments. *Advanced Polymer Science, 86*, 1-86.
2. Mark, J. E. (1990). Silicon Based Polymer Science, J.M. Zeigler & F. W.G. Fearon, (Eds) *Adv. Che. Ser. 224*, Washington, DC, p. 47.
3. Ratner, B.D., Hoffman, A.S., Schoen, F.J. & Lemons, J.E. (1996). An Introduction to Materials in Medicine. *Biomaterials Science,* 2nd Edition, Academic Press.
4. Lehmann, R.G. (1998). Degradation of silicone polymers in nature: *Dow Coming Corp*.
5. Baker, D., Charlesby, A. & Morris, J. (1968). Reinforcement of silicone elastomer by fine particles, *Polymer, vol.9,* 437-448.
6. Boonstra, B.B., Cochrane, H. & Dannenberg, E.M. (1975). Reinforcement of silicone rubber by particulate silica. *Rubber & Chemistry Technology, 48*, 558.
7. Soucek, M.D., Wu, S. & Chakrapani (2000). Silicones and silicone modified materials, *ACS Symp. Ser., 729*, 516.
8. Raghavan, S.R., Walls, H.J. & Khan, S.A. (2000). Rheology of silica dispersions in organic liquids. *Langmuir, 16,* 7920, p48.
9. Iler, R.K. (1979). The Chemistry of Silica Solubility, Polymerization, Colloid and Surface Properties, and Biochemistry, John Wiley and Sons, New York.
10. Brinker, C.J. & Scherer, G.W. (1990). Sol–gel science, the physics and chemistry of sol–gel processing, Brinker C. J. & Scherer G. W. (Eds) Academic Press, Boston.
11. Barthel, H., Rosch, L. & Weis, J. (1996). In Organosilicon Chemistry II: From Molecules to Materials; Auner, N. & Weis, J. (Eds) VCH Publishers: New York, 761.
12. Yoshida, A. (1994). The Colloidal Chemical of Silica, Advance In Chemistry Series 234, Oxford University Press, Oxford.

International Journal of Advance and Innovative Research
Volume 6, Issue 1 (VI): January - March, 2019

ISSN 2394 - 7780

ANTI-MICROBIAL STUDIES OF POTENTIAL CYCLOHEXANONE DERIVED SPIROPYRROIDINES

V. Sriraman
Department of Chemistry, Vels Institute of Science, Technology & Advanced Studies (VISTAS), Chennai
E-mail: sriramanvelsuniv@yahoo.com

ABSTRACT

A Series of Various cyclohexanone derived spiro-pyrrolidines were synthesized using 1,3-dipolar cycloaddition methodology . The compounds found to have very good antimicrobial properties and some of the compounds shown properties greater than the reference compounds. The attachment of cyclohexanone moiety to spiropyrrolidines enhanced the antimicrobial properties and it is shown in the results.

Keywords: Nutrient agar, bacterial culture, spiropyrrolidines, well diffusion method

INTRODUCTION

Great attention has been paid for curing diseases caused by microorganisms. Many infectous of pathogenic microorganisms develop resistance against the prevailing drugs, and this situation has necessitated a search for new source of compounds. Heterocyclic compounds, particularly five- and six-membered ring compounds have occupied a prominent place among the organic compounds in view of their diverse biological activities. The spiro-pyrrolidine and oxindole ring systems have acquired a prominent place among various heterocyclic compounds owing to their specific structural motif in many pharmacologically relevant alkaloids, as typyfied by rhyncoohylline, cornoxeine, mitraphylline, horsifline and spirotryprostatins.[1,2] Bithiophene derivatives are also important synthetic precursors for biologically active materials. [3]

Steroid based compounds turn out to be nontoxic, less vulnerable to multi-drug resistance (MDR) and highly bioavailable because of being capable of penetrating the cell wall[4,,5] Steroids find widespread application as anti-inflammatory, diuretic, anabolic, contraceptive, antiandrogenic, progestational and anticancer agents.[6] Many of the steroidal heterocycles have been found to exhibit potent biological activities, such as anti-inflammatory, anabolic, anti-cancer and anti-microbial activities.[7-15] Recently, heterocyclic estrone derivatives have been found to exhibit potential antibacterial, antifungal and antiproliferative activities.[16]

With this perspective we have carried out bioactivity studies on some of the spiro-pyrrolidines and the results are discussed.

EXPERIMENTAL

Material and Methods

Clinical Bacterial isolates: All the pathogenic bacterial and fungal isolates were obtained from Department of Clinical Medical Microbiology, Apollo Hospital at Chennai-06, India. All the clinical isolates were identified by standard methods. From this departmental culture collection unit, clinically important bacterial isolates were obtained namely *Staphylcoccus aureus, Bacillus subtilis, Pseudomonas aeruginosa, Klebsiella pneumonia, Escherichia coli* strains were used. Screening of antimicrobial activity was performed by following the sequence as given below:

1). Preparation of Nutrient agar,
2) Preparation of McFerland standards,
3) Inoculums preparation and
4) *Invitro* Antimicrobial Sensitivity Determination by Agar well diffusion method.

Preparation of nutrient agar

The nutrient agar was prepared by dissolving beef extract (1.5g), peptone (0.5g), yeast extract (1.5g), sodium chloride (0.5g) and agar (1.5g) in 100mL of distilled water. The pH was adjusted to 7.2 followed by sterilization in an autoclave at 121°C/15 Lb for 15minutes. The sterile molten agar media was then cooled to 50°C. About 15ml of the media was poured on a sterile petriplate and allowed to cool at room temperature.

Preparation of 0.5 Mcferland standards

0.5 mL of solution A (1.175g of barium chloride in 100mL of distilled water) was added to 99.5 mL of solution B (1mL of 0.36 N sulfuric acid in 100mL of distilled water) and mixed well with magnetic stirrer, then disturbed in test tubes with a screw cap of the same size as those containing the bacterial culture, the turbidity of which must be evaluated.

Preparation of bacterial inoculums

The cooled sterile broth medium was poured into sterile petri-plates having a uniform depth of 4 mm; this is equivalent to approximately 25 mL in a 90mm plate. Once the medium had solidified then the culture was inoculated on the medium. The turbidity of the culture was adjusted with sterile cotton swab was immersed in the bacterial/fungal suspension and then rotated and compressed against the wall of the test tube so as to remove the excess fluid.

RESULTS AND DISCUSSION

I*nvitro* Antimicrobial Sensitivity Determination Test by Well Diffusion Method

The invitro antimicrobial sensitivity of the antibiotics and the test compounds synthesized were determined by well diffusion method[9] as recommended by the National Committee for Clinical Laboratory Standards (NCCLS).[10] The well diffusion test was performed using medium, as per the procedure described by Magaldi *et al.*, 2004. A sterilized 10 mm cork borer was used to make agar wells on the sterile cotton swab. Compounds were dissolved in DMSO solvent separately and poured in the wells with varying concentrations ranging from 50µL and 100 µL using a micropipette. Antibiotic kanamycin (10mg/ml) was used as a standard to compare the results. The percentage of inhibition was calculated by the formula.

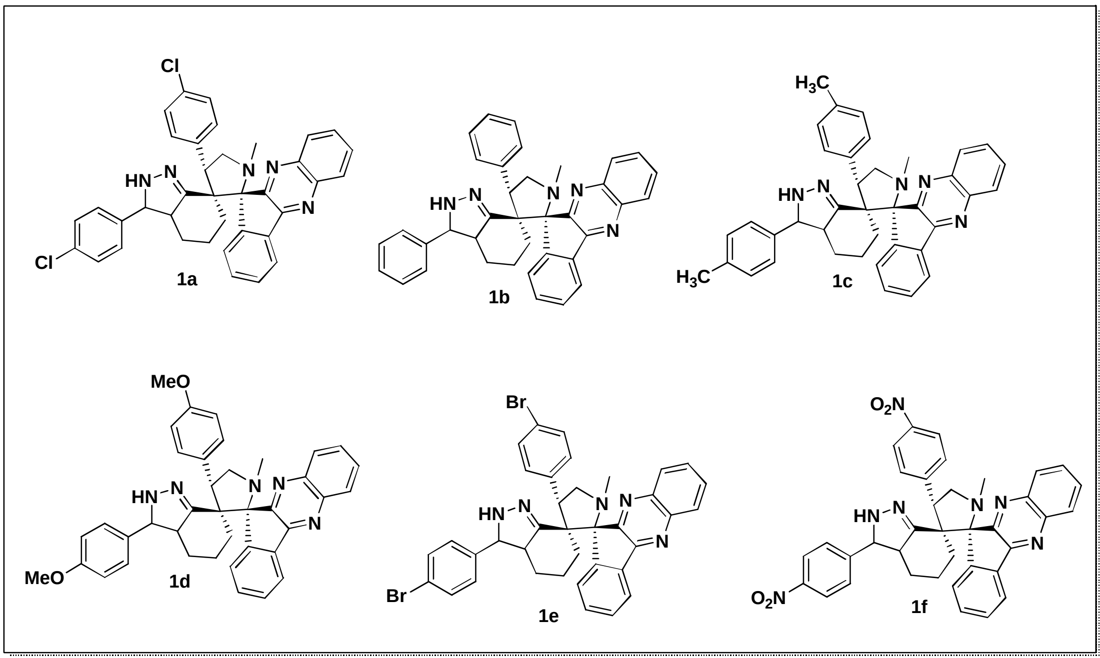

Spiropyyrolidines derived cyclohexanone

Table-1

Compounds	Escherichia coli		Pseudomonas Aeruginosa		Bacillus substills		Staphylococcus Auerus	
	50 µg/ml	100 µg/ml	50 µg/ml	100 µg/ml	50 µg/ml	100 µg/ml	50 µg/ml	100 µg/ml
1a	14.44	17.77	13.33	15.44	-	-	-	-
1b	18.89	21.11	18.89	21.11	-	13.33	-	-14.22
1c	-	13.33	-	-	-	-	-	-
1d	13.33	17.77	13.33	17.78	-	-	13.33	15.35
1e	-	12.22	-	-	-	-	-	-

Table-2: Antibacterial activity of Kanamycin (10 µg/ml) against human pathogens

Organisms	Zone of inhibition (mm) (µg/ml)	Percentage of inhibition (%)
Escherichia coli MTCC 733	26.00±2.13	28.88
Pseudomonas aeruginosa MTCC1688	39.98±2.1	33.33
Bacillus subtilis MTCC 41	28.25±1.81	31.38
Staphylococcus aureus MTCC 96	30.25±2.05	32.50

Given values are mean values of triplicate and standard deviations (Mean ± SD)

Table-3: Minimum Inhibitory concentration (MIC) of compounds against human pathogens

COMPOUNDS	Minimum inhibitory concentration (µg/ml)			
	Gram negative		Gram positive	
	Escherichia coli	Pseudomonas aeruginosa	Bacillus subtilis	Staphylococcus aureus
27a	50	100	ND	ND
27b	50	50	50	50
27c	100	ND	ND	ND
27d	50	100	100	ND
27e	100	ND	ND	100

ND: Not Determined

CONCLUSIONS

Five synthetic compounds were tested for antibacterial activity against four pathogens *Escherichia coli, Pseudomonas aeruginosa, Bacillus subtilis, Staphylococcus aureus.* All the compounds showed moderate activity against the tested pathogens. The bioactivity was tested at two different concentrations 50 to 100 **µg/ml** with reference compound Kanamycin. For the compounds 1**a, 1b and 1d** MIC was found to be 50 **µg/ml** against *E.coli.* and 1**b** exhibited MIC 50 **µg/ml** against *P.aeruginosa. 1***b** showed same MIC against *B.subtilis* and *S.aureus.* The compounds 1**a** and **1d** exhibited MIC at 100 **µg/ml** against *P.aeruginosa* while the same MIC was showed by **1d** against *Bacillus subtilis* and 1**e** against *S.aureus. The* remaining compounds did not show any antibacterial activity against the tested pathogens (Table 3)

ACKNOWLEDGEMENTS

V.S thanks of Vels Institute of Science, Technology & Advanced studies (VISTAS), pallavaram for providing necessary facilities to carried this research work.

REFERENCES

Examples

Journals

1). Bristol, J. A., Ed.; *Annual Reports in Medicinal Chemistry*, Academic Press: San Diego, 1990; Vol. 25 and earlier volumes in this series.

2) (a) Henrickson, J. B.; Silva, R. A. *J. Am. Chem. Soc.* 1962, 34, 643. (b) Shavel, J.; Zinnes, H. *J. Am. Chem. Soc.* 1963, 35, 1320.

3). Taylor R. In: *Thiophene and Its Derivatives*. part 1. Gronowitz S, editor. Vol. 44. Wiley; New York: 1985. ch.3.

4). (a) Ismail, M. A.; El-baily, S. A.; Brun, R.; Wenzler, T.; Nanjunda, R.; Wilson, W. D.; Boykin, D. W. *Bioorg & Med. Chem Lett.* 2011, *19*, 978. (b) Chou, Y.; Lai, M.C.; Hwang, T.; Ong, C.W. *Bioorg & Med. Chem Lett.* 1999, *9*, 2643.

5). Pettit, R. K.; Cage, G. D.; Pettit, G. R.; Liebman, J. A. *Int J Antimicrob Agents* 2000, *15*, 299.

6). Savage, P. B. *Eur. J. Org. Chem.* 2002, *5*, 759.

7). Savage, P. B. *Microbiol Lett.* 2002, *217*, 1.

8). Banday, A. H.; Mir, B. P.; Lone, I. H.; Suri, K. A.; Kumar, H. M. S. *Steroids* 2010, *75*, 805.

9). Shan, L. H.; Liu, H. M.; Huang, K. X, Dai, G. F, Cao, C. *Bioorg. Med.Chem. Lett.* 2009, *19*, 6637.

10). Lange, C.; Holzhey, N.; Scho¨necker, B.; Beckert, R.; Mollmann, U.; Dahse, H. M. *Bioorg. Med. Chem.* 2004, *12*, 3357.

International Journal of Advance and Innovative Research
Volume 6, Issue 1 (VI): January - March, 2019

ISSN 2394 - 7780

VOLTAMMETRIC STUDIES OF A, B-UNSATURATED ORGANIC COMPOUNDS

P. Indra Priyatharesini
Department of Chemistry, School of Basic Sciences, VISTAS, Chennai

ABSTRACT

Cyclic voltammetric reduction of various α,β-unsaturated Organic compounds such as Allyl bromide, Diethyl fumarate, Diethyl maleate in aprotic media (DME), containing 0.1M TBAI, have been reported at glassy carbon as working electrode. Allyl bromide undergoes one electron irreversible diffusion controlled process. The other two compound produce two peaks show that there is two one electron diffusion controlled process. For the compounds Diethyl fumarate the 1st peak is reversible and 2nd peak is irreversible. For Diethyl maleate both peaks are irreversible. The intermediate formed during the reduction process is traced out by using trapping agent such as CO_2.

INTRODUCTION

The electrolytic hyrodimerzation of activated olefins and the mechanistic work has been devoted by Baizer [1] himself and by other works.

Electrohydrodimerization of activated olefins and related substances has been subjected to numerous mechanistic investigations, have been studies by Rolando and co workers [2]. By far the majority of these mechanistic investigations have been carried out in media of low proton availability. In fact, the anion radical $R^{\cdot -}$ which is formed by transfer of one electron from the metal to the activated olefin R is relatively unstable and may undergo either a dimerization reaction or else a protonation and immediate subsequent reduction of the protonated radical RH.

The Electrochemical reduction of organic halides in aprotic medium generally proceeds via a two-electron cleavage of the carbon-halogen bond follows the order I>Br>Cl>F.

In the literature paper of D.Vasudevan, Russian J.Electrochemistry [3] they have studied the direct as well as superoxide-assisted reduction of the 17 organic halides in aprotic media was studied by cyclic voltammetry and CPE. The products have been characterized by TLC, chromatographic, or chemical methods. According their studies, $O_2^{\cdot -}$ is act as a strong nucleophile or base in the reactions.The cyclic voltammetry results from its ability to rapidly provide considerable information on the the thermodymaincs or redox processes and the kinetics of heterogeneous electron transfer reaction, and on coupled chemical reactions or adsorption processes [4]. Potential sweep valtammetry is divided into Linear sweep voltammetry and cyclic voltammetry [5&6]

The Voltammetric data for ester reduction are available for several aromatic esters and in particular cyclic voltammetry shows that in the absence of proton donors reversible formation of radical-anions occurs [2]. A study of the electrochemical reduction of monoethyl maleate on a mercury electrode has been carried out and the results obtained are compared with those corresponding to the reduction of monoethyl fumarate [7]. Cyclic voltammetry and controlled-potential electrolysis have been employed to investigate the electrochemical reductions of benzyl iodie, benzal bromide and benzal chlorobromide at glassy carbon cathodes in the presence of nitric oxide in acetonitrile containing tetra methyl ammonium tetrafluoroorate [8].

The reduction of the cis- and trans- isomers of thioindigo at a platinum electrode was studied by Lun-shu R.Yeh and Allen J.Bard [9] by cyclic voltammetry, controlled potential coulometry, rotating ring-disk electrode voltammetry, and e.s.r spectroscopy. According to their study the trans- isomer produces predominantly the radical anion upon one-electron reduction while the cis- radical anion isomerized to the trans form and dimerizes much more rapidly than trans- TI. Reduction of both forms at the second reduction wave or in the presence of benzoic acid proceeds by a two electron reaction probably to a protanated dianion species. Both the dimeric dianion and the protonated dianion can be oxidized back to trans-TI dimeric dianion and the protonated dianion can be oxidized back to trans- TI.

In cyclic voltammetry, the electrode potential ramps linearly versus time. The ramping is known as the scan rate (V/s) [10&11].

In the current studies we have reduced, α,β-unsaturated Organic compounds in an aprotic medium (DME) using 0.1M TBAI as a supporting electrolyte. The potential and current of the organic compounds have been reported at various sweep rates and various concentration. The compounds undergoes diffusion controlled process have been investigated by various voltammetric analysis. The intermediate formed in the reaction have been trapped by passing CO_2 and the current and potential of the intermediate also reported. From the potential obtained after passing CO_2 the stability of the intermediate have been determined from the difference between the potential obtained after and before passing CO_2

MATERIALS AND METHODS

Solution Preparation

The stock solutions of 0.1M Allyl bromide, Diethyl fumarate, Diethyl maleate are prepared by using the prepared solvent-supporting electrolyte as a solvent.

Working electrode and its pretreatments

In this study 5mm dia glassy carbon electrode is used as a working electrode. The geometric area of cross-section of GC electrode used is 0.1964cm^2. This type of material is treated by heating up to 3000^{0}C. The impurity level in this type is very low when compared to other Tokai GC materials. The electrical contact was achieved through the mercury poured into the glass tube.

Pretreatments

The GC electrode was polished to mirror finish using gradually finer emery papers up to 4/0(John Oakey and Sons). Such polished electrodes were scratch free by visual examination. The polished electrode was thoroughly rinsed with triple distilled water to remove any powdery particles on the surface and then cleaned with trichloroethylene using cotton. The electrode was immediately put into the electrochemical cell. In non-aqueous studies, the moisture present on the electrode surface was completely removed by drying with cotton. Such a mechanically pretreated electrode was electrochemically pretreated by adopting the procedure described in a literature by M.Noel and P.N.Anantharaman and the level of activation and its reproducibility was often checked with the standard redox system, ferrocyanide/ferrocyanide in KCl solution. The GC electrode was potentiodynamically cycled for 1 minute. Stirring as well as deareation of the electrode was continued during potential cycling. Background current was recorded, then potassium ferrocyanide(2mm) solution was added and potential was scanned from -0.250V to +0.500V. The reversible peak with separation ΔE_p of 60mV was observed [10]. This was taken as a measure of electrode activity. Such activated electrode was able to give reproducibile resuls for few hours shown in Fig 1.

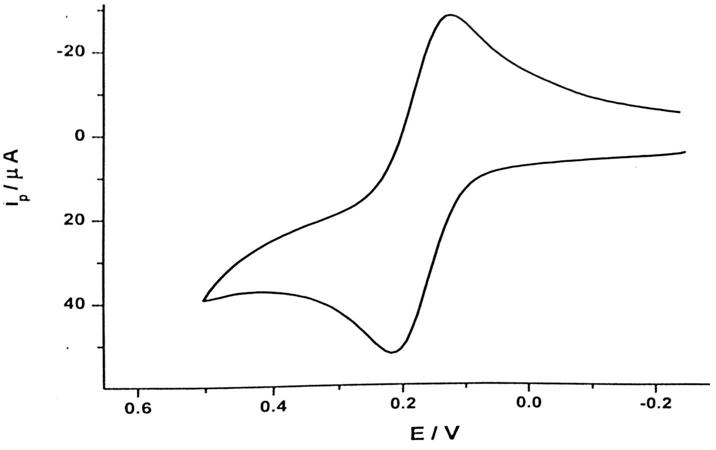

Fig-1: Cyclic voltammogram of potassium ferrocanide on GCE at 20mV/sec in 0.1 KCl at 2mM concentration.

Reagents

Each of the following reagents was used as received are shown Table 1

Table-1: Reagents used for the study

Chemicals used	MAKE
DMF	Merck
Tetra butyl ammonium iodide (AR Extra pure)	SRL
Allyl bromide (98%)	Merck
Diethyl fumarate (97%)	Merck
Diethyl maleate (95%)	Merck

EXPERIMENTAL PROCEDURE

Voltammetry

Care was taken to record reproducible voltammograms particularly in non-aqueous media, where lot of difficulties may be encountered which can arise from cleaning the cells, solvent-supporting electrolyte, purifications, preparation of solutions etc., Before each set of experiments the electrochemical cell was scrupulously washed with nitric acid, triple distilled water and dried in an oven at about 150^{0}C. GC electrode was placed in the cell which is electrochemically pretreated. In this experiment platinum wire is used as a reference electode

High purity nitrogen gas was further purified by passing through molecular sieve 4A, DMF and finally through the solvent-supporting electrolyte solution. Long time deareation (for and hour) was carried out by bubbling purified nitrogen gas through the electrolytic solution in the cell, until no oxygen was present in the system. All the electrochemical studies were carried out by thermosetting the electrochemical system at 25^{0}C±1^{0}C.

RESULT AND DISCUSSION

Electro reduction of Diethyl fumarate

The main cathodic peaks around -1.5V and -2.0V and a reverse peak around +1.3V were observed for the voltammetric reduction of diethyl fumarate on GCE in DMF media. A small peak around -2.1V move negative to the second main peak was also observed. This post peak is clearly noticed at lower sweep rates. On recording the voltammograms for this reduction process a small perpeak less negative to the second main peak was observed. The reverse peak observed its complimentary to the first main peak. The peak current of the two main peaks and reverse peak increase with the increase in sweep rates shown in Fig 2 and also increase in concentration shown in Fig 3. The peak potentials of the two peak vary wih sweep rate and slightly vary with the concentration. The plot of ip Vs $\nu^{1/2}$ shown Fig 5 is linear and passes through origin at lower concentration. The peak current constant ($ip/AC\nu^{1/2}$) for the first main peak is almost constant in the sweep rate and concentration ranges studied given in Table 2. The peak current constant value for the second main peak is greatly less than that of the first first peak current constant value. This is due to the difficulty in ascertaining the base line for second peak. The value of peak current constant for the first main peak is approximately close to one electron process. All the above voltammetric analysis suggests that the reduction of diethyl fumarate proceeds in two one electron diffusion controlled processes. The first one electron process is reversible and the second one electron process is irreversible. The linear line shown in the calibration curve shown in Fig 6 indicates that, as the concentration increases, the current also increases.

The stability of anion radical and dianion produced in the electro reduction of diethyl fumarate was studied by recording the voltammograms in the presence of dissolved carbon dioxide the peak potential of the first peak remain unaltered and the second peak completely disappears shown in Fig 4. the peak current increased. The anodic peak is unaltered. The anion radical generated in the first reduction process coupled with the carbon dioxide molecule and gets further reduced. The non-availabiliy of anion radical for second electron transfer is shown by the absence of the second peak in the the presence of carbon dioxide.

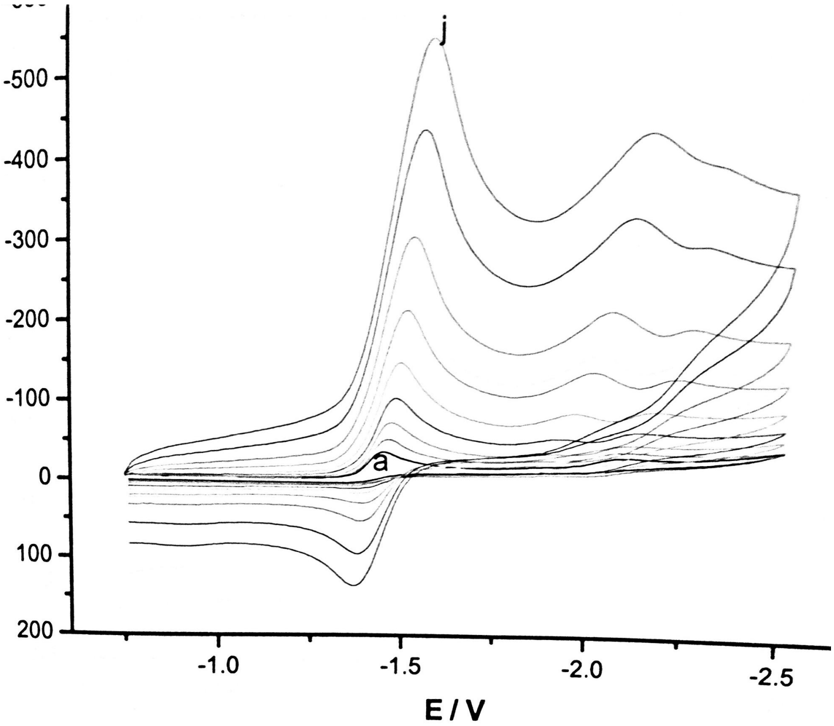

Fig-2: Cyclic voltammetry of Diethyl fumarate in 0.1M TBAI/DMF on GCE, Sweep Rate Effect with 2mm concentration (a)5mV/s, (b) 10mV/s, (c)20mV/s, (d)40mV/s, (e)80mV/s, (f) 160mV/s, (g) 200mV/s

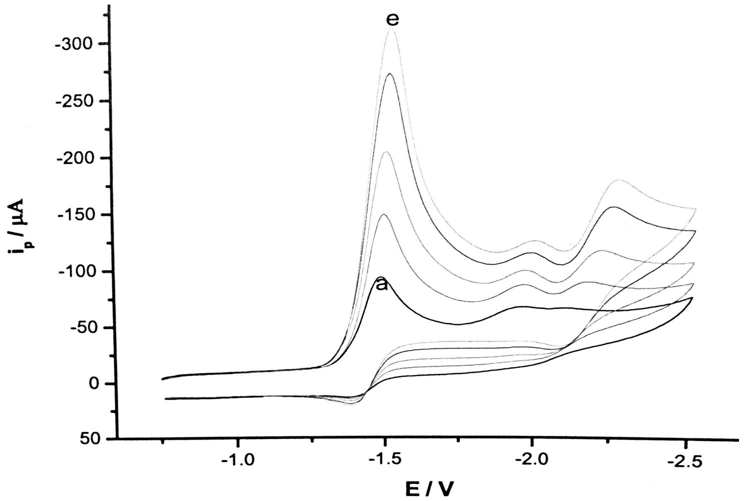

Fig-3: Cyclic voltammetry of Diethyl fumarate in 0.1M TBAI/DMF on GCE, Concentration with scan rate of 80mV/s

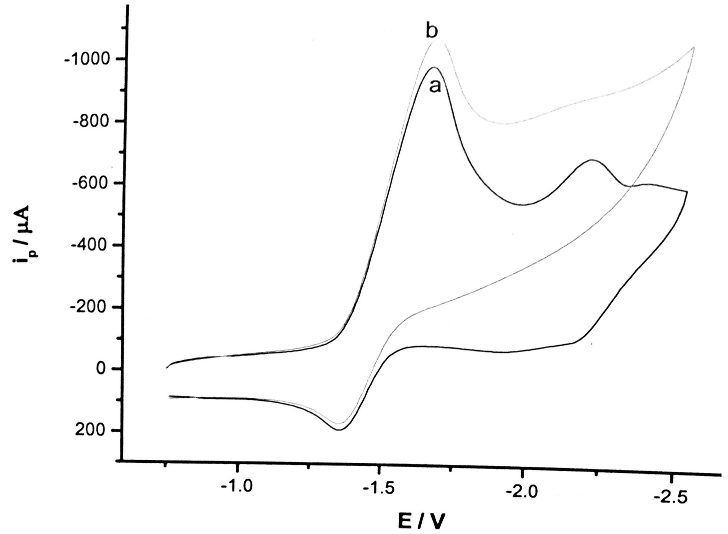

Fig-4: Cyclic voltammetry of Diethyl fumarate in 0.1M TBAI/DMF on GCE, Passing CO_2 at 12mm concentration with scan rate of 1V/s (a) with out CO_2 and with CO_2

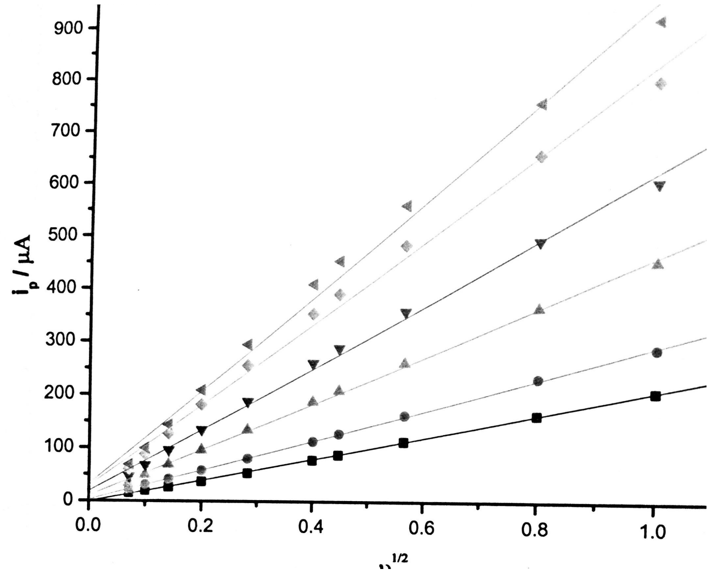

Fig-5: Cyclic voltammetry of Diethyl fumarate in 0.1M TBAI/DMF on GCE

Relationship between concentration of Allyl bromide and reduction peak current at different sweep rates (a)5mV/s, (b) 10mV/s, (c)20mV/s, (d)40mV/s, (e)80mV/s, (f) 160mV/s, (g) 200mV/s and at different concentrations: (2mm, (b) 3mm (c) 5mm (d)7mm, (e) 10 mm (f) 12mm.

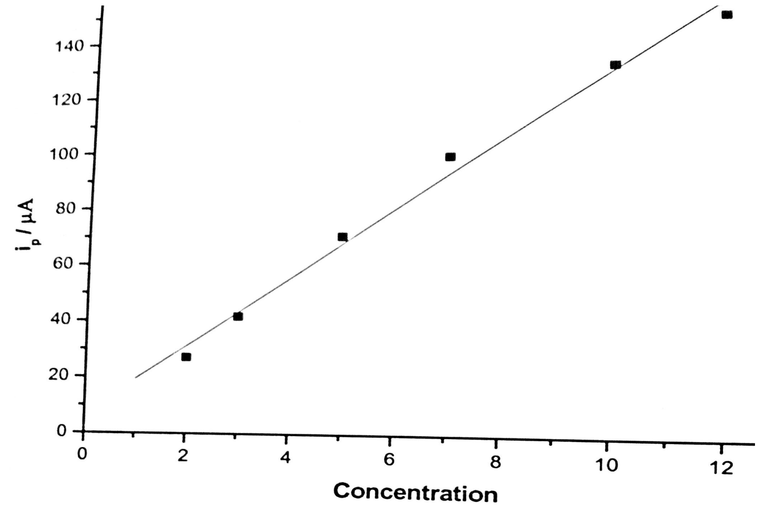

Fig-6: Calibration curve of Diethyl fumarate

Table-2: Cyclic voltammetric peak parameters for the reduction of Diethyl fumarate in 0.1M TBAI/DMF on GCE

Conc. (mM)	Sweep rate (V/s)	$\nu^{1/2}$	$-E_{p1}$ (V)	I_{p1} (μA)	E_{p1}-$E_{p/2}$ (mV)	$I_p/AC\nu^{1/2}$	$-E_{p1}$ (V)	I_{p1} (μA)	E_{p1}-$E_{p/2}$ (mV)	$I_p/AC\nu^{1/2}$
2mM	0.005	0.0707	1.470	15.50	66	558.15	-	-	-	-
	0.01	0.1	1.460	20.2	54	514.25	-	-	-	-
	0.1414	0.1414	1.470	27	62	486.12	-	-	-	-
	0.2	0.2	1.480	37.35	70	475.43	1.944	11.45	109	145.74
	0.2828	0.2828	1.480	53.27	66	479.55	1.964	16.91	117	152.22
	0.4	0.4	1.490	78.35	71	498.66	1.974	21.51	126	136.90
	0.4472	0.4472	1.490	88.57	70	504.21	2.004	31.74	148	180.68
	0.5656	0.5656	1.501	113.6	75	511.32	1.994	30.28	140	136.29
	0.8	0.8	1.521	161.2	84	512.98	2.024	45.34	147	144.28
	1	1	1.531	199.5	85	507.89	2.044	61.50	142	156.56
3mM	0.005	0.0707	1.450	22.01	47	528.37	-	-	-	-
	0.01	0.1	1.465	30.39	58	515.78	-	-	-	-
	0.2	0.1414	1.465	41.43	54	497.28	-	-	-	-
	0.4	0.2	1.475	57.47	62	487.69	-	-	-	-
	0.8	0.2828	1.485	80.15	70	481.02	1.958	15.38	95	92.30
	0.160	0.4	1.495	113.8	76	482.85	1.989	22.31	102	94.66
	0.200	0.4472	1.495	128.2	74	486.54	2.009	26.45	115	100.38
	0.320	0.5656	1.505	162.6	79	487.92	2.029	37.75	125	112.07
	0.640	0.8	1.525	228.4	88	484.55	2.079	61.23	157	129.90
	1	1	1.546	277.3	97	470.63	2.110	85.36	166	144.87
5mM	0.005	0.0707	1.445	34.43	45	495.96	2.089	12.92	86	186.11
	0.01	0.1	1.465	49.28	58	501.83	2.099	14.33	94	145.92
	0.2	0.1414	1.475	69.08	62	497.51	2.110	14.96	83	107.24
	0.4	0.2	1.485	96.70	66	492.36	2.140	19.94	93	101.52
	0.8	0.2828	1.495	135.1	71	486.49	-	-	-	-
	0.160	0.4	1.505	188.5	77	479.88	2.009	34.85	86	89.72
	0.200	0.4472	1.515	209.5	85	477.05	2.019	42.37	86	96.48
	0.320	0.5656	1.525	260.7	89	469.38	2.059	61.79	105	111.25
	0.640	0.8	1.556	357.2	107	454.68	2.110	94.09	123	119.76
	1	1	1.576	435.2	116	443.17	2.140	107.8	129	109.77
7mM	0.005	0.0707	1.445	46.54	48	478.81	2.110	14.42	87	148.35
	0.01	0.1	1.455	67.41	50	490.32	2.130	18.38	96	133.68
	0.2	0.1414	1.475	96.07	62	494.19	2.150	25.28	99	130.04
	0.4	0.2	1.485	135.0	64	490.98	2.180	35.57	101	129.72
	0.8	0.2828	1.505	188.5	77	484.83	-	-	-	-

	0.160	0.4	1.525	261.4	89	475.34	-	-	-	-
	0.200	0.4472	1.525	289.4	87	470.71	-	-	-	-
	0.320	0.5656	1.546	357.3	100	459.49	2.059	67.69	85	87.05
	0.640	0.8	1.576	480.8	116	437.15	2.120	126.4	102	114.92
	1	1	1.596	579.0	124	421.15	2.160	133.6	106	97.177
10mM	0.005	0.0707	1.445	9.98	51	431.96	2.140	19.67	100	141.65
	0.01	0.1	1.455	88.29	52	449.54	2.150	23.44	95	119.3
	0.2	0.1414	1.475	127	62	457.32	2.150	37.61	106	135.42
	0.4	0.2	1.495	182.2	72	463.84	2.180	40.44	88	102.95
	0.8	0.2828	1.515	256.0	82	460.92	-	-	-	-
	0.160	0.4	1.535	352.9	91	449.21	-	-	-	-
	0.200	0.4472	1.546	390	97	444.03	-	-	-	-
	0.320	0.5656	1.566	478.9	108	431.11	-	-	-	-
	0.640	0.8	1.606	636.8	132	405.29	2.120	127.4	90	81.08
	1	1	1.636	759	149	386.45	2.180	164.7	101	83.85
12mM	0.005	0.0707	1.445	68.53	51	411.29	2.150	20.17	97	121.05
	0.01	0.1	1.455	99.53	52	422.30	2.170	28.72	101	121.86
	0.2	0.1414	1.475	143.6	62	430.90	2.190	36.36	95	109.10
	0.4	0.2	1.495	209	71	443.39	2.220	56.70	95	120.29
	0.8	0.2828	1.525	295.2	89	442.91	2.271	85.89	103	128.86
	0.160	0.4	1.546	408.3	96	433.10	-	-	-	-
	0.200	0.4472	1.556	450.9	102	427.81	-	-	-	-
	0.320	0.5656	1.576	553	12	414.85	-	-	-	-
	0.640	0.8	1.626	732	144	388.23	2.140	123.4	85	65.44
	1	1	1.656	869.9	160	369.10	2.100	179.2	104	76.03

Electro reduction of Diethyl maleate

Two voltammetric peak around -1.5V and -1.9V for the electron reduction of diethyl maleate was observed. In addition to these two main peaks a small prepeak was also noticed. The peak potential and peak current of the two main peaks icreases with the increase in sweep rates shown in Fig 7 and concentrations shown in Fig 8. No sharp reverse peak was observed. The i_p increases linearly with square root of sweep rate shown in Fig 10. The linear line passes through origin at low concentration. The peak current constant value ($i_p/AC\nu^{1/2}$) for the first main peak remains constant at low concentration and slowly decreases with the increase in sweep rates given in Table 3. The peak current constant value is very low for second main peak due to the uncertainty in ascertaining the correct base line. The (I_p /$AC\nu^{1/2}$) value is comparable to the value for the one electron transfer process reported in the literature. The above voltammetric data suggests that the electro reduction of diethyl maleate proceeds through two one electron process. The linear line shown in the calibration curve shown in Fig 11 indicates that, as the concentration increases, the current may increases.

The stability of anion radicals and dianion produced in the voltammetric experiments is studied. The peak potential almost remain constant and the peak current increases in the presence of carbon dioxide shown in Fig 9.

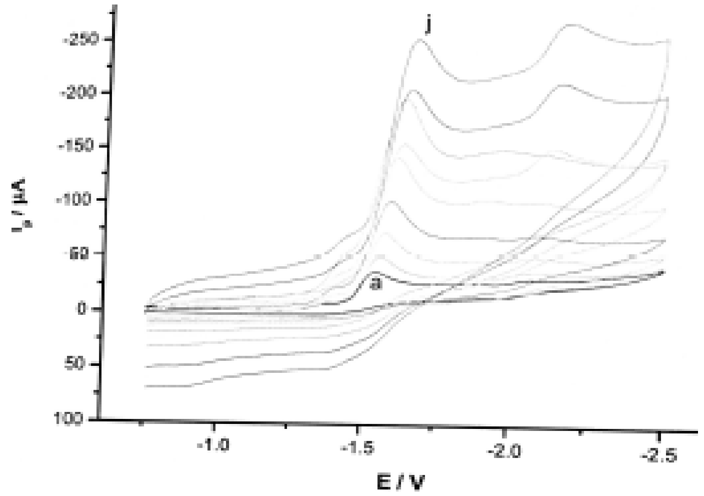

Fig-7: Cyclic voltammetry of Diethyl maleate in 0.1M TBAI/DMF on GCE, Sweep Rate Effect with 2mm concentration (a)5mV/s, (b) 10mV/s, (c)20mV/s, (d)40mV/s, (e)80mV/s, (f) 160mV/s, (g) 200mV/s

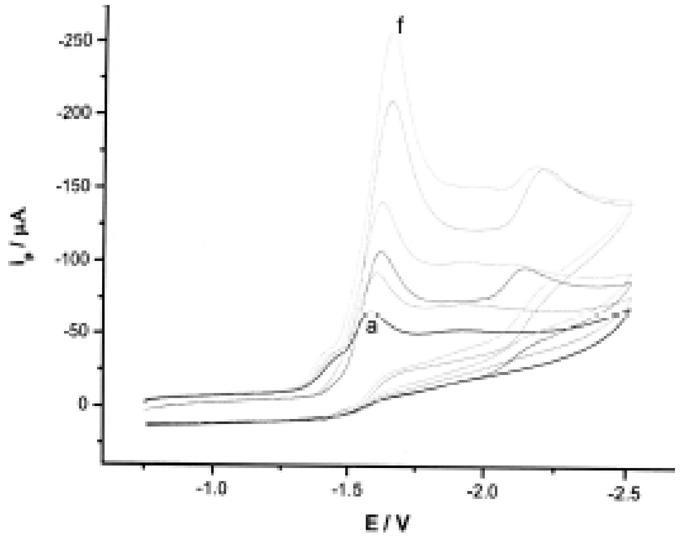

Fig-8: Cyclic voltammetry of Diethyl maleate in 0.1M TBAI/DMF on GCE, Concentration with scan rate of 80mV/s

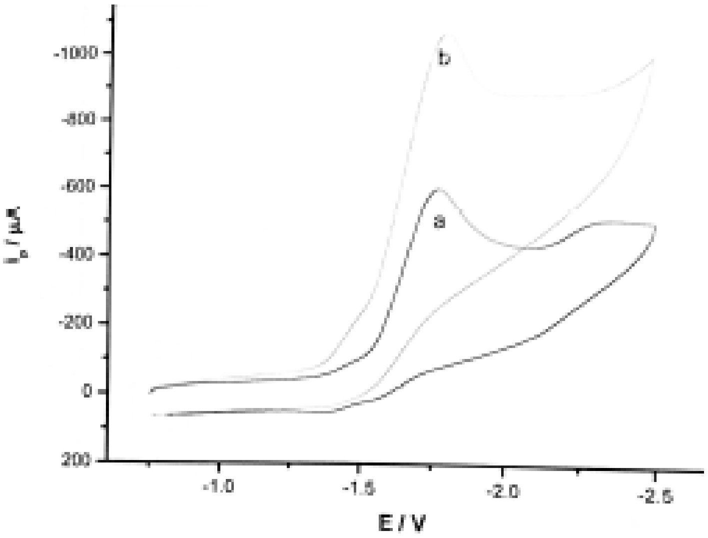

Fig-9: Cyclic voltammetry of Diethyl maleate in 0.1M TBAI/DMF on GCE, Passing CO_2 at 12mm concentration with scan rate of 1V/s (a) with out CO_2 and with CO_2

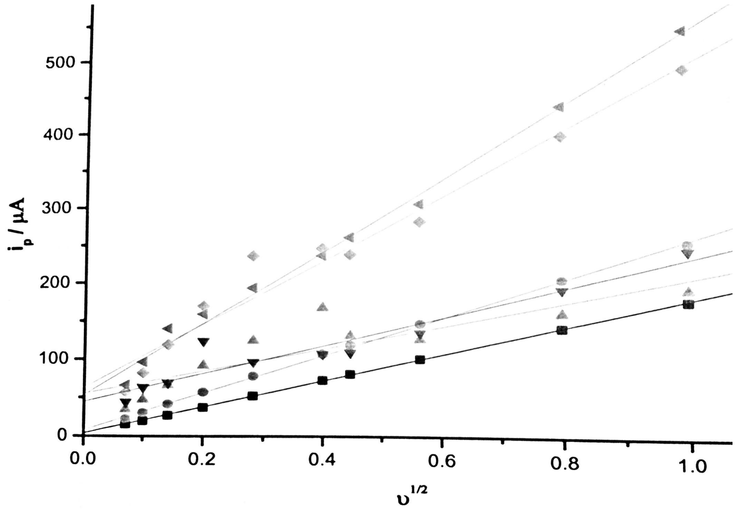

Fig-10: Cyclic voltammetry of Diethyl maleate in 0.1M TBAI/DMF on GCE

Relationship between concentration of Allyl bromide and reduction peak current at different sweep rates (a)5mV/s, (b) 10mV/s, (c)20mV/s, (d)40mV/s, (e)80mV/s, (f) 160mV/s, (g) 200mV/s and at different concentrations: (2mm, (b) 3mm (c) 5mm (d)7mm, (e) 10 mm (f) 12mm.

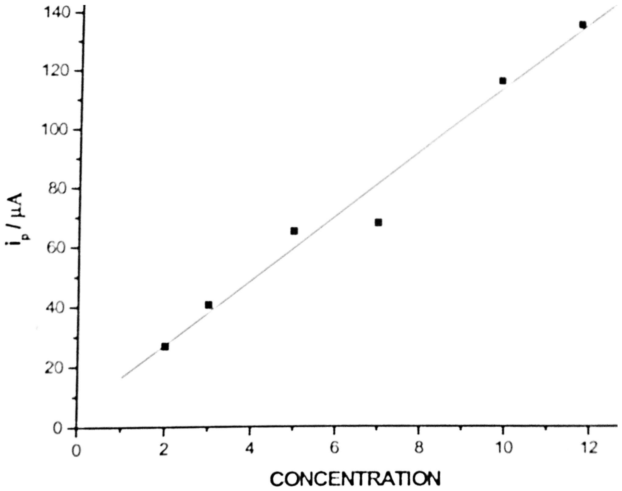

Fig-11: Calibration curve of Diethyl maleate

Table-3: Cyclic voltammetric peak parameters for the reduction of Diethyl maleate in 0.1M TBAI/DMF on GCE

Conc. (mM)	Sweep rate (V/s)	$\nu^{1/2}$	-E_{p1} (V)	I_{p1} (µA)	E_{p1}-$E_{p/2}$ (mV)	$I_p/AC\nu^{1/2}$	-E_{p1} (V)	I_{p1} (µA)	E_{p1}-$E_{p/2}$ (mV)	$I_p/AC\nu^{1/2}$
2mM	0.005	0.0707	1.536	15.69	77	564.99	-	-	-	-
	0.01	0.1	1.544	19.99	76	508.91	-	-	-	-
	0.1414	0.1414	1.564	27.18	89	489.36	1.900	1.300	85	23.40
	0.2	0.2	1.572	37.41	90	476.19	1.900	1.566	76	19.93
	0.2828	0.2828	1.581	52.29	91	470.72	1.900	1.526	67	13.73
	0.4	0.4	1.598	72.91	104	464.04	1.925	2.487	80	14.15
	0.4472	0.4472	1.598	81.31	102	462.88	1.917	2.685	63	12.08
	0.5656	0.5656	1.614	101.3	114	455.96	1.917	2.686	55	12.09
	0.8	0.8	1.631	140.1	117	445.83	1.967	5.229	80	16.64
	1	1	1.648	173.0	122	440.42	1.975	5.035	70	12.81
3mM	0.005	0.0707	1.547	22.10	70	530.53	-	-	-	-
	0.01	0.1	1.556	30.08	73	510.52	-	-	-	-
	0.2	0.1414	1.564	41.26	73	495.24	-	-	-	-
	0.4	0.2	1.581	57	81	483.70	1.925	2.405	86	20.40
	0.8	0.2828	1.598	78.06	89	468.47	1.925	2.024	76	12.14
	0.160	0.4	1.614	107.1	97	454.42	1.942	3.957	79	16.78
	0.200	0.4472	1.614	119.1	94	452.00	1.967	6.196	99	23.51
	0.320	0.5656	1.631	146.9	103	440.80	1.984	6.198	97	20.97
	0.640	0.8	1.656	202.7	116	430.03	2.042	13.09	119	27.77
	1	1	1.673	246.8	122	418.87	2.059	13.14	109	22.30
5mM	0.005	0.0707	1.547	34.62	64	498.70	2.076	5.183	67	74.23
	0.01	0.1	1.564	47.19	69	480.54	2.076	4.768	56	48.55
	0.2	0.1414	1.581	66.32	75	477.63	2.093	8.676	79	62.48
	0.4	0.2	1.598	91.58	82	466.29	2.101	8.886	86	45.24
	0.8	0.2828	1.614	124.7	89	449.04	2.110	5.508	211	19.83
	0.160	0.4	1.640	168.6	104	429.22	1.984	7.151	89	18.20
	0.200	0.4472	1.631	131.2	87	298.75	2.126	19.53	82	44.47
	0.320	0.5656	1.640	126.9	87	228.47	2.143	31.73	83	57.12
	0.640	0.8	1.656	158.8	88	202.13	2.168	38.73	83	49.29
	1	1	1.682	186.9	101	190.32	2.185	54.40	89	55.39

7mM	0.005	0.0707	1.547	44.27	62	455.46	2.084	8.229	61	84.66
	0.01	0.1	1.564	63.25	65	460.06	2.101	10.80	71	78.55
	0.2	0.1414	1.581	69.26	69	356.28	2.110	15.34	75	78.91
	0.4	0.2	1.606	123.9	79	450.61	2.126	14.98	77	54.48
	0.8	0.2828	1.614	96.60	80	248.46	2.135	25.54	77	65.69
	0.160	0.4	1.631	107.4	83	195.30	2.143	34.36	72	62.48
	0.200	0.4472	1.640	109.4	87	177.94	2.151	37.66	75	61.25
	0.320	0.5656	1.656	135.5	94	174.25	2.168	42.65	78	54.84
	0.640	0.8	1.682	190.5	102	173.20	2.193	53.50	81	48.64
	1	1	1.698	237.8	105	172.97	2.227	68.12	99	49.54
10mM	0.005	0.0707	1.547	56.76	60	408.77	2.110	12.81	72	92.25
	0.01	0.1	1.564	82.01	62	417.56	2.118	14.52	66	73.93
	0.2	0.1414	1.589	118.9	69	428.15	2.135	15.92	68	57.32
	0.4	0.2	1.623	169.7	84	432.02	2.151	16.27	64	41.42
	0.8	0.2828	1.648	236.9	90	426.53	2.168	13.28	55	23.91
	0.160	0.4	1.656	247.4	95	314.91	2.185	31.27	71	39.80
	0.200	0.4472	1.665	239.2	101	272.34	2.185	40.45	70	46.05
	0.320	0.5656	1.682	282.3	106	254.13	2.210	51.69	81	46.53
	0.640	0.8	1.715	390.6	118	248.59	2.252	66.79	95	42.50
	1	1	1.740	474.3	127	241.49	2.286	70.84	103	36.06
12mM	0.005	0.0707	1.547	65.81	60	394.97	2.126	15.92	91	95.54
	0.01	0.1	1.572	95.82	69	406.56	2.135	21.64	79	91.81
	0.2	0.1414	1.598	139.8	75	419.50	2.151	26.46	75	79.39
	0.4	0.2	1.601	159.2	79	337.74	2.168	30.84	73	65.42
	0.8	0.2828	1.635	194.2	92	291.37	2.192	43.89	79	64.78
	0.160	0.4	1.656	237.7	98	252.14	2.227	55.72	92	59.10
	0.200	0.4472	1.656	262	107	248.58	2.244	58.56	99	55.56
	0.320	0.5656	1.676	305.5	109	229.18	2.277	70.63	116	52.98
	0.640	0.8	1.726	429.7	128	227.90	2.361	84.53	165	44.83
	1	1	1.734	525.3	145	222.88	2.412	85.14	186	36.12

CONCLUSION

The following conclusions are drawn in the present work. The α.,β unsaturated organic compounds investigated in the present work undergo smooth reduction on GCE in DMF media.

1. Diethyl fumarate undergoes two one-electron diffusion contolled process. The first reduction process is a reversible and the second reduction process is irreversible.
2. Diethyl maleat undergoes two one electron diffusion controlled processes. Both the process is irreversible.
3. A slow time-dependent adsorption/blocking prewave is observed for the reduction of Diethyl maleate.

The calculation for number of electron transferred in all the reduction process is only qualitative. Actual determination of electron transfer is to be determined by coloumetry at constant potential. The constant potential or controlled potential electrolysis experiments have to carry out to determine the actual mechanisms involved in the reduction process. It will be interesting to isolae and characterize the carbon dioxide coupled product with the α,β unsaturated compound. Chemically modified glassy carbon electrode can be tried to investigate the reduction process of α,β unsaturated compound without any possible adsorption/blocking effects.

REFERENCE

1. Manuel M. Baizer & Henning Lund: Organic Electrochemistry, 3rd Edition, (1991) by Marcel Dekker Inc, Denmark.
2. Rolando Guidelli Giovanni Piccardi and Maria Rosa Moncelli, J.Electroanal. Chem, 129(1981) 373-378.

3. D.Vasudevan, Russian J.Electrochemistry, 41(30) (2005) 310-314.
4. L.A.Matheson and N.Nichols, Trans.Electrochem.,300,73(1938)193.
5. A.Sevick, Coll. Czech. Chem. Commun. 13 (1948) 349.
6. Bard, Allen J; Larry R. Faullener (2000-12-18) Electrochemical Methods Fundamentals and Applications (2.ed.).Wiley.
7. Luis Camacho and Juan Jose Ruiz, J.Electroanal. Chem., 170 (1984) 281-292.
8. Chang Ji, Dennis G. Peters, J.Electroanal. Chem., 516 (2001) 39-49.
9. Lun-Shu R.Yeh and Allen J. Bard, J. Electroanal. Chem., 70 (1976) 57-169.
10. Heinze, Jurgen (1984) “Cyclic Voltammetry, Electrochemical Spectroscopy”; New analytical Methods (25), Angewandte Chemie Internaltional Edition in English (23).
11. H. Matsuda.Z. Electrochem.61(1957) 489.

International Journal of Advance and Innovative Research
Volume 6, Issue 1 (VI): January - March, 2019

ISSN 2394 - 7780

CORROSION STUDIES OF BIODIESSEL IN COPPER METAL – A MINI REVIEW

P. Indra Priyatharesini, S. Tamijselvy and P. Andal
Department of Chemistry, VISTAS, Chennai

ABSTRACT

Biodiesel is a suitable eco friendly and an alternative fuel. It is used as a blend with diesel, as the constituent of biodiesel matches to that of diesel. The engine parts of automobiles such as tankers, storage tanks, pipes and pumping equipment are normally constructed using carbon steel, stainless steel, copper, brass and aluminium. It is well known that biodiesel form sediments, when it is contact with metal. In this review the corrosion study of copper metal in biodiesel of various vegetables oil has been discussed.

Keywords: Diesel, Biodiesel, Corrosion, Copper, Aluminium, Corrosion inhibitors.

INTRODUCTION

Now a days, biodiesel has been used as an alternative fuel in order to reach demand of fuels and to reduce fossil fuel combustion. It is produced from renewable sources such as vegetable oils or animal fats. The properties of biodiesel from various vegetable oils and animal fats has properties very close to that of petroleum diesel (Barnes *et.*,2010, Fazal *et al.*, 2011). However, biodiesel has more corrosive nature compare to that of diesel (Fazal *et al.*,2012). The physical and chemical properties of biodiesel are different from that of diesel since its raw materials are different (Sharma *et al.,* 2008). The corrosive nature of biodiesel is due to its auto-oxidation behavior and also due to the moisture absorption, attack by microorganisms during storage and use (Fazal *et al.*,2010). The oxidation of biodiesel leads to the formation of of oxidation products such as peroxides and hydroperoxides. During degradation the peroxides and hydroperoxides are converted into aldehydes, ketones and acids that are volatile products of short chains. The higher molecular weight species can be also formed through oxidative polymerization (Karavalakis *et al.,* 2010, Karavalakis *et al.,* 2011). This enhances the corrosive nature of biodiesel and alter the properties of biodiesel (Aquino *et al.,* 2012). The corrosive nature of biodiesel also due to the presence of impurities such as water, alcohol, free fatty acids, glycerol and catalyst excess of the process (Haseeb *et al.*,2011) as well as purification method.

Corrosive behavior of different metals such as copper, brass, bronze, cast iron, carbon steel etc. in diesel and biodiesel was investigated by several researches (Sgroi *et al.*,2005, Geller *et al.*,2008, Fazal *et al.*,2010 , Haseeb *et al.*,2010). The corrosion of biodiesel in metal is due to the following factors:

1. Microbial corrosion: The ester group present in biodiesel forms hydrogen bond with water and becomes more hygroscopic compared to diesel. This causes hydrolysis of biodiesel, and forms fatty acids and glycerol which increases metallic corrosion or microbial corrosion occurs due to the growth of microbes (Fazal *et al.*,2011, Wang *et al* 2011, Fazal *et al.*,2013).
2. Biodiesel act as good lubricity than diesel so that it dissolves more metallic parts and these metals in solution enhance biodiesel degradation and enhances metallic corrosion (Kaul *et al.*,2007, Norouzi *et al.*,2012).
3. The metals such as aluminium, copper, brass in biodiesel act as catalysts for biodiesel oxidation. Therefore, the acid number of biodiesel increases proportionally with the corrosion rate for different metals (Kaul *et al.*,2007, Norouzi *et al.*,2012).

The metals such as bronze, brass, copper, zinc, lead and tin undergoes oxidation when in contact with diesel or biodiesel and create sediments (Kaul *et al.*,2007). Moreover, aluminum, carbon and stainless steels have been reported as materials compatible with biodiesel. Corrosion problems caused by biodiesel after tests have been performed in different motors were found by automobile manufactures and are considered a big challenge to be overcome (Fazal *et al.*,2010).

There are many papers studied about corrosion of metals such as stainless steel, copper, aluminium etc in acid medium (Al-Mobarak *et al.*,2010, Alejandra Carreon-Alvarez *et al.*,2012, Sameerah *et al.,* 2016). Also the studies carried overed about the corrosion of metal such stainless steel, copper, aluminium etc in biodiesel (Fernandes *et al.*,2013, Meenakshi *et al.*,2017).

Number of potential feedstocks available for use in biodiesel. Some of the vegetable oils used for the production of biodiesel are rapeseed oil, castor oil, sunflower oil, soybean oil, pongamita glabra, Madhuca indica and salvadora oleoides, palm oil, linseed oil etc., (Benjumea *et al.*,2008, Mamat et al.,2009, IIham *et al.,* 2010, Kousoulidou *et al.,* 2010).

As the biodiesel act as an alternative fuel, the main draw back of the usage of biodiesel is corrosion. The current studies is the review of corrosion of copper metal in some of the biodiesel which is synthesized from natural feed stock Pongamia, Jatropha, Palm biodiesel and Rapeseed biodiesel.

An introduction about the raw oil taken for the synthesis of biodiesel are as follows

Palm oil
Over 70% of the world's oils come from 4 plant species: soybean, palm, sunflower and rapeseed, and currently, the palm oil is the most traded oil in the world. It is used in the food industries. It is also used in the industry of hygiene and cleanliness in the composition of soaps, detergents and cosmetics. In the chemical industry, it is part of the lubricant composition and can also be used as biofuel. This oilseed has the largest oil content among the raw materials for the biodiesel production reaching the yield of 6000 kg/hectare/year.

Rapeseed
The rapeseed (*Brassica napus*) is a winter oilseed of Brassica genus, from Cruciferae family and it has 39-45% oil with excellent quality for fatty acid composition. It is the main oil used for biodiesel production in Europe, and is usually known as “colza . It represents, in percentage, 15.32% of world productionof vegetable oils, considering the 2011/2012 crop, behind only the production of palm oil (33.14%) and soybean (27.28%). The rapeseed oil contains mostly oleic acid (18:1), 62% followed by 32% linoleic acid (18:2) (Georgogianni *et al.*,2009).

Jatropha curcas
The jatropha (*Jatropha curcas*) is an economically important plant for the production of biodiesel (Endalew *et al.*,2011). The jatropha contains mostly 40.3% linoleic acid (18:1), 37% linolenic acid (18:2) which indicates a good quality of biodiesel to be produced from this source because the lower the amount of raw material unsaturation, the better is the stability to oxidation (Sarin,*et al.*,2010).

Pongamia pinnata
Pongamia pinnata (Legumnosae; Pappilona-ceae) is a non-edible oil of Indian. It is found mainly in the native Western Ghats in India, northern Australia, Fiji and in some regions of Eastern Asia. In general, Indian mills extract 24–27.5% oil, and the village crushers extract 18–22% oil. The oil contains primarily eight fatty acids. Of these, the four which are commonly found in most oils, including Pongamia, are the saturated acids, palmitic (Hexadecanoic acid) and stearic (Octade-canoic acid) and the unsaturated acids, oleic (Octadec-9-enoic acid) and linoleic (9,12-octadecadienoic acid).

Pongamia oil contains oleic acid (44.5–71.3%) as the major fatty acid followed by linoleic (10.8–18.3%), palmitic (3.7–7.9%) and stearic (2.4–8.9%) acids. In addition to these four fatty acids, Pongamia oil also contains eicosenoic acid (9-eicosenoic acid) in reasonable amounts (9.5–12.4%). This dark brown oil has a repulsive odor and shows fungicidal properties (Sanjib Kumar *et al.*, 2005).

The following Table 1 shown about the general characteristics of biodiesel.

Table-1: Physicochemical properties of the biodiesel

Property	Unit	Biodiesel
Appearance	-	Clear, light yellow
Odor	-	Mild
Physical state	-	Liquid
Boiling point	-	235
Kinematic viscosity at 40^0C	mm^2/S	4.19
Specific gravity at 25^0C	-	0.865
Flash point	^{0}C	165
Pour point	^{0}C	0
Water content	wt%	0.05
Total acid number	Mg KOH/g	0.39
Solubility in H_2O	-	Insoluble
Ph	-	Not applicable

PROCEDURE FOR THE SYNTHESIS OF BIODIESEL
Typical procedure for the synthesis of biodiesel: The vegetable oil (0.1 mol), methanol and the catalyst were mixed together in a three necked round bottomed flask equipped with magnetic stirrer,thermometer and condenser. The mixture was heated at 70 °C for the specified period. The process of the reaction was monitored

by GC analysis. On completion, the excess methanol was distilled off under vacuum. After the mixture was centrifugated, it formed three phases. The top layer was biodiesel, and the lower was the catalyst and a small amount of glycerol. The biodiesel was collected for chromatographic analysis first. The catalyst was recycled by filtration and washed with petrol ether. The quantitative analysis of the product was carried out on a temperature-programmed shimadzu (GC-14B) gas chromatograph (Xuezheng Liang *et al.*,2009).

Considerable amount of work has been done on the corrosion mechanism of copper in aqueous media and atmospheric conditions. Literature shows that the mechanism of copper corrosion depends on the environment. When copper is exposed to urban atmosphere, the corrosion layers formed on the exposed surface are unstable and partially leached away by rain water (T.E. Graodel *et al.*,1987, Benardi *et al.*,2009, C. Chiavari *et al.*, 2010). When copper is exposed to marine atmosphere, enhanced corrosion may occur due to chloride salts, higher concentration of oxygen resulting from water movements (L. Nunez *et al.*,2005). In acidic medium the corrosion of copper is also studied (Scendo , 2005) where the corrosion is initiated by oxygen and proceeded in two stages:

$2Cu+1/2\ O_2 + 2H^+ \Leftrightarrow 2Cu^+ + H_2O$

$2Cu+1/2\ O_2 + 2H^+ \Leftrightarrow 2Cu^{2+} + H2O$

The Metallic copper Cu(II) ions may also further enhance the corrosion process:

$Cu^{2+}+ Cu \Leftrightarrow 2Cu^+$

In neutral solution, the reaction could be as follows:

$2Cu+1/2\ O_2 + 2H_2O \Leftrightarrow 2Cu^+ + 2OH^-$

CORROSION OF COPPER METAL IN VARIOUS BIODIESEL

Corrosion in palm biodiesel on copper is found to be composed of Cu_2O, CuO, $Cu(OH)_2$ and $CuCO_3$. Dissolved O_2, H_2O, CO_2 and $RCOO^-$ radical in biodiesel seem to be the leading factors in enhancing the corrosiveness of biodiesel (Fazal *et al.,* 2013). In this study corrosion of copper is investigated by immersion test at room temperature (25^0C – 27^0C) for different time periods. The surface morphology and the elemental composition of the corrosion products were determined by SEM and XRD. The XPS analysis of corroded copper compounds formed on the biodiesel has also been studied. The impact of biodiesel-diesel-bioethanol (BDE) fuel blend in the corrosion behavior of copper has been studied (Thangavelu *et al.,* 2014). Static immersion tests in B45D35E20 (45% palm biodiesel, 35% diesel and 20% bioethanol) were carried out at room temperature (25°C) and 50° for 408 hours. The changes of fuel properties of the blend such as total acid number (TAN) and color changes were also investigated. The results showed that the corrosion rate of copper in B45D35E 20 at high temperature (50°C) is comparatively lower than the previous studies reported for pure biodiesel (B100) (Fazal *et al.*,2013). The corrosion rate of zinc and copper materials at room temperature, 40°C and 60°C in biodiesels obtained from olive, groundnut and soya oils were studied. The study showed that copper metal show a higher corrosion rate in the biodiesels compared to that of zinc metal. The corrosion rate of zinc materials increased with increase in temperature of the biodiesels over a period of time (Donnell Sylvester *et al.,* 2015).

Comparition study of the corrosion rates of copper and brass in Pongamia pinnata oil (O100), 3% NaCl, and oil blend with NaCl (O99) obtained by static immersion test and using rotating cage. The corrosivity and conductivity of the test media are positively correlated. This study suggested that the corrosivity of copper is higher than brass in Pongamia pinnata oil (PO) (Donnell Sylvester *et al.*,2015). Corrosion characteristics of different proportions of diesel and biodiesel on metal were studied at the room temperature in this paper. The experimental results show that all metals are corrupted by different proportions of diesel and biodiesel. The corrosion of metal is enhanced along with increasing of biodiesel in sample. After 45 days, in B0, B10, 50, B100 oil sample, the corrosion rate of aluminum is $0.13^0/_{00}$, $0.28^0/_{00}$, $0.33^0/_{00}$, $0.41^0/_{00}$ respectively, the corrosion of copper rate is $0.38^0/_{00}$, $0.48^0/_{00}$, $0.58^0/_{00}$, $0.60^0/_{00}$ respectively, the corrosion of iron rate is $0.30^0/_{00}$, $0.39^0/_{00}$, $0.66^0/_{00}$, $0.91^0/_{00}$ respectively. The corrosion resistance of iron is worst while the aluminum is the best among three metals (Youyong Su *et al.,* 2013). The effect of biodiesel fuel made from rapeseed oil and methanol on the corrosion properties of copper,mild carbon steel, aluminum, and stainless steel was studied and compared with those of commercial diesel fuel. The results show that the metals mentioned above corroded with variable degrees as they were immersed in the biodiesel fuel at 43 C for 60 days. Their corrosion rates were 0.02334, 0.01819, 0.00324, and 0.00087 mm/year, respectively. However, the corrosion rates of the metals immersed in commercial diesel fuel were relatively lower under the same corrosion conditions. The effects of corrosion in bio-diesel of copper and mild carbon steel were more significant than on aluminum and stainless steel. The corrosion process of metal surfaces in the biodiesel was mainly attributed to the chemical corrosion according to the experimental results with the help of SEM/EDS, AAS, and XPS (Enzhu Hu *et al.*,2012). Studies for the synthesis and characterization of biodiesel from non-edible oils like *Jatropha curcas*, *Pongamia glabra* (Karanja), *Madhuca indica* (Mahua) and *Salvadora oleoides* (Pilu) are studied in this paper. Corrosion characteristics of biodiesel are important for long term durability of engine parts, and very little information is available on this aspect. The studies were therefore taken up to assess the corrosion of synthesized biodiesel from the above mentioned non-edible oils.

Using long duration static immersion test method corrosion studies on engine parts like piston metal and piston liner were carried out with neat diesel procured from one of the Indian refinery and biodiesel synthesised from these non-edible oils. Biodiesel from *Salvadora* showed marked corrosion on both metal parts of diesel engine whereas biodiesel from other oils showed little or/no corrosion as compared to neat diesel (SavitaKaul R.C, 2007). Copper showed strongest corrosion effect in this study. The dependence of the oxidation stability on the type of metal showed that long-term storage tests in different types of metal containers for examining the influence of container material on oxidation stability of biodiesel may be replaced by significantly faster (AmitSarin *et al.*,2009). The study of corrosion of aluminium and copper in ultra low sulphur diesel fuel and its blends with rapeseed methyl ester were carried out by ShahrouzNorouzi et.,. Tests were carried out at wide ranging contents of rapeseed methyl ester (0%, 50%, 75% and 100%) at 80 °C for 600 h. Results showed that increasing the biodiesel content enhanced the corrosiveness of blend to both metals; this was confirmed by analyses of fuel properties and damage on metal surfaces exposed to fuels. Also it was found that copper was more vulnerable to attack compared with aluminium for all blends (Shahrouz Norouzi *et al.,* 2012).

CONCLUSION

Biodiesel has distinct chemical characteristics compare to that of petroleum diesel. Compositional differences of biodiesel derived from different feed stocks complicate the situation. The automobile fuel systems, has different types of metals which is contact with the fuel. Mainly there are different types of metals – Ferrous and non- Ferrous alloy and also elastomers. These can be mainly grouped into ferrous alloys, non-ferrous alloys and elastomers. Generally elastomers undergo degradation to a greater extent in biodiesel. So that elastomers like natural rubber, nitrile, chloroprene/neoprene etc. are not suitable for use in biodiesel. Among the two different types of metals, viz. ferrous alloys and non-ferrous alloys, the former are more resistant to attack in biodiesel. Among non-ferrous alloys, copper alloys and lead alloys are the most vulnerable which appear to be followed by aluminum.

Corrosion studies done so far showed that biodiesel is more corrosive than diesel. The corrosiveness of biodiesel increases with the concentration of biodiesel in the blend and the extent of oxidation.

Copper alloys are more susceptible to corrosion than ferrous alloys and aluminum alloys. The presence of impurities and water increases the corrosion tendency of biodiesel. The degree of degradation of biodiesel, is not directly related to the corrosiveness when it is in contact with the metal, for short immersion times.

The biodiesel degradation degree and corrosiveness as well as corrosion resistance presented by metals depends on a set of variables including raw material (feedstock), biodiesel purity summed to external factors like incidence of light, heat, oxygen and presence of metallic ions. Further studies are carried over for the inhibition of corrosion of various metals including copper using natural inhibitors.

REFERENCE

1. Alejandra Carreon-Alvarez, Rocio Castaneda Valderrama, Jorge Avalos Martinez, Arturo Estradda-Vargas, Sergio Gomez-Salazar, Maximiliano Barcena-Soto, Norberto Casillas. 2012. Corrosion of Aluminium, Copper, Brass and Stainless Steel 304 in Tequila. Int. J. Electrochem. Sci. 7 : 7877 -7887

2. Al-Mobarak N.A, Khaled D.F, Elhabib O.A, Abdel-Azim K.M. 2010. Electrochemical investigation of corrosion and corrosion inhibition of copper in NaCl solutions. J.Mater.Environ.Sci. 1 : 9-19.

3. Amit Sarin, RajneeshArora, Singh. N. P, Meeta Sharma, Malhotra. R.K. 2009. Influence of metal contaminants on oxidation stability of Jatropha biodiesel. Energy. 34(1): 1271-1275

4. Aquino I.P ,Hernandez R.P.B, Chicoma D.L, Pinto H.P.F , Aoki I.V. 2012. Influence of light, temperature and metallic ions on biodiesel degradation and corrosiveness to copper and brass. Fuel 102:795–807.

5. Barnes C.D, Garwood D.R, Price T.J 2010. The use of biodiesel blends in domestic vaporizing oil burners. Energy. 35: 501-505.

6. Benardi. E,Chiavari . C, Lenza. B, Martii . C, Moreselli . L, Ospitali . F, Robbiola .L. 2009. The atmospheric corrosion of quaternary bronzes: the leaching action of acid rain, Corros. Sci. 51: 159-170.

7. Benjumea P, Agudelo J. Agudelo A. 2008. Basic properties of palm oil biodiesel-diesel blends. Fuel. 87:2069-75.
8. Chiavari C, Bernardi . E, Martinin,. C, Passarini . F, Ospitali . F, Robbiola .L. 2010. The atmospheric corrosion of quaternary bronzes: The action of stagnant rain water. Corros. Sci. 52 : 3002-3010.
9. David M. Fernandes , Rodrigo H.O. Montes , Eduardo S. Almeida , Angerson N. Nascimento, Pedro V. Oliveira b, Eduardo M. Richter a, Rodrigo A.A. Muñoz . 2013. Storage stability and corrosive character of stabilised biodiesel exposed to carbon and galvanised steels. Fuel. 107: 609–614.
10. Endalew A.K, Kiros Y, Zanzi R. 2011. Heterogeneous catalysis for biodiesel production from *Jatropha curcas* oil (JCO). Energy. 36, 2693–2700.
11. Enzhu Hu, Yufu Xu, Xianguo Hu,, Lijun Pan, Shaotong Jiang. 2012. Corrosion behaviors of metals in biodiesel from rapeseed oil and methanol. Renewable Energy. 37: 371-378.
12. Fazal M. A, Haseeb A.S.M.A, Masjuki H.H 2011., Biodiesel feasibility study: an evaluation of material compatibility; performance: emission and engine durability. Renew. Sustain. Energy Rev. 15: 1314-1324.
13. Fazal M. A, Haseeb A.S.M.A, Masjuki H.H 2012. Degradation of automotive materials in palm biodiesel. Energy. 40:76-83.
14. Fazal M.A, Haseeb A.S.M.A, Masjuki H.H 2010. Comparative corrosive characteristics of petroleum diesel and palm biodiesel for automotive materials. Fuel Process Technology. 91:1308–15.
15. Fazal M.A, Haseeb A.S.M.A, Masjuki H.H. 2011. Biodiesel feasibility study: an evaluation of material compatibility; performance; emission and engine durability. Renew sust Energ Rev. 15: 1314-24.
16. Fazal M.A, Haseeb A.S.M.A, Masjuki H.H. 2013. Corrosion mechanism of copper in palm biodiesel. Corros Sci. 67:50-9.
17. Geller D.P, Adams T.T, Goodrum J.W, Pendergrass J.2008, Storage stability of poultry fat and diesel fuel mixtures: specific gravity and viscosity. Fuel. 87:92-102.
18. Georgogianni K.G, Katsoulidis A.K, Pomonis P.J, Manos G, Kontominas M.G. 2009. Transesterification of rapeseed oil for the production of biodiesel using homogeneous and heterogeneous catalysis. Fuel Processing Technology. 90 :671-676.
19. Graodel T.E, Nassau K., Franey J.P. 1987. Copper patinas formed in the atmosphere –l. Introduction. Corros. Sci. 27: 639-657.
20. Haseeb A.S.M.A, Fazal M.A, Jahirul M.I, Masjuki H.H. 2011. Compatibility of automotive materials in biodiesel: a review. Fuel. 90:922–31.
21. Haseeb A.S.M.A, Masjuki H.H, Ann L.J, Fazal M. 2010. Corrosion characteristics of copper and leaded bronze in palm biodiesel. Fuel process. Technol. 91: 329-334.
22. IIham Z, Saka S. 2010. Two-step supercritical dimethyl carbonate method for biodiesel production from Jatropha curcas oil. Bioresour Technol. 101:2735-40.
23. Karavalakis G, Hilari D, Givalou L, Karonis D, Stournas S.2011. Store stability and ageing effect of biodiesel blends treated with differents antioxidants. Energy. 36:369–74.
24. Karavalakis G, Stournas S, Karonis D 2010. Evaluation of the oxidation stability of diesel/biodiesel blends. Fuel.89:2483–9.
25. Kaul S, Saxena R.C, Kumar A, Negi M.S, Bhatnagar A.K, Goyal H.B. 2007. Corrosion behavior of biodiesel from seed oils of Indian origin on diesel engine parts. Fuel Process Technol. 88:303-7.
26. Kousoulidou M. Fontaras G. Ntziachristos L, Samaras Z. 2010. Biodiesel blend effects on common-rail diesel combustion and emission. Fuel. 89:3442-9.
27. Mamat R. Abdullah NR, Hongming Xu, Wysynski ML, Tsolakis A. 2009. Effect of fuel temperature on performance and emissions of a common rail diesel engine operating with rapeseed methyl ester (RME), SAE Technical.1:1896.
28. Meenakshi H. N. Parameswaran, Anisha Anand, and Shyamala R. Krishnamurthy. 2013. A Comparison of Corrosion Behavior of Copper and Its Alloy in Pongamia pinnata Oil at Different Conditions. Journal of Energy. Article ID 932976.

29. Meenakshi H.N, Anisha Anand, Shymala R, Sarath R. 2017. Comparision on the corrosion rate of copper, zinc and brass in Pongamia and Jatropha biodiesel.Indian Journal of Chemical Technology.24: 417-423.
30. Norouzi S, Eslami F. Wyszynski ML, Tsolakis A. 2012. Corrosion effects of RME in blends with ULAD on aluminium and copper. Fuel Process Technol, 104:204-10.
31. Nunez . L, Reguera. E, Corvo . F,Gonzalez . E,Vazquez . C. 2005. Corrosion of copper in sea water and its aerosols in a tropical island. Corros. Sci. 47: 461-484.
32. O’Donnell Sylvester, Feyisayo V. Adams and Linus N. Okoro. 2015. Impact of Biodiesel on the Corrosion of Zinc and Copper Strips. International Journal of Scientific & Engineering Research. 6: 546. ISSN 2229-5518.
33. Sameerah I. Al-Saeedi, Ghadah M. AL-Senani and Rasmiah Almufarij. 2016. Electrochemical investigations on the corrosion inhibition of aluminium by Green Leafy Vegetables in 1M HCl, Life Science Journal. 13:12.
34. Sanjib Kumar Karmee, Anju Chadha. 2005. Preparation of biodiesel from crude oil of Pongamia pinnata. Bioresource Technology. 96: 1425–1429.
35. Sarin, A.; Arora, R.; Singh, N.P.; Sarin, R.; Malhota, R.K.; Sharma, M. Synergistic. 2010. Effect of metal deactivator and antioxidant on oxidation stability of metal contaminated Jatropha biodiesel. Energy. 35 : 2333-2337.
36. Savita Kaul, Saxena R.C, AjayKumar, Negi M.S, Bhatnagar A.K, Goyal H.B, Gupta A K. 2007. Corrosion behavior of biodiesel from seed oils of Indian origin on diesel engine parts. Fuel Processing Technology. 88:303-307.
37. Scendo. M. 2005. Corrosion inhibition of copper by potassium ethyl xanthate in acidic chloride solutions by benzo- hydroxamic acids. Electrochim. Acta. 43:2778-2791.
38. Sgroi M, Bollito G, Saracco G , Specchia S.2005. BIOFEAT: biodiesel fuel processor for a vehicle fuel cell auxiliary power unit – study of the feed system. J. Power Sources. 149:8-14.
39. Shahrouz Norouzi , Farshad Eslami , Miroslaw L.Wyszynski, Athanasios Tsolakis. 2012. Corrosion effects of RME in blends with ULSD on aluminium and copper. Fuel Processing Technology 104: 204-210.
40. Sharma Y.C, Singh B 2008. Development of biodiesel from daranja, a tree found in rural India. Fuel. 87:1740-1742.
41. Thangavelu . S.K, Piraiarasi. C, Ahmed. A.S, Ani.F.N. 2014. Corrosion Behavior of Copper in Biodiesel-diesel-bioethanol (BDE). Advanced Materials Research. 1098: 44-50. ISNN. 1662-8985.
42. Wang W, Jenkins PE, Ren Z. 2011. Heterogeneous corrosion behavior of carbon steel in water contaminated biodiesel. Corrosion Sci. 53:845-9.
43. Xuezheng Liang, Shan Gao, Haihong Wu, Jianguo Yang. 2009. Highly efficient procedure for the synthesis of biodiesel from soybean oil. Fuel Processing Technology. 90:701–704.
44. Youyong Su_; Fei Chen_; Zhenfen Wu_; Hua Wang. 2013. Materials for Renewable Energy and Environment (ICMREE),. INSPEC Accession Number: 14566425.

International Journal of Advance and Innovative Research
Volume 6, Issue 1 (VI): January - March, 2019
ISSN 2394 - 7780

AN ALTERNATIVE ROUTE TO THE PREPARATION OF CARBON NANOTUBES FROM A BIOSOURCE AND THE SYNTHESIS OF NICKEL-DOPED CARBON NANOTUBES

D. Jesudurai[1], K. Arun[2], and V. Sheela Violet Rani[3]
Department of Chemistry[1], School of Basic Sciences, Vels University, Chennai
Arun Tech Impex[2], Padi, Chennai
Department of Chemistry[3], Velammal Institute of Technology, Thiruvallur
E-mail: jesudurai.sbs@velsuniv.ac.in

ABSTRACT

A simple methodology was adopted for the formation of carbon nanotubes (CNTs) from the biological source, egg albumin and the Nickel-doped CNTs were also produced. Metal doped nano structures have recently emerged as a material of choice for solar-to-fuel conversion. Compared to conventional oxide-based photo electrodes, metal doped Carbon Nano Tubes offer several distinct advantages, including a tunable energy band gap across nearly the entire solar spectrum, conduction and valence band edges that can overlap water redox and hydrocarbon potentials under deep visible and near-infrared light irradiation, and high-efficiency charge carrier separation and extraction. Such nano structures also exhibit a high level of stability in aqueous solution.

Keywords: Biosource, Carbon Nanotubes (CNTs), Metal-doping, Ni-doped CNTs.

1. INTRODUCTION

Humanity's reliance on fossil fuels to produce energy and the associated emissions of greenhouse gases which may have unpredictable effects on Earth's climate are arguably the greatest challenges facing society in the 21st century [1-3]. Currently, close to 80% of our energy needs are derived from the burning of fossil fuels in the form of oil, coal, and natural gas generates greenhouse gases as a byproduct [4]. Greenhouse gases have been found to be harmful for the environment and living organisms [5].

Of all renewable energy sources, solar power is by far the most abundant: roughly 120 000 TW of solar power hits the surface of the Earth each year [6, 7]. Photosynthesis is the largest-scale, longest-tested, and most important solar energy conversion system on earth [8]. A special attractive way of achieving this energy storage is to use renewable energy inputs to effect the formation of chemical bonds, to make fuels that can be stored safely and used when required [7].

1.1 NANOSTRUCTURED MATERIALS FOR PHOTOGENERATION OF ENERGY

Nanostructures are powerful tools for the design and realization of integrated microscopic systems, and it is possible that their use will enable practical applications of efficient and affordable solar-to-fuel conversion [1]. The photosynthetic systems of bacteria are the earliest examples of nanostructured solar energy conversion devices; they date back to the beginning of life on this planet [9]. Nano scaling has been shown to improve charge extraction from absorbers with low carrier mobility and short carrier lifetimes [9]. The first experimental work dates back to 1968, when Boddy established photo electrochemical water oxidation with an illuminated TiO_2 electrode, and Freund and Gomez reported similar reactions on ZnO, TiO_2, and WO_3 [4, 5, 9].

Nanotubes with large porosity can benefit the photo conversion efficiency from two aspects. First, the large surface areas ensure the stronger light absorption and simultaneously a much shorter path towards wall surface than the hole diffusion length. Second, a larger inner space of nanotube is important to accelerate the ion migration in the tube and overcome the kinetic bottleneck [6].

Single-wall carbon nanotubes can be doped, or intercalated, with electron donors or acceptors, similar to graphite and some conjugated polymers. The resulting materials show many of the same features: enhanced electrical conductivity, conduction electron paramagnetism, partial or complete reversibility, and cyclability. Reactions may be carried out in vapor or liquid phase, or electrochemically [10, 11].

1.2 METAL DOPED CARBON NANO TUBES

In 1991, Iijima [12-15] discovered carbon nanotubes which consisted of several concentric cylinders of graphene sheets [13,15]. Graphene sheets are hexagonal networks of carbon and these layers get stacked one above the other in the *c*-direction to form bulk graphite [19]. The nanotubes can be open-ended or closed end; closed ends are capped by one half of a fullerene-like molecule [13,15] They can be multi or single walled [13]. Depending on the way the graphene sheets fold, nanotubes are classified as armchair, zigzag or chiral [13,15]. The electrical conductivity of the nanotubes depends on the nature of folding [15]. Carbon is the chemical element with atomic number 6 and has six electrons which occupy $1s^2$, $2s^2$, and $2p^2$ atomic orbital [10].

The unique physical and chemical properties of carbon nanotubes (CNTs) have stimulated intense research and have enabled them to be applied in many promising fields including high strength composites, sensors, field emission displays, nanometer-sized semiconductor devices and hydrogen storage media [12,14,16]. Among the two-thirds of possible SWNT structures that are semiconductors, the band gap shows an approximate inverse dependence on tube diameter [17]. It is also significant that several theoretical studies have demonstrated that defect structures on the tubes lead to metal-semiconductor, semiconductor-semiconductor, and metal-metal junctions at the defect sites, which may themselves behave as nanoscale device elements, as demonstrated [17].

Currently, SWNTs are synthesized by one of three different techniques: pulsed laser vaporization, arc discharge growth, or chemical vapor deposition (CVD) on supported or gas phase catalysts [17]. Nanoscale particles of transition metals catalyze the growth processes [17-20].

CNTs doped with different metal atoms, like Fe, Sm, and Pt were investigated for their potential catalytic and material utilities [14, 21]. Among these metals Ni appears as an important one; besides its contact nature there is also its important role as a catalyst in the growth of carbon nanotubes [22 ,23]. Zinc oxide (ZnO) is also an important material and has received considerable attention due to its applications in electrical, optical, mechanical, and scientific research [24].

High-resolution transmission electron microscopy (HRTEM) revealed the orientations of the crystallography planes of the anchored metal nanoparticles. This information can be important for modeling the process of nucleation and growth of the nanoparticles on the nanotubes surfaces. Raman spectroscopy, scanning electron microscopy (SEM), X-ray diffraction (XRD), and X-ray photoelectron spectroscopy (XPS) were also employed for sample characterization [22-25].

2. EXPERIMENTAL

All the chemicals used were of analytical grade and used as such without any further purification. 0.5 Normal Nickel chloride ($NiCl_2$) metal salt solutions were prepared in ethyl alcohol by AR grade chemicals. Then it is allowed to react with 40 g egg albumin, to form lysine-nickel metal ion complex. The nickel-lysine complex formed was decomposed at higher temperature. In order to get CNTs, the complex was decomposed in muffle furnace. The decomposition takes place in 800 °C, 900 °C and 1000 °C. Multi-walled CNTs are prepared mostly at temperature as high as 800-900 °C. As at high temperature than this range the formation tends to single walled structure. Metal doped CNT formation confirmed by SEM, XRD.

2.1 SYNTHESIS OF NICKEL DOPED CARBON NANO TUBES

2.2 REACTION

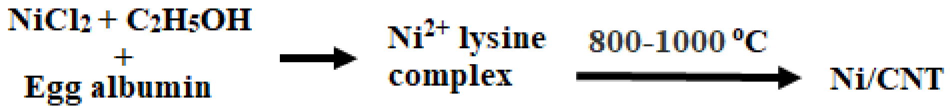

2.3 FLOW CHART

3. RESULTS AND DISCUSSION

3.1 Nickel Doped Carbon Nano Tubes Characterization

The microstructure of Ni/CNT was analyzed by SEM and XRD. SEM images exhibit the formation Carbon Nano Tubes (See Figure **1**) and XRD pattern confirmed Nickel doped CNT (See Figure **2**). The 2θ values of the XRD and the assigned peak for various elements are presented in the adjoined table. Appearance of characteristic peak of graphite shows the presence of Multiwalled carbon nanotubes in the sample. The other diffraction peaks at the angles 2θ with reflections are formation of Nickel doping. Thus, the XRD data obtained further reinforces the formation of the doping of the transition metal nickel on CNTs.

Figure-1: SEM images of Ni/CNT

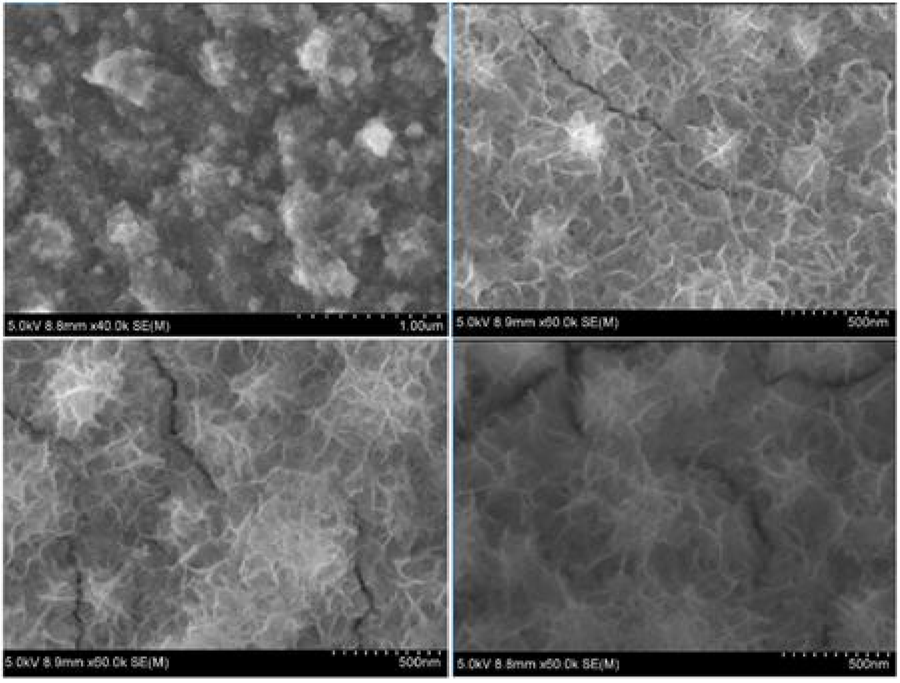

Figure-2: XRD patterns of Ni/CNT [26-28

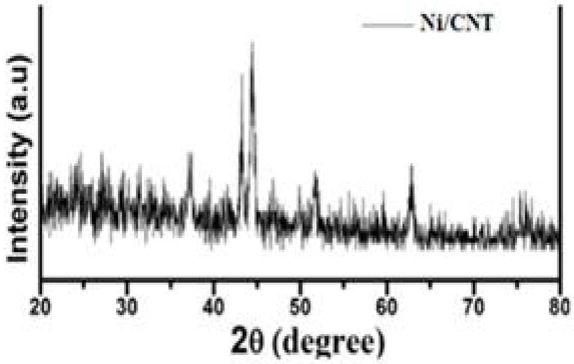

Ni/CNT	
2 θ	Peaks for
25.9	C(002)
42.9	Ni(111)
44.7	C(101)
51.8	Ni(200)
55.9	C(004)
76.2	Ni(220)

4. CONCLUSIONS

An efficient and alternate method was employed for the synthesis of carbon nanotubes (CNTs) from a bio-source of hen egg albumin. In view of applying to the photolytic utilization, nickel-doped on CNTs were prepared. The formation of Ni-doped CNTs was confirmed by the SEM, and XRD analysis.

REFERENCES

1. Chong Liu, Neil P. Dasgupta and Peidong Yang (2014),' Semiconductor Nanowires for Artificial Photosynthesis', Chem. Mater. 2014, 26, 415−422.
2. Peter Mirtchev (2015),' Investigations of Earth- Abundant Metal Oxide Nanomaterials for Solar Fuel Generation', PhD thesis, Department of Chemistry, University of Toronto.
3. Sergey Koroidov (2014), PhD thesis, 'Water splitting in natural and artificial photosynthetic systems', Department of Chemistry, Umea university.

4. Bandar AlOtaibi (2016),' Artificial Photosynthesis for Hydrogen Generation and CO_2 Reduction Using Metal-Nitride Nanowires', PhD thesis McGill University, Montreal, January 2016.
5. Dohyung Kim, Kelsey K. Sakimoto, Dachao Hong, and Peidong Yang (2015),' Artificial Photosynthesis for Sustainable Fuel and Chemical Production', Angew. Chem. Int. Ed. 2015, DOI: 10.1002/anie.201409116.
6. Albertus D Handoko, Kimfung Li and Junwang Tang (2013), 'Recent progress in artificial photosynthesis: CO_2 photoreduction to valuable chemicals in a heterogeneous system', Current Opinion in Chemical Engineering 2013, 2:200–206.
7. Symes MD, Cogdell RJ, Cronin L (2013),'Designing artificial photosynthetic devices using hybrid organic–inorganic modules based on polyoxometalates', Phil Trans R Soc A 371: 20110411.
8. Devens gust et al. (2013),'Artificial photosynthesis', Theoretical and Experimental Plant Physiology, 25(3): 182-185, 2013.
9. Frank E. Osterloh (2015),'Nanoscale Effects in Water Splitting Photocatalysis', Top Curr Chem (2015) DOI: 10.1007/128_2015_633.
10. Ali Eatemadi et al. (2014), 'Carbon nanotubes: properties, synthesis, purification, and medical applications', Nanoscale Research Letters 2014, 9:393.
11. John e. Fischer (2002),'Chemical Doping of Single-Wall Carbon Nanotubes', Acc. Chem. Res. 2002, 35, 1079-1086.
12. Hang Qi, Cheng Qian, and Jie Liu (2006), 'Synthesis of High-Purity Few-Walled Carbon Nanotubes from Ethanol/Methanol Mixture', Chem. Mater., 2006, 18 (24), 5691-5695, DOI: 10.1021/cm061528r.
13. Kannan Balasubramanian and Marko Burghard (2005),'Chemically Functionalized Carbon Nanotubes', small 2005, 1, No. 2, 180 –192, DOI: 10.1021/acsenergylett.6b00059.
14. Kodi Pandyan R et al. (2012), 'Hydrogen adsorption on transition element-doped SWCNT', Elixir Comp. Chem. 50 (2012) 10539-10540.
15. Rao C.N.R and Manashi Nath (2003),'Inorganic nanotubes', Dalton Trans.,2003,1-24, DOI: 10.1039/ b208990b.
16. Shaijumona M.M, Bejoyb N, Ramaprabhu S (2005),'Catalytic growth of carbon nanotubes over Ni/Cr hydrotalcite-type anionic clay and their hydrogen storage properties', Applied Surface Science 242 (2005) 192–198.
17. Bruce Weisman R and Shekhar Subramoney (2006), 'Carbon Nanotubes', The Electrochemical Society Interface, Summer 2006.
18. Rümmeli et al. (2011),'Synthesis of carbon nanotubes with and without catalyst particles', Nanoscale Research Letters 2011, 6:303.
19. Rohini Chavan, Ujwala Desai, Priti Mhatre, Ruchira Chinchole (2012),' A Review: Carbon nanotubes', International Journal of Pharmaceutical Sciences Review and Research, Volume 13, Issue 1, March – April 2012; Article-022 ISSN 0976 – 044X.
20. Sivakumar V.M, Abdullah A. Z, Mohamed A. R and Chai S. P (2011),' Optimized parameters for carbon nanotubes synthesis over Fe and Ni catalysts via methane CVD', Rev.Adv.Mater.Sci.27(2011)25-30.
21. Ya Kun Chen (2011), 'Theoretical Studies of Transition-Metal-Doped Single-Walled Carbon Nanotubes', dx.doi.org/10.1021/jp909490v, J. Phys. Chem. C 2011, 115, 9306–9311.
22. Bittencourt C et al. (2007),'Decorating carbon nanotubes with nickel nanoparticles', Chemical Physics Letters 436 (2007) 368–372.
23. ShunsukeYamanaka et al. (2007),' Fabrication and Thermal Properties of Carbon Nanotube/Nickel Composite by Spark Plasma Sintering Method', Materials Transactions, Vol. 48, No. 9 (2007) pp. 2506 to 2512.
24. Gültekin D, Alaf M and Akbulut H (2013),'Synthesis and Characterization of ZnO Nanopowders and ZnO-CNT Nanocomposites Prepared by Chemical Precipitation Route', Acta Physica Polonica A, Vol.123 (2013), DOI:10.12693/APhysPolA.123.274.

25. Dunieskys G. Larrude et al. (2014),' Synthesis and Characterization of Silver Nanoparticle-Multiwalled Carbon Nanotube Composites', Journal of Nanomaterials Volume 2014, Article ID 654068.
26. Eman, Mwafya A, Dawya M, Abouelsayedb A, Elsabbaghc I.A and Elfassc M.M (2016),'Synthesis and Characterization of Multi-Walled Carbon Nanotubes Decorated ZnO Nanocomposite', Egypt. J. Chem. 59, No.6 pp.1061– 1068(2016).
27. Ruby chauhan, Ashavani kumar, Ram pal Chaudhary (2011),'Structure and optical properties of $Zn_{1-x}Ni_xO$ nanoparticles by co precipitation method', Journal of Optoelectronics and Biomedical Materials Vol. 3 Issue 1, January – March 2011 p. 17-23.
28. Vinod K. Gupta and Tawfik A. Saleh (2011),'Synthesis of Carbon Nanotube-Metal Oxides Composites; Adsorption and Photo-degradation', Chapter from the book Carbon Nanotubes - From Research to Applications, Intech, ISBN 978-953-307-500-6.

MANUSCRIPT SUBMISSION

GUIDELINES FOR CONTRIBUTORS

1. Manuscripts should be submitted preferably through email and the research article / paper should preferably not exceed 8 – 10 pages in all.
2. Book review must contain the name of the author and the book reviewed, the place of publication and publisher, date of publication, number of pages and price.
3. Manuscripts should be typed in 12 font-size, Times New Roman, single spaced with 1” margin on a standard A4 size paper. Manuscripts should be organized in the following order: title, name(s) of author(s) and his/her (their) complete affiliation(s) including zip code(s), Abstract (not exceeding 350 words), Introduction, Main body of paper, Conclusion and References.
4. The title of the paper should be in capital letters, bold, size 16” and centered at the top of the first page. The author(s) and affiliations(s) should be centered, bold, size 14” and single-spaced, beginning from the second line below the title.

First Author Name1, Second Author Name2, Third Author Name3

1Author Designation, Department, Organization, City, email id

2Author Designation, Department, Organization, City, email id

3Author Designation, Department, Organization, City, email id

5. The abstract should summarize the context, content and conclusions of the paper in less than 350 words in 12 points italic Times New Roman. The abstract should have about five key words in alphabetical order separated by comma of 12 points italic Times New Roman.
6. Figures and tables should be centered, separately numbered, self explained. Please note that table titles must be above the table and sources of data should be mentioned below the table. The authors should ensure that tables and figures are referred to from the main text.

EXAMPLES OF REFERENCES

All references must be arranged first alphabetically and then it may be further sorted chronologically also.

- **Single author journal article:**

Fox, S. (1984). Empowerment as a catalyst for change: an example for the food industry. *Supply Chain Management, 2*(3), 29–33.

Bateson, C. D.,(2006), ‘Doing Business after the Fall: The Virtue of Moral Hypocrisy’, Journal of Business Ethics, 66: 321 – 335

- **Multiple author journal article:**

Khan, M. R., Islam, A. F. M. M., & Das, D. (1886). A Factor Analytic Study on the Validity of a Union Commitment Scale. *Journal of Applied Psychology, 12*(1), 129-136.

Liu, W.B, Wongcha A, & Peng, K.C. (2012), “Adopting Super-Efficiency And Tobit Model On Analyzing the Efficiency of Teacher’s Colleges In Thailand”, International Journal on New Trends In Education and Their Implications, Vol.3.3, 108 – 114.

- **Text Book:**

Simchi-Levi, D., Kaminsky, P., & Simchi-Levi, E. (2007). *Designing and Managing the Supply Chain: Concepts, Strategies and Case Studies* (3rd ed.). New York: McGraw-Hill.

S. Neelamegham," Marketing in India, Cases and Reading, Vikas Publishing House Pvt. Ltd, III Edition, 2000.

- **Edited book having one editor:**

Raine, A. (Ed.). (2006). *Crime and schizophrenia: Causes and cures.* New York: Nova Science.

- **Edited book having more than one editor:**

Greenspan, E. L., & Rosenberg, M. (Eds.). (2009). *Martin's annual criminal code:Student edition 2010.* Aurora, ON: Canada Law Book.

- **Chapter in edited book having one editor:**

Bessley, M., & Wilson, P. (1984). Public policy and small firms in Britain. In Levicki, C. (Ed.), *Small Business Theory and Policy* (pp. 111–126). London: Croom Helm.

- **Chapter in edited book having more than one editor:**

Young, M. E., & Wasserman, E. A. (2005). Theories of learning. In K. Lamberts, & R. L. Goldstone (Eds.), *Handbook of cognition* (pp. 161-182). Thousand Oaks, CA: Sage.

- **Electronic sources should include the URL of the website at which they may be found, as shown:**

Sillick, T. J., & Schutte, N. S. (2006). Emotional intelligence and self-esteem mediate between perceived early parental love and adult happiness. *E-Journal of Applied Psychology*, *2*(2), 38-48. Retrieved from http://ojs.lib.swin.edu.au/index.php/ejap

- **Unpublished dissertation/ paper:**

Uddin, K. (2000). A Study of Corporate Governance in a Developing Country: A Case of Bangladesh (Unpublished Dissertation). Lingnan University, Hong Kong.

- **Article in newspaper:**

Yunus, M. (2005, March 23). Micro Credit and Poverty Alleviation in Bangladesh. *The Bangladesh Observer*, p. 9.

- **Article in magazine:**

Holloway, M. (2005, August 6). When extinct isn't. *Scientific American, 293*, 22-23.

- **Website of any institution:**

Central Bank of India (2005). *Income Recognition Norms Definition of NPA.* Retrieved August 10, 2005, from http://www.centralbankofindia.co.in/ home/index1.htm, viewed on

7. The submission implies that the work has not been published earlier elsewhere and is not under consideration to be published anywhere else if selected for publication in the journal of Indian Academicians and Researchers Association.

8. Decision of the Editorial Board regarding selection/rejection of the articles will be final.

INDIAN ACADEMICIANS & RESEARCHERS ASSOCIATION

Major Objectives

- To encourage scholarly work in research
- To provide a forum for discussion of problems related to educational research
- To conduct workshops, seminars, conferences etc. on educational research
- To provide financial assistance to the research scholars
- To encourage Researcher to become involved in systematic research activities
- To foster the exchange of ideas and knowledge across the globe

Services Offered

- Free Membership with certificate
- Publication of Conference Proceeding
- Organize Joint Conference / FDP
- Outsource Survey for Research Project
- Outsource Journal Publication for Institute
- Information on job vacancies

Indian Academicians and Researchers Association
Shanti Path ,Opp. Darwin Campus II, Zoo Road Tiniali, Guwahati, Assam
Mobile : +919999817591, email : info@iaraedu.com www.iaraedu.com

---

EMPYREAL PUBLISHING HOUSE

- Assistant in Synopsis & Thesis writing
- Assistant in Research paper writing
- Publish Thesis into Book with ISBN
- Publish Edited Book with ISBN
- Outsource Journal Publication with ISSN for Institute and private universities.
- Publish Conference Proceeding with ISBN
- Booking of ISBN
- Outsource Survey for Research Project

Publish Your Thesis into Book with ISBN "Become An Author"

EMPYREAL PUBLISHING HOUSE
Zoo Road Tiniali, Guwahati, Assam
Mobile : +919999817591, email : info@editedbook.in, www.editedbook.in